THE CIRCULATION AND INTERNAL TIDE OF INDIAN ARM, B.C.

by

BRADLEY dE YOUNG

B.Sc., Memorial University of Newfoundland, 1977

M.Sc., Memorial University of Newfoundland, 1984

A THESIS SUBMITTED IN PARTIAL FULFILMENT OF

THE REQUIREMENTS FOR THE DEGREE OF

DOCTOR OF PHILOSOPHY

in

THE FACULTY OF GRADUATE STUDIES

Oceanography

We accept this thesis as conforming

to the required standard

THE UNIVERSITY OF BRITISH COLUMBIA

SEPTEMBER 1986

In presenting this thesis in partial fulfilment of the requirements for an advanced degree at the University of British Columbia, I agree that the Library shall make it freely available for reference and study. I further agree that permission for extensive copying of this thesis for scholarly purposes may be granted by the head of my department or by his or her representatives. It is understood that copying or publication of this thesis for financial gain shall not be allowed without my written permission.

Department of Oceanography

The University of British Columbia
1956 Main Mall
Vancouver, Canada
V6T 1Y3

Date 8 Sept 1986

ABSTRACT

The wintertime deepwater exchange in a silled fjord is described. Bottom-water renewal took place in the third year of the study, 1984/85. Hydraulic control of the exchange was consistent with the observations. This control is exerted over the long sill, which restricts access to the fjord. The maximum density at the sill was observed during neap tides. No distinct peaks in the velocity at the sill were observed during the inflows. During each inflow, associated with a neap tide, about 20 % of the water in the fjord was replaced. These exchanges occurred over periods of 5 – 10 days.

An internal tide was observed in Indian Arm in all three winters studied. In the winter of 1983/84, this internal tide was observed to change from a predominantly M_2 internal response to a predominantly K_1. This change in the response is explained as a partial resonance response of the system. During the 1983/84 winter, the resonance period steadily increased from 14 hours at the start, to 22 hours at the end. It is suggested that the enhanced internal response at the K_1 frequency, late in the winter, is due to resonance. Fitting of normal modes was done to look at the energy flux in Indian Arm. About 20 – 30 % of the energy flux is found to propagate from the head of the inlet, supporting the resonance hypothesis, which requires energy to be reflected from the head.

The energy sinks for the barotropic tide are investigated using a variety of data. From an analysis of the tidal data, it is estimated that a total of 10 – 15 % of the barotropic tidal energy which enters Burrard Inlet is dissipated. About 0.7 MW is lost from the barotropic tide in the vicinity of the Indian Arm sill. About 0.3 MW was found in internal waves propagating away from the sill. Of this flux about 60 % was in the internal tide, with 40 % in high frequency internal waves. The vertical diffusion coefficient (K_v) is determined from an analysis of the density data. K_v is found to be related to the buoyancy frequency N by the relationship, $K_v \propto N^{-0.86}$. Using K_v and N, the amount of energy which does work against buoyancy is found to be about 100 kW. From this energy estimate, the flux Richardson number (R_f) is estimated be 0.05 – 0.1.

Table of Contents

List of Figures

List of Tables

Acknowledgements

The efforts of many people went into this work and it is with pleasure that I acknowledge them. Dr. S. Pond, my supervisor, provided advice and assistance whenever needed. Drs. P.H. Leblond, L.A. Mysak, D.M. Farmer and A.G. Lewis, of my supervisory committee, provided useful advice. A. Webb provided hours of discussion concerning the general problem of modal fitting. By this work I am somewhat of a convert. For the Bernoulli equation analysis of the blocking, I am grateful to Dr. I. Gartshore. Technical assistance came from many people, A. Ramnarine, M. Storm, D. English, R. Bigham, A. Stickland, J. Love, K. Thomson and H. Heckl. The officers and crews of the C.S.S. Vector and the C.N.A.V. Endeavour provided the platforms from which all of the data were collected. Computer software for much of the data translation came from D. Laplante, V. Lee and D. Dunbar. V. Lee also helped perform some of the drudgery involved in cleaning up the cyclesonde files.

The Natural Sciences and Engineering Research Council provided support for this project, in the form of an operating grant (**A-8301**) to Dr. S. Pond and a scholarship to me. Personal support and encouragement came from Angel and Duncan.

1. Introduction

1.1 Fjords

A fjord is a type of estuary found at high latitudes in both the northern and southern hemispheres. An estuary can be defined (Pritchard, 1967) as a nearly enclosed body of water in which the salinity is appreciably influenced by freshwater runoff. In the history of the earth, estuaries are transient features which are most abundant following changes in sea level (Schubel and Hirschberg, 1978). Though ephemeral on the geological time scales, they are important in the present oceans, both scientifically and commercially. Although abundant during only part of the last million years, they are numerous at present. Emery (1967) estimates that estuaries make up 80-90 % of the Atlantic coast and 10-20 % of the Pacific coast. Estuaries are important to man for many reasons: large populations live adjacent to them, they are ports for transportation, they are often used as waste dumps by industry and their high productivity allows them to support large populations of fishes and shellfishes.

Four different types of estuaries have been classified: the fjord, the bar-built estuary, tectonically produced estuaries and drowned river valleys. Fjords are formed in areas covered by ice sheets, thus limiting their presence to higher latitudes. They often have U-shaped channels carved by the movements of glaciers, scouring along lines of structural weakness. A distinctive feature is the sill which restricts access to the deep basin. Although this sill is often the terminal moraine left by the glacier, a mark of its greatest advance, it may also be a bedrock structure. The depth of water over the sill is determined by the change in sea level following de-glaciation and by the extent of isostatic rebound which takes place.

Indian Arm is a narrow ($1.3\,km$) and relatively short ($22\,km$) fjord (see *Figure 1*). According to the survey by Pickard and Stanton (1980), Indian Arm falls into the bottom 10 % of west coast fjords with respect to its length. It has an average depth of $200\,m$ in the deep basin, with a sill at $26\,m$ (see *Figure 2*). It is connected to the Strait of Georgia (*Figure 1*) by Burrard Inlet , a narrow connecting channel in which there are two shallow

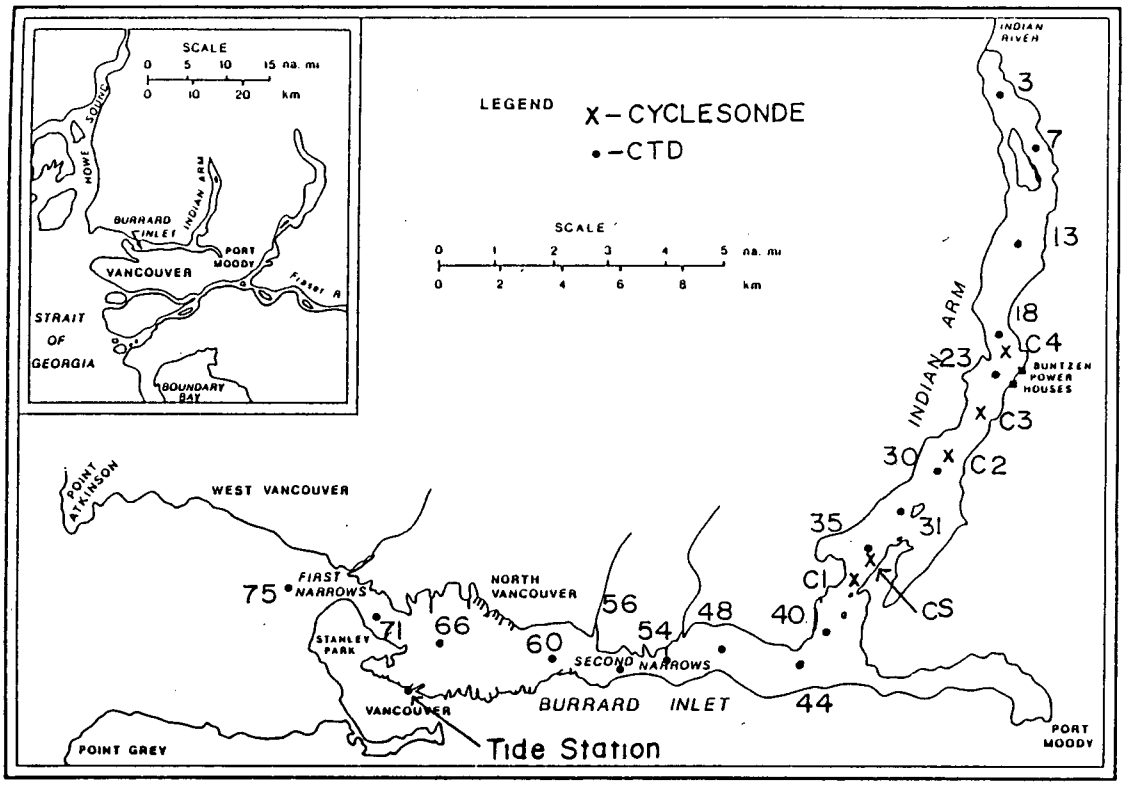

Figure 1 Map of Burrard Inlet and Indian Arm showing the station locations . CTD stations are indicated with a •, current meter stations with a ×.

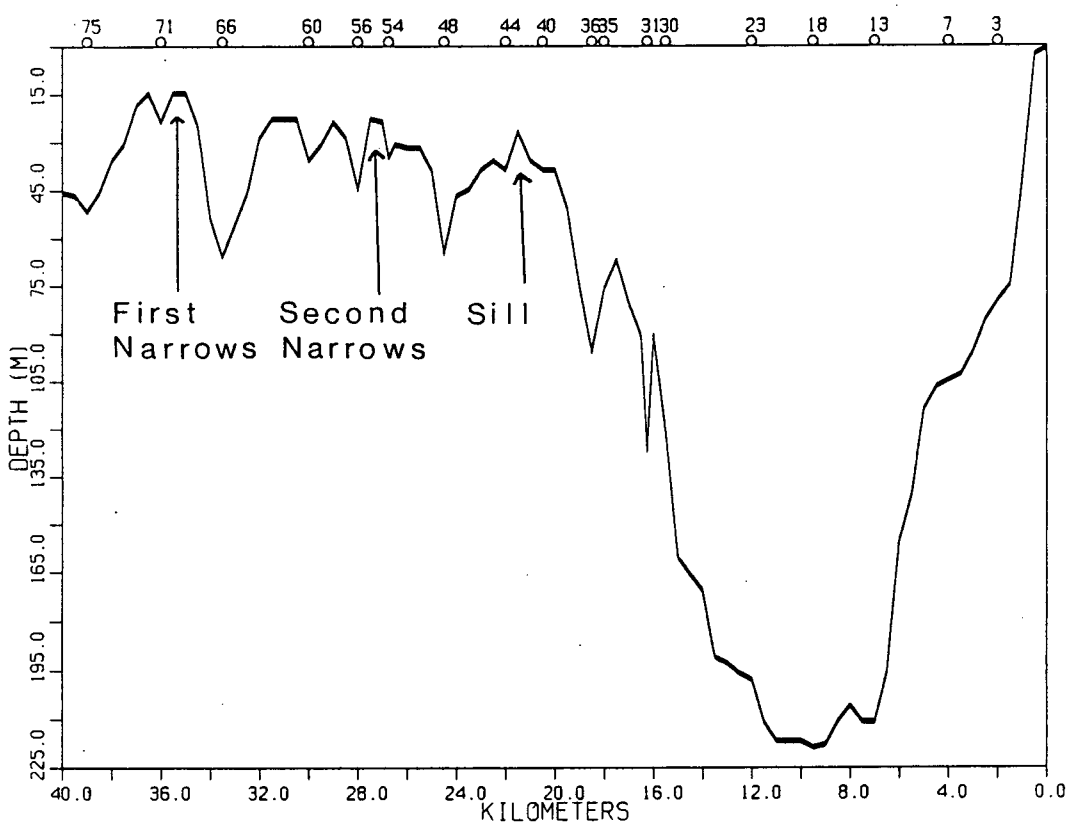

Figure 2 Longitudinal profile from the head of Indian Arm to the mouth of Burrard Inlet.

sills, located at First and Second Narrows (14 and 21 m deep respectively).

1.2 Indian Arm Oceanography

Captain George Vancouver, after a night anchored in Port Moody, passed the narrows of Indian Arm and concluded that it did not provide a navigable route to Europe because of its weak tidal flow. This is the first known oceanographic observation of Indian Arm. Called Sasamat by the Indians, this Arm has not seen the development that has occurred in Burrard Inlet. Malcolm Lowry, living in Dollarton (near the mouth of Indian Arm) during the 1940's, described Vancouver's harbour in *The Bravest Boat* "*... you would be sure you were in hell ... affirmed by the spectacle at first not unpicturesque, of the numerous sawmills relentlessly smoking and champing away like demons, Molochs fed by whole mountainsides of forests ...* ". The beauty of Indian Arm is provided in part at least by the contrast with the industrialization of Burrard Inlet.

Indian Arm, partly because of its proximity to Vancouver, has been studied or monitored for much of the past thirty years. The density regime of the fjord was the main focus of most of this work. The irregular deepwater exchange cycle and the near anoxic bottom water conditions provided the main sources of interest. In recent years there has also been some investigation of the current patterns. Gilmartin (1962) presents a fairly complete 'classical ' description of Indian Arm, based primarily upon bottle-cast data. He describes the fjord as a two-layer system in which a thin layer of brackish water at the surface overlies a more saline water mass. It is the inflow of freshwater from the Indian River and the Buntzen power plant (see *Figure 1*) , about 12 km from the head, that drives the estuarine circulation. The inflowing freshwater creates a pressure gradient which drives brackish water out of the system. Entrainment of underlying saline water into this outflow generates a compensating flow of saline water at depth.

The total annual freshwater inflow averages 42 m^3/s (Dunbar, 1985). Most of this inflow comes from the Buntzen power plant (23 m^3/s) with the majority of the remainder coming from the Indian River (12 m^3/s). Less than 15 % of the total is from peripheral

streams or direct precipitation (Dunbar,1985). Pickard (1961), in a comparison with other B.C. fjords, classified Indian Arm as a low runoff inlet. Because the runoff to surface area ratio is small, it is expected that the estuarine circulation will be weak. Prior to this study, no direct observations of the estuarine circulation in Indian Arm exist, though it has been observed that the flow is primarily tidally driven (Davidson, 1979).

Another feature related to the estuarine circulation is the thickness of the surface layer. Gilmartin (1962) estimates this layer to be $1.5 - 2.5\,m$ thick with a strong halocline somewhere between 2.5 and $5\,m$. Below $5 - 10\,m$ there exists a layer of gradually increasing salinity (see *Figure 3*). The surface salinity was observed to vary between $0 - 25\,‰$, depending upon location and time of year, while the bottom salinity was about $27\,‰$. It would appear that the dynamic effects of this surface layer are weak. Dunbar (1985), for example, was able to create an effective numerical tidal model of the system using a vertical grid spacing of $10\,m$. This result suggests that the effects of the thin surface layer are unimportant to the deeper tidal circulation.

The temperature of the water in Indian Arm is influenced by four factors, solar heating, air temperature, the temperature of the water below sill depth outside Burrard Inlet and to a lesser degree, the amount of freshwater inflow. Gilmartin observed that the cycle of surface temperature is in phase with the air temperature cycle, although it is of a slightly lower amplitude. The minimum temperature is in January, the maximum in August. For most of the year (7 winter months) the air temperature is less than that of the surface water so cooling is important. During the remaining five months of the year, the air temperature exceeds the water temperature and heating takes place. In general, the two do not differ by more than a few $°C$.

The deep water temperature is determined by the quasi-periodic intrusions of water from outside the inlet. Following an exchange, its temperature is a result of the temperature of the source water and the amount of mixing that occurs during its transit through Burrard Inlet and down the slope to the bottom of Indian Arm. Once in the basin, the temperature

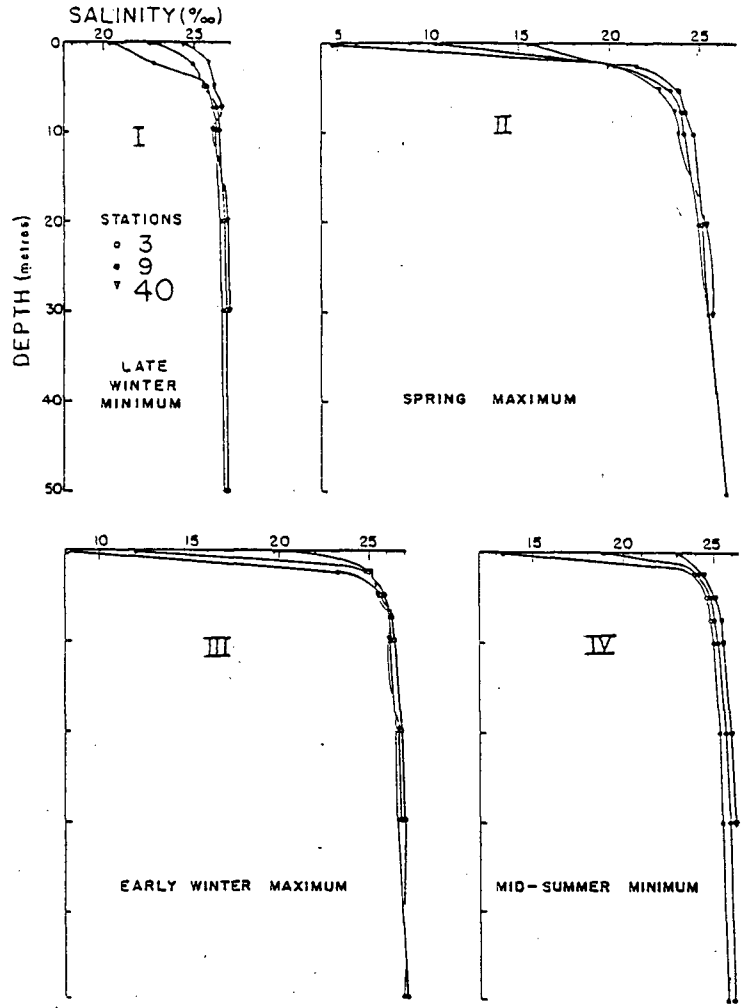

Figure 3 Mean vertical salinity profile at selected stations in 1956 – 1959 .
I - Winter runoff minima. II - Spring runoff maxima. III - Winter runoff maxima. IV - Summer Runoff minima. (From Gilmartin, 1962).

will change as a result of the process of diffusion, or as the result of another inflow event. The effects of winter cooling do not reach the deep water.

Dissolved oxygen (DO_2) concentration is the final physical characteristic important to a description of the Indian Arm system. It is a non-conservative property, because of the influence of biological activity, and is thus somewhat more difficult to interpret than the other scalars. In general, DO_2 is high near the surface and decreases with depth. Gilmartin (1962) describes a seasonal cycle with a maximum in the spring and a smaller overlapping maximum in the fall. The deepwater DO_2 shows periodic increases followed by steady decreases; the increases are a result of inflows of dense near-surface water from

outside the system. The exchange need not necessarily reach the bottom to halt the decrease in DO_2 since diffusion plays an important role. It is because of these quasi-periodic intrusions, usually at mid-depths although in some years reaching to the bottom, that anoxic conditions have not been observed in Indian Arm (Burling, 1982).

Burling (1982) presents a long time-series of DO_2 from Indian Arm showing that the bottom water concentration is usually in the range $2-4\,ml/l$, although it has been below $1\,ml/l$ in a number of years. The mid-depth concentration varies between $2-4\,ml/l$; the surface concentration may reach as high as $10\,ml/l$. It is possible to have either a subsurface maximum or minimum in DO_2 depending upon a number of factors. Advection, stratification and biological renewal will all influence the vertical profile of the dissolved oxygen concentration.

1.3 Deepwater Exchange

In his three year study of Indian Arm, Gilmartin (1962) missed the period of bottom-water exchange, although he was able to infer the event from his observations. Davidson (1979) extended the work of Gilmartin , providing good observations of an exchange event that occurred over the 1974-75 winter. He observed that at least 80 % of the volume of Indian Arm was exchanged over a period of 33 days. A single current meter record, from about 5 m above the bottom at the sill, confirmed this estimate of the transport during the exchange.

Burling (1982) presents a time series of temperature, salinity and DO_2 (see *Figure 4*) collected over a number of years. These data , covering a 14 year period, illustrate the irregular nature of the bottom-water exchange. Exchange at some depth takes place in most years, although there are several years during which no renewal took place. To judge whether or not renewal has occurred, it is sometimes helpful to look at the dissolved oxygen concentration (DO_2) in addition to the temperature and salinity. In 1972 and 1974, for example, there is little change evident in either the temperature or the salinity. The DO_2 data make it clear that exchange took place. In these cases the T-S characteristics of the

exchange water closely match those of the displaced water.

The seasonal timing of the renewals over the 14 year period is reasonably consistent. The paucity of measurements at certain times makes it difficult to be precise but the renewals all begin around the start of the new year. Thus, even though the renewals do not occur in every year, their seasonal timing is regular when they do occur. The precise timing of the renewals cannot be determined from these monthly survey data. Davidson (1979) identified a number of controlling influences on the exchange: freshwater runoff, tidal mixing and the density of the water outside Burrard Inlet in the Strait of Georgia. To these one could add wind effects such as upwelling in the Strait of Georgia. All of these various influences will work together to control the timing of the the exchange. Prior to this study, it was not known whether or not the renewal was steady. It is shown here that the exchange is modulated during the spring/neap tidal cycle.

Figure 4 also indicates the importance of diffusion in conditioning the deep water to permit an exchange. Following the 1978-1979 event, there was a steady decrease in salinity at both 100 and 200 m. Since it is the salinity that controls the density, it is this decrease in density, on account of diffusion, that allows the next exchange to occur. The nature of diffusion, which in the ocean is primarily controlled by turbulent processes, is poorly understood. Gilmartin (1962) made some estimates of the vertical diffusivity of heat and salt based upon bottle data, however, the accurate estimate of such values probably requires greater vertical resolution and longer time series to allow the aliasing effects of the internal tide to be averaged away. The monthly CTD surveys, to be presented here, combined with the current measurements will allow the calculation of improved diffusion coefficients.

It is clear from this brief review of the observations of exchange in Indian Arm that good observations of the renewal processes in the fjord remain to be made. This study seeks to fill this gap. In fact, there are few direct observations of renewal in any fjord. Gade and Edwards (1980) present a review of the work done on deepwater renewal and

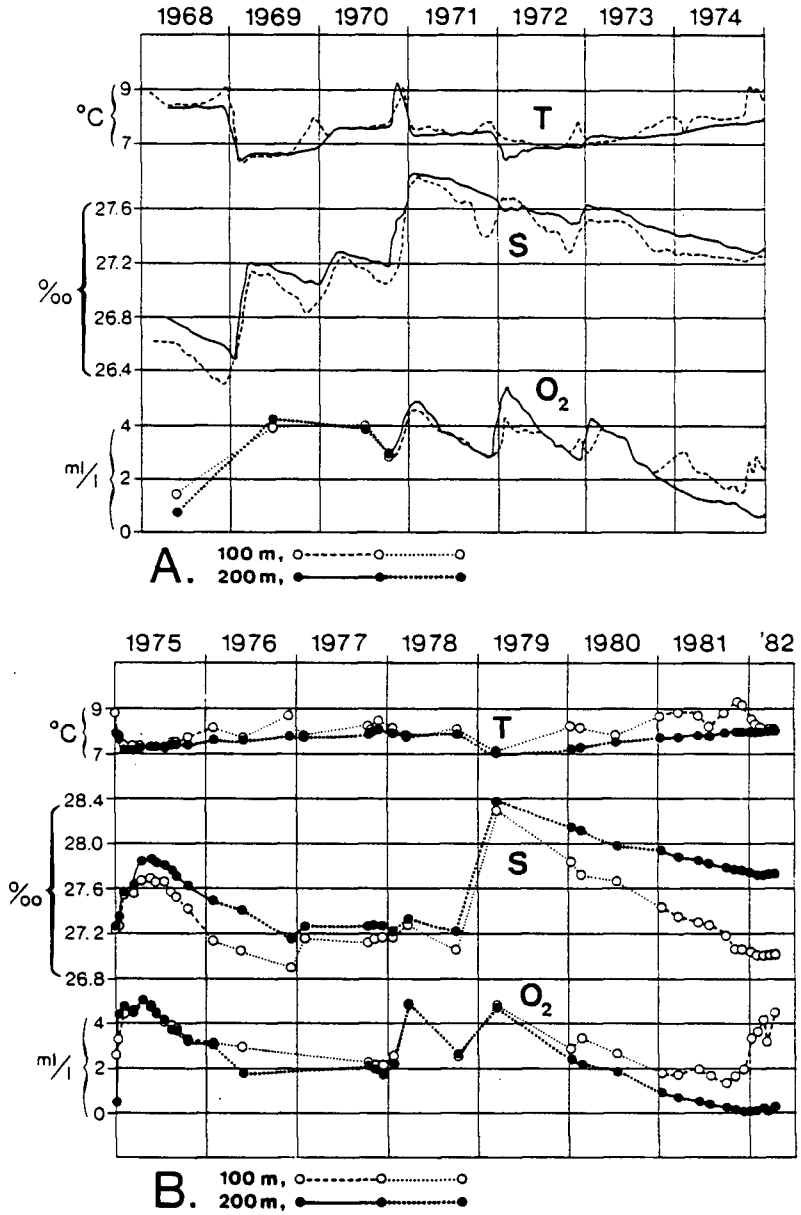

Figure 4 Long term and seasonal changes in Indian Arm. Temperature, salinity and dissolved oxygen at 100 *m* (dashed line) and 200 *m* (solid line) are plotted for 1968-1974 (A) and 1975-1982 (B). Dotted lines are drawn where data are sparse. (From Burling, 1982).

its effects upon the circulation. In their 1983 review of fjord oceanography, Farmer and Freeland also discuss some aspects of deepwater renewal. To place this study of renewal in Indian Arm in context, I shall now review some of the material covered in these two articles, as well as some more recent work.

The first work on deepwater exchange was carried out early in this century in the fjords of Norway (see Gade and Edwards, 1980). Anderson and Devol (1973) studied the renewal of an intermittently anoxic basin, Saanich Inlet, using nitrate budgets with which they were able to estimate the volume and rate of exchange. They estimated that 37 % of the exchange could take place within 12 days. Bell (1973) describes a renewal in Howe Sound where the exchange occurs when freshwater runoff is at a maximum and is augmented by down-inlet winds. Contrary to the observation of Bell, Edwards and Edelsten (1977) found that renewal in Loch Etive was associated with low freshwater runoff. They describe the inflow as a density current flow down a fairly steep slope. Lafond and Pickard (1975) observed replacement in Bute Inlet to occur during the late fall or early winter. With mean flow speeds of $1 - 5\ cm\,s^{-1}$, the exchange took place over many months. Cannon (1975) found that bottom water exchange in Puget Sound occurred in pulses of five days duration. The average speed over the sill ($6\,cm/s$) was enough to permit the complete exchange of all the water below sill depth during each of these five day periods. Geyer and Cannon (1982) discuss the effect of the sill length and tidal mixing on the density of water moving over the sill. Ebbesmeyer and Barnes (1980) describe the effect of tidal action over the sill in Puget Sound in generating a two-layer circulation in the basin. Because of this process, circulation is rapid at all depths throughout the year. Drinkwater and Osborn (1975) describe a similar situation in Rupert Inlet where tidal mixing over the sill controls the density of the inflowing water. Decreases of density in the basin were caused by the mixing of lower salinity water into the basin. Density values over the sill were observed to change during each tidal cycle.

Matthews (1981) observed the effects of freshwater runoff in an Alaskan fjord, Glacier Bay, where a tidewater glacier had a significant influence on the fjord circulation and

water properties. As in Indian Arm, all of the freshwater does not enter at a single point in Glacier Bay. Icebergs break off from the tidewater glacier and drift around the fjord until they have melted enough to escape over the sill. Matthews applied the non-linear internal tidal model of Blackford (1978) to support his contention that the internal tides were responsible for most of the mixing within the fjord.

These various studies show how the controlling physical processes are influenced by the local conditions. Freshwater runoff can either enhance or reduce deepwater exchange. The effects of tidal mixing over a sill depend upon the relative length of the sill and the tidal excursion. Also important in tidal mixing are the velocity of the flow over the sill and the sill depth. Wind forcing can be important both inside the fjord and outside, from where the exchange water must come. In assessing the controlling influences on the exchange cycle of a fjord each of these physical processes, as well as others, must be investigated. The most important ones for a specific fjord will depend upon the local conditions.

1.4 Circulation Of Indian Arm

There have been few current measurements made in Indian Arm. Indeed, there have been few measurements made of the estuarine circulation in any inlet. Rattray (1977), in a review of fjord circulation, identified two main deficiencies: (1) inadequate knowledge of the relevant physical processes and (2) difficulty of calculating and/or describing the actual circulation or transport.

Pickard and Rodgers (1959) made measurements of the circulation in Knight Inlet. They profiled currents at two stations every half-hour for three days. Using two profiling current meters (a Chesapeake Bay drag current meter and an Ekman current meter), they observed outflow in the upper part of the water column and inflow below. The oscillatory component was observed to be in phase from top to bottom. During a period of up-inlet winds, the flow was observed to be three-layered. The flow in the surface was then up-inlet with outflow at mid-depths and up-inlet flow just above the bottom. Although these observations appear to be in keeping with estuarine circulation theory, there is some

inconsistency. The zero-crossing for the current in the two-layered flow is at $40\,m$ while the pycnocline is at $10\,m$ depth. If the flow were simply a result of the freshwater pressure gradient then the outflow would be restricted to the upper $10\,m$. The observations suggest that the tide interacts strongly with the flow.

The measurements made by Davidson (1979) in Indian Arm were at a single depth, just above the bottom at the sill. The flow was observed to be primarily tidal in nature and was aligned with the bathymetry. Cross-channel flow was observed to be weak and transitory. The observations made during a period of deepwater renewal showed a fairly steady mean flow into the fjord.

1.5 The Barotropic and Baroclinic Tide

The main source of energy in most fjords is the barotropic tide. The total tidal amplitude in Indian Arm is about $3\,m$. Both the M_2 and K_1 constituents have surface elevations of about $1\,m$. For the M_2 barotropic tide the wavelength is about $2000\,km$; thus since the length of the fjord is only $22\,km$ barotropic resonance cannot occur. The tide propagates as a Kelvin wave, however, it can be treated as a plane wave since the channel width ($1\,km$) is much less than the external Rossby radius ($(gh)^{1/2}/f \approx 400\,km$). Rotation is therefore not important for the barotropic tide. The tide propagating in an inlet often behaves as a standing wave so that the phase of each constituent is a constant along the inlet. It is possible to think of this standing wave as the sum of two progressive waves, one travelling from the mouth, the other from the head of the inlet. The observed standing wave is the sum of the two waves.

Energy lost from the barotropic tide goes into three main sinks: the internal tide, high frequency internal waves and friction. Freeland and Farmer (1980) found the energy lost from the barotropic tide in Knight Inlet to be correlated with the stratification. The power withdrawn was greatest in the summer when the stratification increased and least in the winter when the stratification decreased. Such an observation does not necessarily imply that the nonlinear processes at the sill are the most important in determining the energy

loss since both the internal tide and the high frequency wave generation and propagation are controlled in part by the stratification. Freeland and Farmer (1980) estimated the loss from frictional drag in Knight Inlet accounted for no more than 3 % of the total loss.

The relative importance of these terms is still in dispute though it seems safe to say that friction is probably the smallest. Stacey (1984) and Stacey and Zedel (1986) describe the relative energy levels of the sinks for the barotropic tide in Observatory Inlet. They found that most of the energy lost from the M_2 barotropic tide went into the internal tide, and that relatively little energy was observed in the high frequency internal waves. This observation was found to hold even in the presence of extreme nonlinearity such as hydraulic discontinuities. These observations seem contrary to the results from Knight Inlet of Farmer and Smith (1978, 1980a, 1980b), who present acoustic images showing the nonlinearity of the flow over the Knight Inlet sill.

Some transfer of energy from the barotropic to the baroclinic tide occurs in all fjords. A number of models of varying complexity have been created to describe this transfer (Baines, 1973, 1974, 1982; Stigebrandt, 1976, 1980; and Blackford, 1978). The transfer occurs during the passage of a barotropic tide over a bump in a stratified fluid. The ability of sills to induce an internal tide was first observed by Zeilon (1912, 1934) as referenced in LeBlond and Mysak (1978).

Baines (1973, 1974, 1982), whose main interest has been the internal tide formed on the continental shelf, solved the equations of motion for the resulting internal modes by applying a forcing function. This forcing function represents the effect of the barotropic tide in a stratified fluid, using something close to the real topography. Stigebrandt (1976, 1980) used a simple linear model to estimate the energy flux away from the sill in an attempt to determine how much of the flux did work against the buoyancy forces. Blackford (1978) presents a non-linear model to predict the effect of the sill in a two-layer system. Because it is a non-linear solution, a significant amount of energy is predicted to be lost at twice the forcing frequency.

The question of what happens to the energy of the internal tide is still unresolved. It must all be dissipated eventually but it is not yet known how much energy goes into either heat or mixing. Stigebrandt (1976) was the first to suggest the breaking of internal waves as a mechanism to explain vertical mixing in a fjord. In a later paper, Stigebrandt (1979) presents data from Oslofjord supporting the theory that internal wave breaking was the main source of energy for mixing of the lower layer of a fjord. The fate of an internal wave propagating up the slope of an inlet is dependent upon the slope of the propagating waves relative to the bottom slope. Because the wave slope depends on the buoyancy frequency, which may be variable over a tidal cycle, particularly near the sill, the reflection characteristics of internal waves are difficult to determine. Wunsch (1968) found an analytical solution for internal wave propagation along a sloping bottom in a fluid with a constant buoyancy frequency. Further solutions were found by Manton and Mysak (1971) and Sandstrom (1976), using a functional equation method. The existence of a critical frequency for propagation was shown experimentally by Cacchione and Wunsch (1974). Using current meter data from several oceanic locations, Eriksen (1982) found reflections to occur over roughly the frequency range anticipated by linear theory.

If a significant amount of energy is reflected from the head of the fjord, and if the sill is shallow enough to reflect energy back into the fjord (Robinson, 1969), then internal resonance is possible. Lewis and Perkin (1982) describe a possible resonant response in an Arctic fjord where the M_2 tidal current velocity was observed to be weak except for short periods (a few days) of greatly increased current speed. Keeley (1984) observed a resonant response in Alice Arm, British Columbia. He Fourier analysed current data in 3-day segments and was able to detect a 180 degree phase shift in the M_2 response. Such a shift is characteristic of a system which moves through resonance.

The internal response of a fjord can also be described using a numerical model. Dunbar (1985) developed a numerical model of Indian Arm based upon the earlier work of Blumberg (1975) and Elliot (1976). An explicit finite difference scheme was used to solve the equations of motion for the velocity field. By tuning the friction term so that the

observed and calculated dissipation rates in Burrard Inlet were matched , the model gave good agreement between the observed and predicted tide. Both the barotropic and the baroclinic tide were modeled and compared with observations.

1.6 Aim of Thesis

In this work I will try to clarify a few of the unresolved problems in fjord research. Three main areas of interest are identified: deepwater exchange, the internal tide and the energy partition. As part of the deep water exchange problem, the estuarine circulation will be investigated. In each of these three areas there exist gaps which this study attempts to fill.

Much previous work has been done in Indian Arm with many biological studies of the fjord conducted (McHardy, 1961; Shan, 1962, Regan, 1968; Whitfield, 1974; Thomas, 1982). As part of each of these studies physical properties were also monitored, though not in a manner detailed enough to be relevant here except in that they provided data on the long term characteristics of the deepwater in Indian Arm. Some early physical oceanographic work was conducted in Burrard Inlet (Gilmartin, 1962; Waldichuk, 1965; Tabata, 1971). The study of Gilmartin was primarily descriptive. He outlined the main features of the Indian Arm system. Waldichuk concentrated on the Port Moody part of the system while Tabata was primarily interested in Burrard Inlet. The work of Davidson (1979) represents an extension of Gilmartin's earlier work. Davidson was able to provide more detailed observations of an exchange event; however, only limited current meter data were available. Burling (1982) provides a useful summary of the data collected but presents no new data. Dunbar (1985), in his numerical model, does make some use of current data but only for the purposes of model verification. A detailed analysis of the dynamics of the system together with an analysis of the data from the entire water column has not been done before and represents an original contribution.

Deepwater exchange events have been observed in many fjords, but detailed measurements of current and density over the entire water column have been rare. Geyer and

Cannon (1982) do provide detailed measurements of exchange in Puget Sound, but only over part of the water column. I will present measurements from the top to the bottom just inside the sill, and in the basin from near the bottom to near the top, during exchange of bottom water. These data will also be used to describe the estuarine circulation, which is fairly weak in a low-runoff fjord like Indian Arm. From the observations of the exchange, analysis of the forcing will be made to determine the effect of local conditions on the inflow.

The generation of the internal tide will be studied with a number of goals in mind. Dunbar's prediction (1985) of a resonant response will be investigated. This is particularly interesting in Indian Arm where the range of the K_1 tide equals that of the M_2. In most systems studied to date, either the K_1 has been ignored or the M_2 so overwhelms the K_1 so as to make it uninteresting. In these data it will be possible to see the difference in the internal response at the two frequencies. Modal fitting to the current meter and density data will be done to determine the energy fluxes in the different modes for the M_2 and K_1 internal tides.

The energy lost from the barotropic tide will be studied using tide gauge data and pressure data from the cyclesonde current meters. These data will be used to estimate the energy lost from each constituent of the tide. The current meter data will allow the determination of the relative energy, at different stations within the inlet, of both the internal tides and the high frequency internal waves. This analysis will seek to resolve the question of the relative energy lost to the various sinks of the barotropic tide. The energy lost through diffusion will be determined following an analysis of the CTD data to determine the vertical diffusion coefficient.

1.7 Outline of Thesis

The instrumentation used and the data collection process will be discussed in Chapter 2. Chapter 3 will contain a presentation of the current meter data. These data will illustrate the nature of the currents in the Indian Arm system and the effects of wind and freshwater forcing upon the currents. In Chapter 4 a detailed discussion of the deepwater exchange process will be given. Starting with the CTD data, a general description of the physical system will be given followed by presentation of the current meter and density data during a series of exchange events. The internal tide will be discussed in Chapter 5, where the varying internal response over the 1983/84 winter is explained as a resonant response of either the M_2 or the K_1 tide. The energy transfer from the barotropic tide will be discussed in detail in Chapter 6 in an attempt to determine the relative importance of the internal tide and the high frequency internal waves. Chapter 7 will present the conclusions together with suggestions for future work.

2. Instruments and Data Collection

2.1 Monthly Surveys

The data for this study were collected over a three year period. Three winters were studied: 1982/83, 1983/84 and 1984/85. Winters were chosen because this was the period when deepwater renewal had been observed to occur (Gilmartin, 1962; Davidson, 1979). Cruises were carried out approximately monthly during the study. On each cruise the current meters were serviced and a CTD survey of the inlet was conducted. Over the course of the study 19 cruises were run. Some results of these surveys are presented in data reports of the Department of Oceanography at the University of British Columbia (Data Report 51, 1982; 52, 1983; 53, 1984; 54, 1985).

The stations occupied during the study are indicated in *Figure 1.* Not all of the stations were occupied on every cruise, particularly in the first field season when a reduced number of stations were occupied. The usual routine was to pick up the current meters and service them while running the CTD survey. After completion of the CTD survey the current meters were redeployed. On cruises when spare current meters were available, it was possible to exchange the spares for the ones in the water, thereby saving time and making it possible to do the servicing of the recovered cyclesondes on land.

At selected CTD stations, usually about 5, water samples were taken using a rosette sampler. These samples were taken to allow measurement of dissolved oxygen and as a calibration check of the CTD. This calibration check was done by measuring the salinity of the water sample using a Guildline Autosal and comparing the result with that determined from the CTD measurement.

2.2 CTD Data

The CTD data were collected using a Guildline Model 8705 digital probe. The digital data were recorded at sea on audio cassette tapes. On land these data were transferred to 9-track computer tapes using an *LSI-11/03* microcomputer. All data processing following this stage was done on the University of British Columbia computer system.

Each CTD profile was despiked using a simple interpolation algorithm. This process removed about 30 % of the data points, a percentage greatly in excess of the number of spikes in the data. The remaining vertical resolution ($10\,cm$) was still more than sufficient, thus the data loss was not considered important. In order to reduce computer time the despiked data were averaged to give temperature, salinity and density at $1\,m$ intervals. This averaging technique is probably not good for the data near the surface, however, the effects of this very thin surface layer upon the analysis presented here are minimal. These averaged data were used in place of the original CTD data.

Although no calibration of the CTD probe was made during the study, regular field checks were carried out. Water samples, taken at standard depths, were analysed for salinity using a Guildline Autosal salinometer. The salinity measured by the CTD was compared with the water sample measurement. Any error in the temperature (T) or conductivity (C) sensor would lead to a discrepancy between the two measurements. It is possible that the T and C sensors could be off in such a manner that a single value of the salinity would appear to be correct but a series of checks would reveal the error. Based upon the original calibrations , and the calibration checks made through the study, the estimated accuracy of the CTD data is: $T \pm 0.005\,^{\circ}C$, $S \pm 0.005$, and $\sigma_t \pm 0.005$.

Samples for measurements of dissolved oxygen (DO_2) were taken at the same time as were the salinity samples. All of these samples were analysed within several hours of collection using the Winkler titration method (Parsons, Maita and Lalli, 1984). It is estimated that the concentration measurements are accurate to better than $0.1\,ml/l$.

2.3 Cyclesonde Data

The primary current meter used in this study was the cyclesonde (van Leer et al., 1974), a profiling current meter into which are built an inflatable bladder and a helium tank. A solenoid valve, under electronic command, is used to control the inflation and deflation of the bladder. When the bladder is inflated the instrument has a positive buoyancy of about $5.0N$, on deflation it has a similar negative buoyancy. Ballast can be added to, or removed from, the instrument to control the trim and to compensate for the density of the water in which the cyclesonde profiles.

Mooring techniques for cyclesondes are similar to those used for other current meters (see Berteaux, 1976). A single point mooring is used. The wire, held taut by subsurface buoyancy at the top, passes through a block in the body of the instrument. The cyclesonde travels up and down the plastic coated steel wire. Below the top of the mooring and above the bottom, a bumper is attached to the wire in order to limit the travel of the cyclesonde. The upper bumper was usually at about $15\,m$ below the surface; the lower bumper was usually at about $10\,m$ above the bottom.

Current speed in the cyclesonde is measured by two Savonius-like rotors, identical to those used in Aanderaa current meters except that they are mounted horizontally on the cyclesonde. This orientation allows the vertical motion of the instrument to be used to overcome the stall speed of the rotors. Temperature, conductivity, pressure, direction and pitch are also measured. Temperature is measured with a thermistor; conductivity with a four-electrode, glass cell; pressure with a strain gauge; direction with a magnetic compass and pitch with a clinometer. These data are recorded internally in binary format on an audio cassette tape.

Sampling time and profile rates for the instrument are set at the beginning of each deployment. For the current meters at the sill, profiles were made every 1 1/2 hours; in the basin the profile rate was 3 hours. The sampling interval, during which rotor revolutions were counted and at the end of which data were recorded on tape, was variable. The

cyclesonde at the sill was set to sample every minute for 30 minutes after the start of a profile and every five minutes for an hour after the end of the first half hour. The basin cyclesonde was set to sample every minute for 60 minutes after the start of a profile and every 5 minutes for 2 hours thereafter. These sampling rates were chosen to optimize the use of tape, which limited the amount of data that could be recorded. The data were transferred from the audio cassette tape to 9-track computer tape on an *LSI-11/03* microcomputer. Further processing of the data was carried out on the University of British Columbia computer system.

Quality control of the data was done in a number of ways. Bit shifting was the first step. If a scan line had a shifted bit, the entire line would be lost. By shifting one or more bits, it was sometimes possible to recover the original data. The cause of the original shift was probably poor recording or playback of the tape. The next step was to translate the raw data into engineering units with the application of the calibration fits. After this step, the file was scanned for spikes, which were plotted and inspected. Suspect data were replaced by linear interpolation. The majority of the spikes found could be attributed to the conductivity sensor. During periods of weak current the cell did not flush well. There was also a problem with the mismatch in the time response between the temperature ($\sim 100\,ms$) and the conductivity ($\sim 1\,s$) sensors.

The computation of the speed involves a number of stages. The raw speed is determined from the number of revolutions of the rotor over the sampling period. Because there are two rotors it is possible to compare the two independent measurements of the speed. If the two rotor speeds did not differ by more than $3\,cm/s$ the average of the two was used, otherwise the higher value was taken with the assumption being that the slower rotor was sticking.

Early in 1984, the method of measuring the rotor rotation and the speed calculation method were changed. Initially, a magnetic follower and optical sensor were used. Because of difficulties with this system, a magnetic reed switch was installed. It was observed,

however, that occasional bursts of very high speed were recorded with this new system. These bursts were clearly not present in the water so the speed algorithm was changed. For all instruments with the reed switch, if the speed difference was greater than $3\,cm\,s^{-1}$, the lower speed was selected. It is suspected that magnetic particles in the water, which are attracted to the rotor magnets, interfere with the magnetic field of the rotor magnets sufficiently to cause the reed switch to count occasionally too high.

The horizontal speed was calculated from the total speed. The vertical component of the velocity, on account of the rising or falling of the instrument, was calculated from the change in pressure. The square of the vertical speed was subtracted from the square of the total speed to give the square of the horizontal speed. At this point two assumptions were made: first, that the vertical component of the water velocity was small enough to be ignored. This assumption was reasonable for small amplitude long, linear internal waves but not for the short, non-linear internal waves at the sill. The second assumption was that the heading varied linearly from the start to the end of the minute.

A plot of the total speed versus the vertical speed was made and an adjustment made so that the rotor speed would almost always be greater than, or equal to, the vertical speed. The stall speed for the rotor was expected to be higher when mounted in the horizontal position than when in the vertical position, as on the Aanderaa current meter, since friction at the horizontal bearing can lead to an increase in the stall speed. The new stall speed, generally $1-2\,cm\,s^{-1}$ higher, was used to recompute, first the total speed and then the horizontal speed.

Calibrations of the cyclesondes were done before and after each field season. Only temperature and conductivity were calibrated routinely. The pressure, direction and tilt sensors were checked occasionally to ensure that their calibrations were stable. CTD profiles, taken at the start and end of each deployment, were used to check the calibrations. The temperature calibration was found to be consistently reliable and needed no correction. The conductivity calibration done in the laboratory was found to differ from that done

at sea using the CTD data. In the laboratory only part of the instrument could be submerged during the calibration run whereas in the sea the rest of the body probably caused the shift in the conductivity measurement. The CTD data were used to correct for this observed conductivity shift. If the shift differed from the start to the end of the deployment, a linear interpolation was used to apply the correction. Because the CTD cast was not always simultaneous with a cyclesonde profile, the comparison between the two was sometimes difficult.

Adjustments to the conductivity and hence salinity data were also made. The conductivity sensor was found to have an offset when in five minute sampling compared to the values in one minute sampling. Because the difference appeared to be approximately constant, it was possible to correct for the change. A least squares linear fit before and after the change in sampling rate was done, and an offset was computed from the difference between the two fits. This offset was then applied to the data.

The data were interpolated to standard depths after the data reduction. Data were interpolated to fixed $10\,m$ intervals, although the data from the top and bottom bumper were also saved. The estimated accuracies of the various data are given in *Table 1.*

Table 1
Cyclesonde Accuracy

Sensor	*Unit*	*Accuracy*	*Precision*
Speed	$cm\,s^{-1}$	$3\,if < 5cm\,s^{-1}$ $2\,if > 5\,cm\,s^{-1}$	Threshold $\sim 2-3\,cm\,s^{-1}$
Direction	°	3	0.3
Temperature	$°C$	0.02	0.005
Salinity	‰	0.1	0.03
Density	$kg\,m^{-3}$	0.1	0.03

Aanderaa current meters were also used during the study. In December 1984, four meters were moored at the sill in the place of a cyclesonde. Salinity results from these four current meters were corrected using the CTD profiles taken at the start and end of each deployment. The second deployment of Aanderaa current meters , from January to March 1985, was from a Geodyne surface float. Because these current meters were placed

in the surface layer (from 3 to 15 m below the surface), corrections using the CTD data could not be made. Estimated accuracies for the Aanderaa current meter data are given in *Table 2*.

Table 2
Aanderaa Current Meter Accuracy

	Unit	*Accuracy*	*Precision*
Speed	$cm\,s^{-1}$	$3\,if < 5\,cm\,s^{-1}$ $2\,if > 5\,cm\,s^{-1}$	Threshold $\sim 2\,cm\,s^{-1}$
Direction	°	5	0.3
Temperature	$°C$	0.1	0.01
Salinity	‰	0.1	0.05
Density	$kg\,m^{-3}$	0.1	0.05

2.4 Other Data

Wind Data

Data from other sources were obtained to supplement those collected during the study. Wind data from Environment Canada were obtained for three stations near Indian Arm: Point Atkinson, Vancouver Airport and Sand Heads (see *Figure 5*). Quality control of these data was carried out by Environment Canada. Two attempts were made at direct measurements of the wind in Indian Arm. An anemometer was placed on the dock at Buntzen Power station (see *Figure 1*) in the winter of 1983/84, but the effects of the local topography on the wind produced such interference as to make the data useless. Another anemometer was placed on the Geodyne surface buoy, during its deployment in January to March 1985; unfortunately, instrument failure occurred and no useful data were recovered.

Tidal Height Data

Sea surface elevation data, at hourly intervals, were obtained from the Canadian Hydrographic Service. The data were collected at Point Atkinson and Vancouver Harbour (see *Figure 1*). Quality control of these data was done by the Canadian Hydrographic Service.

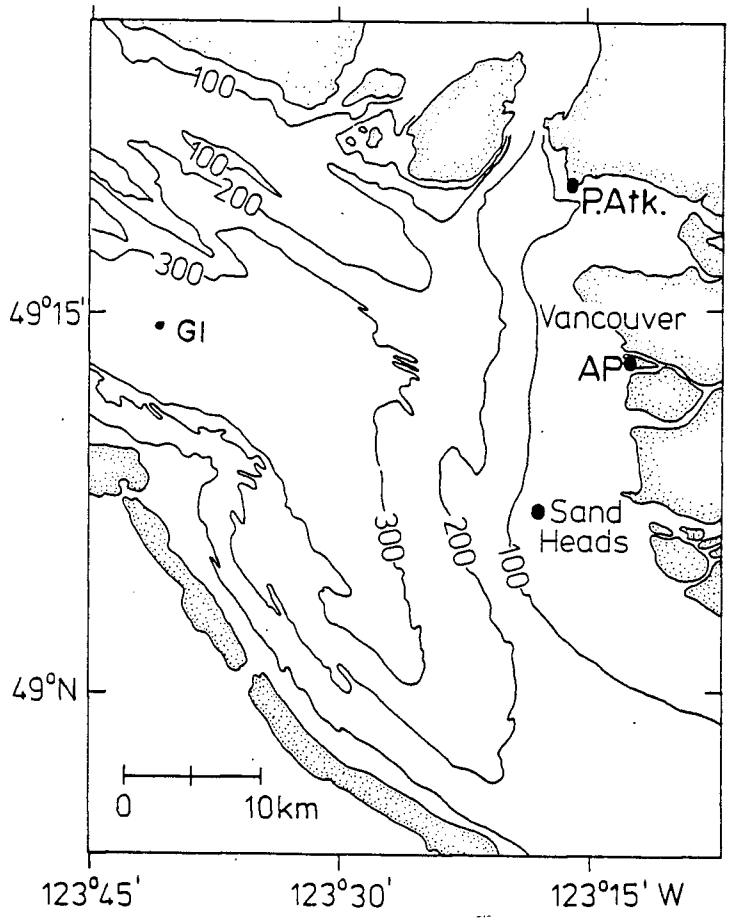

Figure 5 Map of the Strait of Georgia showing anemometer locations. The three anemometer stations are Sand Heads, Vancouver Airport (AP) and Point Atkinson (P.Atk.). Salinity and density data from station G1 in the Strait are discussed in Chapter 4.

Freshwater Inflow

Freshwater inflow data were obtained from two sources. British Columbia Hydro provided daily average outflow figures from the two hydroelectric generating stations in Indian Arm. Information on flow of the Capilano River was obtained from gauge data collected by the Water Survey of Canada.

3. Current Meter Records

3.1 Mooring Location

The five mooring locations are shown in *Figure 1.* The sill and the basin mooring positions (C1 and C3) were chosen to monitor the exchange of the fjord and to provide data on the internal tide. The position of the cove mooring (CS) was chosen to be close to the sill mooring in order to allow comparison with the data from there. These comparisons were used to generate bottom to top current meter profiles. The two extra basin moorings, Twin Islands (C2) and Buntzen (C4), were deployed to add to the data set used to measure the propagation of the internal tide. Their positions were chosen to aid in the separation of the internal modes in the basin.

The cross-channel profiles at each of the five mooring locations are shown in *Figures 6 and 7.* Because they are all plotted at the same scale it is possible to compare the cross-sectional area between moorings. All of the moorings, except CS, were placed in the centre of the channel. The surface mooring at CS could not be placed in the centre because of possible interference from shipping. For this same reason, the subsurface float at each of the cyclesonde moorings was placed at about 15 m below the surface. The characteristics of each of the mooring sites are given in *Table 3.*

Table 3
Characteristics of current meter locations

Mooring	*Depth* (m)	*Cross-section* (km^2)	*Area up-inlet* (km^2)
C1	70	0.02937	24.33
CS	69	0.04978	24.07
C2	166	0.1145	15.68
C3	190	0.1132	14.56
C4	217	0.1568	12.37

The purpose of the surface mooring at station CS was to collect data from the bottom to the surface. Four Aanderaa current meters were used at the top (3, 7, 11 and 15 m below the surface), suspended from a Geodyne surface float. Less than 200 m away, along the same isobath, a cyclesonde mooring with a subsurface float was deployed. These two

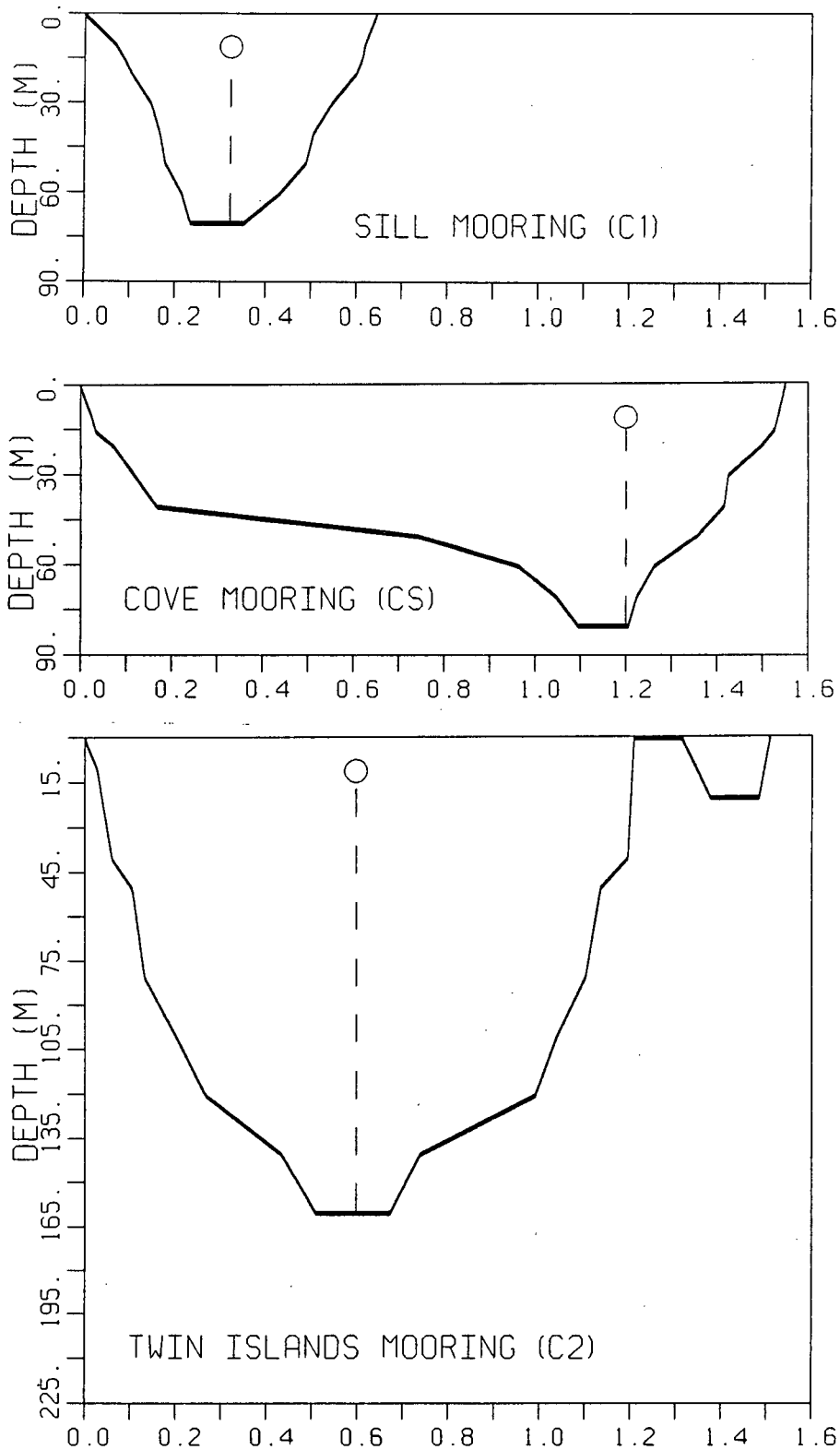

Figure 6 Cross-channel profiles at mooring locations C1, C2 and CS. The cross-channel distances are given in *km* .

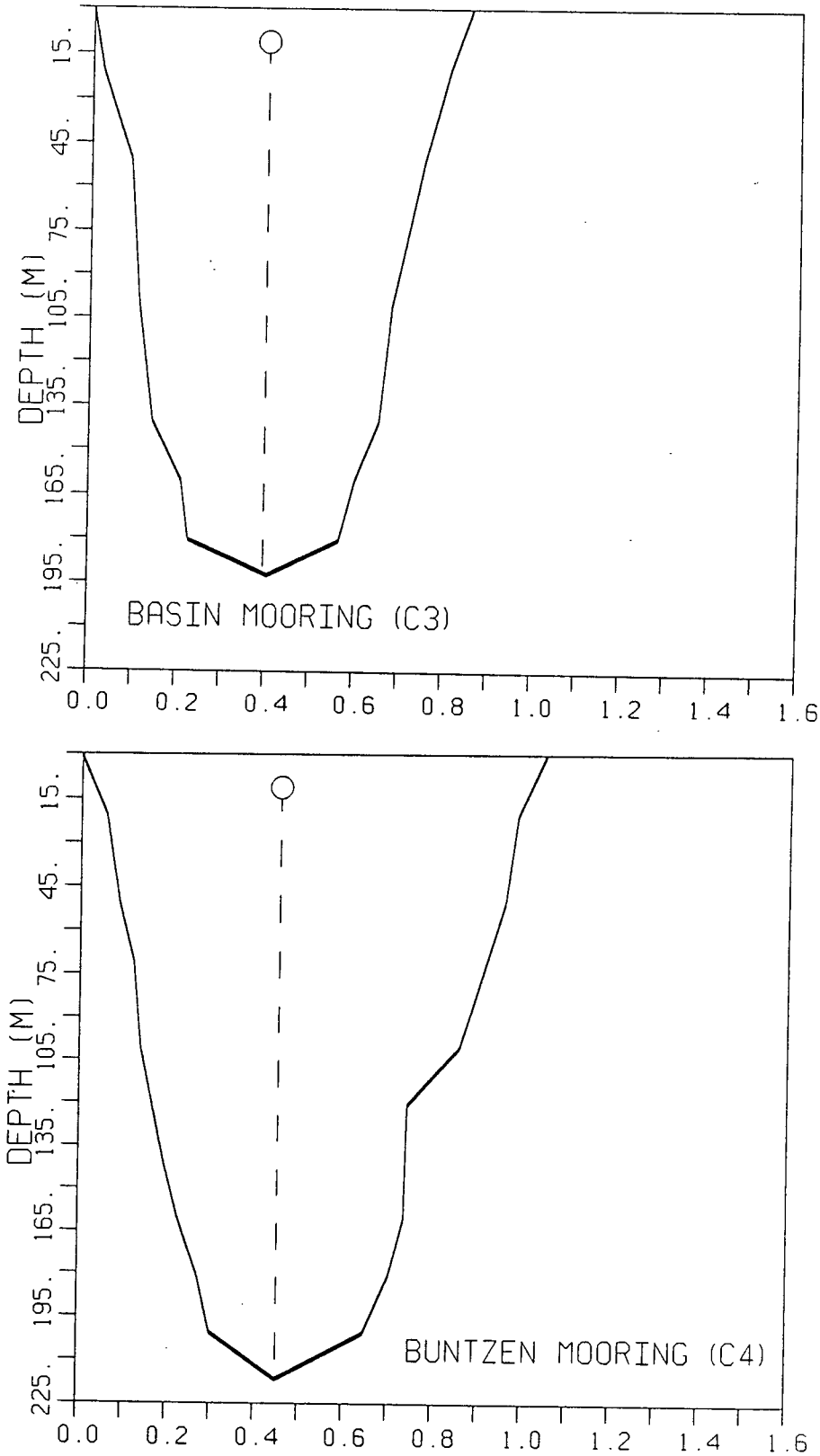

Figure 7 Cross-channel profiles at mooring locations C3 and C4. The cross channel distances are given in *km* .

moorings were placed closely enough together that they can be considered to be at the same point, that is, at station CS. Problems with the Aanderaa current meter when placed in the surface zone have been documented by comparisons made with other current meters (Halpern, Pillsbury and Smith, 1973; Saunders, 1976; Woodward, Huggett and Thomson, 1986). In spite of the recognized problems with the instrument, it is expected that they will perform well at the surface mooring site because of the low wind speeds and limited fetch there. No corrections for the possible effects of wave motion upon the current meter data were applied.

In order to generate a current profile from top to bottom, a comparison was made between cyclesonde data from station C1 and cyclesonde data at station CS. The results of this regression analysis were applied to the Aanderaa current meter data from CS, which were then combined with the cyclesonde data from station C1 to give a consistent bottom to surface current measurement. As a check on the regression analysis, the ratio of the cross-sectional areas between stations C1 and CS was found. By continuity, this ratio should determine the ratio of the along-channel current velocities at the two stations. Approximate agreement ($\sim$ 20% maximum error) between the two methods was obtained.

In all, 29 months of cyclesonde data were collected over the three winters. Each deployment was usually for one month's duration. In *Table 4* the deployment times for all of the current meter moorings are given. One current meter mooring in December 1984 had no cyclesonde attached; 4 Aanderaa current meters were used instead. The times in *Table 4* are given in day-month-year and in Julian days. To obtain the day from the start of the previous year (as is done in some plots) add 365 for 1982/83 and 1983/84, add 366 for 1984/85.

Table 4
Table of Cyclesonde Deployments

Station	*Cyclesonde #*	*Start* (d:m:yr)	*End* (d:m:yr)	*Start* (Julian day)	*End* (Julian day)
1982/83					
C1	20	07–12–82	05–01–83	341	370
C1	67	05–01–83	02–02–83	5	33
C1	20	02–02–83	05–03–83	33	64
C1	67	06–03–83	29–03–83	65	88
C3	22	07–12–82	05–01–83	341	70
C3	21	05–01–83	01–02–83	5	32
C3	22	02–02–83	05–03–83	33	64
C3	21	07–03–83	28–03–83	66	87
1983/84					
C1	21	08–11–83	10–12–83	312	344
C1	67	12–12–83	10–01–84	346	375
C1	21	10–01–84	07–02–84	10	38
C1	22	07–02-84	07–03–84	38	66
C3	22	08–11–83	10–12–83	312	344
C3	22	12–12–83	31–12–83	346	365
C3	67	10–01–84	07–02–84	10	38
C3	20	07–02–84	23–02–84	38	54
1984/85					
C1	Aanderaa	12–12–84	16–01–85	347	382
C1	67	16–01–85	17–02–85	16	48
C1	67	21–02–85	25–03–85	52	84
C1	67	27–03–85	22–04–85	86	112
C1	67	24–04–85	23–05–85	114	143
CS	Aanderaa	16–01–85	27–03–85	16	86
C3	22	12–12–84	12–01–85	347	378
C3	21	16–01–85	17–02–85	16	48
C3	21	27–03–85	22–04–85	86	112
C3	21	24–04–85	22–05–85	114	142
CS	22	16–01–85	17–02–85	16	48
C4	22	21–02–85	22–03–85	52	81
C4	20	27–03–85	22–04–85	86	112
C4	20	24–04–85	23–05–85	114	143
C2	22	24–04–85	23–05–85	114	143

3.2 Current Meter Data

Flow in a narrow channel, where the forcing is at one end, is expected to be aligned with the main axis of the channel. Wind forcing and topographic irregularities will generate cross-channel motion but in most fjords, which can be approximated as channels, the energy in this flow will be small compared to that in the along-channel flow. After preliminary analysis of the current meter data, the direction of the flow at each station was determined.

The rotation required was found by minimizing the variance in the cross channel direction. *Table 5* shows the results of this analysis and compares the results of this work with the rotation estimated from the bottom bathymetry at each station. The error in the estimated bathymetry alignment at each of the stations is about ± 5 degrees.

Table 5
Rotation from variance analysis and bathymetry alignment

Mooring	*Variance Analysis* (°)	*Bathymetry Alignment* (°)
C1	26.0	27
CS	26.0	27
C2	34.0	41
C3	26.0	23
C4	354-15	357

The variance analysis produced different results each month for the rotation at station C4. The variation in the analysis at this station occurs because there is a bend in the fjord at station C4 which makes it difficult to place the mooring on precisely the same bottom contour during deployment. Such variation was not observed at other stations. The variation of the rotation with depth was not always insignificant, at times reaching $10 - 15\,°$. The rotations presented in *Table 5* are depth averaged results. As expected, the flow is along the isobaths.

Figure 8 shows the along-channel and cross-channel current at the sill station C1 in January 1984. The data at the top and the bottom in these plots are from the cyclesonde when it was at either the top or the bottom bumper. Because the position of the bumper below the surface changes with time, no fixed depth can be given for the top and bottom bumper. The top bumper is about $14 - 20\,m$ below the surface and the bottom bumper is about $0 - 6\,m$ below the deepest depth plotted. The data at the $10\,m$ depth intervals were found by linear interpolation so that data points separated by only $10\,m$ in depth in the plot are not entirely independent of one another.

In *Figure 8* it can be seen that the cross channel energy, following rotation of the data, was very weak. For this reason, after rotation only the along-channel current was used in

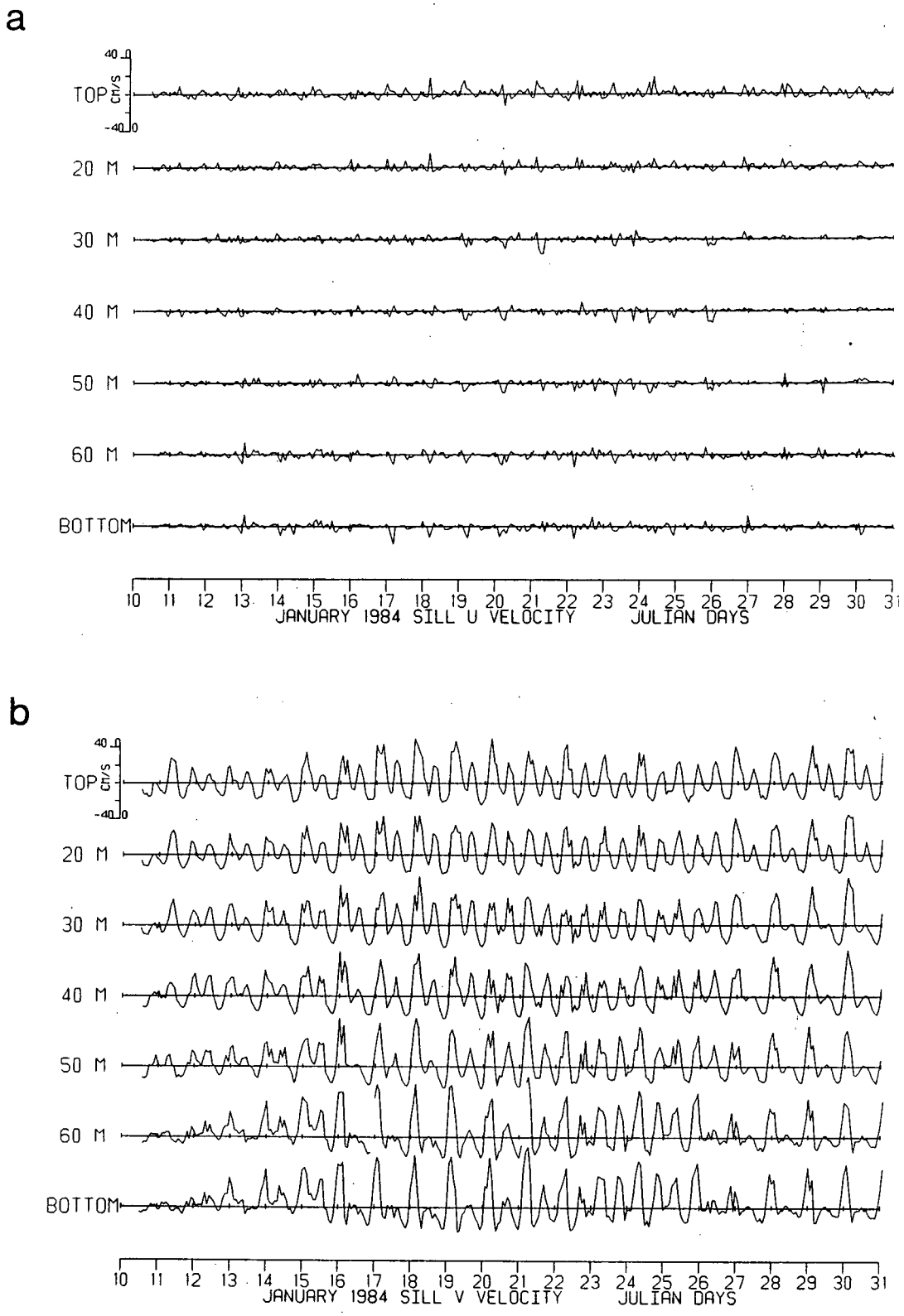

Figure 8 Cross-channel (a) and along-channel (b) velocity components at the sill (C1) in January 1984.

this study. This reduction greatly simplifies the computer analysis since the vector analysis can be replaced by scalar analysis.

3.3 Spectral Analysis

Autospectra of the current at the sill and in the basin are shown in *Figure 9* . The dominant energy is in the diurnal and semi-diurnal bands, specifically at the M_2 and K_1 frequencies. The M_2 constituent is more energetic than the K_1. The M_2 in January 1985 shows baroclinicity in that the amplitude increases towards the bottom. The baroclinic nature of the M_2 can also be seen in the basin record (*Figure 9b*) . The effects of friction are evident in the peak at 0.012 cycles per hour (*CPH*). The interaction of the M_2 and K_1 gives rise to this peak known as the MK_3. As one might expect for a non-linear interaction term, which is strongly influenced by friction, there is a strong depth dependency with the largest amplitude of the MK_3 near the bottom.

Just below the Nyquist frequency ($\frac{1}{2\Delta t}$ where Δt is the sampling interval) in *Figure 9* is the M_4 constituent, the first harmonic of the M_2 tide. Splitting of the M_2 peak, and a side-band on the K_1, also appear in the basin plot of *Figure 9.* A closer inspection of *Figure 9*a reveals a peak at about 0.06 *CPH* which has no corresponding astronomical forcing frequency. The cause for these features is the Doppler shifting of the internal tide. A Doppler shift will occur when the propagating wave moves in a flow relative to the observer. As we shall see later, in January 1985 there was a mean flow in the basin near the bottom for periods of days. It was this mean flow which caused the Doppler shift.

The expected frequency to be observed as a result of a Doppler shift is given by:

$$f_o = f_s \frac{C + V_w}{C} \quad . \tag{3.1}$$

Here f_o is the observed frequency, f_s– the source frequency, C– the wave speed and V_w– the water speed. *Table 6* gives the results of the Doppler shift analysis for the internal tide. The internal wave speed for the first mode is calculated using modal analysis (LeBlond and Mysak, 1980), which will be discussed later in Chapter 5. Modal analysis is a technique for finding the vertical form of the waves which will propagate horizontally in a physical

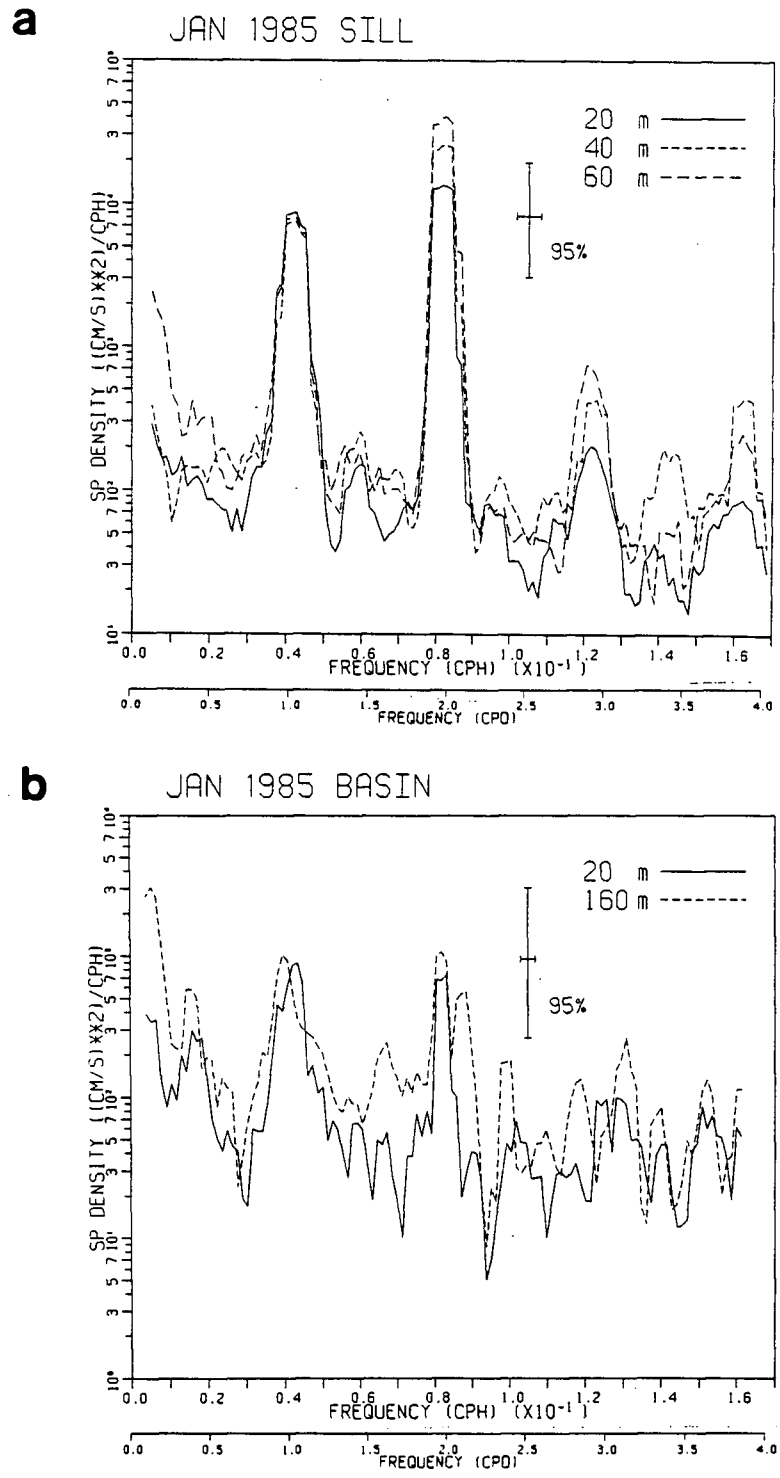

Figure 9 Autospectra of the along-channel current at the sill (a) and in the basin (b) in January 1985. The frequency is plotted with two scales; one in cycles per hour (CPH), and one in cycles per day (CPD).

Table 6
Doppler Shift Analysis

		$f_s(CPH)$	C (ms^{-1})	V_w	f_o
Sill	K_1	0.041	0.48	0.20	0.058
Sill	M_2	0.080	0.48	0.20	0.12
Basin	K_1	0.041	0.48	0.05	0.045
Basin	M_2	0.080	0.48	0.05	0.092

system.

The expected peak at 0.058 *CPH* can be seen in *Figure 9* while the peak at 0.12 *CPH* is masked by the MK_3. The MK_3 peak was removed using harmonic analysis, after which there was still a peak at 0.12 *CPH*, the Doppler shifted M_2 internal tide. In the basin record, the Doppler shifted peaks are not so clearly visible because of the weaker mean flow there. The observed splitting in the basin is consistent, however, with the Doppler shift analysis.

3.4 Harmonic Analysis

Harmonic analysis was used to analyse the tidal height and current meter data. The purpose of the analysis is to compute the Greenwich phase lags and the amplitudes of the chosen constituents. The technique involves the least squares fitting of a series of harmonic functions to the data (Godin, 1972). The program used in this study, developed by M. Foreman (1977, 1979), has the advantage that the data need not be at equally spaced time intervals. It is possible to choose a number of combinations of constituents when doing harmonic analysis. The guidelines of Foreman (1977) were used to select the constituents for this analysis. The requirement for separation used was the Rayleigh criterion which states that the record length must be greater than the reciprocal of the difference between the frequencies. The nine constituents used in this study are given in *Table 7*.

The components chosen represent the largest set that could be reasonably used with the data. The M_4 which arises from the interaction of the M_2 with itself and the MK_3 which arises from the interaction of the M_2 and K_1, could just be analysed. In the basin, where the sampling period was 3 hours, no signal with a period of less than twice this

Table 7
Tidal constituents used in the harmonic analysis

Tidal Harmonic	*Darwin name*	*Period (hours)*	*Frequency (CPH)*
Shallow water constituents			
	M_4	6.21	0.1610
	MK_3	8.18	0.1223
Semi-diurnal			
Principal solar	S_2	12.00	0.08333
Principal lunar	M_2	12.42	0.08051
Longer lunar elliptic	N_2	12.66	0.07899
Diurnal			
Soli-lunar declinational	K_1	23.93	0.04178
Main lunar	O_1	25.82	0.03973
Main solar	P_1	24.07	0.04154
Long period			
Luni-solar fortnightly	MSf	354.4	0.002822
Mean	Z_0	∞	0

period can be resolved without aliasing. For separation of the M_2 and S_2, the record must be as long as the beat frequency (theMSf – 14.76 days). The N_2 constituent could just be determined from thirty day records. Any record shorter than 30 days was not analysed for the N_2 constituent. The K_1 and O_1 are well separated for any record longer than 13 days. Resolution of the P_1 requires a record longer than 178 days so for this constituent inference was used. The tidal station at Vancouver Harbour was used to fix the phase and amplitude of the P_1 constituent relative to the K_1 (as suggested by Foreman, 1979). Some error may be involved in the assumption that the ratio P_1/K_1 is the same for tidal height and current data; however, since the K_1 result is the primary source of interest, the second order effect of such an error should be negligible.

3.5 Wind Forcing

Other than the tide, the wind and freshwater flow are the main sources of energy for this system. In this section I shall discuss the winds, which are generally weak throughout the area. *Figure 10* shows that winds greater than 6 $m\,s^{-1}$ are present less than 10 % of the time. It should also be noted that there are more periods of very calm conditions, with winds less than $2\,ms^{-1}$, in the winter than in the summer.

Wind data were obtained from three stations: Vancouver Airport, Point Atkinson and Sand Heads (see *Figure 5*). Analysis was done to determine the direction of the maximum energy in the same manner as for the current meter data. For Vancouver Airport and Point Atkinson the winds are predominantly E/W while at Sand Heads they were aligned along 300/120 degrees. Topographic steering of the winds is clearly important at the two land stations. Approximately 80 % of the variance is along the E/W line at Vancouver Airport. Over 95 % of the variance was along the same line at Point Atkinson. The relative energy levels at Point Atkinson were greater than at Vancouver Airport. In spite of its greater separation from Indian Arm, the Vancouver Airport data were used because they were of better quality than the Point Atkinson data. The autospectral plot of the wind at the airport (see *Figure 11*) shows that there is more energy in the E/W direction than in the N/S. Two large peaks in the E/W spectrum occur, one at 1 day and the other at 2.5 days, with increasing energy at longer periods. The most significant peak in the N/S spectrum is also at 1 day.

The effects of wind forcing upon the system were investigated using correlation analysis. Cross-spectra of wind and current time series were obtained to look for the response to the wind forcing. Empirical orthogonal functions (EOF) (Lumley, 1970, for example) were used to represent the current time series at each station. These EOF's represent the eigenvectors of the covariance matrix of current components as a function of depth. The eigenvectors are the basis set for the velocity, where the velocity is a function of depth. The eigenvectors can be used to transform the velocity time series into a new time series

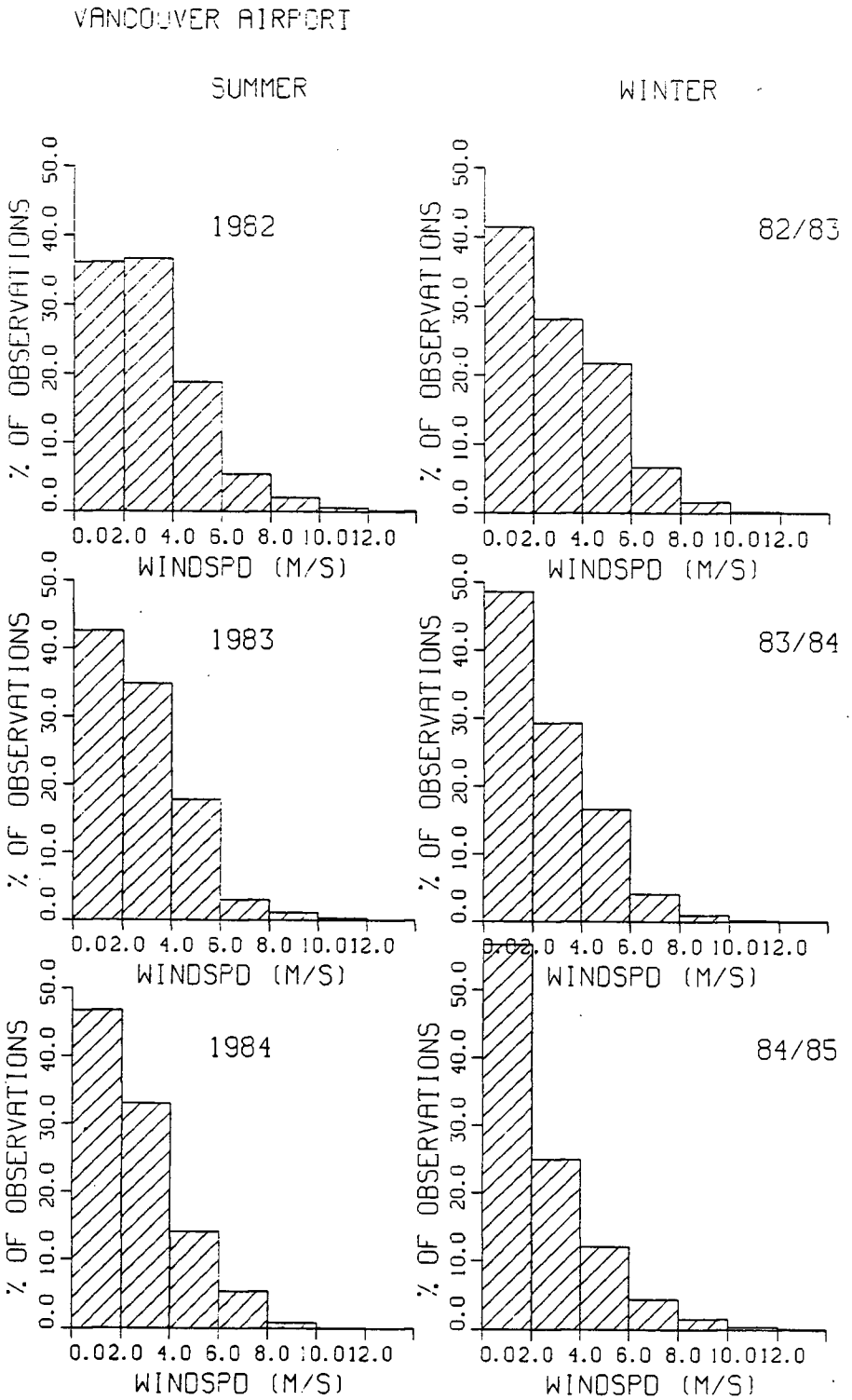

Figure 10 Wind statistics for Vancouver Airport from 1982 to 1985. The summer period is from April to September; the winter period is from October to March.

which will be uncorrelated; that is orthogonal. Thus:

$$\varsigma_i(t) = \sum_j e_{ij} V_j(t) \quad , \tag{3.2}$$

where e_{ij} is the jth element of the ith eigenvector and $V_j(t)$ is the velocity time series (with the tide and the mean removed) at the jth depth. The original time series $V_j(t)$ can be recovered by reversing the procedure;

$$V_j(t) = \sum_i e_{ij} \varsigma_i(t) \quad . \tag{3.3}$$

In Indian Arm, indeed in the ocean in general, one expects that a major portion of the total variance to be explained by the lowest few terms in equation (3.3). The fraction of the total variance of the jth velocity time series explained by the ith empirical orthogonal function is given by

$$\frac{Var(\varsigma_i)\, e_{ij}{}^2}{Var(V_j)} \quad . \tag{3.4}$$

If the empirical orthogonal functions explain more than 20 % of the variance (or have a cross-correlation of 0.4) then they are significant to the 95 % level. The first and second functions, the only two to be discussed in any detail, always explain greater than 20 % of the variance.

The structure of the first four EOF's for 1985 are shown in *Figure 12.* The tides and the mean were removed from the current meter data before performing the EOF analysis. The first mode accounted for over 40 % of the variance, the second mode for over 20 %. The first three modes accounted for about 80 % of the total variance. It is not surprising that the first four EOF's at the sill so closely resemble the structure of the first four modes from modal analysis (see sections 10 and 15 of LeBlond and Mysak, 1978). The EOF's in the basin do not look like the expected modes because the time series is dominated by the exchange event. The first EOF in the basin (*Figure 12*) shows inflow at the bottom and outflow in the upper layer.

The cross-spectra of the two lowest modes at the sill and the Vancouver Airport wind (*Figure 13*) show no coherence at low frequencies, less than 1 cycle per day (CPD). There

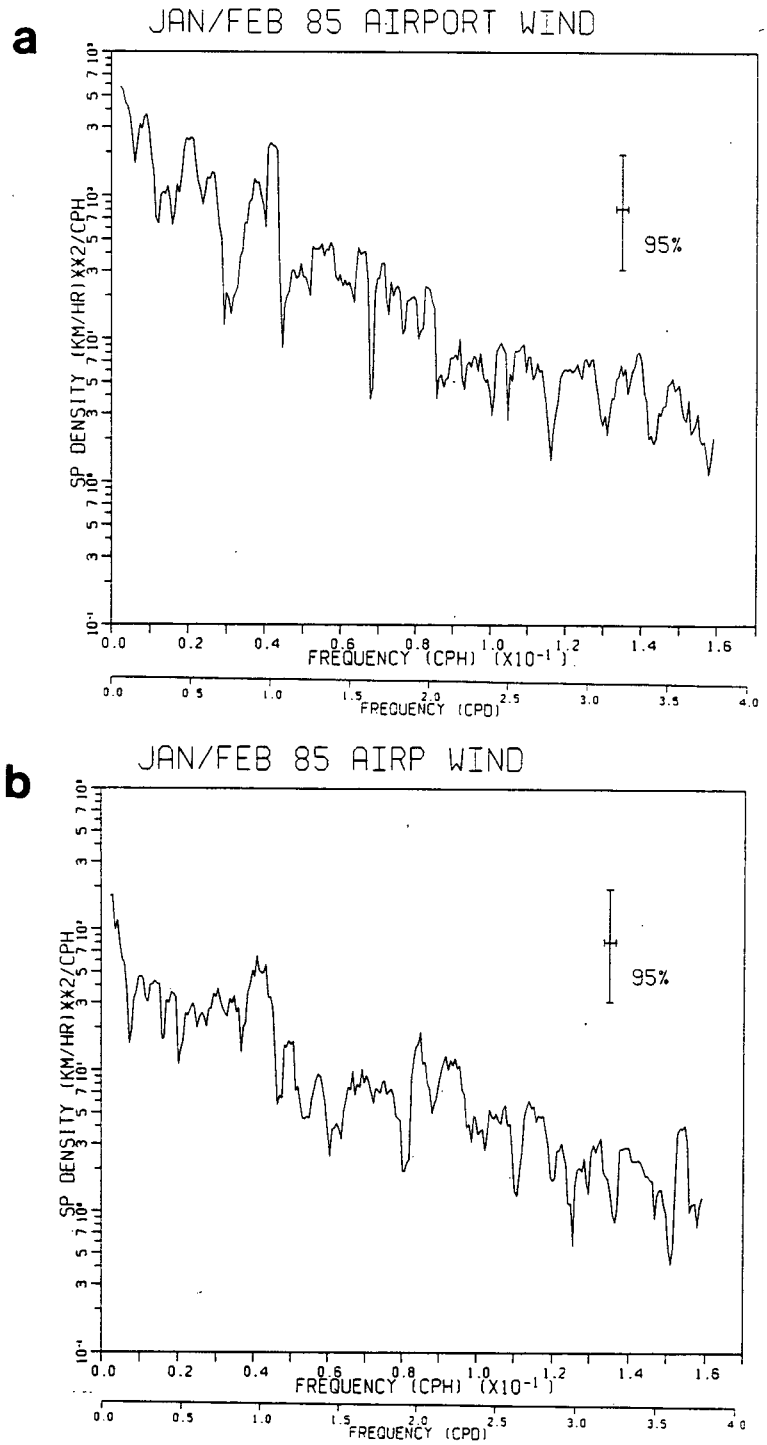

Figure 11 Autospectra of the E/W (a) and N/S (b) component of the wind velocity at Vancouver Airport in Jan-Feb 1985.

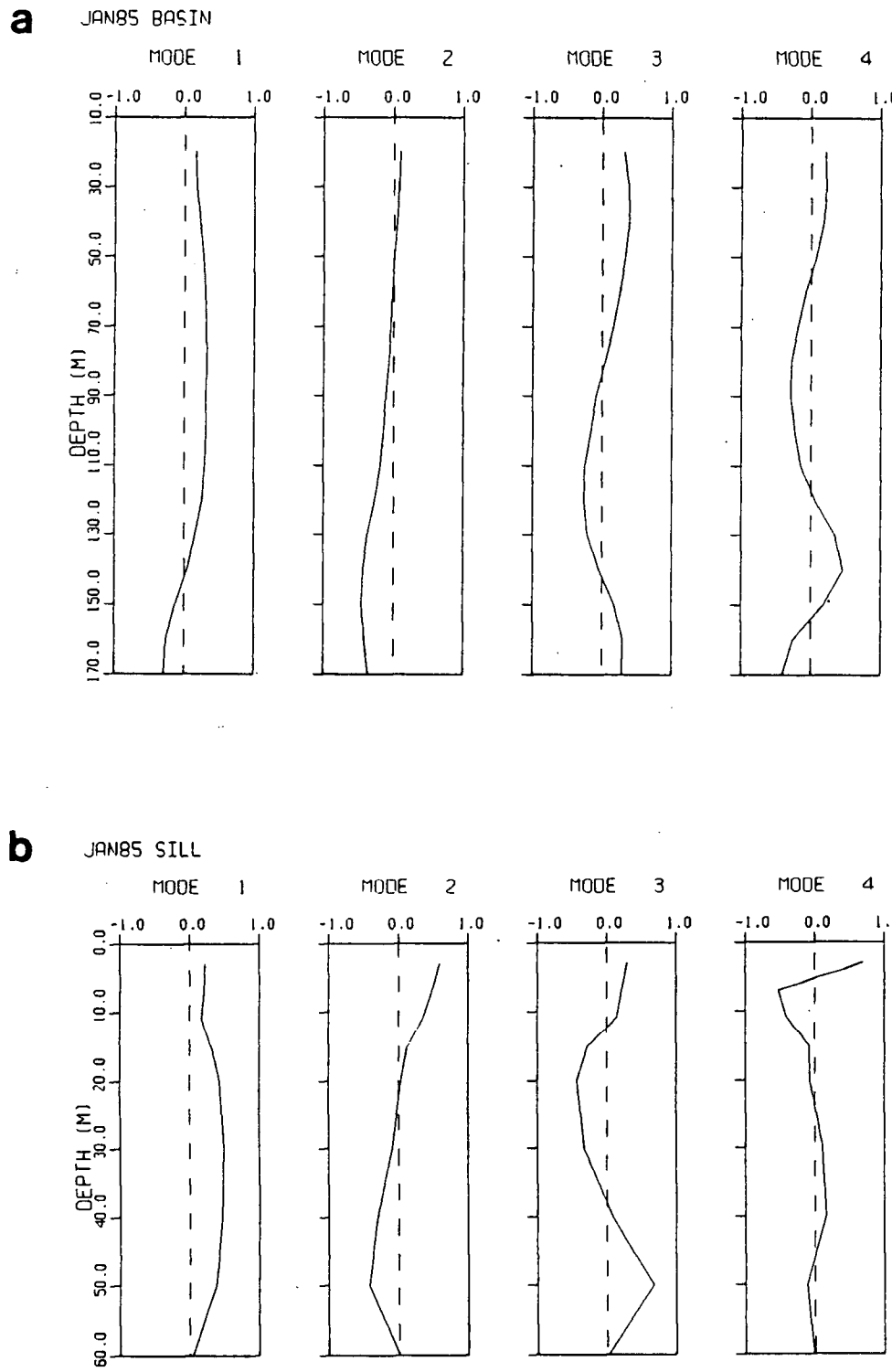

Figure 12 Empirical orthogonal functions in the basin (a) and at the sill (b) in January 1985. Current data at the sill were at 3, 7, 11, 15, 20, 30, 40 , 50 and 60 *m* below the surface. Current data in the basin were at 10 *m* depth intervals between 20 and 170 *m* depth.

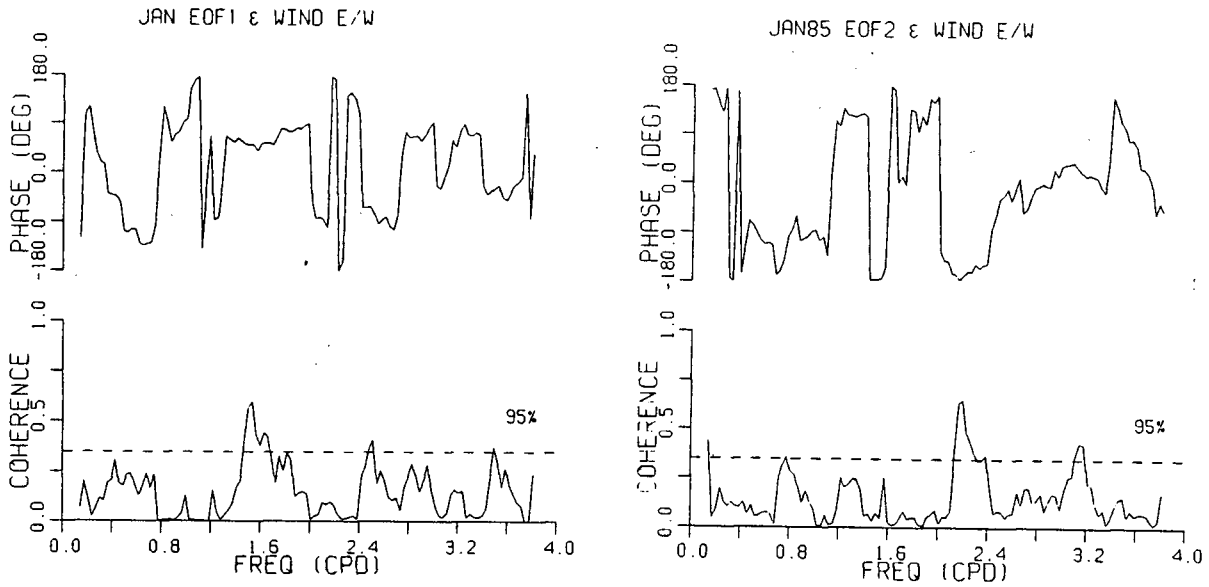

Figure 13 Cross-spectra between the two lowest EOF's at the sill and the E/W wind at the airport in January 1985. A positive phase means that the current leads the wind. The 95 % confidence level is indicated by the dashed line.

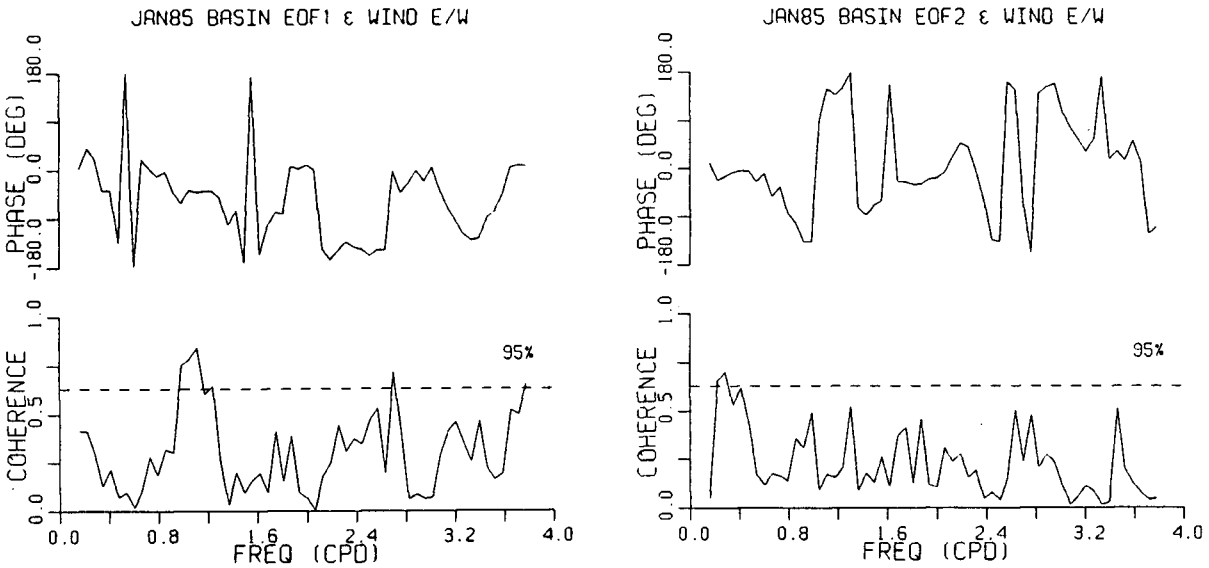

Figure 14 Cross-spectra between the two lowest mode EOF's in the basin and the E/W wind at the airport in January 1985. A positive phase means that the current leads the wind. The 95 % confidence level is indicated by the dashed line.

is coherence at the sill for the first mode EOF at about 1.6 CPD (or about 16 hours). In the basin (*Figure 14*), the lowest frequency coherence was found at about 1 CPD (or 24 hours). Some energy is found in both the wind and the current data at these frequencies, though it is difficult to be sure about their significance. The very high coherence, greater than 0.8, makes it difficult to disbelieve in a physical transfer of energy at these frequencies; however, the lack of a distinct peak in the autospectra of the currents means that not all that much energy is going into water motion. The wind speeds are so low that the weak forcing leads to a weak response.

3.6 Freshwater Forcing

Although the freshwater inflow into Indian Arm is not as great as in other British Columbia fjords (Gilmartin, 1962; Pickard, 1975; Davidson, 1979), its effects upon the water properties of the fjord can be detected. Gilmartin (1962) described the effects from the outflow of the Buntzen power plant on the salinity of the surface layer. Davidson (1979) described changes in the surface water properties of English Bay, just outside Burrard Inlet. In this section I shall discuss the effects of the changing inflow on the surface salinity and circulation at the sill.

Table 8
Freshwater inflow into Indian Arm

Source	*Drainage Area* (km^2)	*Mean Annual Discharge* ($m^3 s^{-1}$)	*% of total*
Buntzen Power Plant	–	23.0^a	55
Indian River	121	11.8^b	28
Peripheral streams	44	4.3^c	10
Direct Precipitation	32	3.0^d	7
Total	–	42.1	100

Note:

a - Davidson (1979)

b - mean of 1914-21 streamflow data (Dunbar, 1985)

c - based on drainage area ratio, from Dunbar (1985)

d - based on 3.0 m annual precipitation (Hay and Oke, 1976)

Table 8 describes the sources of freshwater for Indian Arm. The outflow from the

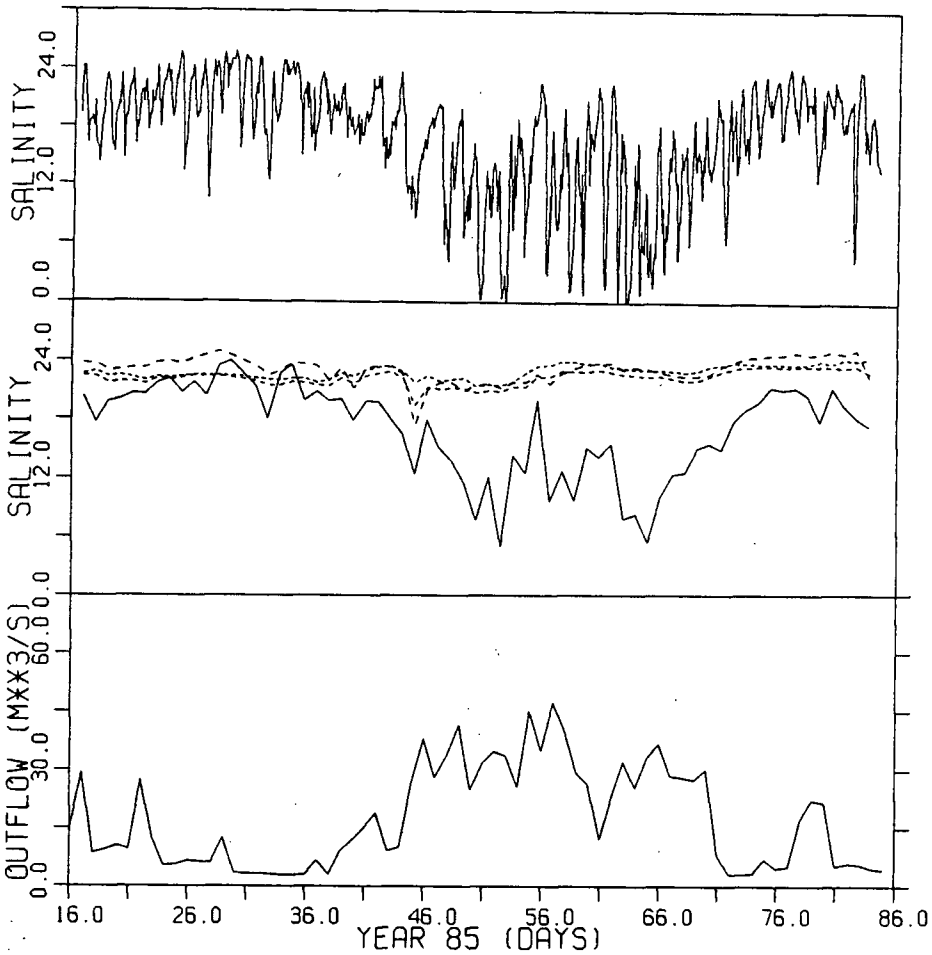

Figure 15 Salinity and freshwater runoff at the sill. The top panel shows the hourly salinity at $3\,m$ below the surface in 1985. The middle panel shows the 24 hour averaged salinity at $3\,m$ (solid line) and 7, 11 and $15\,m$ (dashed lines) below the surface. The bottom panel shows the freshwater inflow during the period. The time is given in Julian days from the start of 1985.

Indian Arm River is estimated by using data which were obtained for the Capilano River. This procedure was necessary because there are no flow measurements made on the Indian Arm River, though there once were. Dunbar (1985) performed a regression of Indian Arm River runoff (R_I) against the Capilano River runoff (R_C), $R_I = a + bR_C$, for an eight year period (1914-1921) when both rivers were gauged. He found $a \simeq 1.5$ and $b \simeq 0.5$. These values were used to estimate the Indian Arm River runoff. The effects of peripheral streams and direct precipitation were ignored in computing the freshwater input, since the relative nature of the signal is of more interest than its absolute value.

The surface salinity at the sill in the early winter of 1985 is shown in *Figure 15.* The salinity at 3 m is reduced to near zero on the ebb tide. The conductivity cell does not work well at these salinities , however, so the result is probably not too accurate. The sharp decrease in salinity at 3 m at day 40 is a result of the increased freshwater inflow starting at the same time. This inflow does not significantly influence the salinity at depths of 7 m or greater except at the very beginning of the event.

Lagged correlations were attempted between the daily freshwater input and the daily averaged salinity and the daily averaged current at various depths. Significant negative correlations were found between the inflow and the salinity at different depths. The maximum correlations were found at a lag of 1 day. The degree of correlation decreased from a value of about 0.7 at 3 m to insignificant correlations at 11 m (less than 0.4). The correlation with current was less strong, no significant correlation was found between the freshwater and lagged currents.

The correlation between the freshwater input and the salinity in the surface layer was expected. The difficulty in determining any lag between the freshwater input and the salinity is probably because of the long sampling interval of the inflow data (1 day). The lack of correlation between the freshwater input and the current indicates that although the freshwater flow influences the stratification no strong circulation is set up as result. The residual flows at the sill are driven by the tide and the exchange of water into and out of Indian Arm.

4. The Deepwater Exchange Cycle

4.1 Introduction

Deepwater exchange has been observed in many fjords. The sill of the fjord blocks access to the deep water of the system thus leading to potentially stagnant conditions. In fact such conditions are not isolated to fjords. Okuda (1981) presents observations of renewal events in the Gulf of Cariaco in Venezuela. This gulf has a deep basin with a sill, and the water in the basin undergoes periodic renewals and stagnations. Because of the narrowness of fjords the flow is often approximately two-dimensional, which simplifies the observation and modeling of the exchange.

The renewal process in Indian Arm has been previously described (Gilmartin, 1962; Davidson, 1979; Burling, 1982 and Dunbar, 1985). These studies were discussed in the introduction. The general nature of the exchange process was documented, primarily using CTD or bottle data, without discussing the importance of the flow through Burrard Inlet or the response within Indian Arm itself. Here, with the addition of the cyclesonde current meter data, obtained during an exchange cycle I shall discuss deepwater exchange in Indian Arm in greater detail.

I present first the CTD data collected from Burrard Inlet and Indian Arm during 1984/85. These data describe the general water properties of the system and also show the changes which occur in the basin during an exchange period. These data will also allow comparison with earlier measurements. Current meter data are then presented, together with an analysis of the forcing and response of the system. The nature of the flow through Burrard Inlet is described and a dynamical explanation of the exchange cycle is provided.

4.2 CTD Data

Exchange in Indian Arm has been observed to be a quasi-periodic event (Burling, 1982). Data covering the period 1975 to 1986 are presented in *Figure 16*. The data from mid-1982 on were collected during this study, data from before that time were taken from data reports of the Department of Oceanography, University of British Columbia.

Figure 16 shows that bottom water renewal has taken place only four times in the last 11 years: 1974/75, 1977/78, 1978/79 and 1984/85. Generally such renewals are indicated by an increase in the density of the water at 200 m depth. The bottom water density increased very little in 1977/78; although there was a noticeable increase in the bottom water oxygen concentration. Exchange of water at mid-depths can be observed in several years in which bottom water exchange did not occur. In such years, the density of water reaching the sill is sufficient to displace water at mid-depths in the fjord but not great enough to drive out the bottom water.

The saw-toothed nature of the curves in *Figure 16* is a feature common to many British Columbia fjords (Pickard, 1975). Following an exchange event, the water properties show a steady decrease (or increase, depending on the sign of the vertical gradient) until the next exchange. These variations are more irregular at 100 m because of mid-depth exchanges. Advection of new water disrupts the diffusion process. The regular nature of the diffusion at 200 m indicates that the energy which goes into this process is a constant which does not change seasonally. Further discussion of vertical diffusion is put off until Chapter 6, where energy sources in the fjord will be discussed.

Even though 7 years may pass between exchange events, the water in Indian Arm has never been observed to become anoxic, although before the 1981/82 winter the mid-depth exchange the bottom water was nearly anoxic. *Figure 16* illustrates part of the reason for this failure to go anoxic. The more frequent mid-depth inflows of high oxygen water reform the vertical oxygen gradient in the basin, thereby providing a source of oxygen for the deep water. This oxygen diffuses down the oxygen gradient helping to keep the bottom water

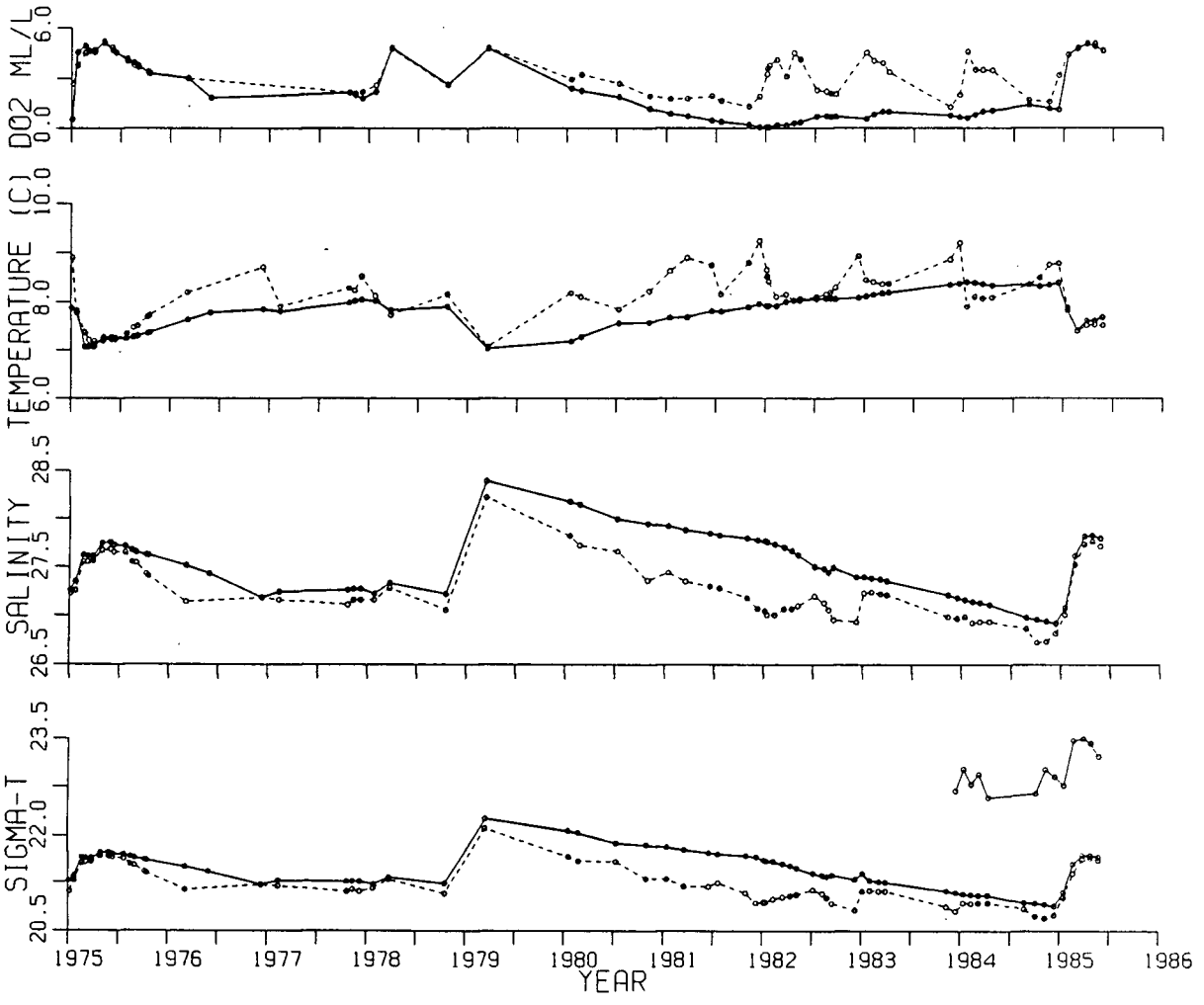

Figure 16 Time series of DO_2, temperature, salinity and σ_t at station 23 in Indian Arm. The solid line represents data at 200 m , the dashed line data at 100 m. The extra density data at the end are from 40 m depth at station 75 outside First Narrows.

from becoming anoxic. That the bottom water should ever be anoxic cannot be ruled out. If the mid-depth inflow of early 1982 had not occurred, the basin would probably have become anoxic sometime in the spring of 1982. It would appear from this observation that the basin can go for about 3 years, without exchange at depths greater than $75 - 100\,m$, before anoxic water will form.

Contour plots of the temperature, salinity and σ_t for the Indian Arm system for April 1984 are presented in *Figure 17*. This survey was the last complete CTD transect prior to the 1984/85 winter exchange. A comparison of the salinity and density plots indicates that the density is controlled almost entirely by the salinity. For this reason, only the density plots will be discussed for most of the remaining CTD data. The temperature plots will be retained because of their value in illuminating some aspects of the fjord exchange cycle.

The weak stratification in the inlet is a constant feature. Even just before exchange events the stratification in Indian Arm is weak. The brackish surface layer does not extend below $10\,m$ and is often less than $5\,m$ in depth. The length and shallow nature of Burrard Inlet leads to effective mixing of the water which makes it into Indian Arm. Thus, even though there is strong stratification at station 75, outside Burrard Inlet, there is only weak stratification inside Indian Arm.

The effects of vertical mixing are particularly apparent at Second Narrows, between stations 54 and 56. In April 1984 (*Figure 17*), the 21.0 isopycnal drops from just below $15\,m$ to the bottom at about $40\,m$. Although it is at the two outside sills, First and Second Narrows, where most of the mixing occurs, mixing of the water throughout all of Burrard Inlet will take place. It is expected, however, that such isolated features in these CTD surveys will depend upon the phase of the tide. Because no time series of data were collected in the Burrard Inlet part of the system, the detailed nature of the flow there will not be discussed.

The temperature in Burrard Inlet and Indian Arm, contoured in *Figure 17a*, exhibits a small range in the vertical. In the basin the vertical range is about $1\,^{\circ}C$. Through Burrard

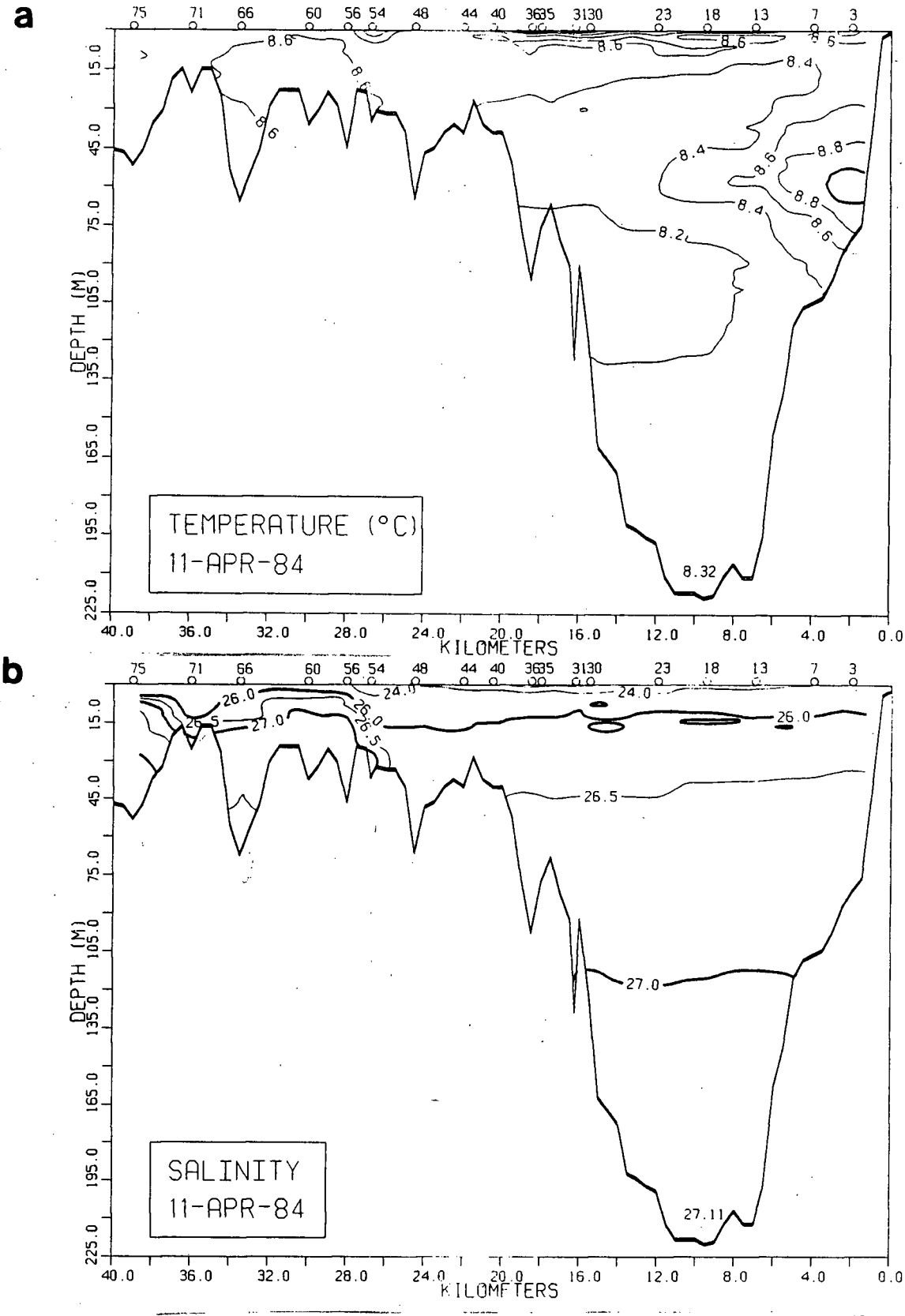

Figure 17 Temperature (a), salinity (b) and σ_t (c) in Indian Arm on 11-April-1984. The station numbers on the top correspond to those in *Figure 1*. The number at the bottom of station 18 indicates the conditions at that depth. 11-April-84 is Julian day 102.

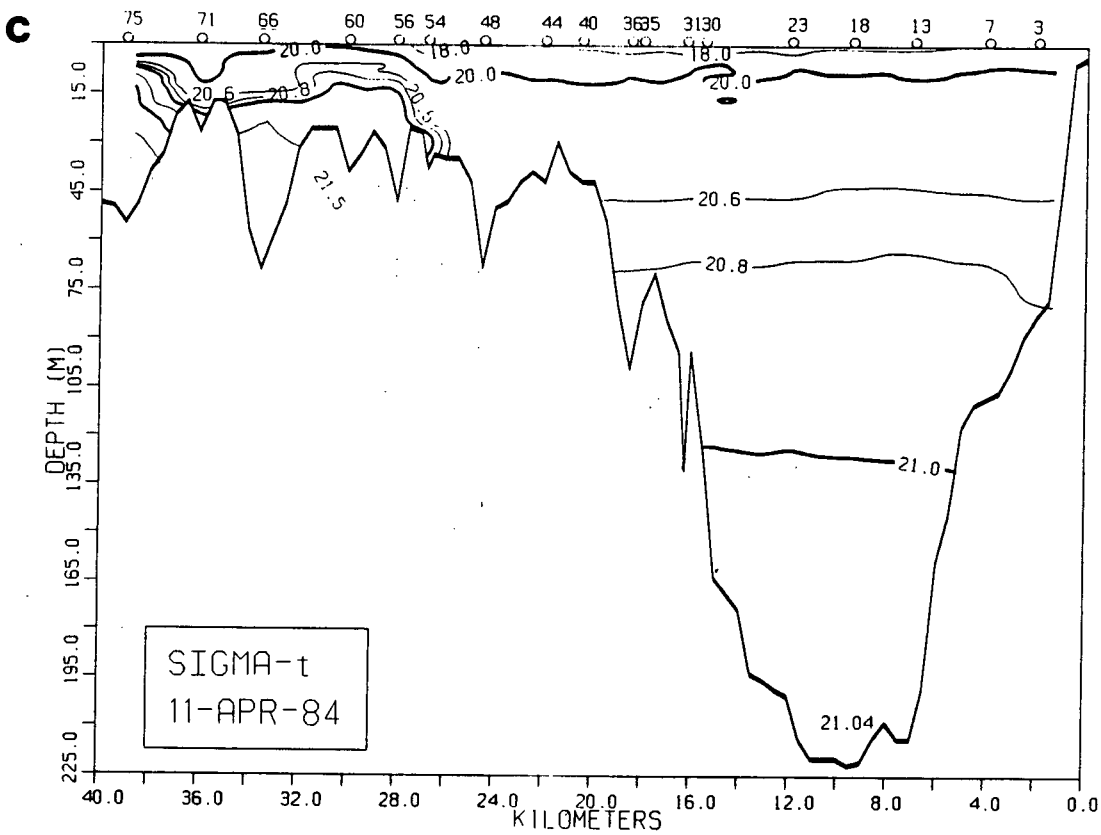

Figure 17 (continued) (c) Sigma-t in Indian Arm on 11-April-1984.

Inlet it is much less, often appearing vertically homogeneous in temperature. A remnant of warm water at the end of the fjord can be seen at about 50 m depth. This lens takes its form because of the winter-cooling/summer-heating cycle which controls the vertical gradient of temperature in the upper waters of the inlet.

By October (*Figure 18*), the effects of summer heating on the temperature distribution can be seen. Bottom water exchange has not yet taken place (see *Figure 16*) but some mid-depth inflow has occurred. The depression of the 20.8 isopycnal from 70 to 120 m has taken place. By November (see *Figure 19*) this isopycnal has been depressed still further near the sill . In the basin there is also a noticeable slope of the isopycnals towards the sill. A mid-water temperature maximum has developed in the basin as a result of the start of winter cooling. The water density, 20.4 at station 48, is still less than that of the bottom water in the basin though there is a strong horizontal density gradient across the sill. This gradient indicates that dense water could be advected towards station 48 on the flood tide.

The changes from November to December (see *Figure 20*) 1984 indicate that a significant inflow has occurred. The 20.6 isopycnal has risen from about 100 m in November to less than 75 m in December. The mid-depth temperature maximum has risen dramatically and has decreased in temperature. At the same time it is clear that bottom water exchange has not taken place. *Figure 16* shows that the bottom water DO_2 was still decreasing through December 1984. The concentration at 100 m had gone up, however, supporting the view that a mid-depth inflow of cold water took place.

From October to November the density just outside the Indian Arm sill, at the bottom of station 48, increased steadily. In October it was 20.2, in November 20.4 and in December 20.6. By December the difference in σ_t between this water and the bottom water was only 0.28.

The January 1985 data (see *Figure 21*) show that the bottom water density had increased by 0.20 while the temperature decreased by 0.57 $^\circ C$. The density plot shows an unstable tongue of water extending over the sill into Indian Arm. The 21.0 isopycnal at

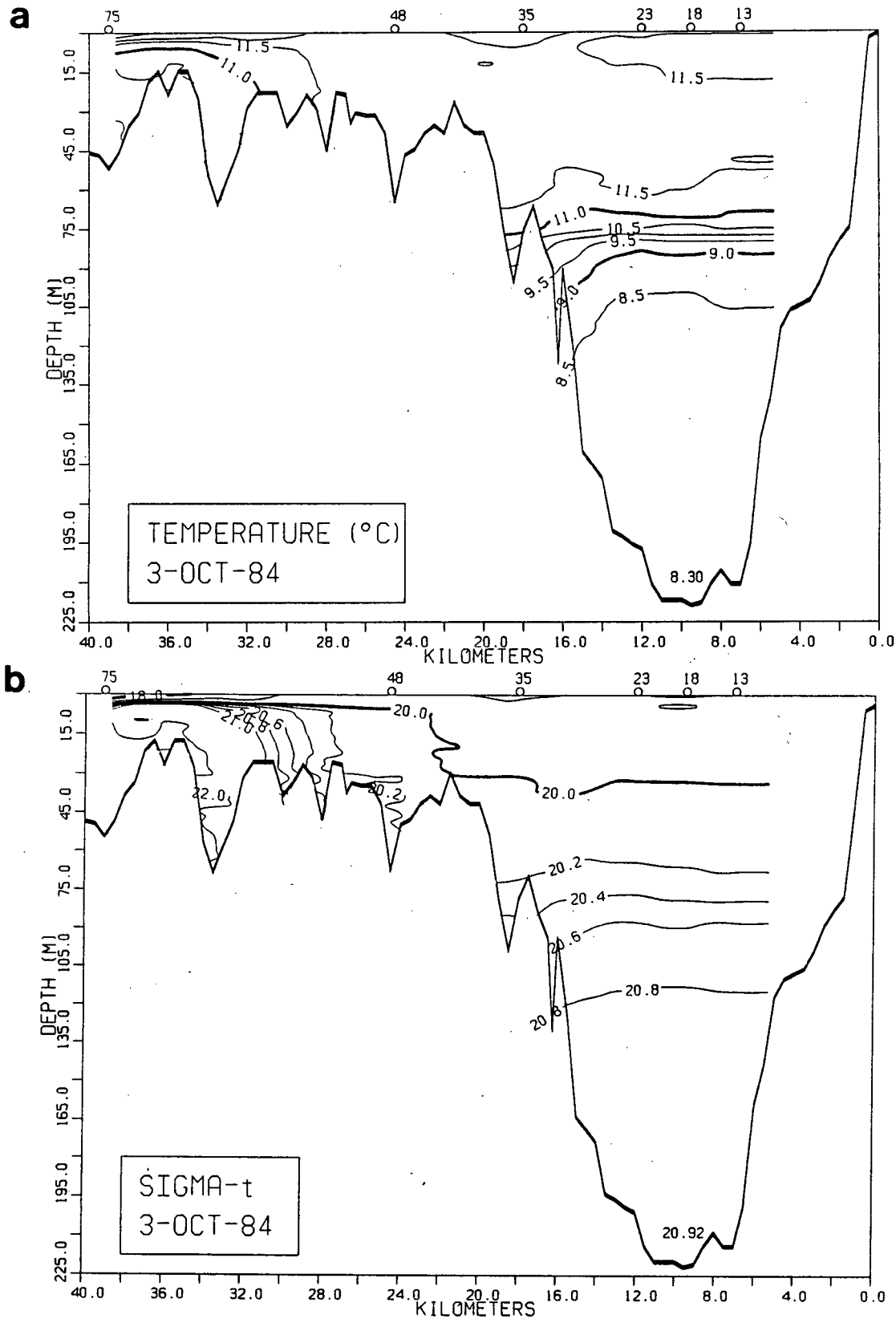

Figure 18 Temperature and σ_t in Indian Arm on 3-October-1984. Note that only six stations were occupied. 3-October-84 is Julian day 277.

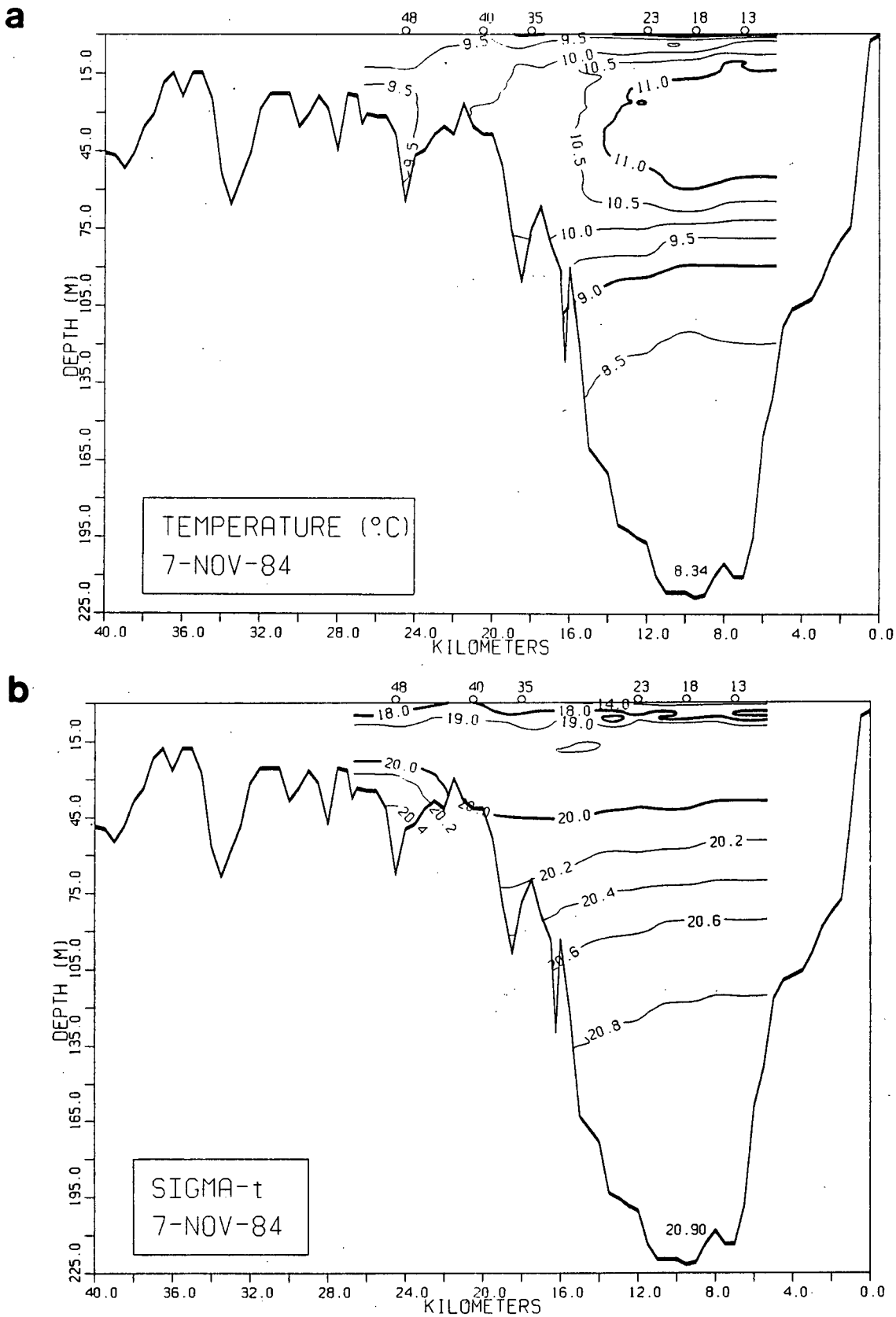

Figure 19 Temperature and σ_t in Indian Arm on 7-November-1984 (Julian day 312).

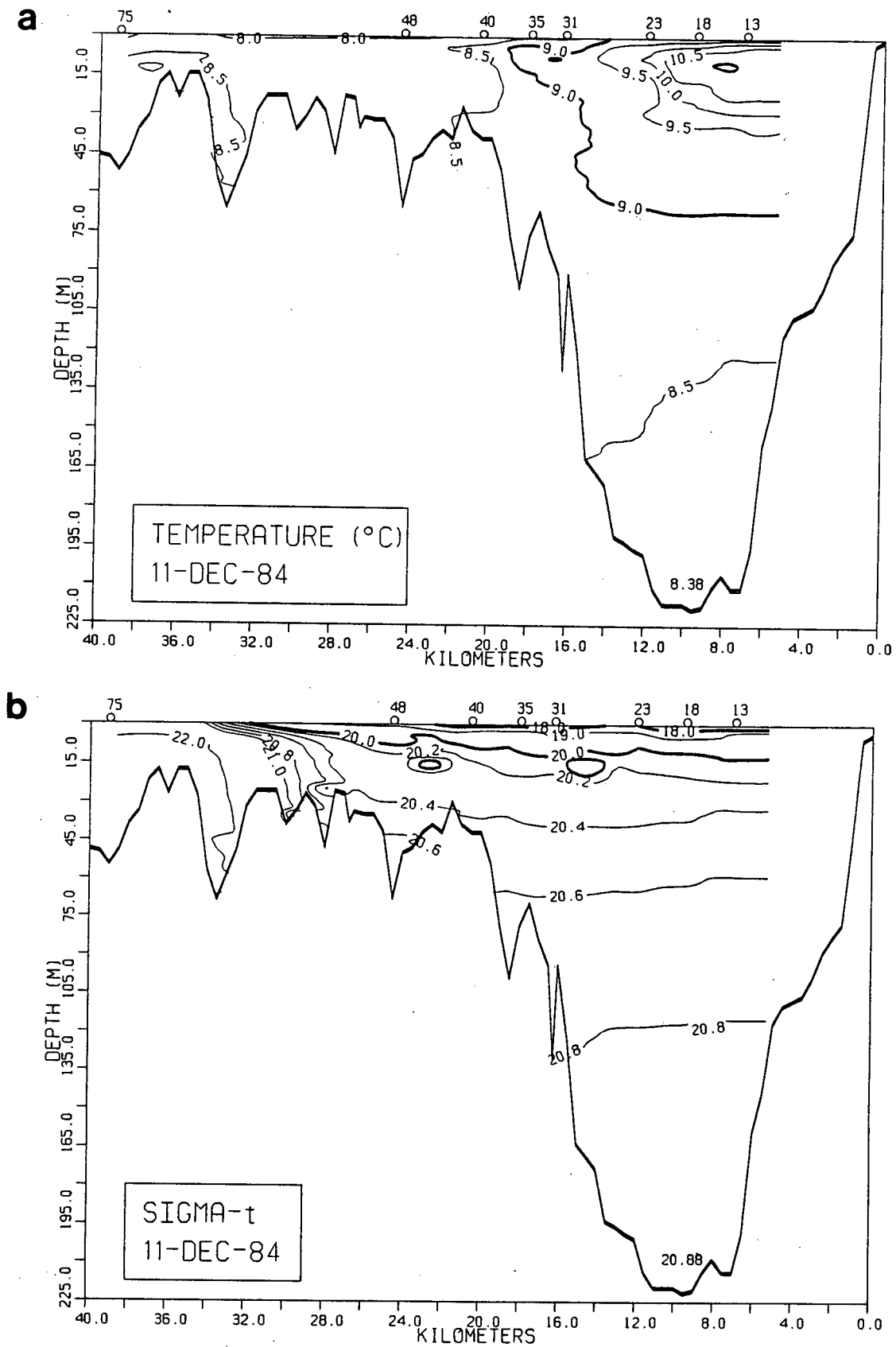

Figure 20 Temperature and σ_t in Indian Arm on 11-December-1984 (Julian day 346).

station 30 looks as if it were being drawn downward by the inflow. The density at the bottom of station 48 was greater than 21.5, more than 0.4 higher than that at the bottom of the basin. Following the exchange, the stratification in the fjord weakened. From the bottom to 15 m, there is a density difference of 0.9 before the exchange (see *Figure 18*), after the exchange the difference was 0.28.

The effects of this bottom water flushing on the DO_2 were also observed. Prior to the exchange, the DO_2 above 50 m was greater than 3 ml/l. Below 100 m the concentration was less than 2 ml/l (see *Table 9*). In January the DO_2 level at 15 m was less than 2 ml/l at some stations in the fjord. At the same time the bottom water oxygen concentration was greater than 4 ml/l. The low-oxygen water was forced upwards by the inflow of oxygen-rich water.

The effects of further inflow can be seen in February 1985 (see *Figure 22*). The density of the bottom water increased to 21.55. The water at the sill (21.7) is still more dense than that at the bottom of the fjord. The horizontal density gradient through Burrard Inlet is intense with several subsurface fronts visible in *Figure 22*. *Figure 22* shows that the mid-water temperature maximum has become re-established.

The vertical temperature gradient near the bottom was reversed by March 1985 (*Figure 23*), while the density increased by 0.13. The vertical temperature gradient near the bottom in February was positive, but in March it was negative. *Figure 23* shows that the density at the bottom of station 48 was somewhat less than that at the bottom of the fjord. The strong horizontal gradient in Burrard Inlet was still present, with dense water (22.4) at the bottom of station 60, so the possibility of inflow still existed. The effects of the spring warming can be seen in the temperature plot. The mid-water temperature maximum which existed in February has turned into a mid-water temperature minimum.

The April 1985 contour plots (see *Figure 24*) show no change in the bottom water density from the previous month. The density at the sill in April was less than that at the bottom of the basin indicating that the exchange period was over. Dense water ($>$ 22.0)

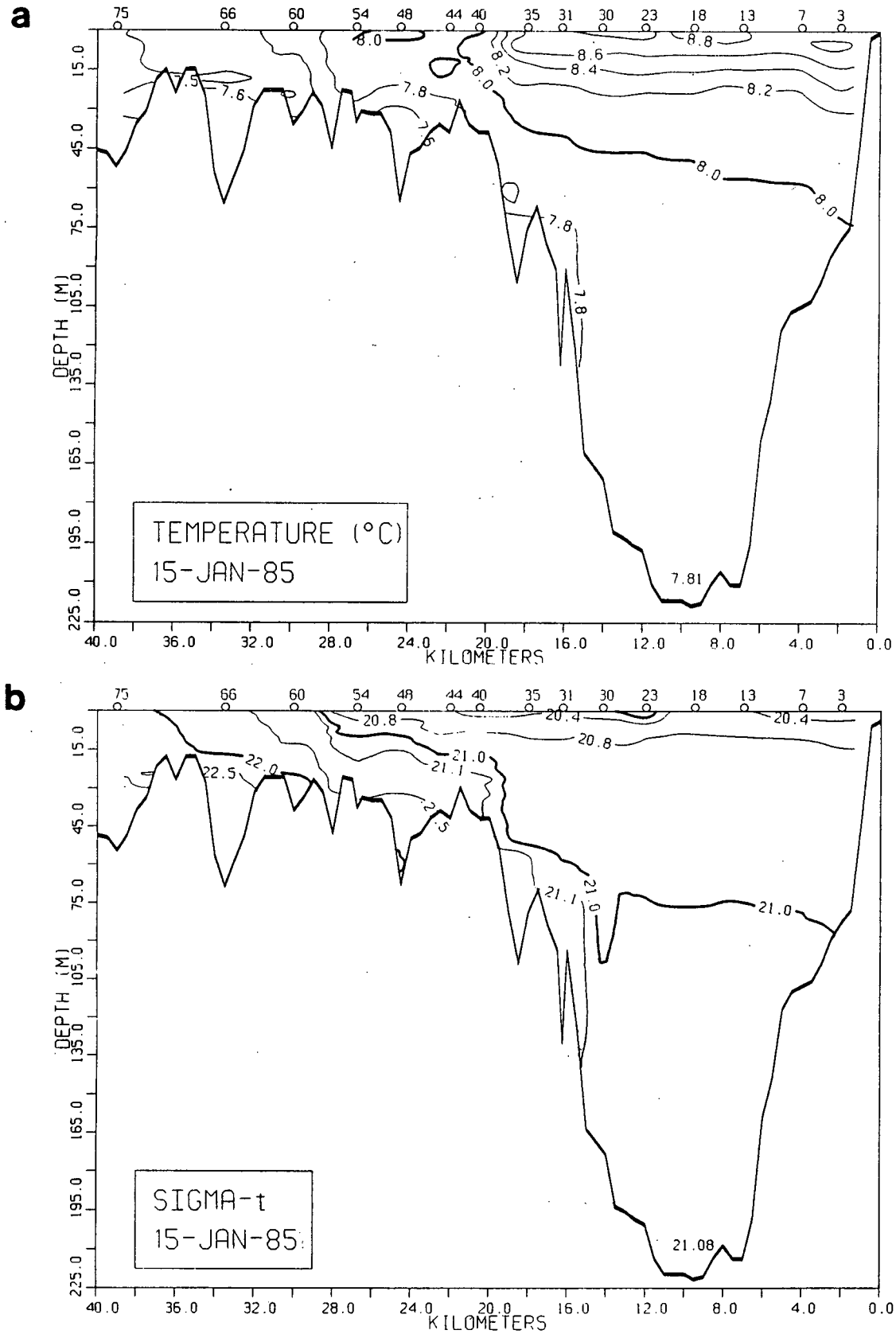

Figure 21 Temperature and σ_t in Indian Arm on 15-January-1985 (Julian day 15).

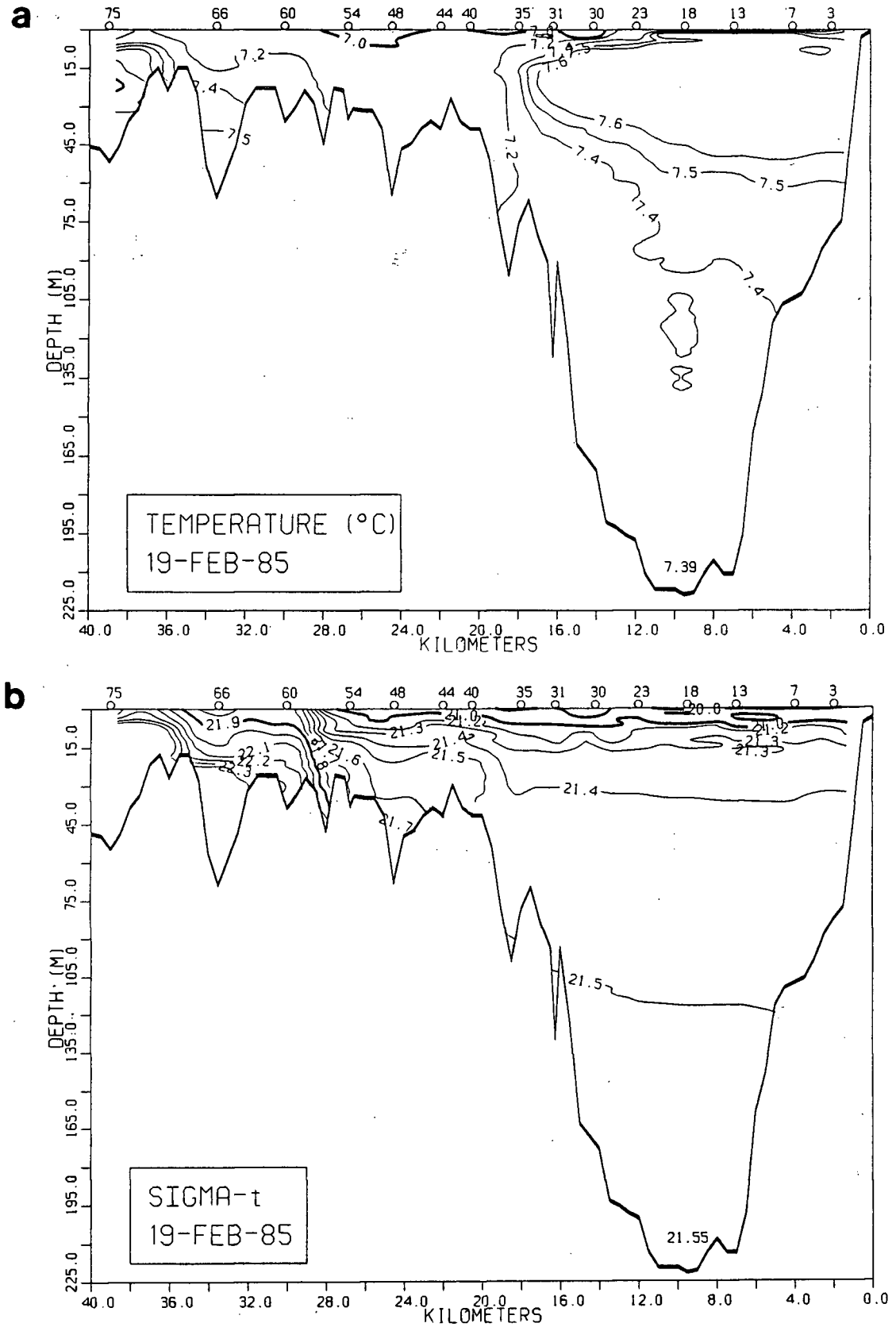

Figure 22 Temperature and σ_t in Indian Arm on 19-February-1985 (Julian day 40).

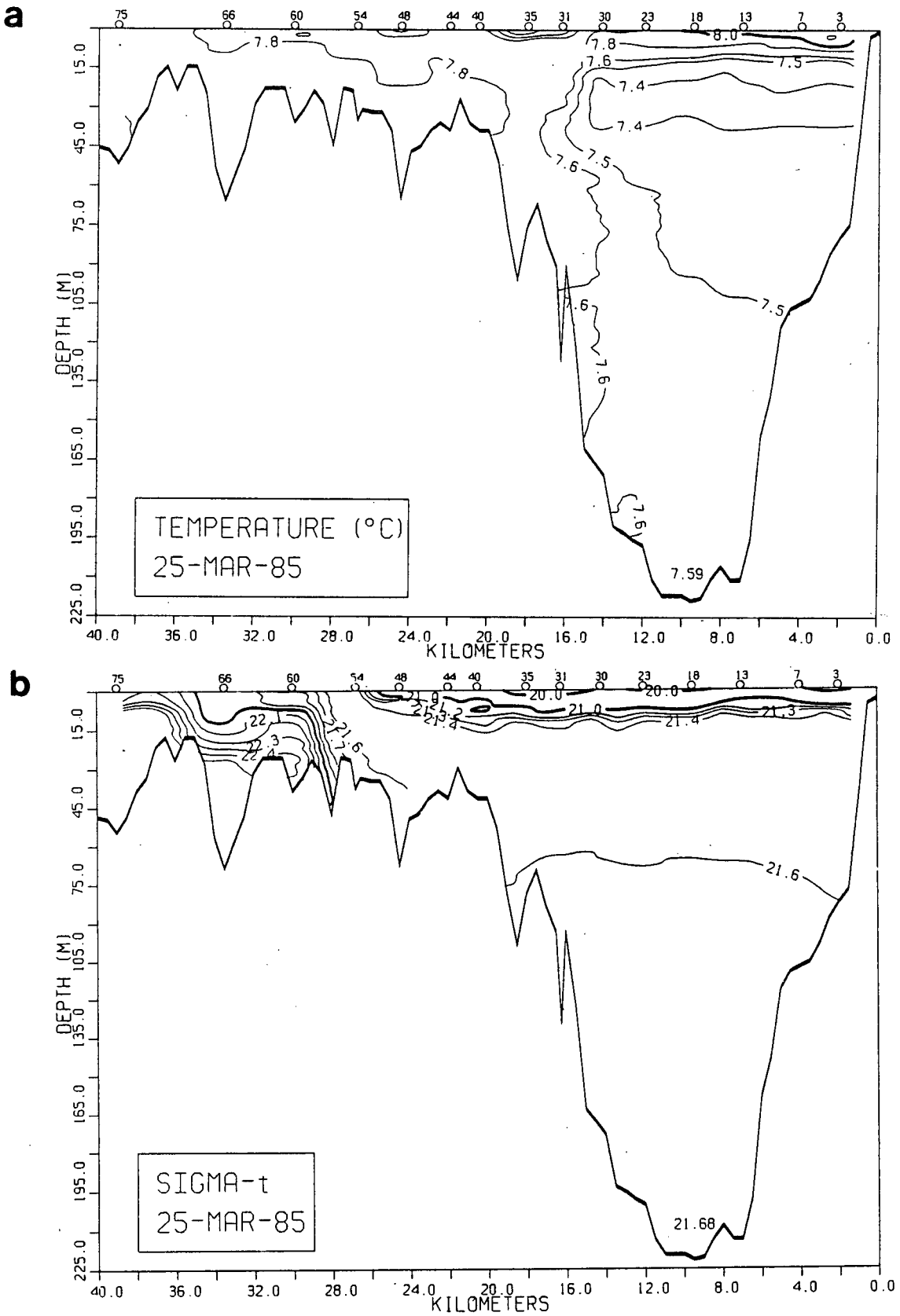

Figure 23 Temperature and σ_t in Indian Arm on 25-March-1985 (Julian day 84).

Table 9
Dissolved oxygen concentration in the basin of Indian Arm. The concentration is in ml/l, with an estimated error of ±0.1 ml/l.

Date	*Depth (m)* 10	30	50	100	150	200
1982/83						
7-Dec-82	–	–	–	–	–	0.69
5-Jan-83	3.06	3.75	4.78	4.50	1.52	0.54
1-Feb-83	5.15	4.98	4.11	4.02	1.20	0.82
5-Mar-83	5.37	5.32	4.32	3.88	1.58	0.98
29-Mar-83	5.04	5.56	4.52	3.35	1.39	0.97
1983/84						
9-Nov-83	4.04	3.53	3.67	1.28	0.83	0.75
13-Dec-83	3.29	4.01	4.53	1.83	0.67	0.64
11-Jan-84	5.22	3.52	3.47	4.53	1.17	0.60
8-Feb-84	4.90	4.71	4.35	3.48	1.56	0.79
7-Mar-84	4.58	4.69	4.28	3.46	1.33	0.98
11-Apr-84	5.84	4.57	3.91	3.45	1.37	1.05
24-Aug-84	4.17	4.12	3.87	1.68	1.47	1.38
1984/85						
7-Nov-84	4.28	3.50	3.46	1.58	1.27	1.16
11-Dec-84	2.87	3.33	2.14	1.78	1.12	1.03
15-Jan-85	2.05	4.12	4.44	4.33	4.25	4.33
19-Feb-85	4.38	4.41	4.55	4.72	4.75	4.75
25-Mar-85	4.49	4.83	5.10	5.07	5.13	4.99
22-Feb-85	5.30	4.37	4.38	4.87	4.93	4.83
22-May-85	7.72	5.20	4.83	4.64	4.79	4.58

was still present on the far side of Second Narrows sill but extended no further. The midwater temperature minimum in Indian Arm was deeper, centered at $40 - 60\,m$ now rather than $20 - 30\,m$ as it had been in March.

The midwater temperature minimum had all but disappeared by May 1985 (*Figure 25*). The density at the bottom of station 18 was lower than in April, indicating that no bottom water exchange had taken place in the time between the surveys. The decreased density was a result of diffusion of salt along the salinity gradient. Dense water in Burrard Inlet was even further west of Second Narrows than it had been in the previous month. The water at the bottom of station 48 was much less dense than that at the bottom of the fjord. The outflow of freshwater from the fjord increased from April to May, as evidenced by the extension of the 16.0 isopycnal from station 3 to a point between stations 31 and 35. The increasing stratification of the upper $50 - 100\,m$ is apparent from February to

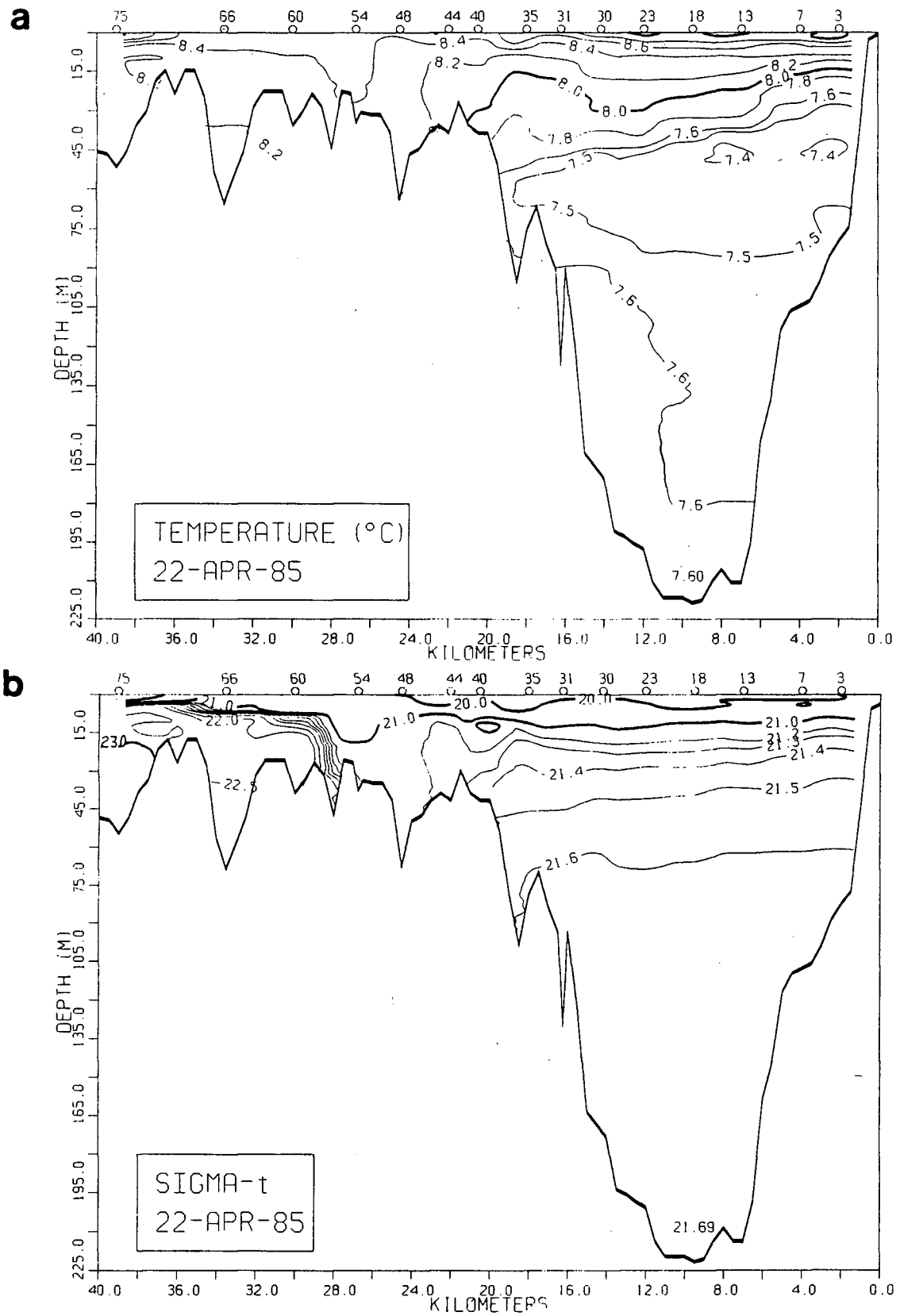

Figure 24 Temperature and σ_t in Indian Arm on 22-April-1985 (Julian day 112).

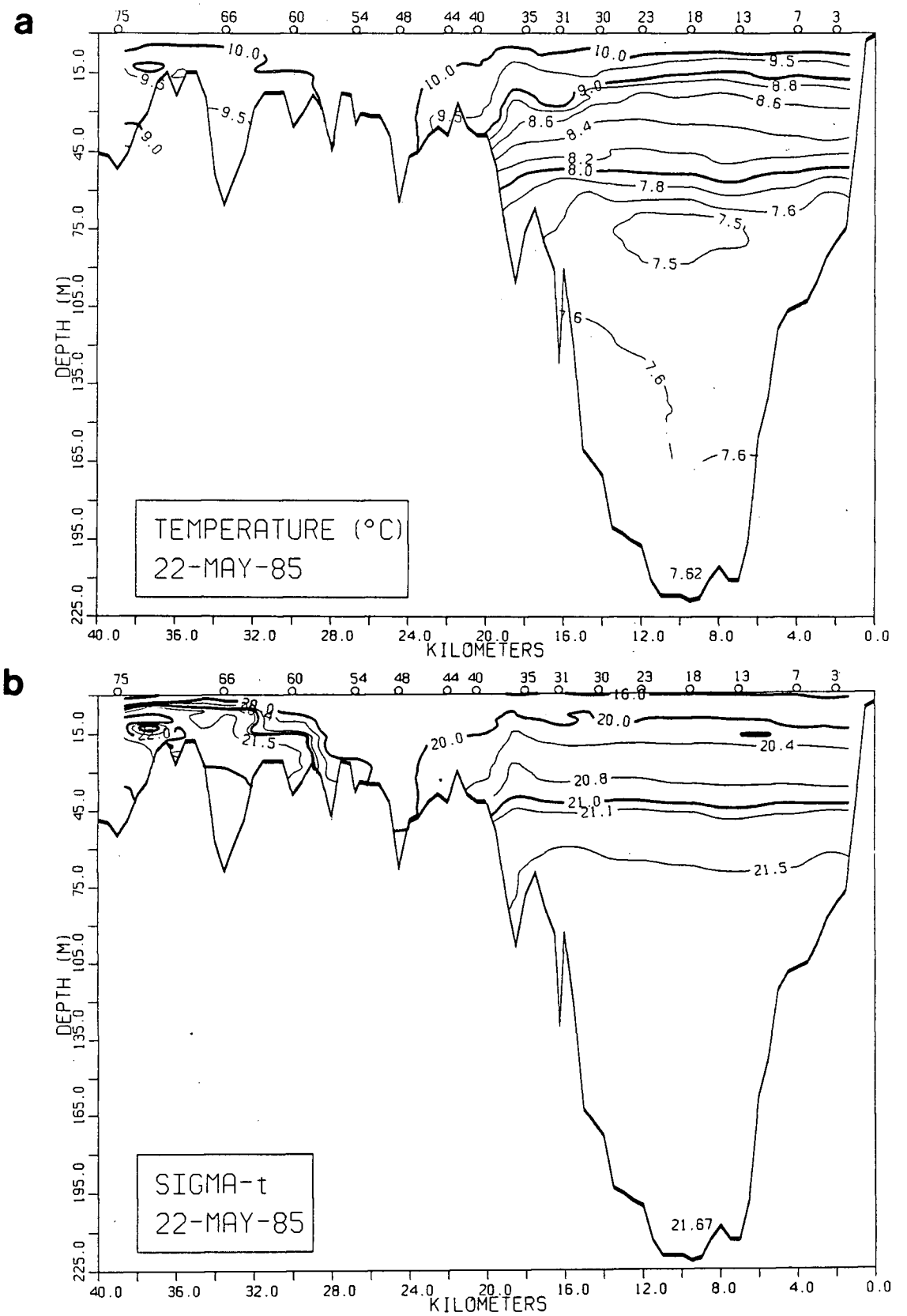

Figure 25 Temperature and σ_t in Indian Arm on 22-May-1985 (Julian day 142).

May.

4.3 Forcing of the Deepwater Exchange

The timing of the exchange events is expected to be controlled by the tide, freshwater inflow, the wind and the density outside First Narrows. The density of the water at station 75 will also be a function of the physical forcing, but in a much more complex way since it will also depend upon the exchange cycle in the Strait of Georgia (Pickard, 1975).

Energy is required to lift the dense water up over the sill of Indian Arm. In determining the source water for the exchange, it is important to determine from what depth the flow is capable of drawing water. This phenomenon is known as blocking and occurs in a number of different situations (Gill, 1982). For a mean flow approaching a barrier of height h, one can apply a form of Bernoulli's equation:

$$\frac{p_1}{\rho} + \frac{{u_1}^2}{2} = \frac{p_2}{\rho} + gh + \frac{{u_2}^2}{\rho}. \tag{4.1}$$

The left side of equation (4.1) gives the kinematic energy of the approaching flow. The right side gives the energy of this water after reaching the top of the barrier. Water at the at the top of the barrier has increased potential kinematic energy given by gh, where g is the acceleration due to gravity. It is assumed that the flow at the top of the barrier has no remaining kinetic energy so $u_2 = 0$. If the average density of the surrounding water through which the water parcel moves is ρ_s then:

$$p_1 - p_2 = \rho_s gh \quad . \tag{4.2}$$

It is now possible to rewrite equation (4.1) to give

$$\frac{\rho_s gh}{\rho} = gh - \frac{U^2}{2} \tag{4.3}$$

where the velocity of the approaching flow is now just written as U. Equation (4.3) can be rewritten to give

$$gh\left(\frac{\rho - \rho_s}{\rho}\right) = \frac{U^2}{2} \tag{4.4}$$

The density difference term can be rewritten in terms of the observed stratification which is assumed to be approximately linear in z. Since ρ_s is the average density, for an approximately linear gradient ρ_s is reached for a height change of $h/2$.

$$\frac{\rho - \rho_s}{\rho} \simeq -\frac{1}{\rho}(\frac{\partial \rho}{\partial z})\frac{h}{2} = N^2 h/2g \quad , \tag{4.5}$$

where $N^2 = (-g/\rho)\frac{\partial \rho}{\partial z}$. Inserting equation (4.5) into equation (4.4) gives an equation for the blocking height:

$$h \simeq \frac{U}{N} \quad . \tag{4.6}$$

The form of this equation can also be derived from dimensional analysis since one expects the blocking height to be a function of the stratification and the velocity of the approaching flow. Any dissipation in the region of the sill will lead to a reduction in the energy on the right hand side of equation (4.1). The blocking height given by equation (4.6) should not be treated as a precise estimate.

The parameters controlling the blocking of the flow into Indian Arm are approximately known. At First Narrows the velocities for the M_2 and K_1 tide are 0.61 and 0.31 ms^{-1} respectively, thus the barotropic velocity is about 0.91 ms^{-1}. For the winter of 1985, the buoyancy frequency N was about 0.014 s^{-1}. Inserting these numbers into equation (4.6), gives a blocking depth of about 65 m. This value is not meant to be precise but does give some estimate of the blocking depth. It indicates that the blocking depth is much deeper than the sill depths and thus water from the bottom of station 75, outside First Narrows, will not be blocked even during periods of neap tides. This estimate shows that the source water for the exchange is available throughout the spring/neap tidal cycle.

Figure 26 shows the annual variation of water properties in the Strait of Georgia. Waldichuk (1957) discussed the deepwater renewal process in the Strait, a problem that was investigated in more detail by Samuels (1979). In the winter, cold but relatively fresh water mixes in the passages leading into the Strait. This water then sinks down into the deeper part of the Strait. In the summer, a warm salty water inflow enters the Strait reaching neutral buoyancy at mid-depths. Samuels interpreted this process to be very

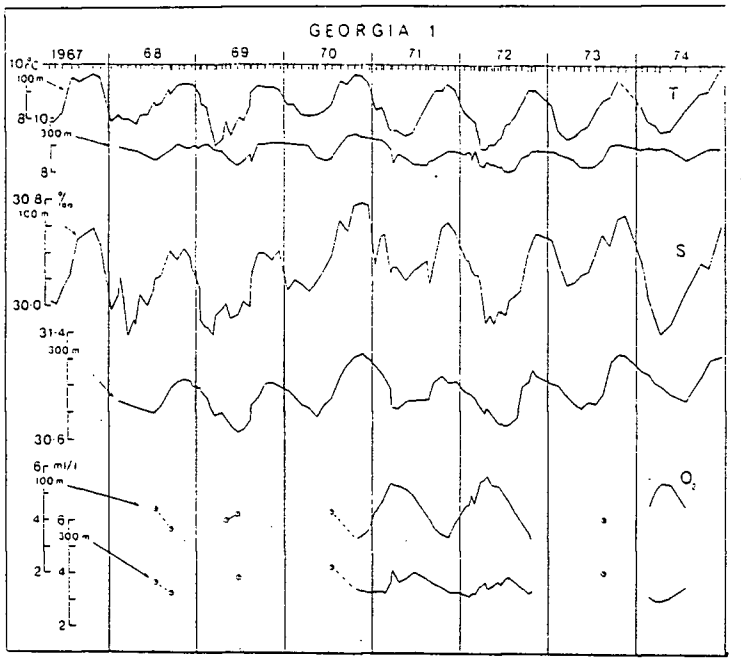

Figure 26 Long term variation of temperature, salinity and DO_2 at depths of 100 and 300 m in the Strait of Georgia. The station location (G1) is shown in *Figure 5*. From Pickard (1975).

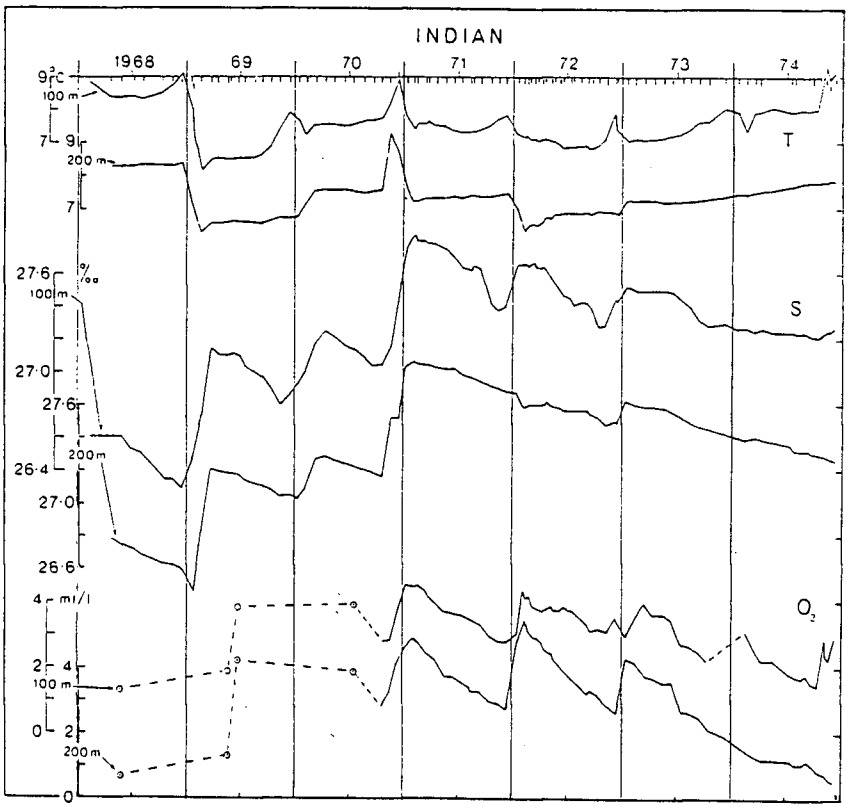

Figure 27 Long term variation of temperature, salinity and DO_2 in the basin of Indian Arm. From Pickard (1975).

regular, subject to occasional intensification, rather than one where strong intermittent overturns occurred.

The source water for the Indian Arm exchange is probably in the top 100 m of the Strait of Georgia. *Figure 26* shows that the maximum salinity (or density) occurs late in the year. This timing is undoubtedly a controlling factor of the exchange in Indian Arm, as a comparison of water properties makes clear. *Figure 27* shows the long term properties in Indian Arm covering the same period as in *Figure 26*. The exchange in Indian Arm does not occur at the same time as does the maximum density at 100 m in the Strait of Georgia, indicating that the Strait water does not simply flood over the sill when it is at its maximum density. There is, however, a relationship in that the exchange in Indian Arm occurs early in the winter, following the exchange in the Strait.

The forcing of the flow in Burrard Inlet and Indian Arm will now be looked at, to investigate the control of the exchange. Three years of data are available: 1982/83, 1983/84 and 1984/85. In discussing control of the exchange, I shall concentrate on the last year because it was in that year when full bottom-water renewal took place.

Figure 28 presents some of the data for the 1982/83 period. An estimate of the tidal kinetic energy per unit volume is plotted with the observed density and current data. This energy is calculated using the tidal height data. Harmonic analysis of the data yielded the various constituents which were used, together with data on the geometry of the sill, to determine the barotropic tidal velocity over the sill. A 24 hour running average of the resulting kinetic energy term was then taken to allow visualization of the changing energy level. One of the main points of the plot is to indicate the changing amount of energy available for mixing.

Only mid-water exchange was observed in 1982/83 (*Figure 28*), thus basin data at 70 m are presented together with the sill data at 60 m. It should be noted that these *sill* data are in fact taken from mooring C1 just inside the sill. The sill is at 26 m depth – station C1 is 70 m below datum. The observations from station C1 are of water that has made

it over the sill and into Indian Arm. The density data presented should also be remarked upon because of the quality of the cyclesonde salinity and density data. The estimated error in σ_t as measured by the cyclesonde is ± 0.1. Fortunately the relative accuracy at a particular station is much better and so comparisons of the data within a month are quite good. Month to month comparisons between different cyclesondes, or even between data from the same instrument in two different months, need to be made cautiously. As well it should be noted that the error at the basin station is probably greater than the error at the sill because of the much lower flow speeds in the basin.

Several major bursts of current at the sill occurred in 1982/83 (see *Figure 28*). They varied in length from 5 to 20 days and in speed from $15 - 30\,cm\,s^{-1}$. Between these periods, the mean flow was weak and directed out of the inlet near the bottom at station C1. (A more detailed discussion of the vertical structure of the changing mean flow will be given in a later section.) All of these bursts , except the one centered at day 364, were associated with neap tides. Most were also associated with increasing densities, though this relationship is less clear. The basin speeds will be large only during inflow events. The 1982/83 inflow events occurred at different depths, though never at the bottom, so large responses in the basin speed at $70\,m$ are not seen clearly. Increased basin speed around day 400, associated with an inflow event, can be seen.

A comparison between the E/W wind velocity and freshwater flow for 1982/83 (see *Figure 29*) provides no clear relationship with the sill data. The main sources of freshwater are the Indian Arm River and the Buntzen power plants located about $10\,km$ from the head. The position of this freshwater source halfway down the inlet is important for the surface circulation and salinity within Indian Arm (Gilmartin, 1962) but is probably not important in driving the circulation at the sill. The other major source of freshwater in this area is the Fraser River whose effects in English Bay and Burrard Inlet have been previously described (Davidson, 1979). It may be that the freshwater from the Fraser River is as important as the outflow from Indian Arm in influencing the water at the sill and in Burrard Inlet. The increase in density at the sill around day 360 may be related

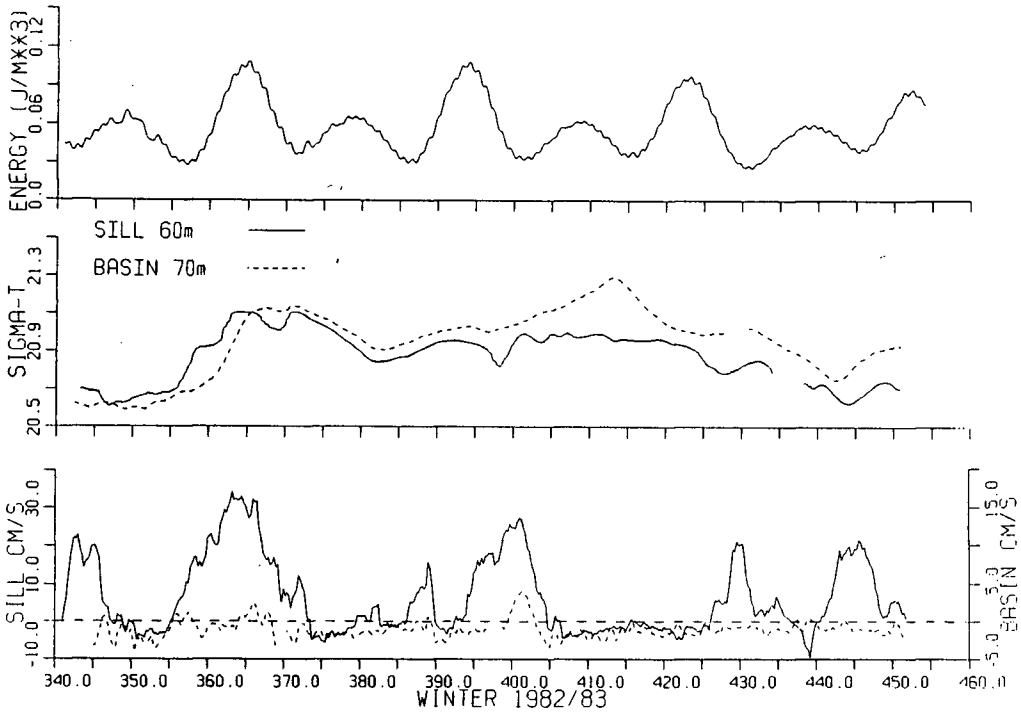

Figure 28 Tidal energy, density and along-channel current for the 1982/83 exchange. At top is the tidal kinetic energy plotted as a 24-hour average. The middle frame presents σ_t from the basin and sill cyclesonde stations. The bottom frame presents the along-channel current, with the tidal signal removed using harmonic analysis. Note that the basin and sill current data are plotted at different scales. Positive current is directed into the inlet, negative out. Time is in Julian days from the start of 1982.

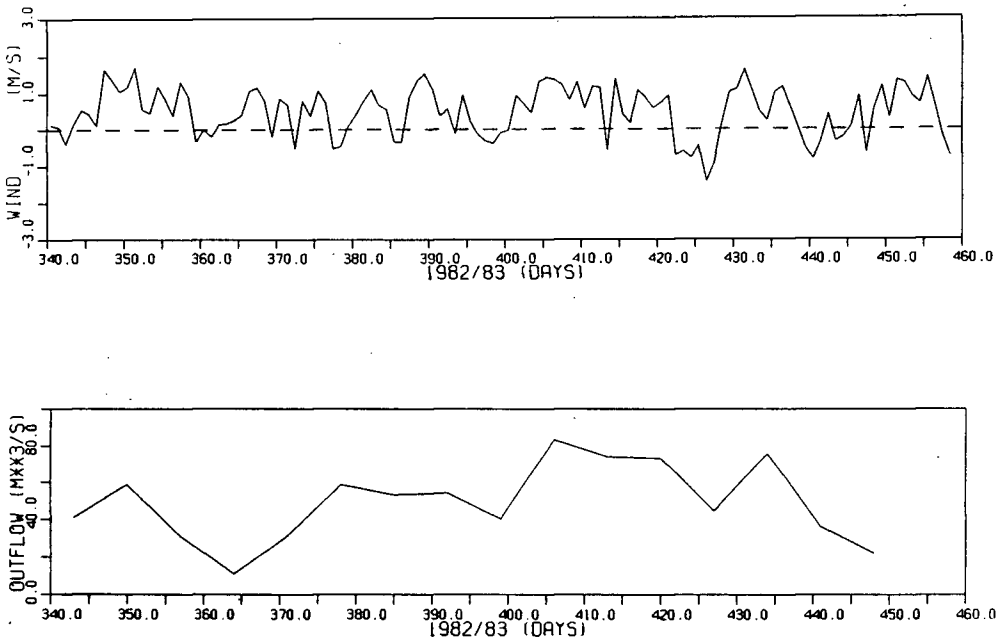

Figure 29 E/W wind at Vancouver airport in 1982/83 and freshwater flow into Indian Arm. The wind data are averaged over one-day intervals; the freshwater inflow data are averaged over three-day intervals. Time is in Julian days from the start of 1982.

to the decrease in freshwater flow which begins at about the same time. The density in the Strait of Georgia is probably increasing at the same time (Pickard, 1975) and so this observed increase at the sill may not be a direct freshwater effect at all. Some relationship between the current flow at the sill and the wind is expected, although, no strong forcing is expected from the weak winds. Forcing of the flow by the wind is discussed in more detail in Chapter 3.

This association of maximum density and flow speed at the sill was also observed in 1983/84 and 1984/85. In *Figure 28* most of the peaks in the density curve occur near neap tides. The current at the sill in 1983/84 cannot be described so easily. Other physical effects are at work here. The period of inflow, starting at day 335 and extending to day 370 (see *Figure 30*), does begin on a neap tide and is associated with a density increase of 0.4 over this period, however, the current speed is fairly constant throughout the period.

The increasing density from day 325 to 360, seen in *Figure 30*, may be related to the decreased freshwater runoff. Freshwater inflow and the E/W wind for the 1983/84 period are presented in *Figure 31*. This period is also one of reduced wind velocities following stronger (about $1\,m\,s^{-1}$) winds from day $310-320$. The density at the sill drops after day 360 when the freshwater flow increases to about $50\,m^3 s^{-1}$.

The 1984/85 record (see *Figure 32*) shows the effects of the tide during a period of bottom water renewal. Four strong renewal events are observed at days: 380, 395, 405 and 435. Three of these events (at days 380, 395 and 435) have peak inflows which occur during neap tide. One (405) takes place just before the neap tide.

As in 1983/84, inflow at the sill occurred for extended periods, although there was somewhat more variability in 1984/85. The inflow speed at the sill varied from $10-30\,cm\,s^{-1}$. Maximum inflow speeds at the sill on days 380, 395, 405 and 435 are associated, roughly at least, with the exchange events and with the neap tide. Large basin velocities, up to $10\,cm\,s^{-1}$, occur during these inflow events. Increases in the density at the bottom of the basin are also observed. The increase in the density at the sill shows distinct maxima

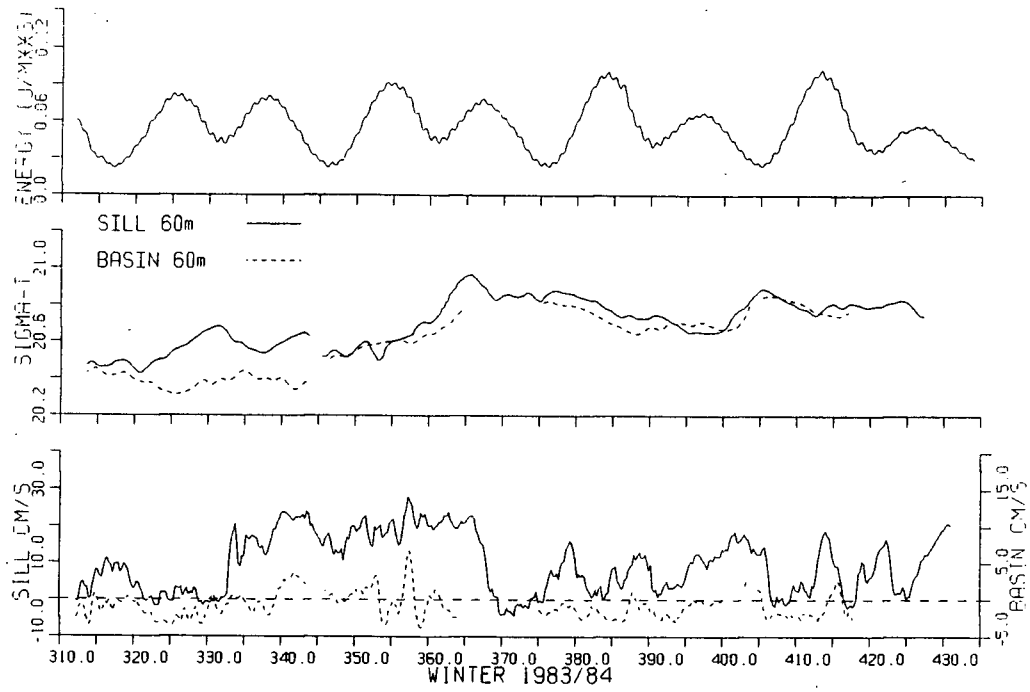

Figure 30 Tidal energy plus density and current at the sill and in the basin in 1983/84. Time is in Julian days from the start of 1983. Plotted as in *Figure 28.*

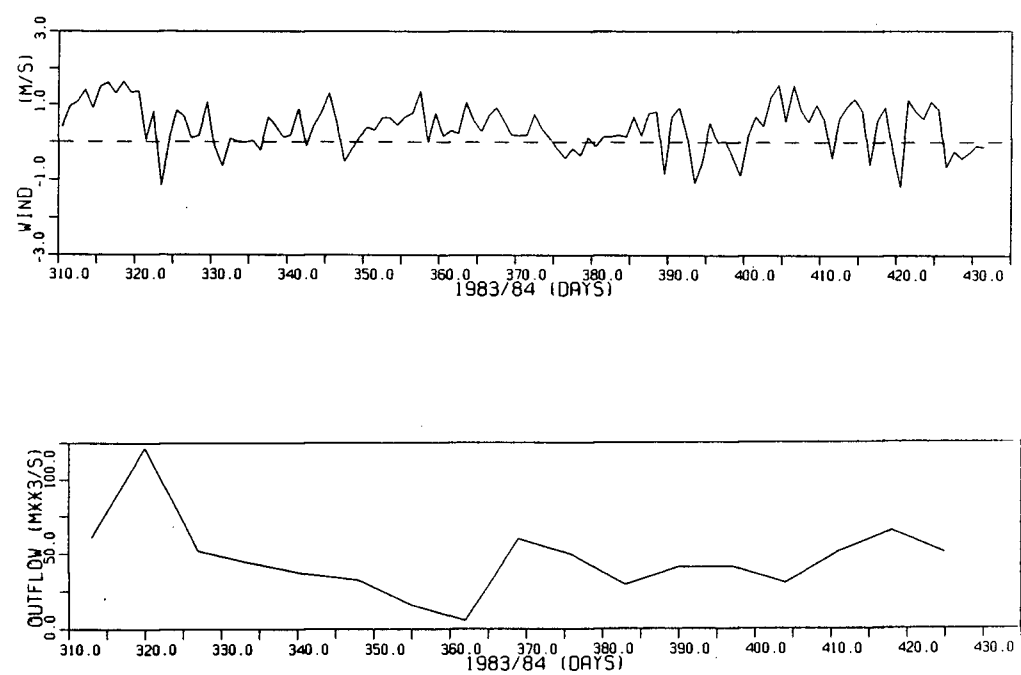

Figure 31 E/W wind at the airport and freshwater flow into Indian Arm in 1983/84. Time is in Julian days from the start of 1983. Details of the data are described in *Figure 29.*

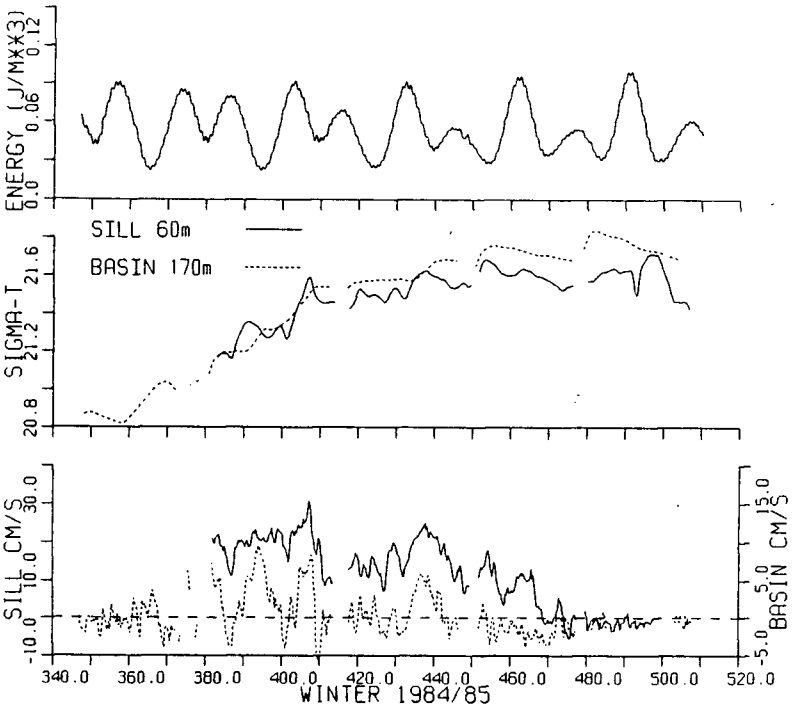

Figure 32 Tidal energy plus density and current at the sill and in the basin in 1984/85. Time is Julian days from the start of 1984. Plotted as in *Figure 28.*

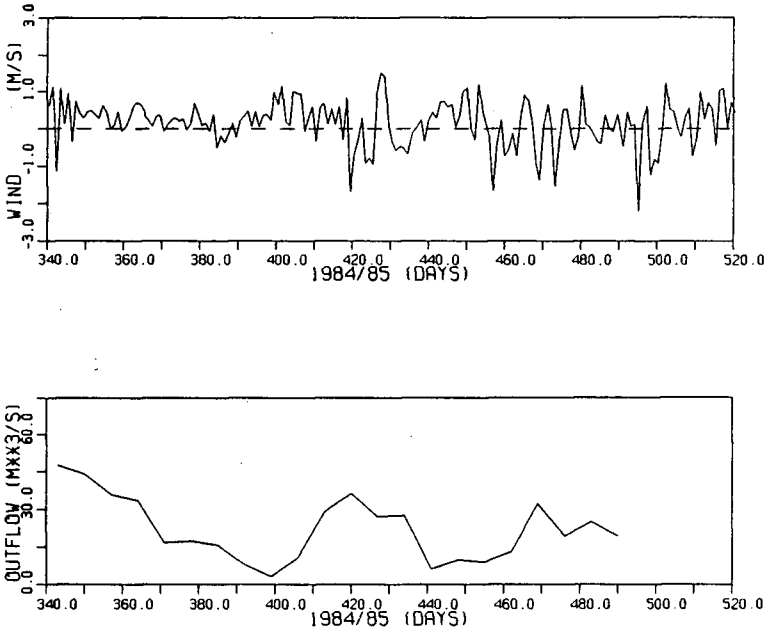

Figure 33 E/W wind at the airport and freshwater flow into Indian Arm in 1984/85. Time is in Julian days from the start of 1984. Details of the data are described in *Figure 29.*

not apparent in the basin record. The peaks in the sill density are the result of the mixing of the water in Burrard Inlet. Most of the observed peaks are associated with the neap tides. Between days 410 and 440, however, the peaks seem to occur halfway between spring and neap tides. At this time the tidal excursion is sufficient to carry the dense water up to the sill, while the mixing is weak enough that the density will not be as greatly reduced as it would during spring tides.

The tidal excursion in Burrard Inlet is about 18 *km*, approximately the length of Burrard Inlet. If the tidal excursion in a shallow silled fjord is less than the sill length then mixing will be critically important since the water cannot make it over the sill on one tidal cycle. The water must be dense enough to reach the far end of the sill with sufficient negative buoyancy to sink. Bottom water renewal associated with neap tides has been observed in Puget Sound (Cannon and Laird, 1978; Geyer and Cannon, 1982) where the tidal excursion is just slightly less than the length of the sill. In Rupert-Holberg Inlet, where the sill is short in comparison with the tidal excursion, exchange has been observed to be associated with spring tides (Stucchi and Farmer, 1976). Here in Indian Arm, with Burrard Inlet acting as the sill, mixing and the tidal excursion will be crucial in determining the exchange timing.

Figure 33 shows the freshwater inflow and the wind for 1984/85. The freshwater inflow data provide an explanation for the lack of an inflow at day 422. A strong surge of freshwater begins at day 400 and continues until day 440. From day 380 to 420, there is an increase in the density at the bottom of station 75, outside First Narrows. In spite of this density increase, there is no inflow of water at day 422. There is a drop in the density at the sill from day 410 to 435 associated with the freshwater surge.

4.4 Current and density averages during an exchange episode

The dominant signal in the current meter records is the tide (see Chapters 3 and 5). Plots of the raw data show the strong diurnal/semi-diurnal flow. Filtering or averaging of these data is useful to allow us to see the lower frequency signal present in the record. Three possible techniques can be employed to enhance the low frequency signal: deconstitution, filtering and simple averaging. Deconstitution is the removal of the tidal signal following harmonic analysis. In some ways this is the *purest* technique in that only energy at the chosen tidal frequencies is removed. Some problems are associated with this type of signal removal. Part of the tidal signal is the internal tide which may not be constant over the month, so the time series is only partially non-stationary. There is also the problem of the Doppler shift of the internal tide, whose energy will not appear in the harmonic analysis. Filtering has the advantage of selectively removing energy at a broad range of frequencies (Godin, 1972), with fairly sharp cutoffs. Averaging is the same technique applied in a simpler fashion leading to much broader cutoffs. The advantage of averaging lies in its computational simplicity.

The along channel current speed in 1982/83 at C1 is shown in *Figure 34*. These data have had the M_2, S_2, N_2, K_1, O_1 and P_1 tides removed following harmonic analysis. The P_1 tide was determined using inference with the Vancouver Harbour tidal height record providing the amplitude ratio and phase difference information. A simple 24 hour running average of the data was then done to reduce the noise level.

The vertical structure of the inflow events is indicated by the strong currents in 1982/83 at the sill (see *Figure 34*) and in the basin (*Figure 35*). The strong inflows increase in strength towards the bottom. At station C1 on the sill the water is flowing as a density current down the slope. None of these flows made it to the bottom in 1982/83, but separated from the bottom near the point along the slope where they reached neutral buoyancy. As the current flows down the slope, its momentum probably causes it to overshoot the point of neutral buoyancy. The inflow at day 365 reached a depth of 130 m in the basin, however, the weaker flow at day 446 only reached to $30 - 40\,m$.

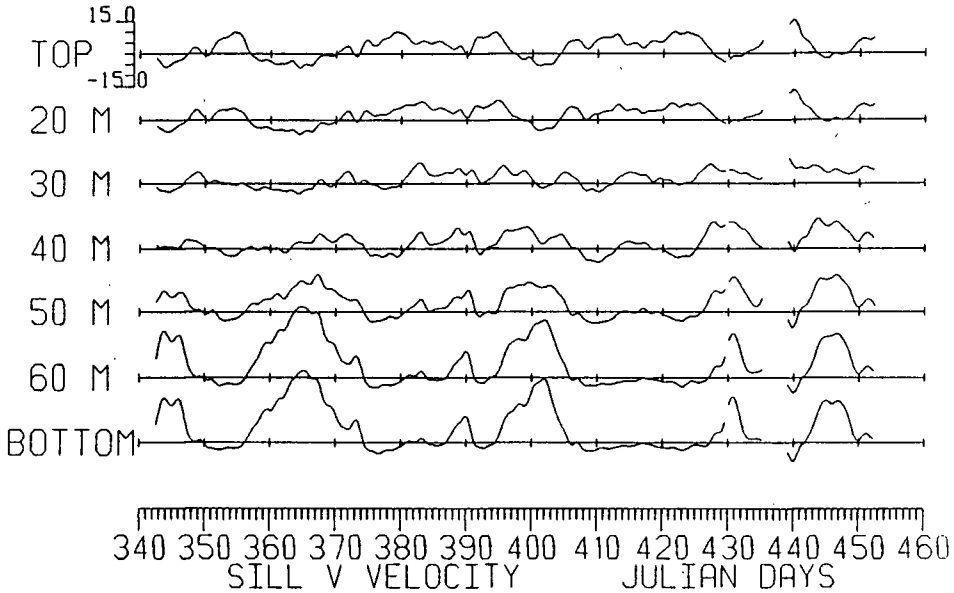

Figure 34 Along-channel current in 1982/83 at the sill station (C1). Positive currents (in $cm\,s^{-1}$) are directed into the fjord. Top and Bottom show data from the cyclesonde when sitting at the top and bottom bumper. Julian days are from the start of 1982.

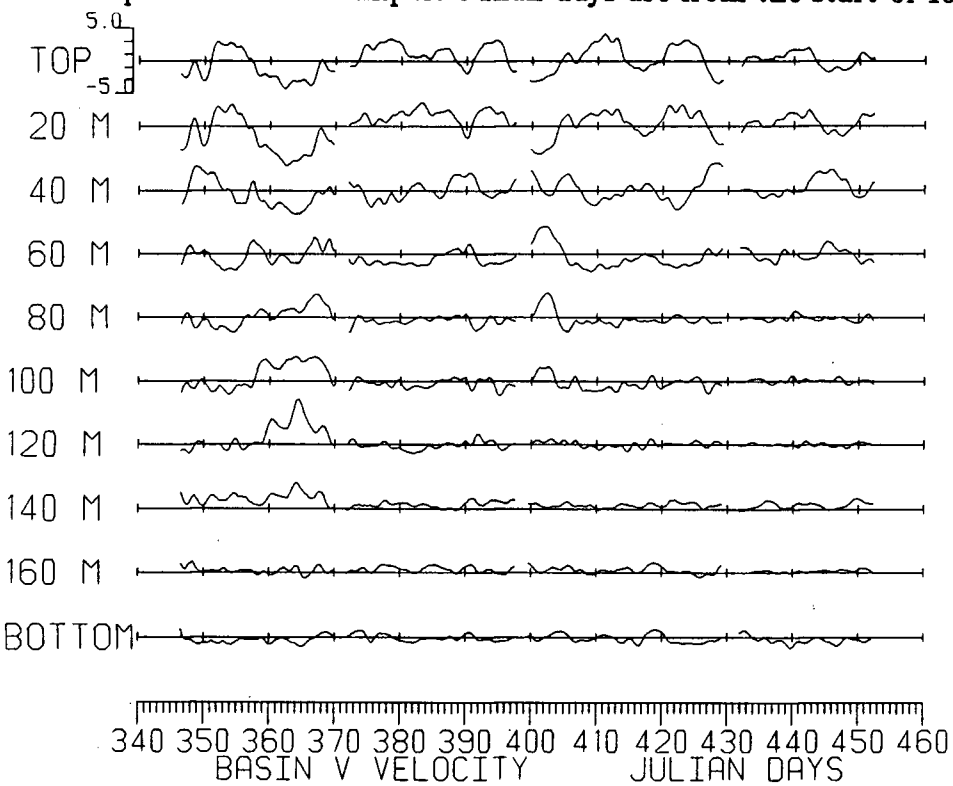

Figure 35 Along-channel current in 1982/83 at the basin station (C3). Positive currents (in $cm\,s^{-1}$) are directed into the fjord, negative outward. Julian days are from the start of 1982.

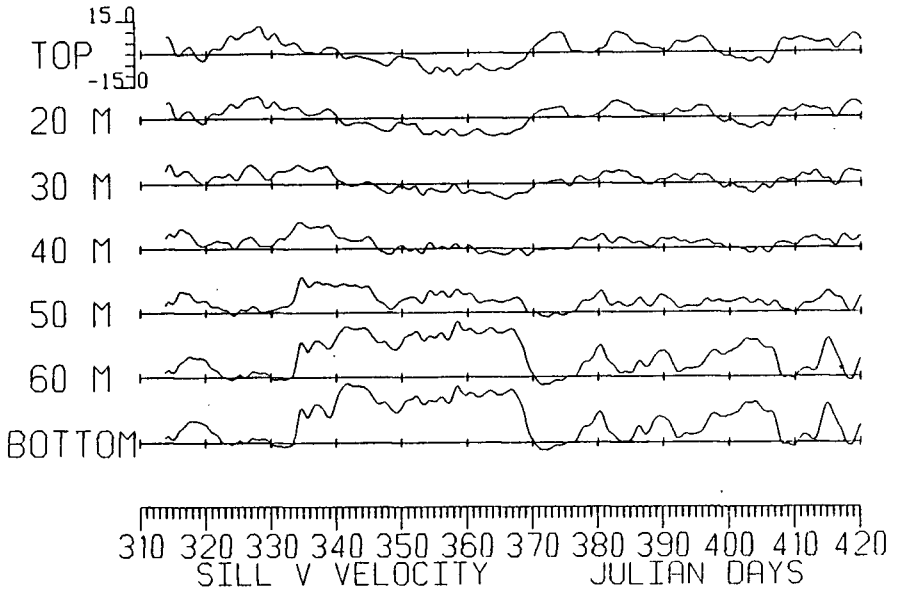

Figure 36 Along-channel current in 1983/84 at the sill station (C1). Positive currents (in $cm\,s^{-1}$) are directed into the fjord. Julian days are from the start of 1983.

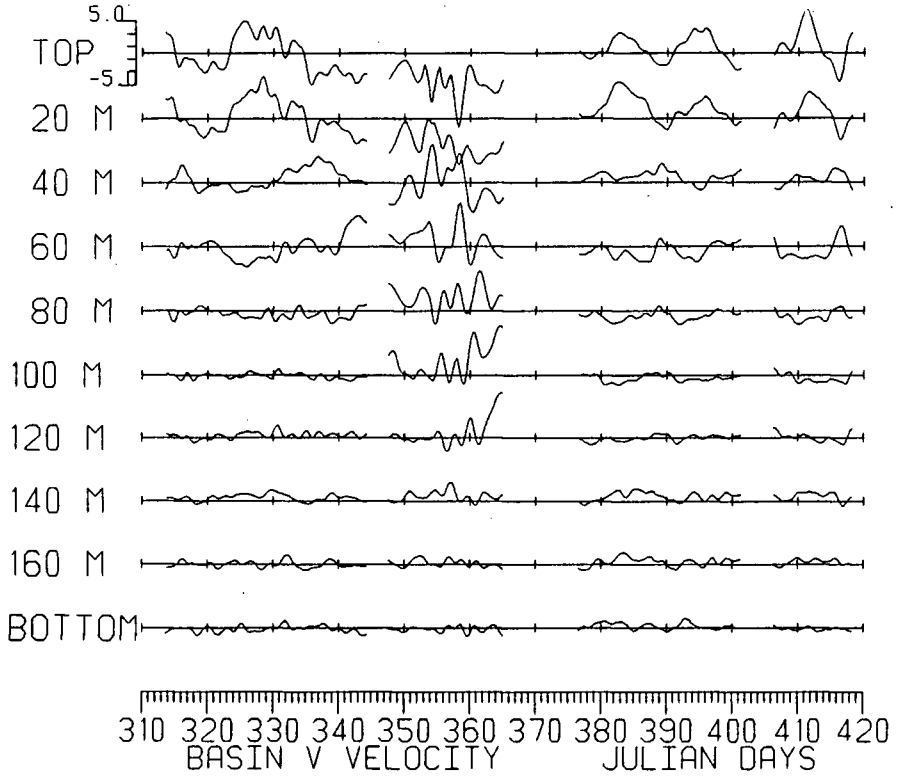

Figure 37 Along-channel current in 1983/84 at the basin station (C3). Positive currents (in $cm\,s^{-1}$) are directed into the fjord. Julian days are from the start of 1983.

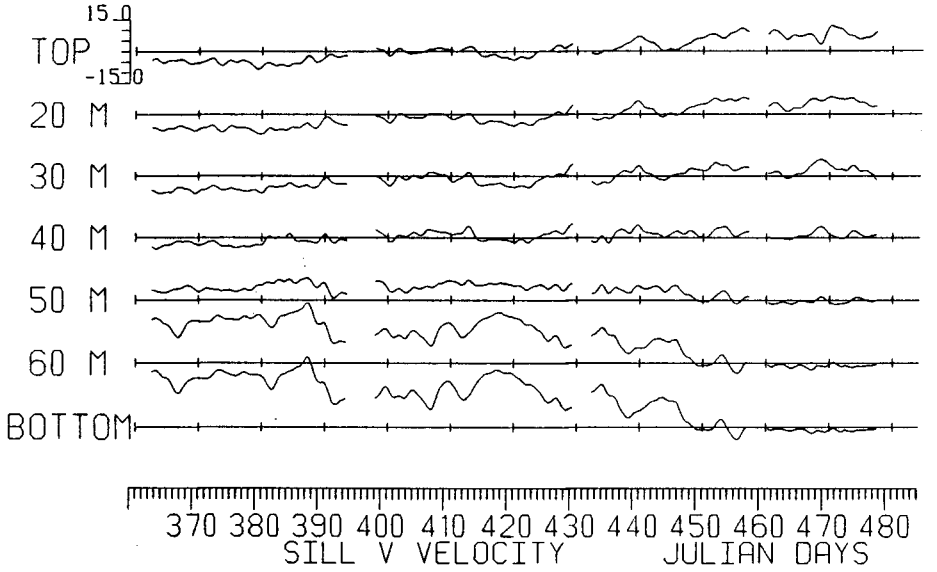

Figure 38 Along-channel current in 1985 at the sill station (C1). The units are $cm\,s^{-1}$. Julian days are from the start of 1984.

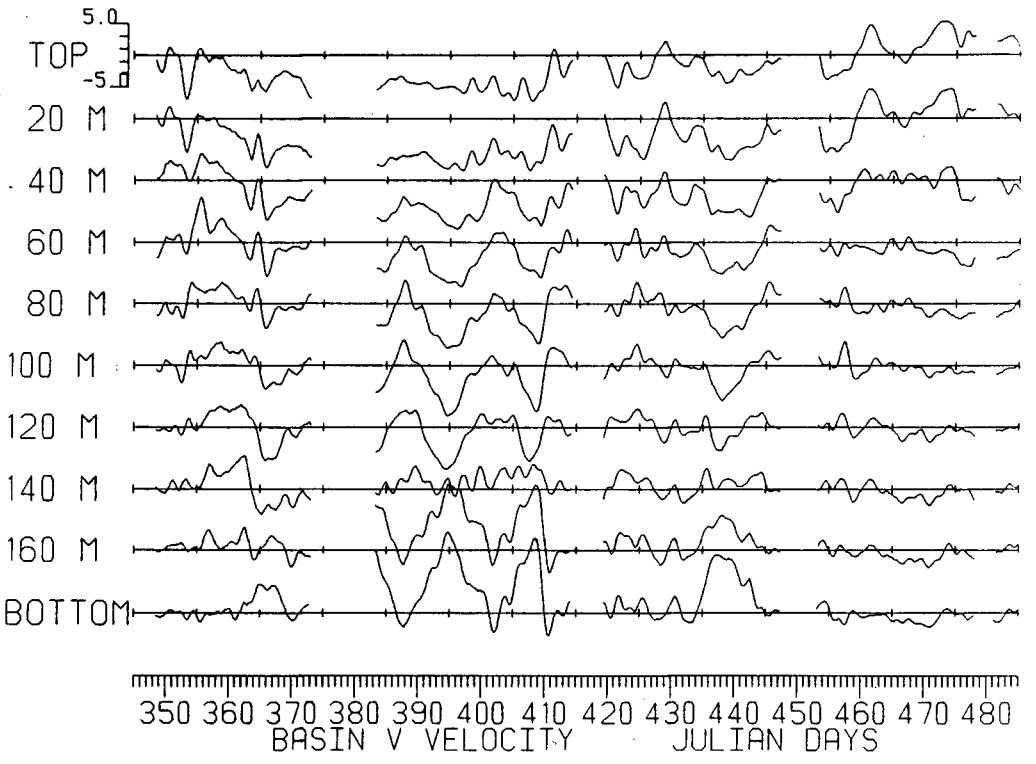

Figure 39 Along-channel current in 1984/85 at the basin station (C3). The units are $cm\,s^{-1}$. Julian days are from the start of 1984.

The 1983/84 sill (*Figure 36*) and basin (*Figure 37*) records show similar events. No strong flow reached deeper than $70 - 80\,m$. There may be an inflow in the basin between 100 and $200\,m$ just after day 360 but because of a gap in the record it is uncertain. There is a strong basin oscillation around days 355-360 which appears to be have a period of about 40 hours. This response may be a mode 2 resonance response (see the discussion in section 5.7), although the source of the forcing cannot be identified. The maximum amplitude of the horizontal current in this event is at $40\,m$ with a monotonic decrease to the bottom. The internal response of the fjord to tidal forcing will be discussed in Chapter 5.

Complete renewal of the fjord occurred in 1984/85. *Figures 38 and 39* show the along-channel current at the sill and in the basin. The inflows at the sill hug the bottom; they appear to be about $20 - 30\,m$ in thickness, an observation based upon the weakness of the inflow at $50\,m$ and the depth of the station ($70\,m$). The strong inflows in the basin are $30 - 40\,m$ thick during the two major inflow events between days 388 and 410. (The inflow is weak at $140\,m$ and the station depth is $190\,m$ below datum.) Between the inflow events, there is a reversal in the current at the bottom in the basin. The response of the fjord to these flows in the upper section of the fjord is seen in the steady outflow down to a depth of $40 - 50\,m$ and the pulses of outflow to $120\,m$ depth at days 396 to 410.

Contoured along-channel currents in *Figure 40* show the structure of the flow in the basin more clearly. For these plots the raw data were averaged over 25 hours and then contoured. The two large inflow events centered at days 30 and 44 show mean bottom speeds as high as $10\,cm\,s^{-1}$. The zero crossing rises and falls with the inflow, dropping to a depth of $140\,m$ during an exchange. The contour plot at the sill (*Figure 41*) during the same period shows that the zero crossing does not change appreciably in depth. The inflow at the sill appears quite steady during the period. There is some indication that the flow speeds up at day 44 but no evidence of this behaviour at day 30.

Averages over 29-day periods at the sill and in the basin are presented in *Figure 42*. In the first month (days $16 - 45$) the inflow was much stronger than in the second month

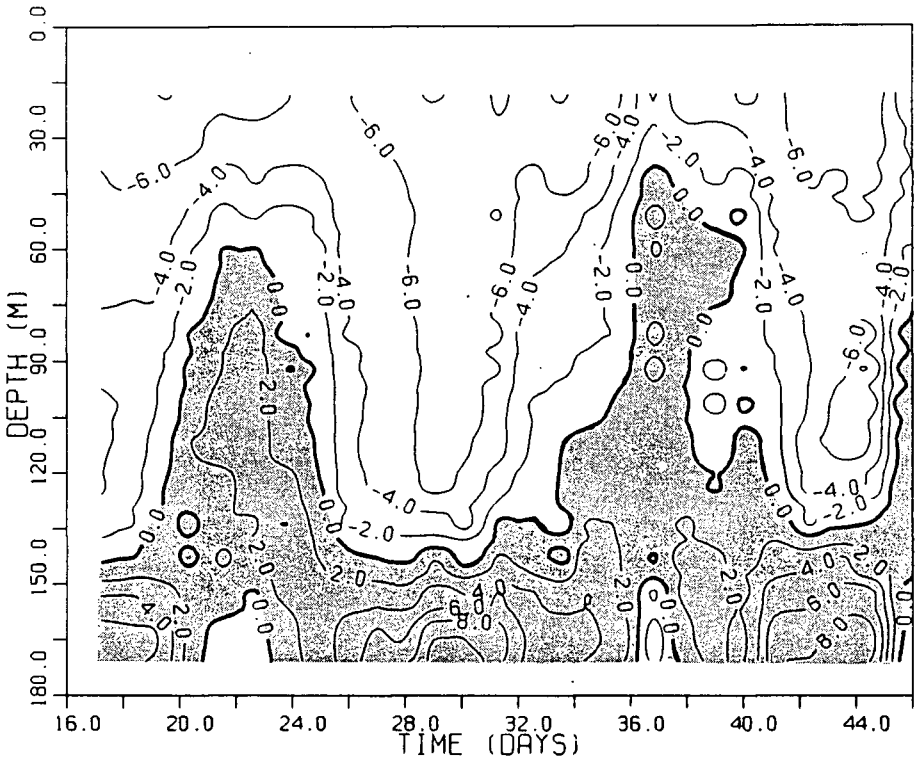

Figure 40 Contours of the along-channel current (in $cm\,s^{-1}$) at the basin station (C3) in 1985. The data have been averaged over 25-hour intervals. Time is in Julian days from the start of 1985 (corresponds to days 382-412 of *Figure 39*). Up-inlet flow is shaded.

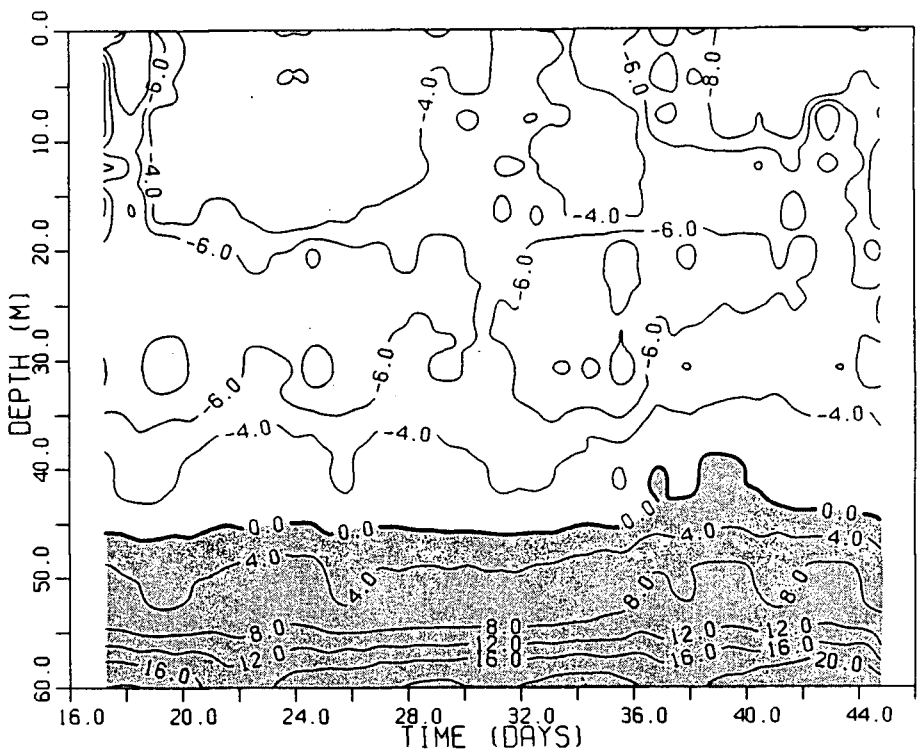

Figure 41 Contours of the along-channel current (in $cm\,s^{-1}$) at the sill station (C1) in 1985. The data have been averaged over 25-hour intervals. Time is in Julian days from the start of 1985 (corresponds to days 382-412 of *Figure 38*). Flow into the basin is shaded.

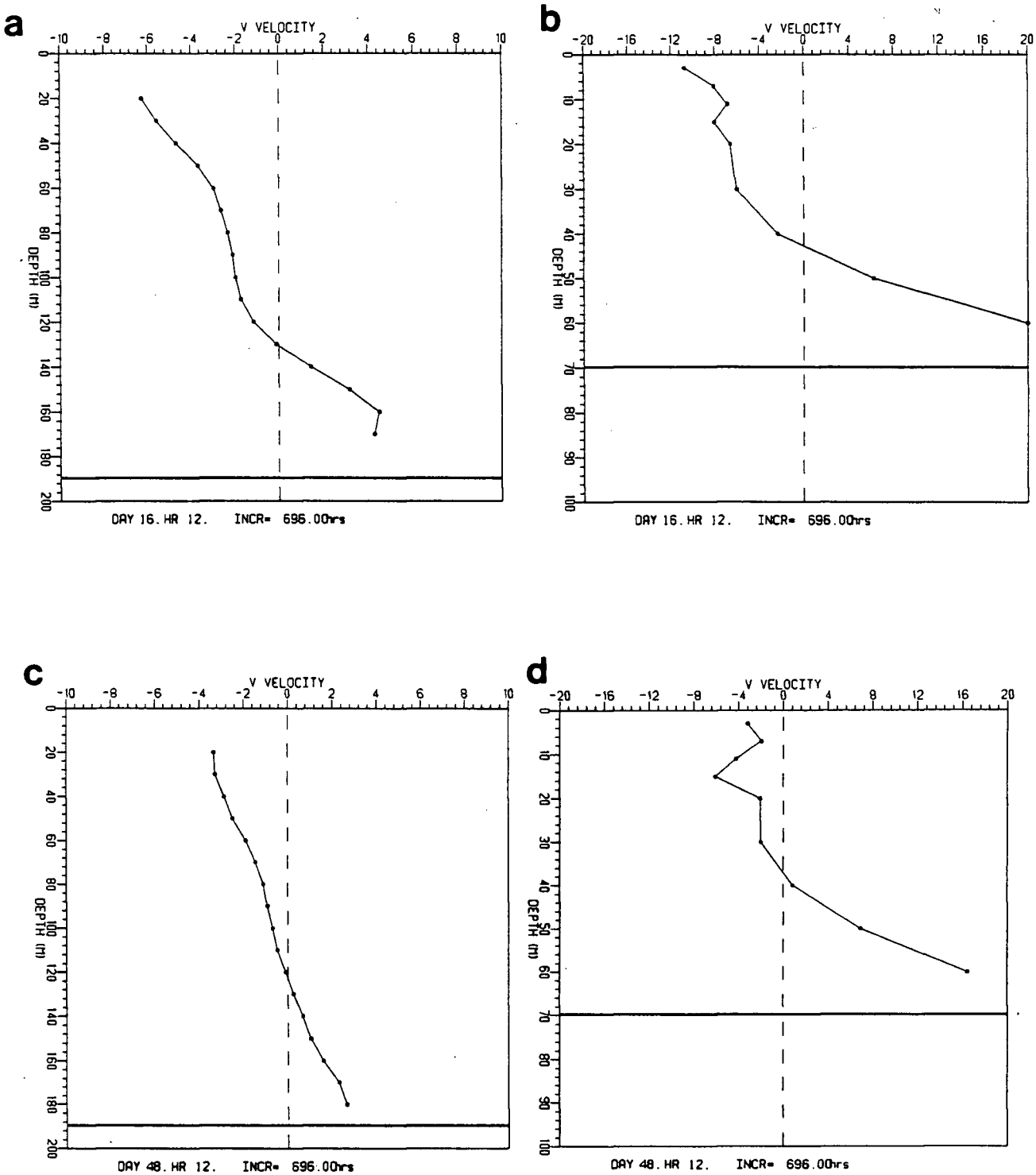

Figure 42 29 day averages of the along-channel current at the sill and in the basin. The first averages (a and b) begin at day 16 (1985), the second (c and d) at day 48(1985). Data from the sill (b and d) include Aanderaa current meter data from station CS interpolated to the sill station (C1). The basin data are from the cyclesonde at C3 for the first period (a) and from C4 for the second period (c). All currents are in $cm\,s^{-1}$.

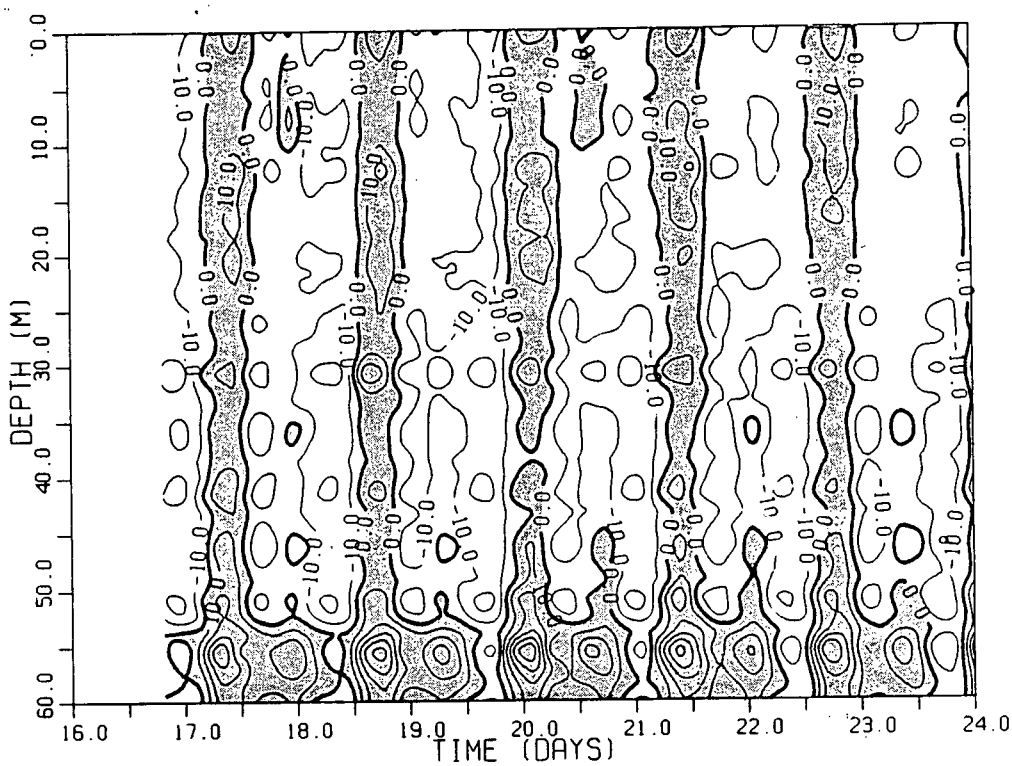

Figure 43 Contours of the raw along-channel current (in $cm\,s^{-1}$) at the sill station (C1) in 1985. The sampling interval for the data is approximately 1.5 hours. Time is in Julian days. The inflows are shaded.

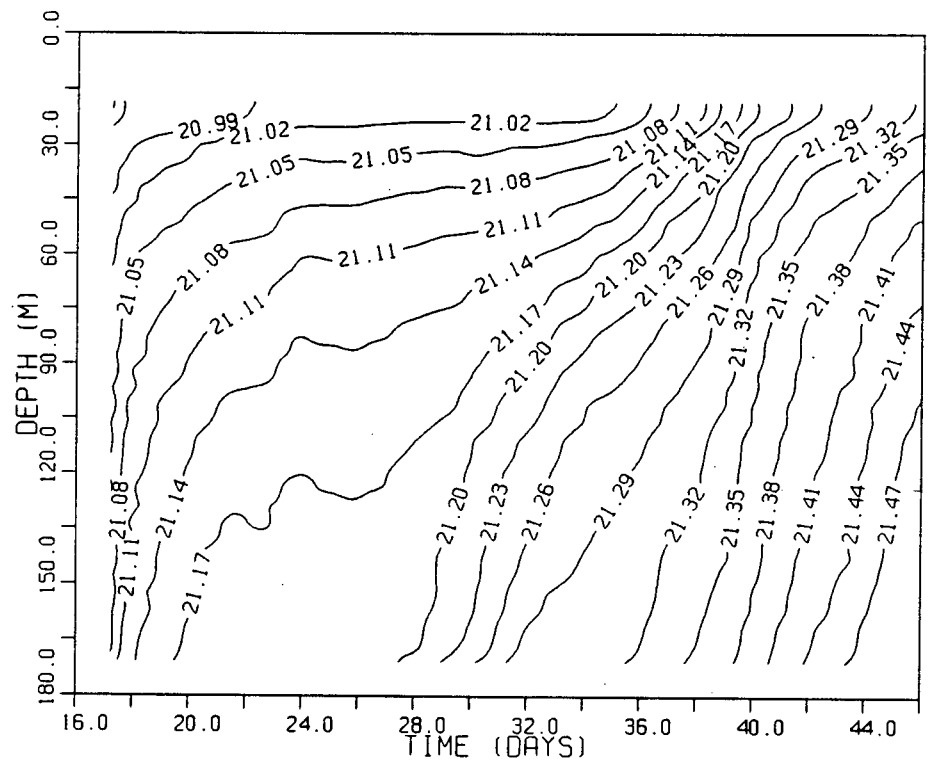

Figure 44 Sigma-t, averaged over 25-hour intervals, at the basin station (C3) in 1985. Time is in Julian days.

(days 48 – 77). Inflow did occur, however, at the end of the second period so there is some contamination of this record by an inflow (see *Figure 38*). Nevertheless, the two periods do make possible some comparison between the average flow conditions during and after an inflow.

Figures 42a and 42b show the 29-day average of the along-channel current in the basin and at the sill for the first record. A 29-day average was chosen to remove not only the shorter period tides, the semi-diurnal and diurnal, but also the longer period tides such as the MSf (14.7 days) and the Mm (27.5 days). The effects of the inflow are apparent both at the sill and in the basin. At the sill (*Figure 42b*) the velocity shows a linear increase towards the bottom from a depth of 40 m indicating the weak effects of bottom friction at the deepest point 60 m. Both at the sill and in the basin, the zero-crossing is found approximately two-thirds the way from the surface, at $\sim$ 130 m depth in the basin and $\sim$ 45 m at the sill. The velocity generally increases from the zero-crossing point to the surface at both stations.

In the second record (days 48 – 79), when much less inflow occurred, the 29-day averaged flow shows the same basic pattern (see *Figures 42c and 42d*). The zero-crossings at the sill and in the basin have not moved much and the general shape of the curves is the same as it was for the earlier averages (*Figures 42a and 42b*). The amplitude of the along-channel current is noticeably reduced from the first record, by about a factor of two at the basin station. At the sill the bottom velocity is reduced, but by much less.

A contour plot of the raw data at the sill (*Figure 43*) indicates how the tidal flow changes there. Because the data are at 10 m depth intervals, some of the closed contours shown in *Figure 43* must be interpreted with care. On strong flood tides there is inflow from the top to the bottom. On weak ebbs and floods, there is inflow below 50 m depth, stronger on the flood than on the ebb, with outflow above. On strong ebb tides there is outflow from the top to the bottom. The figure shows that the flow is in phase during strong flood and ebb tides. These observations are in accord with those of Pickard and

Rodgers (1959) in Knight Inlet where the observed flow at the sill was in phase from top to bottom.

With such large volumes of water entering the fjord, it is expected that the stratification will change quickly. *Figure 44* shows a contour plot of the density in February 1985. During the strong inflows, at the beginning and end of the record, there is almost no stratification below $60\,m$. At other times (days 20-28), there is a considerable stratification to $130\,m$ depth. This changing stratification will be important when the internal response of Indian Arm is investigated in Chapter 5.

4.5 Control of the Exchange

Control of the deepwater exchange in Indian Arm depends on a variety of factors. The first condition requires that water of sufficient density be available outside the sill at First Narrows. This water must then make it over the sill and into Burrard Inlet. Control of the exchange can still be exerted in the area between First Narrows and the Indian Arm sill where either hydraulic control or friction can control the exchange of water from outside the sill to inside the basin. A discussion of the control of Indian Arm will be given in this section. Because of a lack of data in the Burrard Inlet part of the system, the conclusions will be tentative. Future work might serve to resolve some of these problems.

Much work has been done on the nature of hydraulic control of flow in channels (see Turner, 1973). The first such work in estuaries was by Stommel and Farmer (1952, 1953) who looked at the effect of an abrupt change in the channel width on the flow. Farmer and Armi (1986) show that the application of Stommel and Farmer's results to maximal two-layer exchange over a sill is incorrect. They show that either the sill or the contraction may act as the control with different results in each case. Farmer and Armi (1986) also discuss the effects of barotropic flow on the exchange process.

In Indian Arm, which has three sills (First Narrows, Second Narrows and the Indian Arm sill, see *Figures 1 and 2*) and three contractions, the control of the exchange might be expected to be complex. Adding to the complexity is the fact that the third contraction,

that near the Indian Arm sill, is about $1 - 2\,km$ away from the sill. Some arguments can be made, however, that not all of Burrard Inlet is important in determining the control of the exchange with the basin.

Figure 45 shows a schematic of the exchange system as described by Farmer and Armi (1986), whose theoretical development shall be followed here. The flow will be considered to be two-layered. Such an assumption is not always valid in Indian Arm, but may not be a bad assumption for the exchange problem where there is inflow of dense water and outflow of less dense basin water. The source of the dense water (Burrard Inlet) is on the right, with the basin (Indian Arm) on the left. The flow is said to be critical (Turner, 1973) when

$$G^2 = F_1{}^2 + F_2{}^2 = 1 \quad , \tag{4.7}$$

where $F_i{}^2 = U_i{}^2/g'y_i$ is the densimetric Froude number for layer i, U_i is the flow speed, y_i is the layer thickness and $g' = g\Delta\rho/\rho_2$ is the reduced gravity ($\Delta\rho = \rho_2 - \rho_1$). The upper and lower layers are indicated by the subscripts 1 and 2.

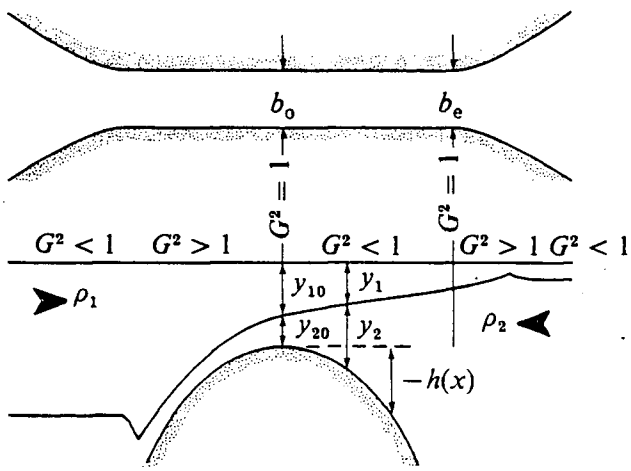

Figure 45 Schematic for maximal two-layer exchange over a sill.

In their discussion of the flow over a sill, Farmer and Armi (1986) use the Bernoulli equations and the Froude number for each layer. They write the combined Bernoulli

equations in terms of the Froude numbers. They show that the interface height at the sill for maximal exchange, when the flow is supercritical on either side of the sill, is about 0.375 times the sill depth. If the flow is supercritical on only one side, the reservoir on that side can exert no control on the exchange.

Figure 21 shows the density in the basin on a tide which was just beginning to flood. The 21.0 isopycnal, which runs from outside Second Narrows to inside the basin, looks much like the interface trace presented in the schematic of *Figure 45*. The dip in the isopycnal on the far side of the sill can be explained as a hydraulic jump as the flow reverts to subcritical from supercritical. A calculation of the lower layer Froude number at the sill cyclesonde station shows it to be, ${F_2}^2 \geq 1$ (if $\Delta\rho \sim 0.2$ and $U \sim 0.4\, m\, s^{-1}$); thus the conditions for supercritical flow on one side of the sill are met. At Second Narrows where the flow is greater than $1\, m\, s^{-1}$, it is expected that the flow should be supercritical in spite of the stronger stratification there. Supercritical flow at these two points simplifies the analysis since it means that only the area between Second Narrows and the sill will be important in controlling the exchange.

The effect of the barotropic tide on the exchange process is also considered by Farmer and Armi (1986) who define a dimensionless barotropic speed U_0 which is scaled by $\sqrt{g'(y_1 + y_2)_0}$. In Indian Arm U_0 is about 1 in the neighbourhood of the sill and thus the schematics of *Figure 46b to 46g*, taken from Farmer and Armi's barotropic analysis, should apply here in Indian Arm. These diagrams are based upon the solutions to the combined Bernoulli equations in the upper and lower layer with an imposed barotropic flow. As the tide moves from weak to strong flood (from d to h in *Figure 46*) the dense water moves over the sill forcing the upper layer Froude number in the basin of Indian Arm to zero. At maximum flood over the sill, there is only a single layer flowing over the sill. On ebb tide (from d to b in *Figure 46*), the water from the basin forces its way over the sill eventually establishing single layer flow over the sill in the opposite direction. *Figure 43* supports this interpretation. On flood tide all of the flow is directed into the basin. On ebb tide the flow is arrested, though on weak ebbs the flow is not always arrested all the

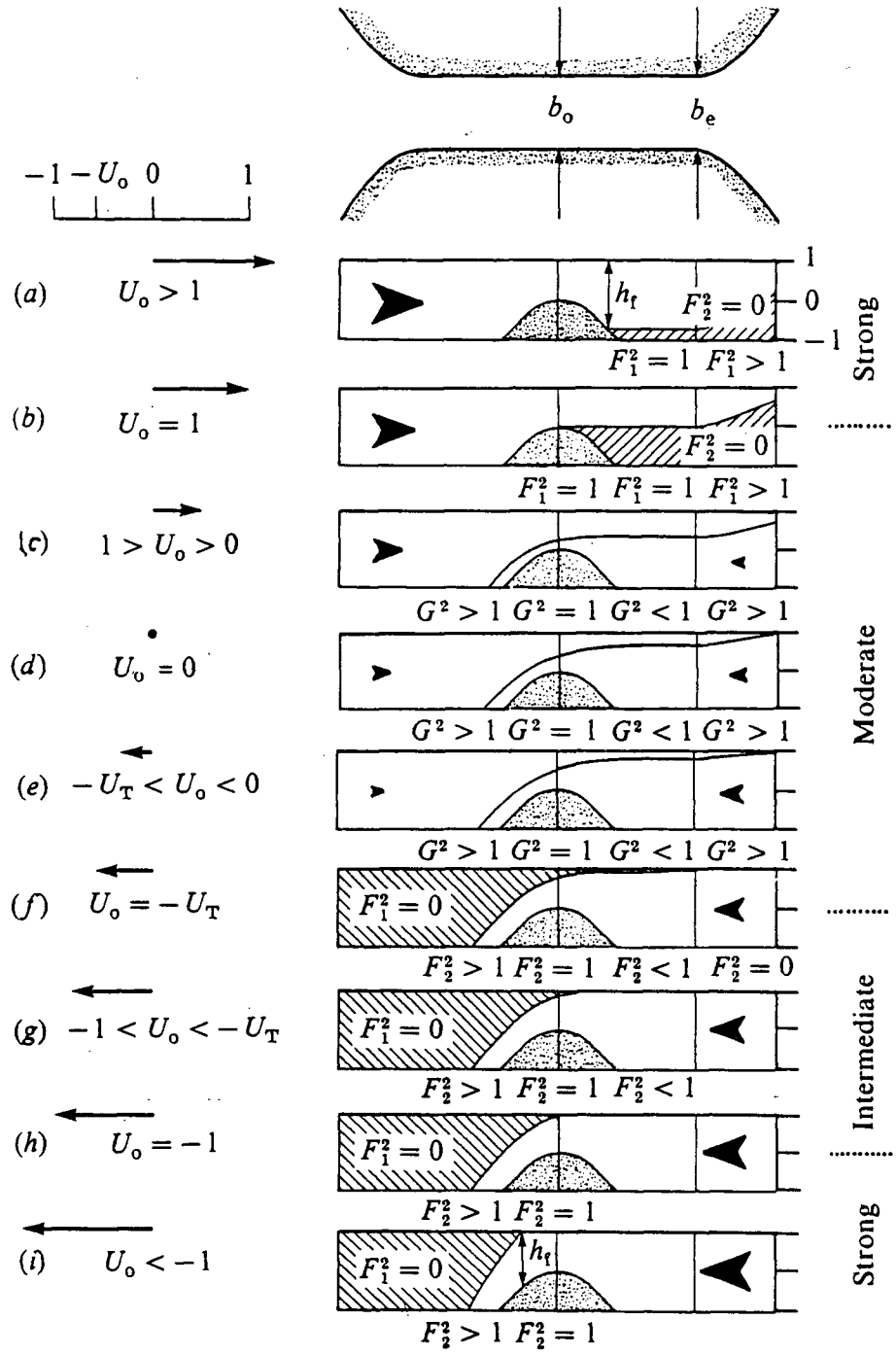

Figure 46 Schematic for the exchange over a sill with a barotropic flow. The dimensionless barotropic speed U_0 is indicated at left. In Indian Arm U_0 is about 1. From Farmer and Armi (1986).

way to the bottom. In comparing these observations to the theory, it must be remembered that the data in *Figure 43* are from just inside the sill, about 30 m below sill depth at the bottom.

This brief comparison suggests that the theory of Farmer and Armi (1986) may be applicable to the Indian Arm exchange problem. The contractions in Indian Arm have been ignored in this discussion. In reality they may play an important part in controlling the exchange. Better information about the flow, and the Froude numbers , in the sill region are required to determine how important all these various factors might be. For two-layer flow, both bottom and interfacial friction must also be considered in determining the nature of the control. The influence of friction in long straits has been treated by Assaf and Hecht (1974), however, there is not enough information available here to apply their theory. If the flow at Second Narrows is supercritical then the rest of Burrard Inlet inlet may be ignored. Only the 8 km from Second Narrows to the basin of Indian Arm would then be important. Over such a comparatively short distance, friction may not be important in controlling the exchange. Numerical modeling, which applies reasonable friction coefficients at the bottom and at the interface between the two layers, may help to resolve the problem.

4.6 Transport Estimates

There are many difficulties with estimating the transport in a fjord, even in a system as simple as a channel leading into the fjord. Measurements from the top to within 10 m of the bottom were made at the sill but there is a lack of surface measurements in the basin. The measurements at the sill do not extend all the way to the bottom. *Figures 42b* and *42d* suggest that the maximum flow speed and density near the bottom have probably not been measured. There is the further problem of cross-inlet variability. No measurements were made across the channel so it is impossible to estimate the effect of this factor. It is recognized, however, that sidewall friction and topographic effects may be important in determining the extent of any variation across the channel. With these problems in mind, I shall press on and estimate the transport as best as possible using the available

measurements.

In this section an estimate of the transport and volume of the exchange events of 1984/85 will be made. The sill record (*Figure 38*) does not differentiate the inflow periods clearly enough to allow determination of the length of the inflow. The sill data will be useful, however, in determining the transport since it is at the sill that the inflowing water enters Indian Arm. The duration of the exchange events can be determined from the basin data (*Figure 39*) which clearly shows when the exchanges occurred. It is not possible to judge the transport of the exchange from the basin data because of entrainment into the flow which occurs when the dense water moves down the slope from the sill into the basin.

Table 10
Period of duration, speed and thickness, transport and % volume of Indian Arm bottom water during renewal events of 1984/85

Period (Julian days)	*Speed at C1 cms^{-1} (Thickness (m))*	*Transport m^3s^{-1}*	*% of Indian Arm Volume*
380 – 386	14 (25)	700	16
390 – 400	14 (25)	700	27
405 – 410	16 (25)	800	15
435 – 443	14 (25)	700	22

Table 10 shows the estimated characteristics of the four main inflow events which occur during the the winter of 1984/85. The data given in this table were estimated from the analysis of *Figures 38 and 39* in which the current at the sill and the basin are shown. Because some inflow at shallower depths will take place between these episodes, these results will underestimate the total exchange during 1984/85. The duration of renewal varies from 5 – 10 days in length. Flow speeds at the sill are fairly constant during the renewal, although this is not true in the basin where a distinct peak can be seen. As the tidal energy decreases during the renewal, the density increases and the speed of the density current flow into the basin reaches a maximum.

The vertical resolution of the current data at the sill is such that the estimated average thickness of the flow is not well known. The current data in *Figure 38* do indicate, however, that this thickness does not change much in the early winter of 1985. The average thickness

is about $25\,m$. The speed in *Table 10* is an average taken over the inflow. The width of the channel, which is U-shaped at station C1 (see *Figure 6*), was determined from bathymetric charts. The mean width over the inflow was $200\,m$. Above the inflow the mean width was $500\,m$. Taking into account the ratio of the cross-sectional areas, it can be seen that to maintain continuity the return flow need only have been $\frac{25(200)}{45(500)} = 0.22$ times the inflow speed. *Figures 42b and 42d* show that the measured speed, averaging about $5\,cm\,s^{-1}$, is close to the expected speed of $3\,cm\,s^{-1}$. The percentage volume estimates show that nearly all of the water in Indian Arm was exchanged during the 1984/85 winter. About one-fifth of the inlet was overturned during each exchange event.

The inflow of the water down the slope will take place as a density current (Ellison and Turner, 1959; Benjamin, 1968; Bo Pedersen, 1980). The density difference provides the negative buoyancy force that drives the flow down the slope. Three other factors control the flow speed: (1) the thickness of the flow, (2) the angle of the slope and (3) the friction the current feels (both at the bottom and the top of the layer) as it moves down the slope. The equation describing this relationship has been derived by a number of workers (for example Bo Pedersen, 1980):

$$U = \left(\frac{g\left(\frac{\rho' - \rho}{\rho'}\right) h \sin\beta}{\frac{f}{2}} \right)^{1/2} \tag{4.8}$$

where h is the flow thickness, g the acceleration due to gravity, β the angle of the slope, ρ' the density of the inflow , ρ the density of the overlying water and f/2 the dimensionless friction parameter. From the January 1985 CTD survey $\Delta\rho \approx 0.1\,kgm^{-3}$, the bottom slope is 0.0185 and from an earlier analysis h is about $25\,m$. In his review of the literature, Bo Pedersen (1980) estimated the dimensionless friction parameter $f/2$ to span the range $2 \times 10^{-3} < f/2 < 3 \times 10^{-2}$. Substituting into equation (4.8) one finds that U should span the range $12 < U\,(cm\,s^{-1}) < 46$ (depending upon the friction coefficient), in good agreement with the observations.

Close inspection of the current and sill velocities indicates that the basin velocity lags the sill velocity by as much as one day. This is consistent with a velocity of the density

current down the slope of 10 $cm\,s^{-1}$. As the density current penetrates deeper into the fjord, the density difference may decrease and thus a slower speed might be expected.

5. The Internal Tide

5.1 Introduction

The energy transfer to the internal tide from the barotropic tide is important because the energy remains in the fjord; the shallow sill effectively traps the energy (Robinson, 1969). Relatively little energy is lost via friction in the transfer process (Freeland and Farmer, 1980). Energy from the barotropic tide may also go into high frequency internal waves, a topic to be discussed in the next chapter.

Most of the energy in the internal tide will turn into heat. Turbulent mixing processes are inefficient so that nearly 90% of the energy of the internal tide will be converted into thermal energy (Osborn, 1980). The remaining 10% is enough to drive many important processes in the fjord. Diffusion in the fjord is controlled by turbulent processes, the energy level of which has been proposed as being controlled by the internal tide (Stigebrandt; 1976, 1980). Trapping of the internal tidal energy in the upper part of the water column may be important in driving the estuarine circulation via critical layer absorption such as occurs in the atmosphere.

An internal tide is generated by the interaction of the barotropic tide with a bump in a stratified fluid. In Indian Arm the bump is the sill which separates the basin from the Strait of Georgia. A number of factors influence the nature of the internal tide which propagates away from the sill. The energy level of the barotropic tide will be important since it provides the forcing for the internal waves. The combination of the various tidal constituents leads to a variable barotropic tidal velocity at the sill. The stratification of the fluid over the sill is also important and changes in response to the tide, wind and freshwater runoff.

After generation, the propagation of the internal tide is determined by the nature of the medium. Stratification will influence the angle, relative to the horizontal, at which the waves travel. If there is a mean flow, the frequency of the waves may be shifted. In general, the group velocity of the internal tide is low enough that this Doppler shift can be

important, as is indeed the case in Indian Arm (see Chapter 3). The group velocity of the barotropic tide is large enough for most geophysical flows that this effect will be negligible.

As the internal tide propagates along the inlet, side and bottom friction will withdraw energy from it. If the amplitude is large enough, nonlinear interaction may lead to energy transfer between the different internal tides generated. When the internal waves reach the head, the bottom slope and stratification will determine whether reflection or wave breaking will occur. Nonlinear effects may also be important at the head if the amplitude of the internal tide is sufficiently large.

In this chapter the focus will be on the generation of both the M_2 and K_1 baroclinic tides. Both of the M_2 and K_1 barotropic tides are large in Indian Arm, each having a surface elevation of about $1\,m$. In most previous studies either the diurnal or the semi-diurnal constituent was investigated, whichever was dominant. In this chapter it will be shown that the internal response, of either or both of these constituents, may be large and that the response changes with time.

In section 5.2 the current meter data will be presented to illustrate the nature of the internal tide. Harmonic analysis of these data will be presented to describe the M_2 and K_1 tides. In section 5.3 an analysis of the energy lost from the barotropic tide will be made to determine how much energy is available to the internal tide. In 5.4 the forcing function will be discussed and plotted. In 5.5 plots of the ray paths are given. In 5.6 the general theory of modal decomposition will be presented, and in 5.7 a computation of the resonance period of Indian Arm is made. The fitting of the modes to the cyclesonde data will be discussed in 5.8; followed, in the penultimate section, by a review of the results of this chapter and a comparison between the observed energy levels and those predicted by theory. A brief discussion of the major points of the chapter will be given in section 5.10.

5.2 Cyclesonde data and harmonic analysis

The internal tide appears in the current meter data as a variation in velocity with depth and as large excursions of the isopycnals (much larger than the amplitude of the surface tide). In *Figure 47* contours of the isopycnals in January 1984 are plotted. Excursions of greater than $15\,m$ are apparent around day 21 with a strong depth dependency visible. The vertical change of the excursions will depend upon the variation of the vertical velocity with depth, which in turn depends upon the modal structure.

Over the two week period plotted in *Figure 47*, there is a shift in the type of internal tide exhibited. From days 14–19, there is a semi-diurnal internal tide with an amplitude of $5 - 10\,m$ at the 20.90 isopycnal, centered at about $90\,m$ depth. After day 20, the internal tide appears to be predominantly diurnal in nature with an amplitude of $10 - 15\,m$, a noticeable increase in the amplitude. From inspection of a plot such as this one, it is difficult to pick out the modal structure since many modes may be present at a single time. Such a task is also difficult because of the changing internal response. It is clear from *Figure 47* that the internal response can change over a period of days or less.

Harmonic analysis of the data was carried out as discussed in section 3.4. This technique yields an amplitude and phase for each of the tidal constituents at depth intervals of $10\,m$. In this chapter, the discussion shall be limited to the M_2 and K_1 tides since these two frequencies are the most energetic in Indian Arm. Phase plane plots for the three winters of data are presented in *Figures 48–53*. These plots show the amplitude and phase of the tide. The amplitude is given by the distance to the origin, the phase by the angle from the x axis.

The plots for 1982/83, *Figures 48 and 49*, show that in general the M_2 tide is stronger than the K_1 at a given station. As one would expect the amplitude at the sill is greater than that in the basin. The difference in the amplitude ratio of the M_2 and K_1 tides is different from the sill to the basin possibly indicating a stronger internal response at the K_1 frequency to a weaker driving force.

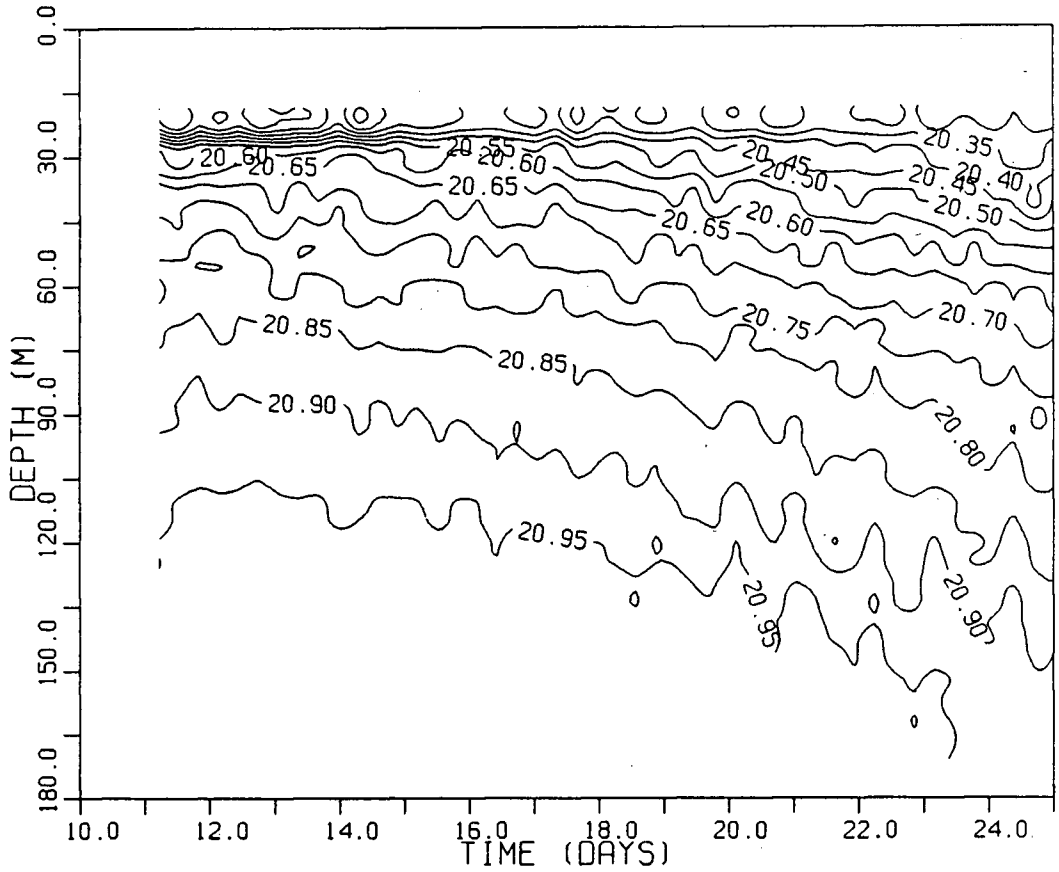

Figure 47 Contours of σ_t at the basin station (C3) in January 1984. The sampling interval for the data is approximately 3 hours. Time is in Julian days from the start of 1984.

Another difference between the sill and the basin plots in 1982/83 lies in the shapes of the curves. If all of the points coalesce to a single point, indicating no variation in amplitude or phase with depth, then no internal tide is present. If a straight line is produced then just a single mode is present; if a curve is produced then more than one mode is present. All of the sill plots, save for the K_1 plot in December 1982, are almost straight lines indicating that only one mode is present. In the basin the plots are more complex. Most of the curves form half-circles, indicating that more than one mode is present. There is some variation from month to month in 1982/83, more in the basin than at the sill, but the position and general shape of the curves does not change drastically.

The plots for 1983/84 are presented in *Figures 50 and 51* . The structure at the sill is somewhat confused, changing from month to month. Once again, however, the M_2 tide is

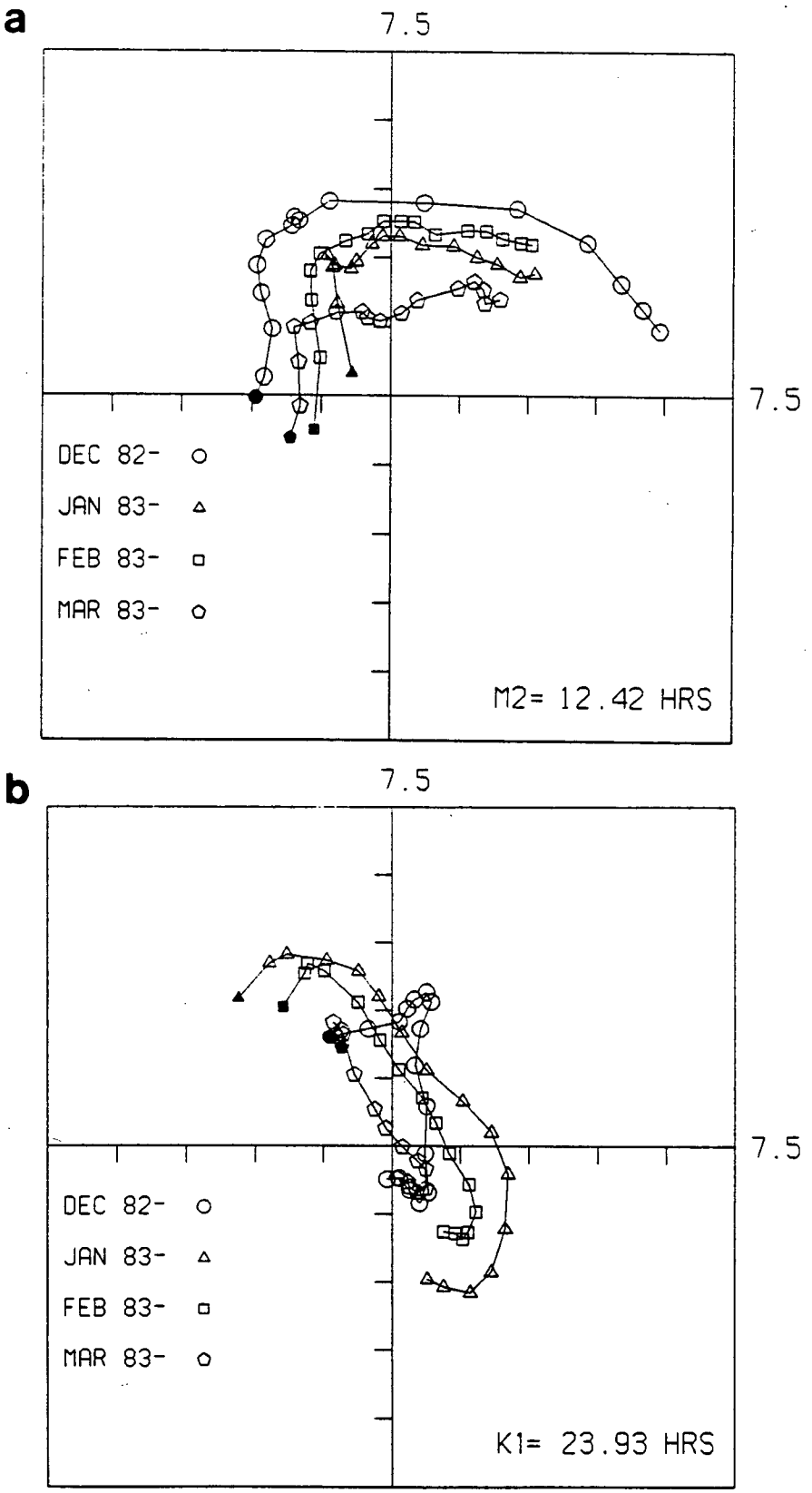

Figure 48 Phase plane plots of the M_2 (a) and K_1 (b) tides in 1982/83 at the basin station (C3). The velocity scale is in $cm\,s^{-1}$. The solid marker is at $20\,m$ depth with other points at $10\,m$ depth intervals.

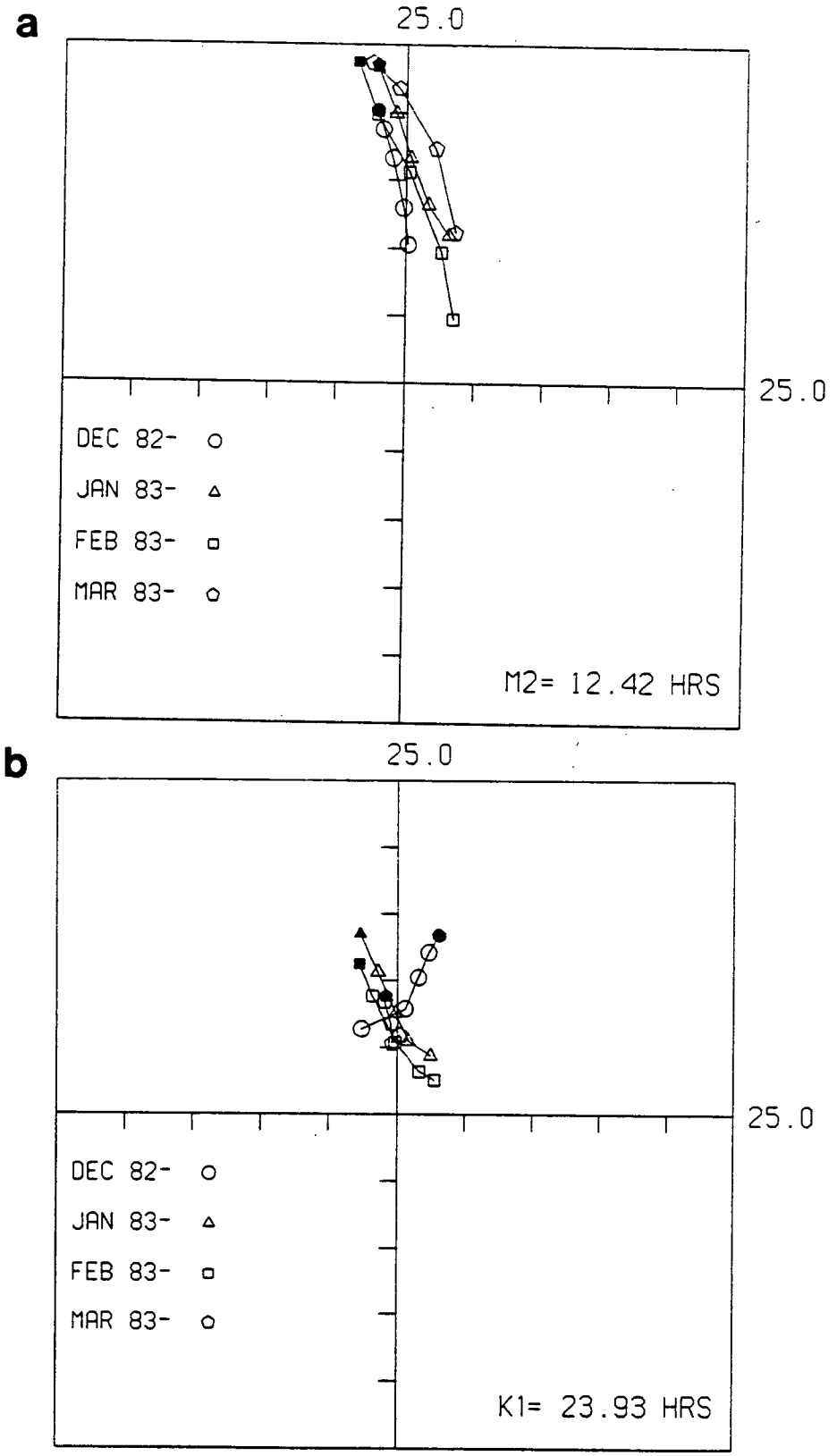

Figure 49 Phase plane plots of the M_2 (a) and K_1 (b) tides in 1982/83 at the sill station (C1). The velocity scale is in $cm\,s^{-1}$. The solid marker is at $20\,m$ depth with the other points at $10\,m$ depth intervals.

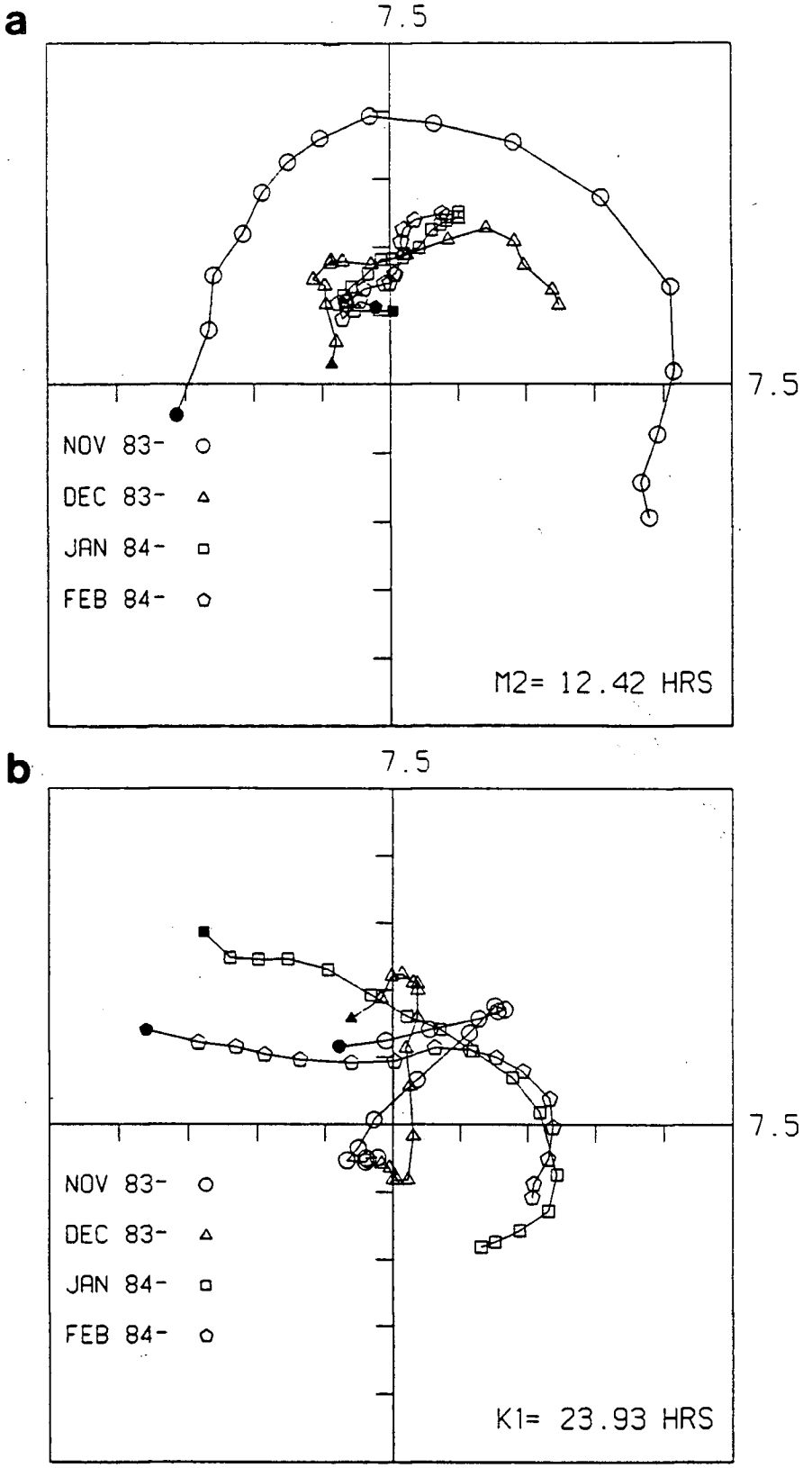

Figure 50 Phase plane plots of the M_2 (a) and K_1 (b) tides in 1983/84 at the basin station (C3). The velocity scale is in $cm\,s^{-1}$. The solid marker is at $20\,m$ depth with the other points at $10\,m$ depth intervals.

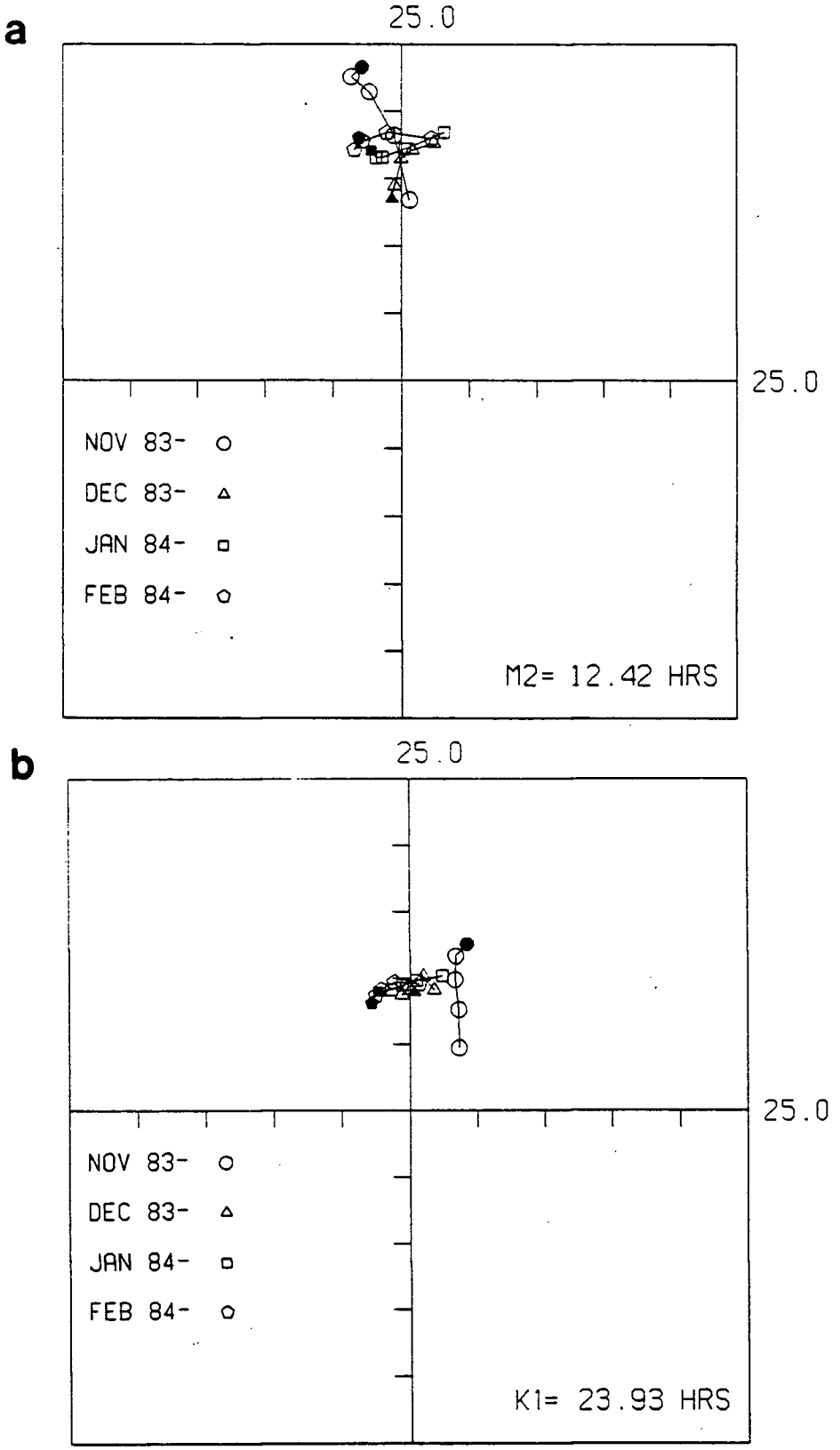

Figure 51 Phase plane plots of the M_2 (a) and K_1 (b) tides in 1983/84 at the sill station (C1). The velocity scale is in $cm\,s^{-1}$. The solid marker is at $20\,m$ depth with the other points at $10\,m$ depth intervals.

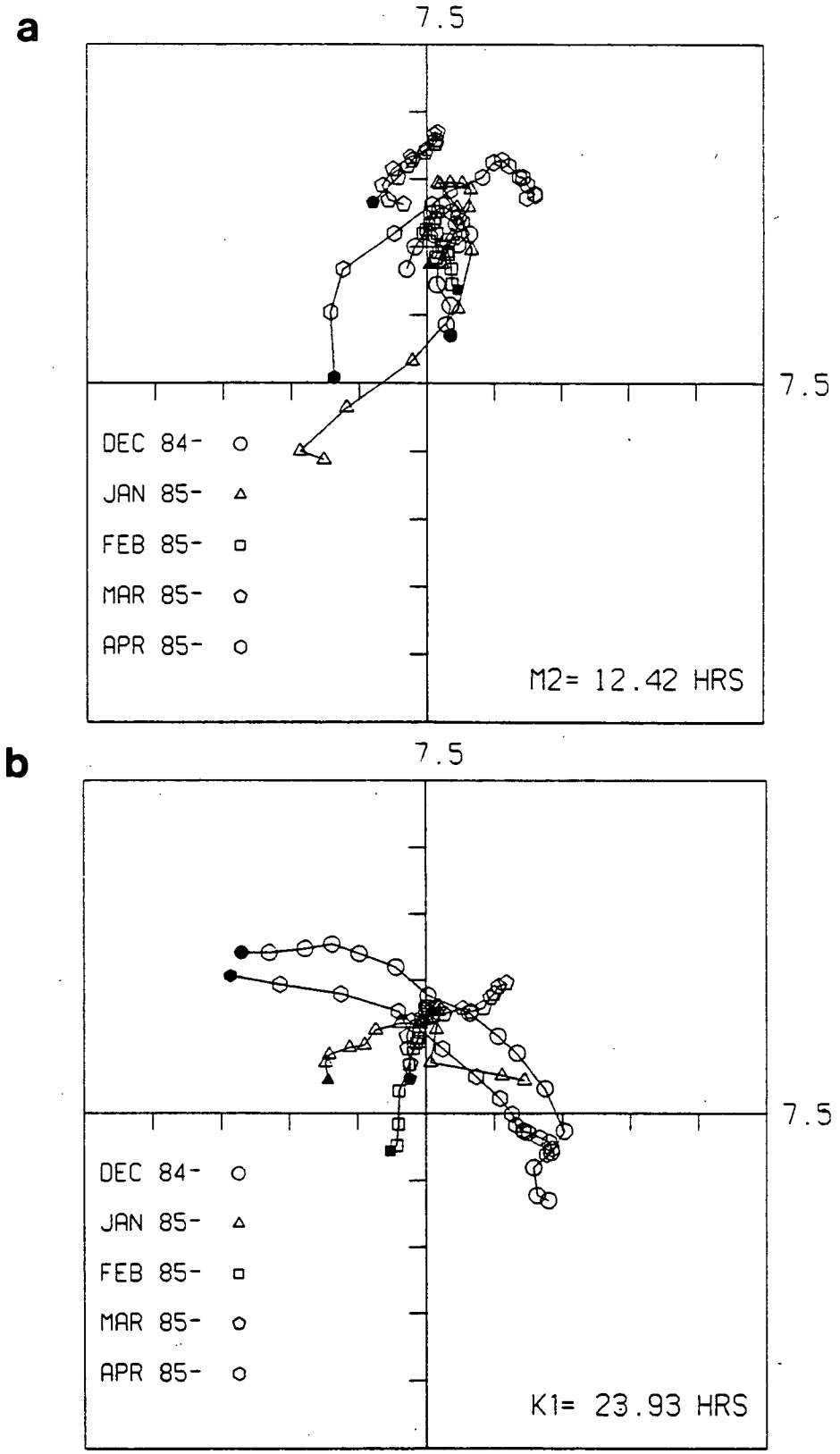

Figure 52 Phase plane plots for the M_2 (a) and K_1 (b) tides in 1984/85 at the basin station (C3). The velocity scale is in $cm\,s^{-1}$. The solid marker is at $20\,m$ depth with the other points at $10\,m$ depth intervals.

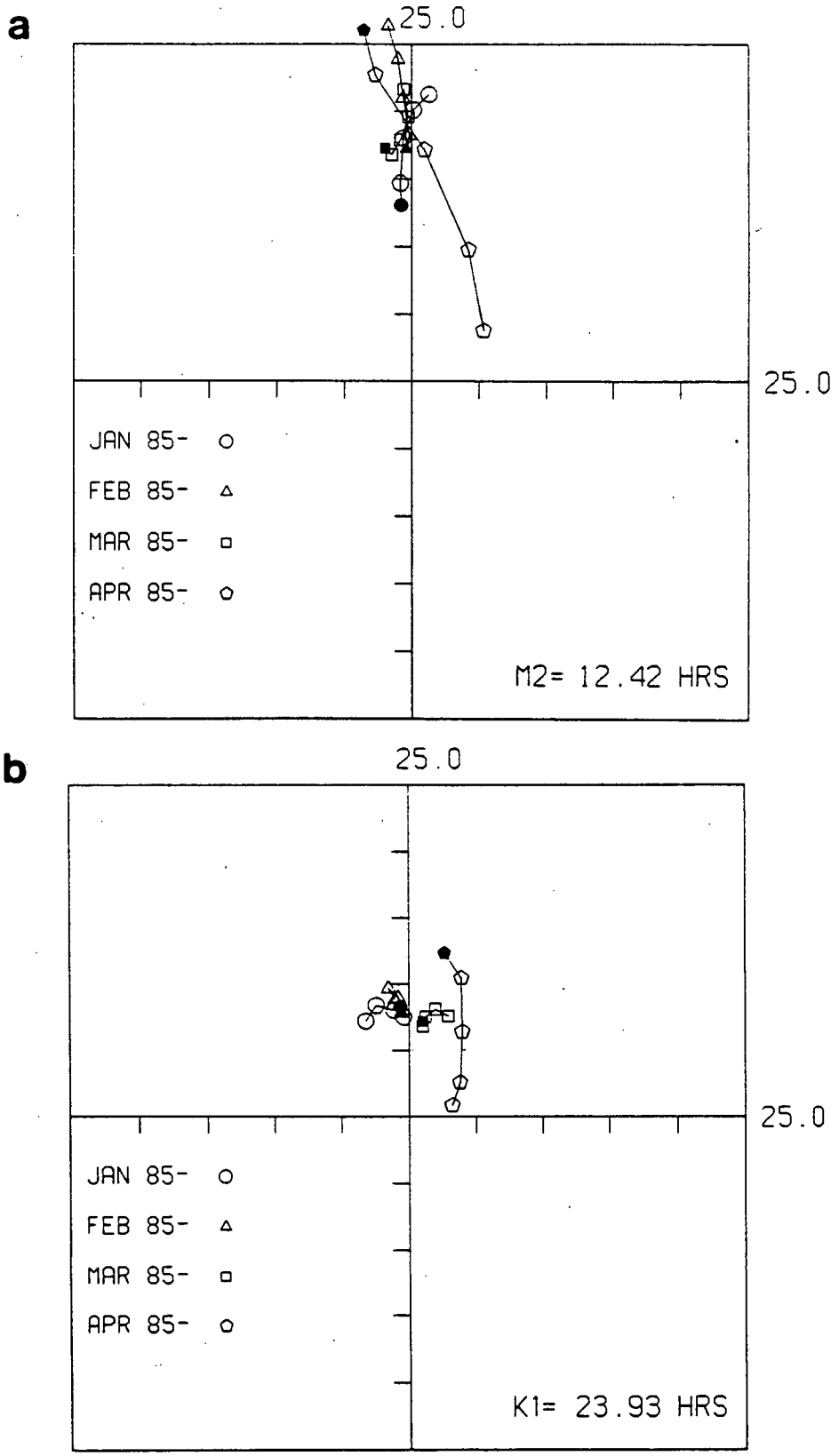

Figure 53 Phase plane plots for the M_2 (a) and K_1 (b) tides in 1984/85 at the sill station (C1). The velocity scale is in $cm\,s^{-1}$. The solid marker is at $20\,m$ depth with the other points at $10\,m$ depth intervals.

stronger than the K_1. The structure in the basin is interesting, though a little difficult to disentangle from these plots. The M_2 response is strongest in November and December, with a distinct crescent shape to the curve. In November and December, the K_1 tide is weakest and shows no clear internal response. In January and February the K_1 plot shows the same crescent shape as did the M_2 earlier. The M_2 no longer shows this lunate shape in January and February. The system has gone from a predominantly M_2 internal response to a predominantly K_1 internal response.

The plots for 1984/85 are shown in *Figures 52 and 53*. The curves in the basin are quite confused. As in 1982/83, all the points from near the top of the mooring (at $20\,m$ depth) are clustered together. At the K_1 frequency, the response seems the same in December and January though this does not hold for the M_2. The M_2 is stronger than the K_1 at the sill (*Figure 53*), as was observed for most of the time during the previous winters. Once again there also appears to be only a single mode present at the sill.

These three winters of data show that there can be significant month to month variations in the internal response at the M_2 and K_1 frequencies. The most striking case of such a change occurred in 1983/84, when there was a shift from a strong M_2 internal tide in November-December to a strong K_1 internal tide in January-February. *Figure 54* shows the baroclinic energy summed over 16 depths in the basin. The barotropic tide was computed from the basin geometry, the tidal height amplitude and by invocation of continuity. The computed barotropic velocity was removed from the signal and the baroclinic velocity calculated. *Figure 54* shows that the M_2 is much stronger than the K_1 in November and December. There is a change in January and February, with the K_1 internal tide finally emerging as the most energetic. This shift is consistent with the contour plot of density at the sill (see *Figure 47*), which shows a shift from a semidiurnal to a diurnal response at about the same time. Such a shift from a semidiurnal to a diurnal tide has not been documented before.

An analysis of the 1983/84 data and an explanation for this shift in internal response

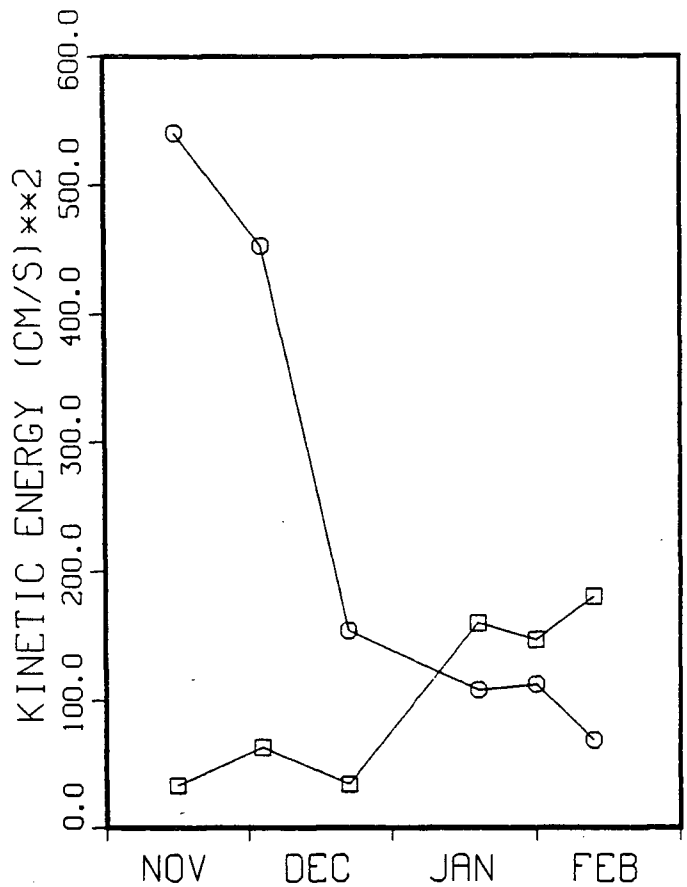

Figure 54 Baroclinic kinetic energy in 1983/84 at the basin station (C3). The K_1 (□) and the M_2 (○) tides are plotted.

will take up the rest of this chapter. Some analysis of the 1984/85 cyclesonde data will be presented but the 1983/84 data set will be at the centre of attention.

5.3 Determination of the Dissipation from tidal height data

The most sensitive measure of the energy lost from the barotropic tide lies in the phase change of the surface elevation as the tide propagates along the inlet. Friction and energy transfer to other processes slow the barotropic tide causing a phase change. An analysis of tidal height data will permit the investigation of the energy lost in the Indian Arm system. Both tide gauge and cyclesonde pressure data will be used in this analysis.

The net energy flux through any cross section in an inlet is given by (Garrett, 1975):

$$P = \int\int_{Area} \rho g < u\eta > dA \quad , \tag{5.1}$$

where ρ is the water density, g the acceleration of gravity and u and η the barotropic tidal velocity and height. The integration is over the cross-section of interest. The <> represents a time average of the velocity-tidal height term.

If there were no dissipation up-inlet of the section, then the tidal height and the velocity would be in quadrature. The time average of the $< u\eta >$ term would therefore be zero. Since there is dissipation, the velocity and the elevation are not in quadrature; however, measurement difficulties make it impossible to observe directly the deviation from quadrature. The change in the phase of the tidal elevation along the inlet , together with the continuity condition, do permit the evaluation of the integral in equation (5.1).

A schematic of the inlet is shown in *Figure 55.* The deviation from quadrature between the tidal height and velocity is represented by ε in *Figure 55.* Equations (5.2) and (5.3) give the tidal velocity and height at the start of the section.

$$u_1(t) = U_1 cos(\omega t - \varepsilon) \tag{5.2}$$

$$\eta_1(t) = \eta_0 sin(\omega t) \quad . \tag{5.3}$$

In the derivation to follow, it will be assumed that the tidal height (η_0) is a constant along the inlet. The energy withdrawn from the tide retards the tide; that is, it changes the phase, but does not greatly change the amplitude of the tide. Observations in Indian Arm show that the surface elevation is a constant to within about 5 % . The barotropic tidal velocity at any point can be found by invoking continuity to give:

$$U_{bt} = \frac{\eta_0 \omega S}{A} \quad , \tag{5.4}$$

where S is the surface area up-inlet and A is the cross-sectional area. Substituting equations (5.2) and (5.3) into (5.1) and making use of equation (5.4) one finds:

$$\begin{aligned} P &= \rho g U_1 \eta_0 A_1 < sin(\omega t) cos(\omega t - \varepsilon) > \\ &= \frac{\rho g U_1 \eta_0 A_1}{2} sin\, \varepsilon \\ &= \frac{\rho g {\eta_0}^2 S_1 \omega}{2} sin\, \varepsilon \quad . \end{aligned} \tag{5.5}$$

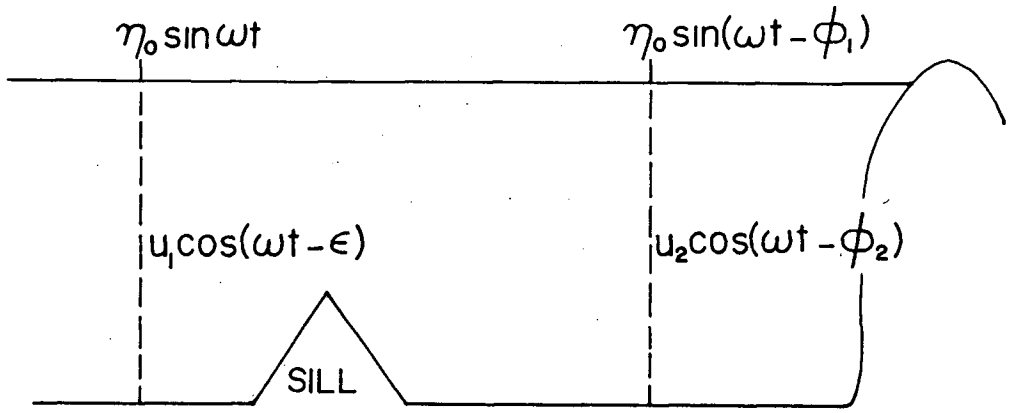

Figure 55 Schematic of Indian Arm for the tidal height analysis. The tidal height and velocity are shown at two points in the inlet.

To find the energy flux it is necessary to find ε. Freeland and Farmer (1980) provided the first derivation for ε. Stacey (1984) generalized their work by dropping the assumption that "all of the energy is lost between sections 1 and 2 ". Dunbar (1985) allowed for a change in the cross-section of the inlet between the ends of the segment. In this derivation a combination of these two generalizations will be presented.

The rate of change of water volume between the sections can be written in two forms.

$$\frac{\partial V}{\partial t} = A_1 U_1 cos(\omega t - \varepsilon) - A_2 U_2 cos(\omega t - \phi_2) \tag{5.6}$$

$$\frac{\partial V}{\partial t} = \frac{S_1 - S_2}{B_1 + B_2} \left(B_1 \frac{\partial \eta_1}{\partial t} + B_2 \frac{\partial \eta_2}{\partial t}\right) . \tag{5.7}$$

The subscripts denote the position of the measurement (see *Figure 55*). B is the breadth of the inlet at the section and U_1 and U_2 are the barotropic tidal velocities at the ends of the section. Freeland and Farmer (1980) assume that $\phi_1 = \phi_2$; Stacey (1984) assumes that $B_1 = B_2$. Here neither of these assumptions will be made. To solve these equations for ε, equation (5.6) is set equal to (5.7) and the cosine terms are expanded. Terms in $cos\ \omega t$ and $sin\ \omega t$ are then equated. In equation (5.7) it has been assumed that the channel width changes linearly along the inlet. This assumption is not particularly defensible, although it does greatly simplify the analysis.

Table 11
Physical Characteristics of the Indian Arm System

Station	S_i *AreaUp − Inlet* (km^2)	B_i *Width* (km)	A_i *CrossSection* (km^2)
Basin	14.56	0.595	0.1132
Sill	24.33	0.419	0.04978
Vancouver Harbour	50.51	3.040	0.0668
Point Atkinson	~ 56	~ 3	0.07

After equating the $sin\ \omega t$ and $cos\ \omega t$ terms one obtains

$$tan\varepsilon = \frac{S_2 sin\phi_2(B_1 + B_2) + (S_1 - S_2)B_2 sin\phi_1}{S_2 cos\phi_2(B_1 + B_2) + (S_1 - S_2)(B_1 + B_2 cos\phi_1)}$$

$$= \frac{S_2 sin\phi_2(B_1 + B_2) + sin\phi_1(S_1 - S_2)B_2}{S_2 cos\phi_2(B_1 + B_2) + (S_1 - S_2)B_2 cos\phi_1 + B_1(S_1 - S_2)} \quad . \tag{5.8}$$

Some simplification can be made if Farmer and Freeland (1980) are followed and $\phi_1 = \phi_2$.

$$tan\varepsilon = \frac{sin\phi(S_2 B_1 + S_1 B_2)}{cos\phi(S_2 B_1 + S_1 B_2) + B_1(S_1 - S_2)} \quad . \tag{5.9}$$

If it is assumed that ε and ϕ are small then equation (5.9) becomes

$$\varepsilon \approx \frac{\phi(S_2 B_1 + S_1 B_2)}{S_2 B_1 + S_1 B_2 + B_1(S_1 - S_2)} \quad . \tag{5.10}$$

If the further assumption is made that the width does not change then the simplest form for ε is obtained:

$$\varepsilon \approx \frac{\phi}{1 + \frac{S_1 - S_2}{S_2 + S_1}} \quad , \tag{5.11}$$

An attempt was made to use the general equation (5.10) to determine the phase shift and dissipation rates. It was found that more energy was lost in a small subsection than was lost in a larger section. Since this result is physically impossible, it indicates that the assumption of a linear change in the basin width is not acceptable in Indian Arm. For this reason, the most simplified relationship (5.11) is used; this equation assumes the inlet to be a constant width. This simplification changed the result by no more than 10 % for all of the sections, except for Vancouver Harbour to the basin, where the change was much greater.

It is now possible to find ε, given the geometry and change in phase along the inlet. *Table 11* shows the physical characteristics required for the calculation of ε from ϕ.

The Point Atkinson station, which is well outside Indian Arm and Burrard Inlet, is taken to be just outside First Narrows. In computing the dissipation between Point Atkinson and Vancouver Harbour, it will be assumed that no energy is lost between Point Atkinson and First Narrows.

Pressure data from the cyclesondes were used to determine the phase of the tide at the sill (C1) and in the basin (C3). The accuracy of the cyclesonde pressure sensor and of the clock make this calculation possible. Corrections were made for the pitch of the cyclesonde, which is measured and recorded internally. It is expected, however, that the measurement of the cyclesonde will be noisier than that of the tide gauge, since the current flow will cause movement of the cyclesonde. That the cyclesondes were not in strong current regimes, never greater than 65 cms^{-1}, and that they were only 10 m (C1) and 18 m (C3) above the bottom helps to reduce the effects of tidal current upon the signal. Data from a cyclesonde in February 1984 are shown in *Figure 56*, together with the harmonic analysis of the record. The data are irregularly spaced in time because of the time spent by the cyclesonde profiling or waiting at the top bumper.

Table 12
Phase Change ε and Dissipation Rates

	M_2			K_1		
	$\phi(°)$	$\varepsilon(°)$	$P(MW)$	$\phi(°)$	$\varepsilon(°)$	$P(MW)$
1983/84						
Pt.Atk.–Van.	5.0	4.8	2.9	3.8	3.6	0.91
Van.–Sill (C1)	6.9	5.1	2.8	4.6	3.4	0.79
Van.–Basin (C3)	9.3	6.0	3.3	5.1	3.3	0.77
Sill(C1)–Basin (C3)	2.4	1.9	0.51	1.6	1.3	0.15
1984/85						
Pt.Atk.–Van.	6.8	6.5	4.0	3.8	3.6	0.93
Van.–Sill (C1)	7.9	5.8	3.7	4.9	3.6	0.83
Van.–Basin (C3)	10.0	6.4	3.6	4.3	2.8	0.65
Sill(C1)–Basin (C3)	2.1	1.7	0.45	−0.6	/	/

Table 12 shows the phase changes ε and dissipation rates for 1983/84 and 1984/85. The

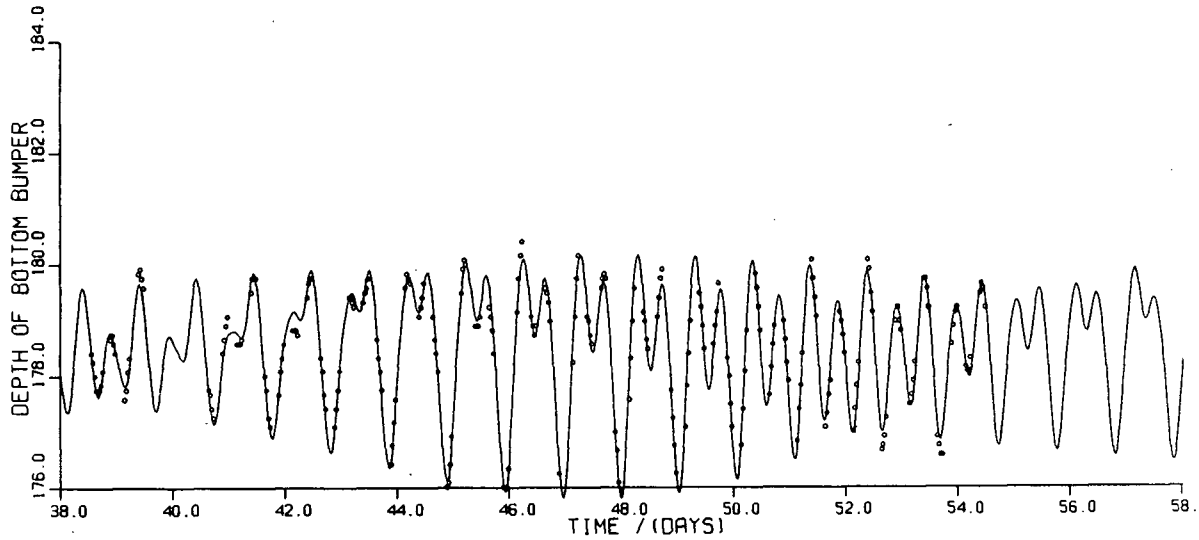

Figure 56 Depth of the cyclesonde at the bottom bumper in February 1984. The open circles are the data, the solid line is the harmonic analysis fit.

M_2 amplitude used was $0.957\,m$, the K_1 amplitude was $0.853\,m$. Each of these estimates of the power dissipation represents an average of four separate months of data. The endpoints of the sections are indicated in the leftmost column. Pt.Atk. is the Point Atkinson tidal station, Van. is the Vancouver Harbour tidal station (shown in *Figure 1*) and sill and basin are the cyclesonde stations C1 and C3. Very little overall difference between 1983/84 and 1984/85 is noted. Seasonal changes may occur, such as those observed by Stacey (1984) in Knight Inlet, but the shortness of the Indian Arm data set does not allow the resolution of such an effect. The K_1 power dissipation from the sill to the basin in 1984/85 escapes detection.

A total of 6.2 MW is lost from the M_2 tide in 1983/84, 1.7 MW from the K_1. In 1984/85, 7.6 MW was lost from the M_2 and 1.6 MW from the K_1. An approximately equal amount of energy is lost between Point Atkinson to Vancouver Harbour (over First Narrows) and Vancouver Harbour to Basin (over Second Narrows and the sill). *Figures 17–25* show that in 6 out of 7 months there is often more stratification over First Narrows

than Second Narrows. It is suggested that most of the energy lost in the first section, over First Narrows, goes into the generation of an internal tide. In the second section, not as much energy can be lost to the internal tide at Second Narrows because of the weaker stratification. More of the energy will be lost to an internal tide generated over the Indian Arm sill. The sill station (C1) used in the analysis presented in *Table 12* is actually inside the Indian Arm sill and therefore misses most of the internal tide generation. It therefore appears that more than 0.5 MW goes into the M_2 internal tide and likewise more than 0.15 MW goes into the K_1 internal tide. Dunbar (1985) analysed one month of tidal height data from two stations: Stanovan, just west of Second Narrows, and Alberta Pool, just east of Second Narrows. Because the data from the two stations were in different years, Dunbar computed the energy loss relative to Deep Cove and took the difference to find the power loss over Second Narrows. He estimated the power loss over Second Narrows , using the same technique as presented here, to be 2.24 MW for the M_2 tide and 0.35 MW for the K_1. These results indicate that about $1 - 1.5$ MW is lost from the M_2 barotropic tide in Indian Arm and $0.3 - 0.4$ MW from the K_1.

To determine the percentage of the tidal energy these power losses represent, it is necessary to compute the total tidal flux at each point in the fjord. This computation is somewhat tricky since the barotropic tide is a standing wave and part of the tide is reflected from the head of the fjord. One way to find the energy flux is through equation (5.5) which, without the $sin\,\varepsilon$ term, represents the total flux in the tide. The $sin\,\varepsilon$ factor determines the amount of energy removed from the total. If ε is zero, no energy is removed from the tide; as ε increases in size, a larger amount of energy is removed from the total amount available.

An alternative approach to this result is through the computation of the total potential energy. For this computation, the potential energy without the tide is subtracted from that with the tide. To get the flux this difference is multiplied by the area and the frequency:

$$Energy\,Flux = 2S\omega\left(\langle \int_{-H}^{\eta} \rho g z\, dz \rangle - \int_{-H}^{0} \rho g z\, dz\right) \quad . \tag{5.12}$$

The first integral must be averaged to represent the appropriate mean. The factor of 2 in front of the the brackets is to give the total flux since the potential energy is equal to the kinetic energy. The result of equation (5.12) is

$$Energy\,Flux = \frac{\rho g \eta_0{}^2 S \omega}{2} \quad , \tag{5.13}$$

which is the same as equation (5.5) without the $sin\,\varepsilon$ factor. *Table 13* presents the total energy flux for the M_2 and the K_1 tide at three points in the inlet. At First Narrows this flux is the tidal energy which enters the inlet. All of this energy, except for that dissipated in the system, leaves the inlet. The fluxes given in *Table 13* are for the positions indicated in the column at the left. The sill position is 0.5 km west of the C1 cyclesonde station.

Table 13
Barotropic Tidal Power Flux at Three Points in Indian Arm

Position	M_2 (MW)	K_1 (MW)
First Narrows	36.0	14.8
Second Narrows	25.8	10.6
Sill	15.8	6.5

The dissipation over First and Second Narrows represents a fairly large percentage of the available energy, as much as 15% . The energy lost from the sill in Indian Arm appears lower , in the range of 5 % of the total available energy. The 7 MW of energy which is lost over the two outer sills of Indian Arm, First and Second Narrows, goes into heat and mixing. If about ten per cent of the energy goes into mixing then about 0.3 MW is available to mix the waters as they pass through Burrard Inlet. The total energy loss corresponds to a dissipation rate of about 16 mW/m^3 in agreement with the observations of Grant, Stewart and Moillet (1962) in Discovery Passage where there are dissipation rates of 0.15 *to* 100 mW/m^3.

5.4 Baines Forcing Function

In an attempt to understand the variation in the M_2 and the K_1 response over the 1983/84 winter, two different possibilities were investigated: either the forcing changes or the internal response of the fjord changes. If the latter, then there are a number of ways in which the change might exhibit itself. In this section, the forcing will be discussed to see how it changes over the 1983/84 winter.

The formulation of Baines (1973, 1974, 1982) will be used to investigate the forcing of the internal tide. Baines writes the equations for a rotating, stratified , inviscid fluid; subtracting from these general equations the terms for the barotropic tide. The momentum equation is written

$$\frac{\partial \vec{U}_i}{\partial t} + \vec{f} \times \vec{U}_i + \frac{1}{\rho_0}\vec{\nabla} P_i + \frac{\tilde{\rho} g \hat{z}}{\rho_0} = \vec{F} = \frac{-g\rho_1}{\rho_0}\hat{z} \quad , \tag{5.14}$$

where ρ_0 is the mean density and $\rho = \rho_1 + \tilde{\rho}$ which has a barotropic and a baroclinic part. Using an equation for the total derivative of the density and one for the vertical velocity in terms of the barotropic tidal flux, Baines writes the forcing function $\vec{F}$ as :

$$\vec{F} = \frac{-QN^2}{\omega}\frac{Z\frac{dh}{dx}}{h^2} sin\omega t\, \hat{z} \quad , \tag{5.15}$$

where Q(x,y) is a flux vector due to the barotropic tide, Z is the subsurface depth, h is the bottom depth, ω is the frequency of the tide and N is the Brunt-Väisälä frequency. Q is equal to the depth times the barotropic velocity; in a channel it is assumed that there is no change in the channel width. This function represents the forcing per unit mass for the internal tide. The buoyancy frequency is the variable term which will determine how the forcing will change in time. Forcing will only take place over bottom slopes, as expected, since over flat bottoms dh/dx is zero.

The N^2 profiles were computed from the CTD data taken on each monthly cruise. The raw N^2 profile was computed from the CTD data, which were previously averaged to $1\,m$ depth intervals. A spline fit to the N^2 profile was then made to reduce the variability in N^2. The solid line over the dashed N^2 profile in *Figure 57* is the spline fit to the N^2 profile.

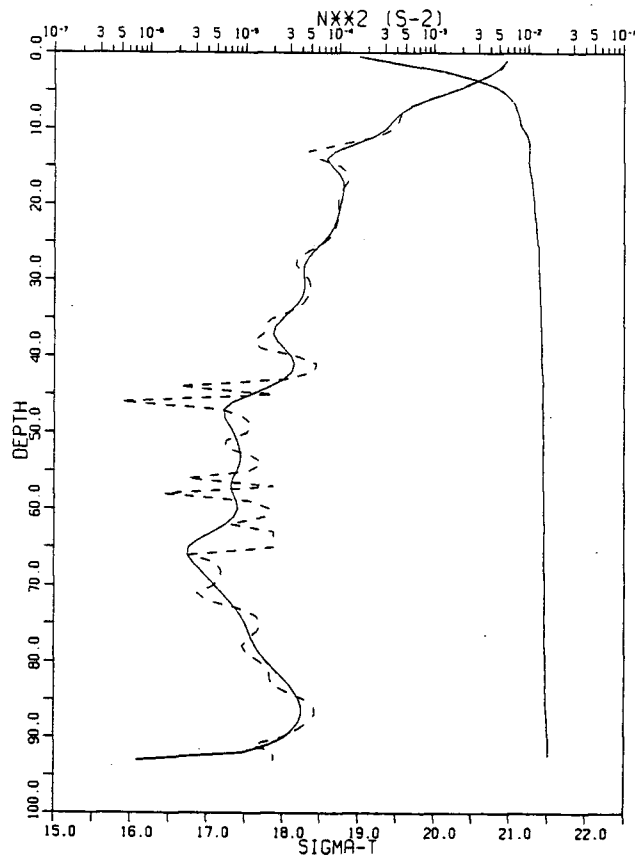

Figure 57 Plot of $N^2\,(rad\,s^{-2})$ and σ_t versus depth on 8-Feb-84 at station 31. The dashed line is the N^{-2} profile computed directly from the CTD data. The solid line is the spline fit.

The forcing function was computed using the N^2 profile from each of the CTD stations. The tidal forcing functions for two months are shown in *Figures 58 and 59.* Because the flux vector of the barotropic tide is approximately constant over the generation zone for each constituent, for these calculations it it is set to an arbitrary value of $1\,m^2s^{-1}$. Thus, the forcing function plotted in *Figures 58 and 59* is relative to a barotropic flux of 1. It is the relative value of the forcing function and how it changes that is of interest in assessing the effect upon the internal tide. A simplified version of the bottom topography was used to make easier the interpretation of the comparison. The function plotted in these two figures has units of force per unit mass.

Figure 58, showing the forcing on 14-Dec-83, indicates that most of the forcing comes from mid-depths between stations 44 and 48. There is also some forcing along the slope

inside the fjord, where the cyclesonde was located at C1. The 8-Feb-84 plot in *Figure 59* shows some reduction in the forcing from a maximum of 750 in December to 500 in February. The area of generation seems even more narrowly confined, between stations 44 and 48, than it was in December. In both plots there is indication of the generation of an internal tide at the head of the fjord, although this forcing is extremely weak in comparison to that at the sill.

That these plots are taken from a single CTD cast clearly limits their reliability as representations of the forcing function over the tidal cycle. For the 1983/84 winter no regular pattern of variations was observed. There are changes from month to month but there is no pattern present in November-December that changes to another pattern in January- February. There was always some forcing, of varying intensity, located between stations 35 and 56.

5.5 Ray Tracing

In section 5.4 it was shown that the forcing function does not change significantly during the 1983/84 winter. The altered internal response in Indian Arm must then be a result of a change in the stratification in the basin. Ray theory was used to investigate one aspect of this possibility. Cushman-Roisin and Svendsen (1983) applied ray theory and modal analysis in their study of the internal tide in a Norwegian fjord.

Two fundamental assumptions are required for the development of ray theory: 1) the waves must be of small amplitude so that linearization can be applied and 2) the wavenumber (k) must change only gradually on the scale of the reciprocal wavenumber (k^{-1}). Neither of these assumptions is particularly robust in Indian Arm; however, it should still be instructive to conduct the analysis since it is relative changes over the 1983/84 winter that are being investigated. In the development of the theory, Lighthill (1978) will be followed. Each variable is written in the form:

$$q = Q(x, z, t)e^{i\alpha(x,z,t)} , \tag{5.16}$$

where Q is the modulated amplitude. The wavenumber and angular frequency are derived

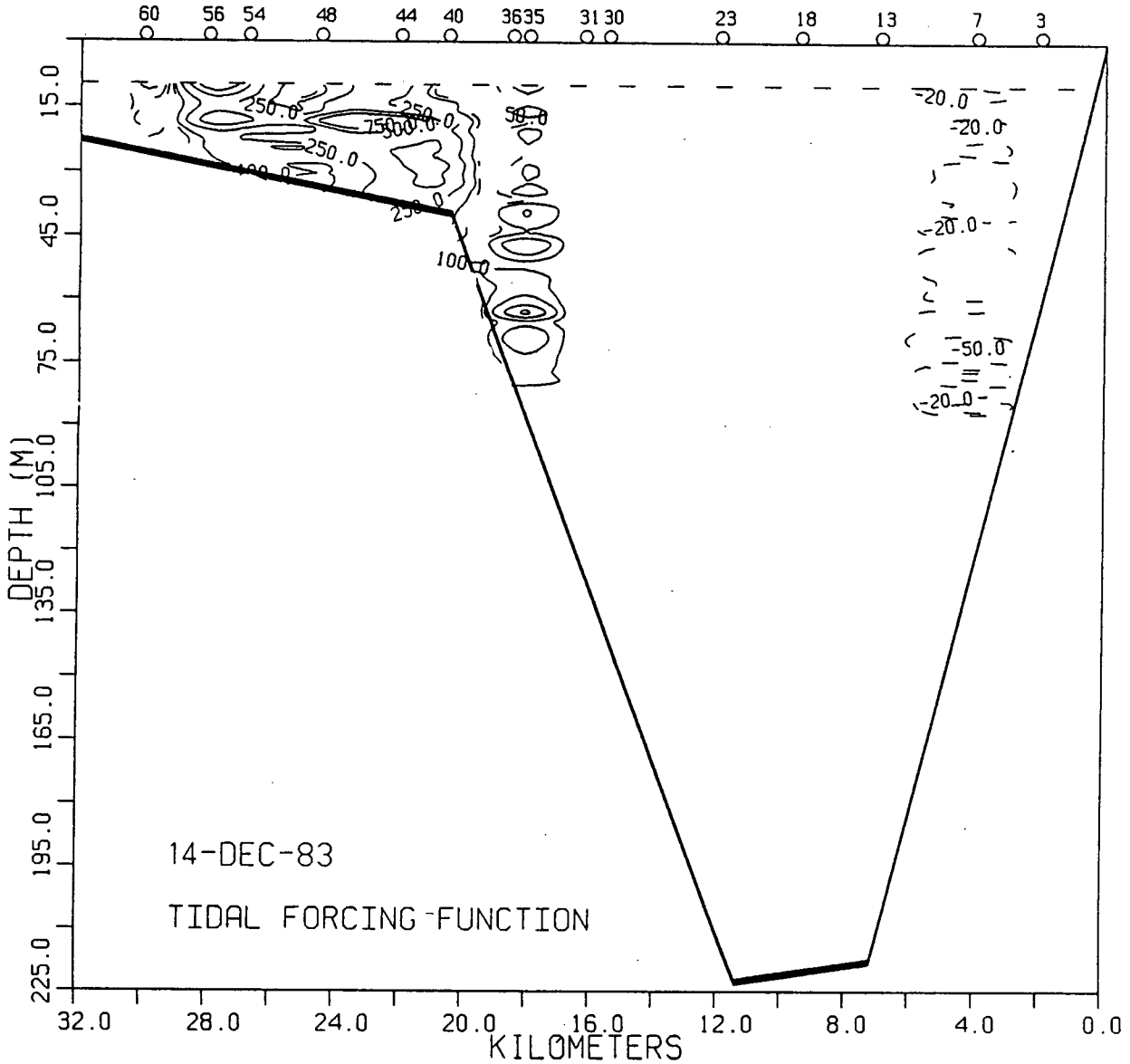

Figure 58 Tidal forcing function in Indian Arm on 14-Dec-83. The units are N/kg, force per unit mass, with the flux vector Q set to 1.

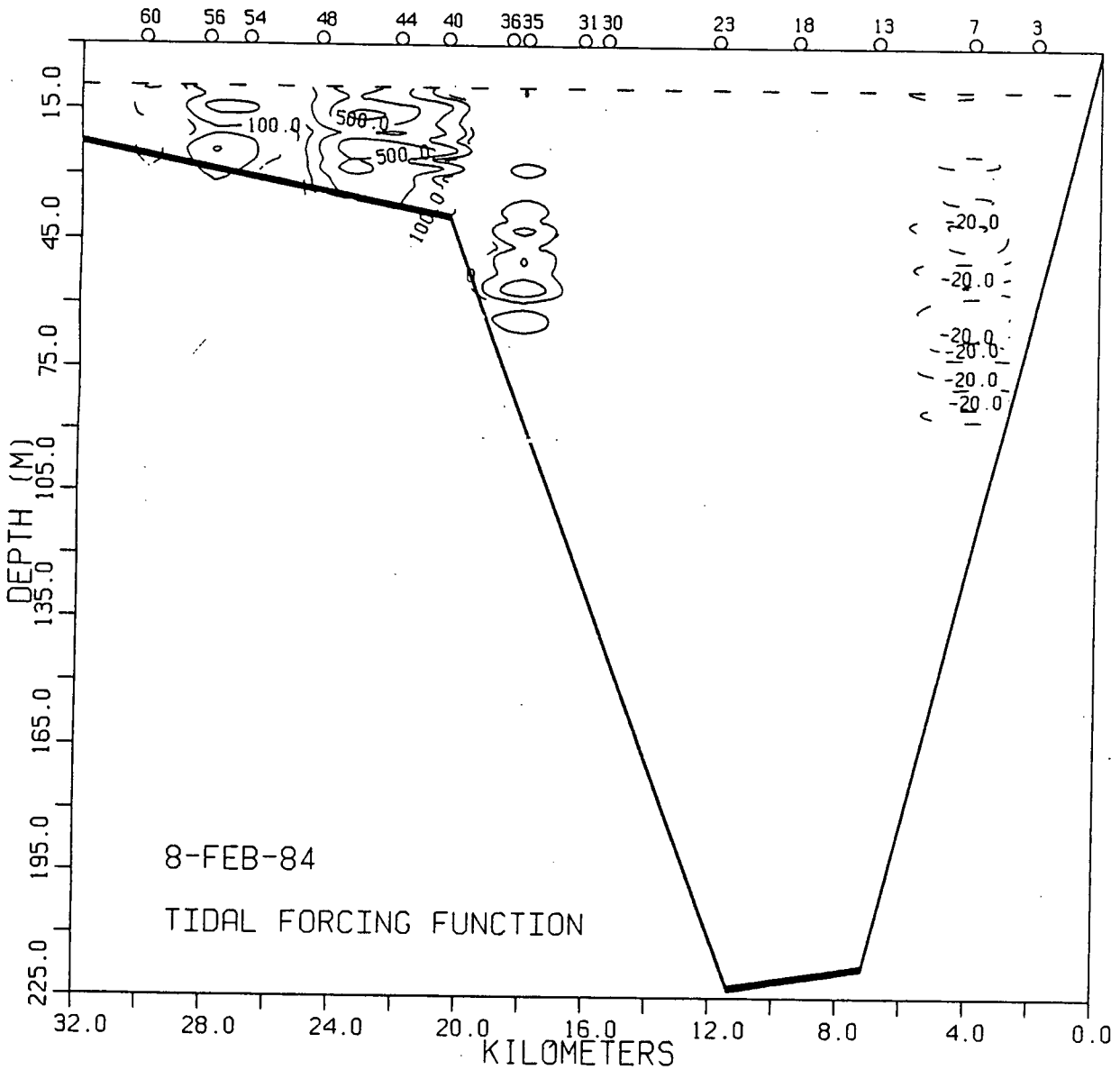

Figure 59 Tidal forcing function in Indian Arm on 8-Feb-84. The units are N/kg, force per unit mass, with the flux vector Q set to 1.

from the phase function:

$$k = -\frac{\partial \alpha}{\partial x} \quad m = -\frac{\partial \alpha}{\partial z} \quad and \quad \omega = \frac{\partial \alpha}{\partial t} \ . \tag{5.17}$$

The dispersion relation for linear gravity waves is:

$$\omega^2 = N^2 \frac{k^2}{k^2 + m^2} \ . \tag{5.18}$$

Equation (5.18) can be rewritten to find m, which is then used to define the ray trajectory in the x-z plane.

$$\frac{dz}{dx} = \frac{dz/dt}{dx/dt} = \frac{C_z}{C_x} = \frac{-k}{m} = \pm\sqrt{\frac{\omega^2}{N^2(z) - \omega^2}} \ , \tag{5.19}$$

where C_z and C_x are the vertical and horizontal components of the group velocity. Equation (5.19) shows that the trajectory is defined by the N^2 profile, which is variable, and the frequency, which is fixed.

The CTD data, which represent the density profile at only one point in time, were combined with the cyclesonde data to give an N^2 profile more representative of conditions over a period of approximately two weeks. N^2 profiles from the CTD and the averaged cyclesonde data were computed separately and then combined together. *Figure 60* shows the N^2 profile computed from the CTD data for November 1983 together with the spliced profile. Over the range that the cyclesonde profiled, density data from the cyclesonde were used to give the N^2 profile. These N^2 values were then substituted for those computed for the CTD data over the same range. A spline fit to the resulting data was then made. The solid line in *Figure 60* is the resulting spline fit.

The ray paths were computed at a number of points in the generation area, identified by the Baines forcing function plots of *Figures 58 and 59*. The results of the ray plots for M_2 and K_1 in early November are shown in *Figures 61 and 62*. Reflections from the head of the inlet have been ignored. Irregularities in the ray plots, such as the crossing of some rays (see the middle of *Figure 61*), are due to local variations in the N^2 profiles. In the search for pattern changes from month to month, these localized irregularities are not important.

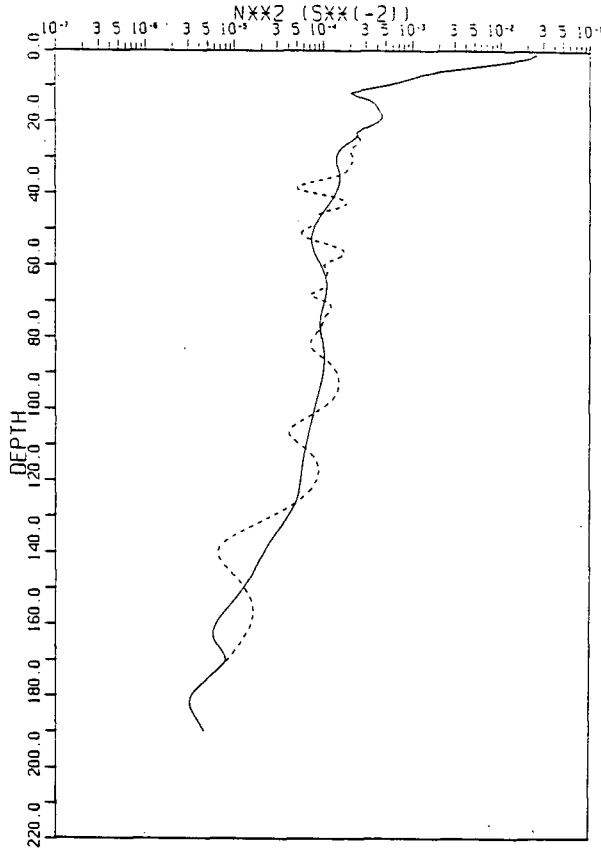

Figure 60 N^2 profile at the basin station for 8-23 November 1983. The dashed line is the N^2 profile computed from the CTD data . The solid line incorporates data from the cyclesonde.

Figure 61 shows the ray path plots for internal waves at the M_2 frequency. Upward and downward propagating energy seem to be balanced throughout much of the fjord. Energy propagating upward (solid lines) is not trapped at the surface but reflects back into the deeper water. Slopes at the K_1 frequency are much shallower (see *Figure 62*). A shadow zone appears towards the head of the fjord. At the basin cyclesonde station C3 (about 13 km from the head) there is not a balance between upward and downward propagating energy. For the modal analysis technique to be valid there must be an equivalence between the upward and downward propagating energy flux. There can be no net flux. *Figure 63* shows the baroclinic along-channel velocity at the basin station for the M_2 and K_1 tide in November 1983. These data were obtained by subtracting the barotropic tidal velocity from the harmonic analysis result. The remaining baroclinic velocity is plotted in *Figure 63*.

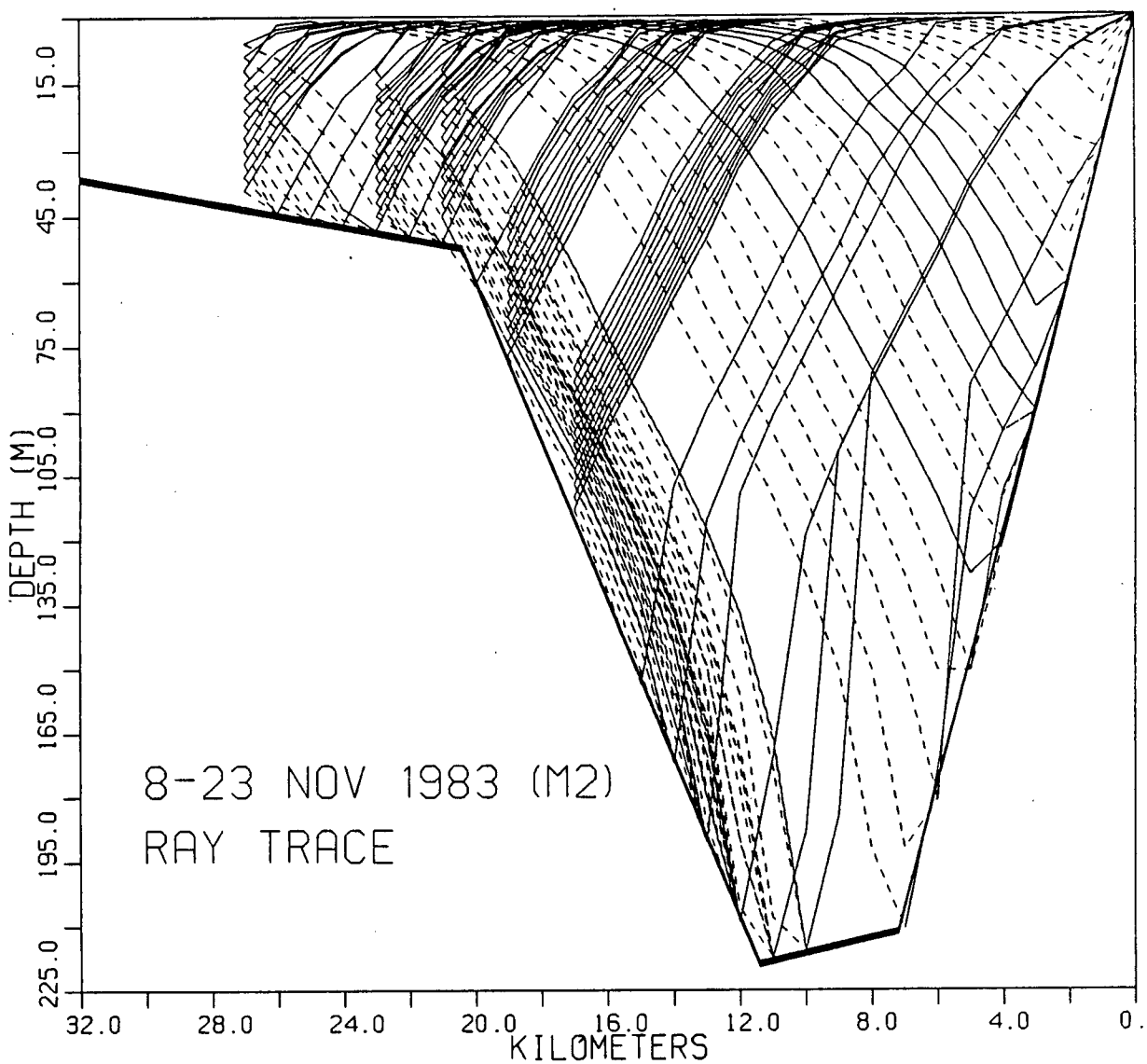

Figure 61 Ray paths for the M_2 internal tide for 8-23 November 1983. Downward propagating waves have dashed lines, upward going waves have solid lines.

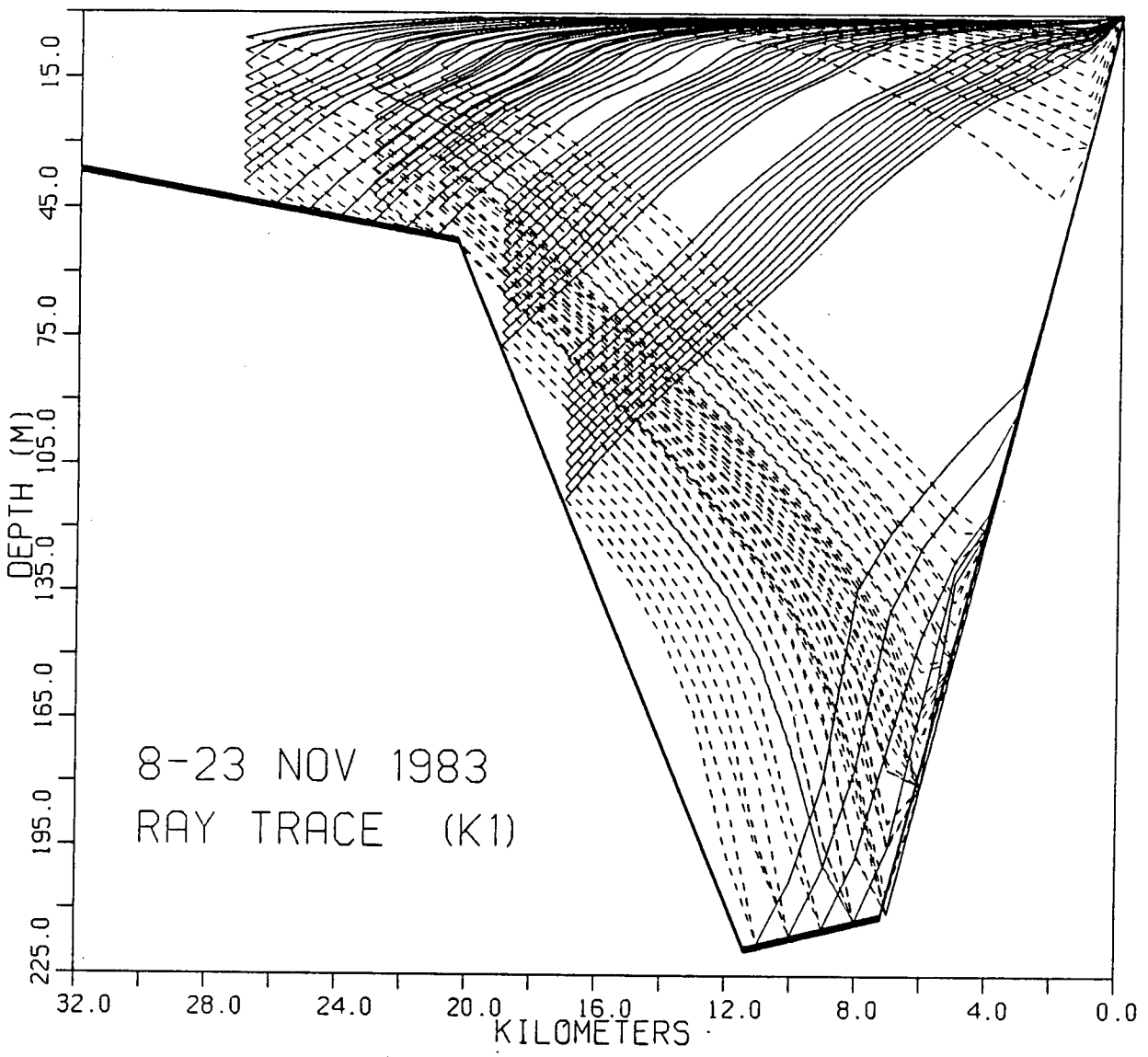

Figure 62 Ray paths for the K_1 internal tide for 8-23 November 1983. Downward propagating waves have dashed lines, upward going waves have solid lines.

The K_1 internal tide shows a minimum at about 100 m. No such minimum appears in the M_2 baroclinic tide. This minimum may be the result of this shadow effect or may be a result of the modal structure in the basin, although the difference between the M_2 and the K_1 tide makes the former seem more likely.

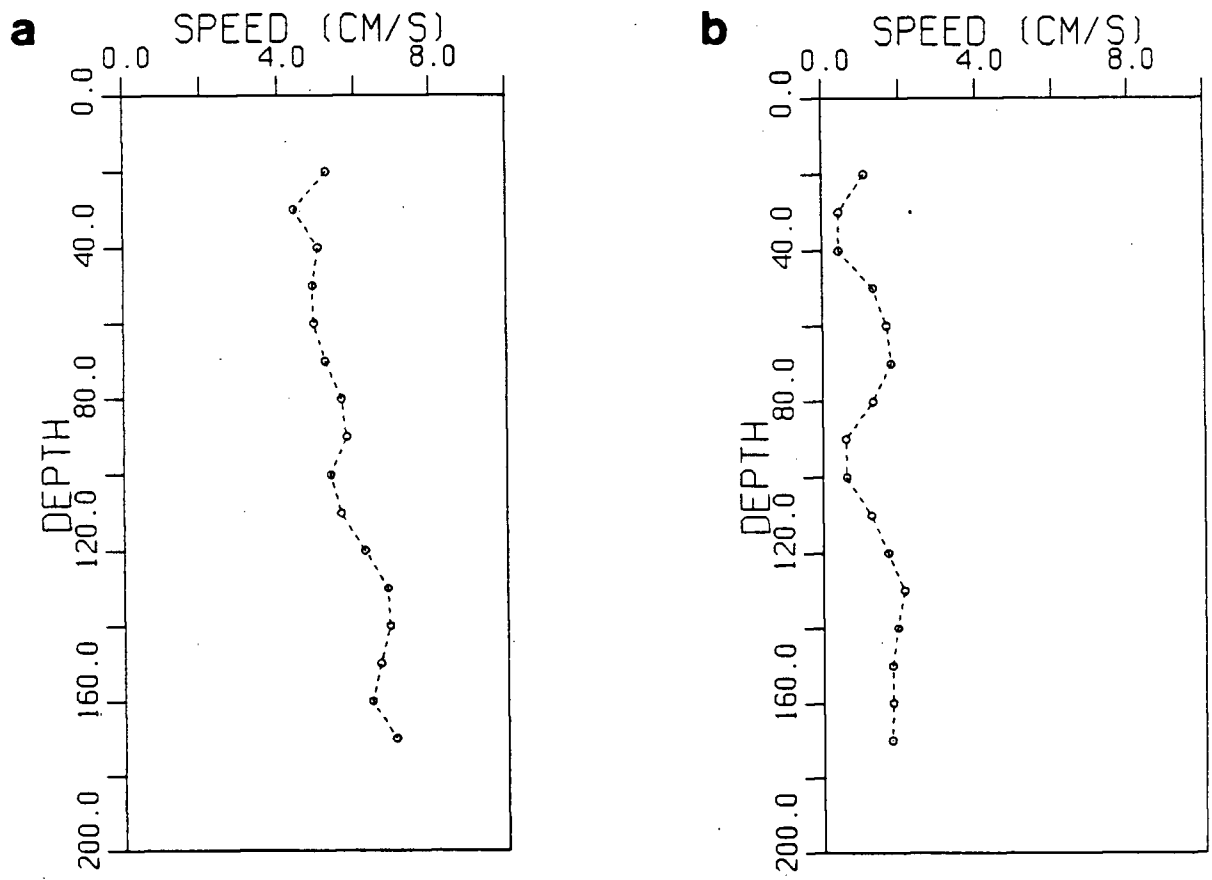

Figure 63 Baroclinic velocity ($cm\,s^{-1}$) in the M_2 (a) and K_1 (b) tide for 8-23 November 1983. The data are from the basin station C3.

Plots were done for two-week sections over the 1983/84 winter to look for systematic differences in the ray paths. It was expected that there might be an identifiable difference between the November-December plots and those for January-February. No common pattern was identified, although variations in the plots from period to period were observed.

Although longitudinal variability will be important, the cyclesonde should provide a good measurement of the variability in the basin over the two-week averaging period. This density measurement should indicate, through these ray tracings, the effects of these

changes upon the internal tide; if such effects are important. Because no systematic shift from the first to the second half of the record was observed, it is concluded that changes in the ray paths are not the cause of the shift from the M_2 to the K_1 internal response.

5.6 Modal Analysis

5.6.1 Theory of Normal Modes

In ray tracing, the waves are considered to travel as packets at the group velocity. In modal analysis, the waves are allowed to have vertical structure. These modes then propagate in the horizontal direction. The normal modes of a channel are searched for in a manner similar to looking for the normal modes of a vibrating string.

The theory of normal modes assumes the ocean to be flat-bottomed and infinite in length with vertical side walls. Since none of these assumptions holds rigidly in Indian Arm, it is natural to question the applicability of this theory. It can be argued that although the assumptions do not hold perfectly, the theory does work reasonably well since the theory has been applied with success in other fjords (Webb, 1985). In Chapter 3 it was observed that the structure of the empirical orthogonal eigenfunctions looked very much like normal modes, indicating that the system probably does respond in the manner predicted by this theory.

In the discussion which follows, I shall follow the work of LeBlond and Mysak (1978). A harmonic time dependence of $e^{-i\omega t}$ will be assumed, consistent with LeBlond and Mysak (1978) and Foreman (1978), whose harmonic analysis programs were used. The first step is to write the set of linearized momentum and continuity equations in the form:

$$\rho_0(-i\omega u - fv) = -p_x \tag{5.20}$$

$$\rho_0(-i\omega v + fu) = -p_y \tag{5.21}$$

$$\rho_0(\omega^2 - N^2)w = -i\omega p_z \tag{5.22}$$

$$u_x + v_y + w_z = 0 \ . \tag{5.23}$$

In these equations ρ_0 is the density, p is the pressure whose subscript indicates differentiation, $i = \sqrt{-1}$, ω is the frequency, N is the Brunt-Väisälä frequency and u, v and w are the components of velocity. To find the vertical modal solution it is necessary to perform a separation of variables.

$$\rho_0(u, v) = \mathcal{D}(z)\left[\mathcal{U}^h(x, y),\ \mathcal{V}^h(x, y)\right] \tag{5.24}$$

$$p = \mathcal{D}(z)\mathcal{P}(x,y) \tag{5.25}$$

$$w = \frac{i\omega}{g} Z(z)\mathcal{P}(x,y) \quad . \tag{5.26}$$

These three equations are substituted into equations (5.20-5.23) and a new set of equations is obtained. After some manipulation the horizontal equations are

$$i\omega\vec{\mathcal{U}}^h - 2\vec{\Omega} \times \vec{\mathcal{U}}^h = \vec{\nabla}.\mathcal{P} \tag{5.27}$$

$$\vec{\nabla}.\vec{\mathcal{U}}^h = \frac{i\omega}{gh_n}\mathcal{P} \quad . \tag{5.28}$$

The vertical equation is

$$\frac{d^2Z}{dz^2} + \frac{N^2 - \omega^2}{gh_n} Z = 0 \quad . \tag{5.29}$$

The bottom boundary condition is

$$Z(-h) = 0 \quad , \tag{5.30}$$

and the surface boundary condition is

$$\frac{dZ}{dz} - \frac{Z}{h_n} = 0 \quad at\ z = 0 \quad . \tag{5.31}$$

The horizontal velocity, vertical velocity and pressure are given by:

$$\vec{\mathbf{u}}^h(x,y,z) = -h_n \frac{dZ}{dz}\vec{\mathcal{U}}^h(x,y) \tag{5.32}$$

$$w(x,y,z) = \frac{i\omega}{g} Z(z)\mathcal{P}(x,y) \tag{5.33}$$

$$p(x,y,z) = -\rho_0 h_n \frac{dZ(z)}{dz}\mathcal{P}(x,y) \quad . \tag{5.34}$$

The solutions to equations (5.32–5.34) form a set of eigenvectors with eigenvalues h_n. The eigenvalues h_n are referred to as equivalent depths and the eigenfunctions Z are the vertical modes. It is necessary to solve the vertical eigenfunction equation (5.29), using the observed stratification to give the buoyancy frequency, subject to the boundary conditions. From these eigenfunctions, the horizontal and vertical velocity eigenfunctions can be found.

It is possible to relate the density perturbations, ρ', and vertical velocity perturbations through rewriting the continuity equation (see LeBlond and Mysak p. 16):

$$\frac{\partial \rho'}{\partial t} + w\frac{\partial \rho_0}{\partial z} = 0 \quad . \tag{5.35}$$

Using equation (5.33), equation (5.35) may be rewritten to give

$$\rho'(x,y,z) = \frac{-\bar{\rho}_0}{i\omega g} N^2(z) w(x,y,z)$$
$$= \frac{-\bar{\rho}_0}{g^2} N^2(z) Z(z) \mathcal{P}(x,y) \quad . \tag{5.36}$$

These equations can be taken even further by considering the solutions to equations (5.27) and (5.28), which represent a horizontal problem with boundary conditions at the sidewalls and at the mouth. The lateral boundary condition states that there be no normal flow at the sides of the channel. For Kelvin waves, which the barotropic and baroclinic tide are, this condition is satisfied everywhere. The expressions for **P**, **U** and **V** are

$$\mathbf{U}(x,y) = U_0 e^{(i\omega x - fy)/c_n} \tag{5.37}$$

$$\mathbf{V}(x,y) = \mathbf{0} \tag{5.38}$$

$$\mathbf{P}(x,y) = U_0 c_n e^{(i\omega x - fy)/c_n} \quad . \tag{5.39}$$

U_0 is an arbitrary constant used to normalize the modes and $c_n = \sqrt{gh_n}$. The decay scale of the wave is given by the Rossby radius $R_n = c_n/f$. This radius represents the e-folding length scale for the wave in the transverse direction.

It is now possible to rewrite the normal modes solution into a form which will be most practical for the computations to be done here.

$$u(x,y,z) = -U_0 h_n \frac{dZ}{dz} e^{(i\omega x - fy)/c_n} \tag{5.40}$$

$$v(x,y,z) = \mathbf{0} \tag{5.41}$$

$$\rho'(x,y,z) = \frac{-U_0 c_n \bar{\rho}_0}{g^2} N^2(z) Z(z) e^{(i\omega x - fy)/c_n} \quad . \tag{5.42}$$

5.6.2 Normal Modes in Indian Arm

In order to find the normal modes, the vertical eigenvalue equation (5.29) was solved subject to the boundary conditions expressed in equations (5.30) and (5.31). As input to the program, the average buoyancy frequency profiles computed from the CTD data and the averaged cyclesonde data were used (for example see *Figure 64*) . The eigenvalue equation was solved using a 4th-order Runge-Kutta technique. Iteration of the eigenvalue using a shooting method was done to satisfy the boundary condition at the surface.

The vertical structure of the first five modes including the barotropic or zeroth mode, is shown in *Figures 65 and 66.* These modal solutions have been normalized so that the maximum horizontal velocity is $1\,m\,s^{-1}$. The horizontal velocity is shown in *Figure 65*, the vertical velocity in *Figure 66.* These modal solutions are based on the buoyancy frequency profile shown in *Figure 64.* Most of the vertical structure differentiating the modes is in the upper part of the water column. Below $20\,m$, for instance, there is very little to differentiate modes 2 and 3 within the vertical resolution of the cyclesonde data ($10\,m$). There are only two data points above the mode three zero crossing at $35\,m$ which can be used to distinguish the different modes. That the structure of the modes below $20\,m$ is so similar and that our data do not extend above $20\,m$ in the basin will make difficult the fitting of the modes to the data.

The phase speeds for the first five modes are given in *Figure 65.* The higher the mode number the lower the speed, the shallower h_n is and the shorter the wavelength. The differences between the modes appear in the vertical velocity as well (see *Figure 66*). Note the scale change ($cm\,s^{-1}$ instead of $m\,s^{-1}$) in this figure from the previous one for the horizontal velocity; the vertical velocity is much weaker than the horizontal velocity.

The structure of these modes, their phase speeds and their wavelengths all change as the stratification changes. The stratification and the water depth control the solution of the vertical mode eigenfunction equation. These changes were observed in Indian Arm and will be used to explain the differing internal response at the K_1 and M_2 frequencies.

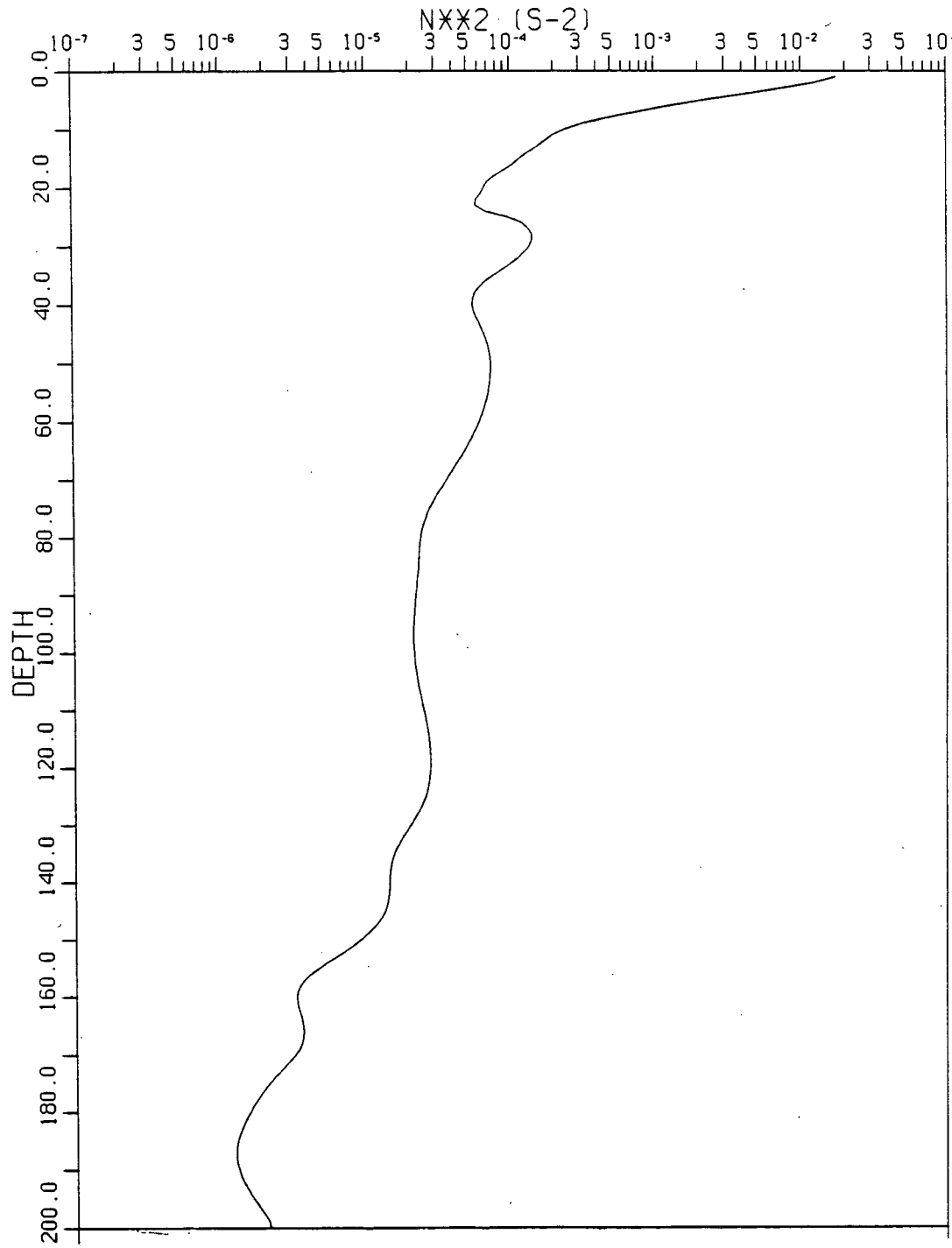

Figure 64 N^2 profile, for 7-22 February 1984, incorporating both CTD and cyclesonde data.

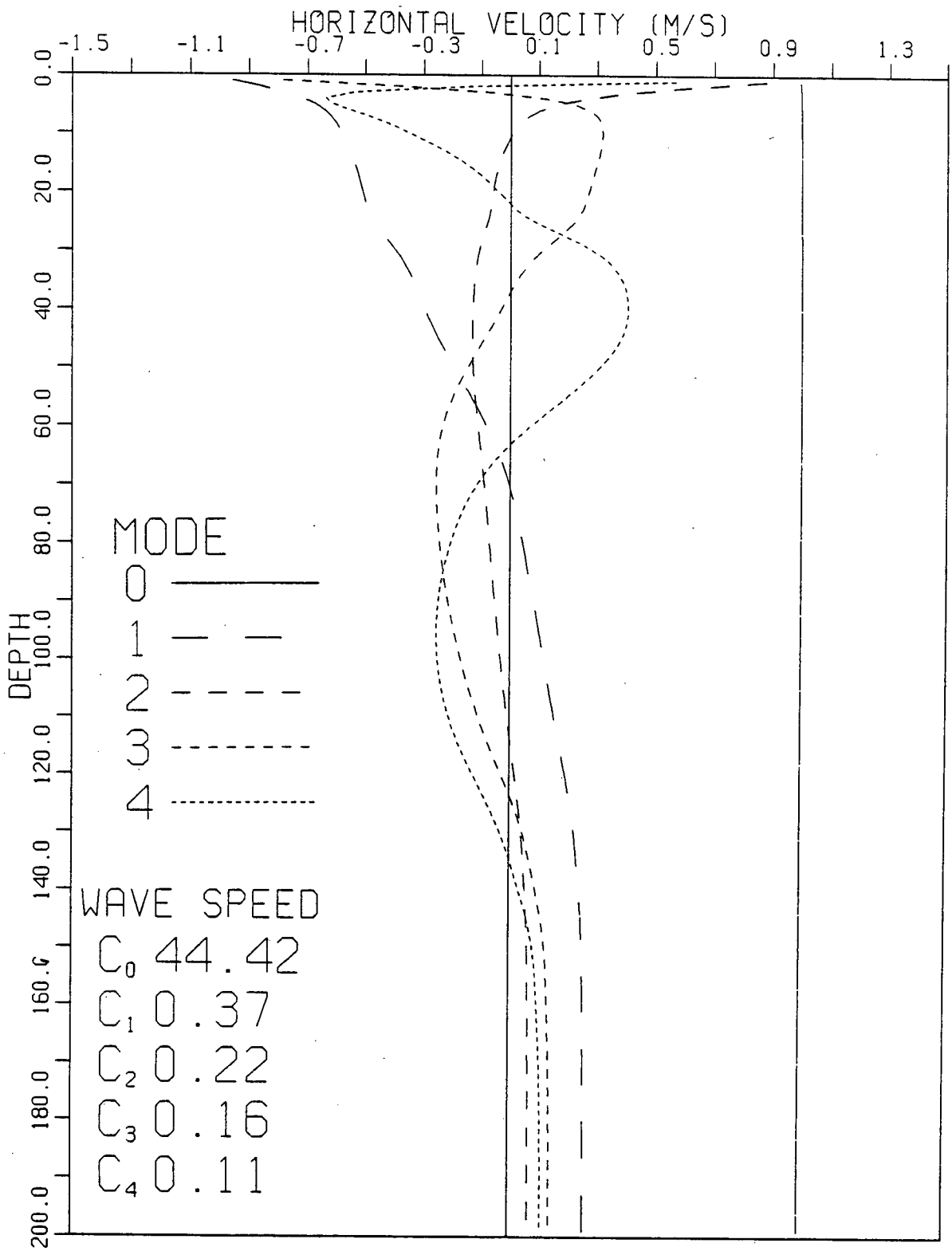

Figure 65 Horizontal velocity for the first five normal modes for 7-22 February 1984. The N^2 profile used is given in *Figure 64*.

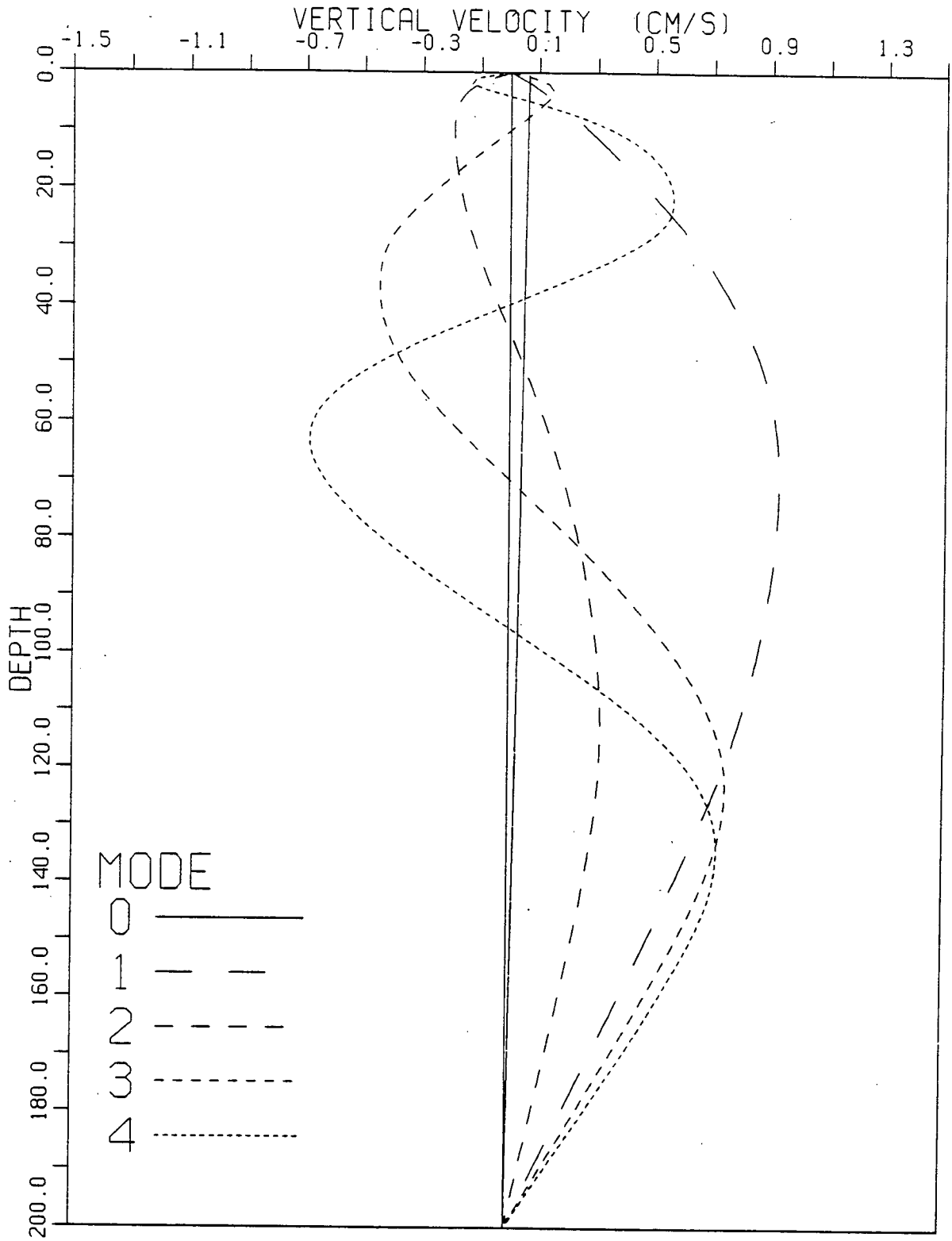

Figure 66 Vertical velocity for the first five normal modes for 7-22 February 1984. The N^2 profile used is shown in *Figure 64*.

A detailed discussion of the varying shapes of the modal eigenfunctions will not be given. Ultimately, fitting the modes to the cyclesonde data explains the dynamical significance of the modes. Such a discussion will be given in Section 5.8.

5.7 Resonance Period

5.7.1 Resonance Theory

In this section the possible resonance of Indian Arm will be discussed. Lewis and Perkin (1982) present observations, from a fjord in Greenland, of current enhancement which they interpret to be a result of resonance. Keeley (1984) describes internal response in a British Columbia fjord, Alice Arm. He observed a phase shift of 180 ° in the M_2 currents during the fall period. Such a phase shift is characteristic of a system which passes through resonance. Alice Arm passed through resonance over a 10 day period, with an increase of about a factor of 3 in the M_2 amplitude.

Resonance occurs in a forced harmonic system when the forcing frequency matches the natural frequency of the system. If there were no dissipation the amplitude of the response would grow steadily in time. The amplitude of the resonance response is limited by friction. Dissipation is also important in controlling the half-width of the resonance response curve.

I shall briefly review some simple ideas about resonance to illustrate the physical effects of the dissipation and to provide some theory to apply to Indian Arm. The starting equation will be the linearized form of the vertical velocity equation (Phillips, 1977):

$$\frac{\partial^2}{\partial t^2}\nabla^2 w + N^2 {\nabla_h}^2 w + \nu \frac{\partial}{\partial t}\nabla^2 w = 0 \ , \tag{5.43}$$

where ${\nabla_h}^2$ is the horizontal component of ∇^2 and ν is the friction coefficient. For the purposes of this discussion rotation will be neglected, that is f=0. If a separation of variables, w=G(x,y)H(z)T(t), is performed then (5.43) becomes three equations:

$$\frac{d^2T}{dt^2} + \nu\frac{dT}{dt} + \omega^2 T = 0 \tag{5.44}$$

$$\nabla^2{}_h G + \alpha^2 G = 0 \tag{5.45}$$

$$\frac{d^2H}{dz^2} + \alpha^2\left(\frac{N^2 - \omega^2}{\omega^2}\right)H = 0 \quad . \tag{5.46}$$

In equations (5.45) and (5.46), α is the separation constant. Only the first equation is of interest here, the last is equivalent to the normal mode equation (5.29). Equation (5.44) is in the form of a one-dimensional harmonic oscillator and can be used to illustrate some of the characteristics of the resonant response. If a forcing function of the form $T_o \cos \omega t$ is added, representing the tidal forcing, then the equilibrium solution for T is

$$T = \frac{T_0}{\sqrt{\nu^2\omega^2 + (\omega_0{}^2 - \omega^2)^2}} cos(\omega_0 t - \varphi) \quad , \tag{5.47}$$

where ω_0 is the undamped resonant frequency and

$$tan\varphi = \frac{\omega\nu}{(\omega_0{}^2 - \omega^2)} \quad . \tag{5.48}$$

Since T_0 is fixed it is clear that resonance will occur when the denominator in equation(5.47) is at a minimum. This will occur when

$$\omega_r{}^2 = \omega_0{}^2 - \frac{\nu^2}{2} \quad . \tag{5.49}$$

The resonance frequency is not at the precise frequency of the non-dissipative system but is lower. Some estimate of the ratio of the amplitude of the response at some fixed frequency, to that at resonance, can be obtained by substitution of equation (5.49) into (5.47). Some simplification is made by assuming that only frequencies near resonance are of interest, since then

$$\omega^2 - \omega_r{}^2 \simeq 2\omega(\omega - \omega_r) \quad .$$

After some manipulation the final amplitude ratio is

$$\frac{T^2}{T_r{}^2} = \frac{\nu^2}{4(\omega - \omega_r)^2 + \nu^2} \quad . \tag{5.50}$$

The curve of the function is symmetric in $(\omega - \omega_r)^2$. The half-width occurs at $\Delta = (\omega - \omega_r)$ where

$$\Delta = \frac{\nu}{2} \quad . \tag{5.51}$$

Equation (5.51) shows that the width of the resonance curve is directly proportional to the friction coefficient in a resonant system. The larger the friction coefficient, the wider the range of frequencies at which a strong response will be detected.

5.7.2 Conditions for Resonance

Once it is established that the forcing frequency matches the resonance frequency, two conditions must be met before internal resonance can occur in a fjord. First, the internal tide must reflect off the end of the fjord, or at least enough energy must reflect to make it back to the sill. Second, the energy reflected from the head must also be reflected from the sill; it cannot be allowed to leak out.

The first condition concerning reflection has been discussed earlier. The critical parameter is the ray slope given by $\sqrt{\omega^2 - f^2}/\sqrt{N^2 - \omega^2}$. This subject has been investigated (Wunsch, 1969; Cacchione and Wunsch, 1974) and the general reflection criteria described (Phillips, 1977). Eriksen (1982) showed that observations near continental shelves, seamounts and islands provided reasonable agreement with theory. In Indian Arm, the complex bottom topography at the head of the fjord (see *Figures 1 and 2*) makes the application of even simple theory difficult.

The second condition, that of reflection of internal energy from the sill, has been discussed by Robinson (1969) who found an analytical solution to the reflection problem in an exponentially stratified fluid. For different modes Robinson is able to compute the effect of a vertical barrier on the internal modes. In Indian Arm the ratio of the barrier height to the total depth is approximately 180/200, for which the theory of Robinson predicts that over 90% of the energy at modes 1, 2 and 3 will be reflected.

5.7.3 Computation of Resonance Period

There are several different approaches available for the computation of the resonance period in a fjord. Because of the nature of the data, and the type of result being looked for, it was decided to apply a fairly simple technique. The desired result was a comparison of the changing resonance period.

Keeley (1984) found the resonance period in Alice Arm by computing the following integral:

$$2 \int_{head}^{mouth} \frac{dx}{c_i}, \tag{5.52}$$

where c_i is the phase speed of the ith internal mode and x is the distance along the inlet. Because the fjord has sloped ends, from which energy must reflect for resonance to occur, this equation will overestimate the resonance period. It is difficult to predict the degree of this overestimation since it will depend upon the fjord geometry and the process of reflection. A further problem with this method is the calculation of the modal phase speeds over sloping bottoms.

Here a simpler technique will be applied, one which does not overestimate the resonance period but probably underestimates it. The calculation will be made assuming a basin 15 km long and 200 m deep, essentially the same assumptions made in the modal analysis in the basin. This length fairly closely matches the effective length of the fjord. The N^2 profiles, spliced together from the CTD and the averaged cyclesonde data, used for the ray tracing analysis will be used here.

The resonance period for 1983/84, calculated for two-week blocks, is shown in *Figure 67.* The mode 1 period increases, except for the early January period, from 14 hours in early November to 22 hours by the end of February. The mode 2 period changes from 26 hours in early November to 38 hours in early February, with a drop to 25 hours in early January. The precise values of these periods are not expected to be very accurate but the trends should hold. If these estimates are wrong they probably err on the low side.

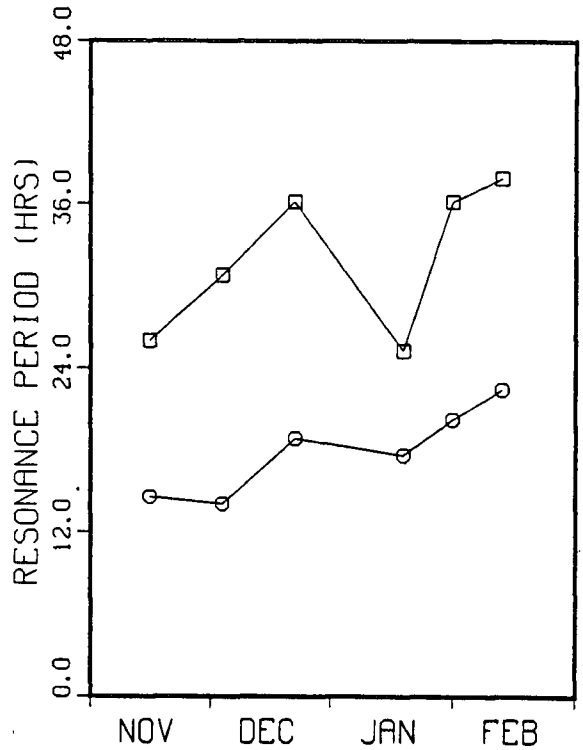

Figure 67 Resonance period versus time in 1983/84. The circles (○) represent the mode 1 period, the squares (□) the mode 2 period.

The trend in the resonance period corresponds reasonably well with the trend in the internal response. In the first half of the period (November-December) there is a predominantly M_2 internal response. During this period the mode 1 resonance period is between 14 and 18 hours, closer to the M_2 period of 12.42 hours than to the K_1 period of 23.93 hours. In the second half of the period (January-February), there is a strong K_1 internal response. Early in the second half, the K_1 is not stronger than the M_2 though it does become so by the end of February. This strong K_1 response corresponds to a time when the resonance period is between 18 and 22 hours, closer to the K_1 period than to the M_2 period. It is reasonable to hypothesize that the enhanced K_1 response late in the record is a result of a partial resonance response shift from an M_2 response early in the period to a K_1 response towards the end.

From the ratio of the amplitude at a fixed period to that at resonance, it is possible to determine the effective half-width of the resonance. Data given by Keeley (1984) was used to compute the factor ν, so that the amplitude ratio could be calculated. Alice Arm, where

Keeley's observations were made, has a geometry similar to Indian Arm. It is about 16 *km* long and is just under 400 *m* deep at its deepest point. It may, therefore, be expected that dissipation will take place in a manner similar to Indian Arm. *Table 14* shows the ratios of the amplitude (T) to the amplitude at resonance (T_R), for the M_2 and K_1 constituents in Indian Arm.

Table 14
Amplitude ratio (T/T_R) for the M_2 and K_1 constituents.

Period (hrs)	Amplitude Ratio (T/T_R) M_2	K_1
13	0.82	0.15
15	0.36	0.21
17	0.24	0.25
19	0.19	0.44
21	0.16	0.68
23	0.14	0.95

Table 14 indicates that the amplitude response of the M_2 tide should change by about a factor of 3-4 from November to February. The K_1 should increase by about the same amount. The plot of the baroclinic energy in *Figure 54* shows that the M_2 amplitude decreased by a factor of 2.7 while the K_1 increased by a factor of 2.5. Reasonable agreement with the prediction based upon the observations of Keeley (1984) is obtained. These results show that the resonance period explanation is very consistent with the observed variations in the internal response. The next step is to see how much energy is reflected from the end of the fjord. For resonance to occur there must be energy reflected from the head, a subject to be investigated in the next few sections.

5.8 Fitting Modes to the Cyclesonde Data

5.8.1 Theory of Fitting

In section 5.6.1 on the theory of normal modes, it was shown that it is possible to represent motion in a channel by the superposition of eigenfunctions. Such a superposition for the density and the velocity can be written

$$\mathbf{u}(z) = \sum_{n=0}^{\infty} u_n(z)(a_n^{up} e^{i\phi_n^{up}} + a_n^{down} e^{i\phi_n^{down}}) \tag{5.53}$$

$$\rho'(z) = \sum_{n=0}^{\infty} \rho_n(z)(a_n^{up} e^{i\phi_n^{up}} - a_n^{down} e^{i\phi_n^{down}}) \tag{5.54}$$

No cross channel dependence has been allowed so the e^{-yf/c_n} which appears in equations (5.37) and (5.39) does not appear. If data were available across the channel, it might be of benefit in solving the fitting problem.

The velocity and density eigenfunctions are written as :

$$u_n(z) = U_0 h_n \frac{dZ}{dz} \tag{5.55}$$

$$\rho_n(z) = \frac{U_0 c_n \bar{\rho}_0}{g^2} N^2(z) Z(z) \ . \tag{5.56}$$

The source of the minus sign in equation (5.54) is now apparent from the writing of (5.56). For a wave propagating down-inlet it is necessary to replace c_n by $-c_n$. Because no c_n term appears in the velocity equation, there is no minus sign in equation (5.53).

The problem to be solved consists of finding the complex coefficients which, when multiplied by the normal modes predicted by the stratification, yield the observed velocities and densities. Equations (5.53) and (5.54) can be rewritten

$$\mathbf{u}(z) = \sum_{n=0}^{\infty} u_n(z)(\mathbf{A}_n^{up} + \mathbf{A}_n^{down}) \tag{5.57}$$

$$\rho'(z) = \sum_{n=0}^{\infty} \rho_n(z)(\mathbf{A}_n^{up} - \mathbf{A}_n^{down}) \ , \tag{5.58}$$

where the complex coefficients $\mathbf{A}$ are written

$$\mathbf{A}_n^{up} = a_n^{up} e^{i\phi_n^{up}} \tag{5.59}$$

$$\mathbf{A}_n^{down} = a_n^{down} e^{i\phi_n^{down}} \ . \tag{5.60}$$

If the energy were distributed evenly over all of the modes, or if the energy were distributed randomnly, this problem would be nearly impossible. In practise, it is observed that most of the energy is confined to the first few modes and so the series is truncated appropriately.

Because the coefficients are complex, whereas the normal modes are real, it is possible to do four independent fits:

$$\text{(i) } \Re(\mathbf{u}_{obs}) \text{ to give } \Re(\mathbf{A}_n^{up} + \mathbf{A}_n^{down})$$

$$\text{(ii) } \Im(\mathbf{u}_{obs}) \text{ to give } \Im(\mathbf{A}_n^{up} + \mathbf{A}_n^{down})$$

$$\text{(iii) } \Re(\rho_{obs}) \text{ to give } \Re(\mathbf{A}_n^{up} - \mathbf{A}_n^{down})$$

$$\text{(iv) } \Im(\rho_{obs}) \text{ to give } \Im(\mathbf{A}_n^{up} - \mathbf{A}_n^{down}) \quad .$$

By adding and subtracting, one can solve for the two complex quantities, $\mathbf{A}_n^{down}$ and $\mathbf{A}_n^{up}$, that describe the modal distribution.

5.8.2 Constraints to Modal Fitting

The knowledge of the tidal elevations in, and geometry of, Indian Arm allow the constraint of the least squares fit of the observations to the normal modes. The first eigenfunction, mode 0, corresponds to the barotropic tide. Harmonic analysis of the sea surface elevation data, combined with knowledge of the inlet geometry, allow the calculation of the u and ρ-oscillations of the barotropic tide.

The analysis of the tidal height data showed that there was little phase change along the inlet and no measureable change in the amplitude. The estimated total energy loss from the tide was about $10 - 15$ % . It is, therefore, possible to consider the barotropic tide as a standing wave, or as the sum of two waves travelling in opposite directions, one from the mouth, the other from the head. It is possible to write

$$a_n^{up} = a_n^{down} \quad . \tag{5.61}$$

The amplitude of the tide η_0 together with the frequency ω, the surface area landward of the chosen station S and the cross-sectional area A give:

$$u_{bt} = \frac{\eta_0 \omega S}{A} \quad . \tag{5.62}$$

In fitting the barotropic tide to the modal analysis, the equation for the barotropic mode is

$$u_{bt}e^{i\phi_{bt}} = U_0(\mathbf{A}_0^{up} + \mathbf{A}_0^{down}) \quad . \tag{5.63}$$

To evaluate this equation it is necessary to consider the phase speed of the wave at a point in the inlet. If the inlet is flat bottomed, then the phase at the head of the inlet will be $(\phi_0^{up} + \frac{l\omega}{c_0})$. The distance to the head is l and c_0 is the barotropic phase speed. The phase speed of the barotropic wave will be $(\phi_0^{down} - \frac{l\omega}{c_0})$ at the head. Since these two waves must be out of phase by 180° then:

$$\phi_0^{up} + \frac{l\omega}{c_0} = \phi_0^{down} - \frac{l\omega}{c_0} + \pi \quad . \tag{5.64}$$

It has already been argued that the amplitude of the up-inlet wave is equal to that of the down-inlet wave so it is possible to rewrite equation (5.63) to give

$$u_{bt}e^{i\phi_{bt}} = a_0^{up}U_0(e^{i\phi_0^{up}} + e^{i(\phi_0^{up} + \frac{2l\omega}{c_0} - \pi)}) \quad . \tag{5.65}$$

After some manipulation this equation becomes

$$u_{bt}e^{i\phi_{bt}} = 2a_0^{up}U_o sin(\frac{l\omega}{c_0})e^{i(\phi_0^{up} + \frac{l\omega}{c_0} - \frac{\pi}{2})} \quad , \tag{5.66}$$

and the amplitude is written

$$a_0^{up} = a_0^{down} = \frac{u_{bt}}{2U_0 sin(\frac{l\omega}{c_0})} = \frac{u_{bt}csc(\frac{l\omega}{c_0})}{2U_0} \quad . \tag{5.67}$$

For the phases the equations are

$$\phi_0^{up} = \phi_{bt} - \frac{l\omega}{c_0} + \frac{\pi}{2} \quad , \tag{5.68}$$

$$\phi_n^{down} = \phi_{bt} + \frac{l\omega}{c_0} - \frac{\pi}{2} \quad . \tag{5.69}$$

From these equations (5.67 – 5.69), it is possible to compute the amplitude and phase of the up- and down-inlet barotropic modes.

In an inlet with varying depth, c_0 will change along the inlet and so $\frac{l\omega}{c_0}$ should really be evaluated as an integral

$$\Delta\phi = \int_{Station}^{Head} \frac{\omega}{c_0(x)}dx \quad .$$

This integral was computed using the bottom bathymetry to find the value needed for the phase computation.

In *Table 15* are given the physical characteristics needed to solve the equations. The mean depth listed was used to compute the mean phase speed needed for the phase calculations.

Table 15
Indian Arm Physical Characteristics and the Barotropic Phase Speed

Station	S (km^2)	A (km^2)	l (km)	$\sqrt{h_{mean}}$ $(m^{1/2})$	c_{mean} (ms^{-1})
Buntzen (C4)	12.37	0.1568	10.0	11.65	33.79
Basin (C3)	14.56	0.1132	12.0	12.11	37.89
Twin (C2)	15.68	0.1145	13.0	12.24	38.88
Cove (CS)	24.07	0.04977	17.5	11.77	36.85
Narrows (C1)	24.33	0.02937	18.0	11.77	36.85

The amplitudes and phases for the M_2 and K_1 barotropic tide are given in *Table 16.*

Table 16
Amplitudes and Phases of Up and Down Inlet Barotropic M_2 and K_1 Tides

Station	u_{bt} (cms^{-1})	$\Delta\phi$ $(°)$	a_0U_0 (cms^{-1})	ϕ_0^{up} $(°)$	ϕ_0^{down} $(°)$
M_2 Tide					
Buntzen	1.03	2.38	12.40	172.6	357.4
Basin	1.69	2.55	18.99	172.5	357.6
Twin	1.80	2.69	19.18	172.4	357.7
Cove	6.33	3.82	47.51	171.4	359.0
Narrows	10.87	3.93	79.30	171.0	358.5
K_1 Tide					
Buntzen	0.52	1.24	12.02	173.8	356.2
Basin	0.84	1.32	18.23	173.7	356.3
Twin	0.90	1.39	18.55	173.6	356.4
Cove	3.16	1.98	45.73	173.2	357.2
Narrows	5.42	2.04	76.13	171.4	355.4

The errors in these computed values may not be small because of their reliance upon the *cosec* of a small angle, however, it is still worth computing the barotropic mode and subtracting it from the rest. The $\mathbf{A}_0^{up}$ and $\mathbf{A}_0^{down}$ terms were subtracted from the right

hand side of equations (5.57) and (5.58) leaving just the internal modes to be fit. Even if in error, the barotropic mode is a constant subtracted from all the fits.

Even though the phase of the barotropic tide ϕ_{bt} is itself difficult to determine accurately, the phases of the ρ and u oscillations relative to it are fixed. The phase of the u-oscillation is $(\phi_{bt} - \frac{\pi}{2})$. The phase of the ρ-oscillations is $(\phi_{bt} + \frac{\pi}{2})$.

5.8.3 Energy Flux of the Internal Modes

To investigate the resonance hypothesis, it is necessary to compute the energy flux in each of the internal modes which have been fit to the data. Gill (1982, pg. 140) shows that the energy density per unit volume of an internal wave can be written

$$E = \frac{1}{2}\rho_0\overline{(u^2 + v^2 + w^2)} + \frac{g^2\overline{\rho'^2}}{2\rho_0 N^2} \ , \tag{5.70}$$

where ρ' represents the perturbation density defined by Gill as

$$\rho' = \rho_0(z) - \rho_0(z + h') \ , \tag{5.71}$$

where h' is the perturbation displacement. Computation of the energy density in the fjord requires integration of equation (5.70) with respect to width and depth.

$$E_l = \int_0^H \int_{-W/2}^{W/2} E dy\, dz \ , \tag{5.72}$$

where E_l is the energy density per unit length, and z=0 is at the bottom. If the theory of normal modes is applied, and the Kelvin wave representation of the internal waves is used since it is now necessary to integrate across the channel, then the velocity and density are written as in equations (5.40-5.42). Upon substitution into equation (5.72) and noting that $h_n = {c_n}^2/g$ and $R_n = c_n/f$, where R_n is the Rossby deformation radius, one obtains

$$E_l = \frac{1}{4}\frac{\rho_0 {U_0}^2 {c_n}^2 W F}{g^2} \int_0^H ({c_n}^2(\frac{dZ}{dz})^2 + \omega^2 Z^2 + N^2 Z^2) dz \ . \tag{5.73}$$

In this equation F is

$$F = \frac{R_n}{W} sinh \frac{W}{R_n} \ . \tag{5.74}$$

The factor of 1/2 comes from the averaging of the velocity and density in equation (5.70). The first term in equation (5.73) represents the kinetic energy from the longitudinal velocity. The second term is the kinetic energy due to vertical velocity and the last term is the energy associated with isopycnal displacements. Because $\omega^2 << N^2$ everywhere in the inlet, the last term is much larger than the middle term. The energy flux is written

$$Flux = E_l c_n \quad , \tag{5.75}$$

where c_n is the group velocity of the nth mode.

For the barotropic mode there is a fourth component to the above equation (5.73) from the sea surface elevation term, which for the internal waves is negligible. For the barotropic tide it is

$$\frac{1}{4}\bar{\rho}_0 g \eta_0{}^2 FW \quad . \tag{5.76}$$

For the purposes of the fitting procedure, only the fluxes of the internal modes are of interest.

5.8.4 Calculation of the Fit

Both the 1983/84 and 1984/85 data were fit with normal modes to investigate the energy flux in the inlet. Only the 1983/84 results will be discussed in any detail since it was in that year that the change in the internal response was observed. The 1984/85 data set was analysed to investigate the change in the phase of the internal tide as it propagated along the inlet. The extra cyclesonde moorings, C2 and C4, were deployed to aid in this analysis. Unfortunately, no reliable results were obtained from this analysis. The internal tide was weak during the period when the extra moorings were in place. This weak internal response made the modal fitting difficult and thus the phase change observations were not good. The 1984/85 internal tide will not be discussed for these reasons.

The error in the fits is difficult to determine since it is just a sophisticated least squares fitting procedure, the significance of the fit may not be determined by a measure of the residual. It may be possible to produce a very good looking fit with 10 modes; however,

there may be only 2 modes present in the real system and it may be that there is no physical significance to 8 out of the 10 modes fit. The technique for the fitting was therefore to accept the best fit with the smallest number of modes. Occam's razor was applied.

Error in the original harmonic analysis of the cyclesonde data was estimated using a technique suggested by Freeland and Farmer (1980). The root mean square noise level in the band between the diurnal and the semi-diurnal was considered to be noise ($\mathcal{N}$). If this noise is added to the harmonic constituent vector of amplitude $\mathcal{A}$, there is a circle of uncertainty about that vector subtending an angle of $\mathcal{N}/\mathcal{A}$ radians. The average error of the angle is ($\mathcal{N}/\mathcal{A}\sqrt{2}$). The error in the computed phase was always less than 10° for both the current and the density data. The largest error was near the bottom, where the signal was weakest. The noise level was, on average, about 10-20% of the signal level.

The 1983/84 data were broken up into intervals of approximately two weeks duration. The N^2 profiles used for the computation of the normal modes were formed by combining the CTD data with the cyclesonde data, which were averaged over the 2 week period.

Fits for the M_2 and the K_1 constituents in the basin in 1983/84 are shown in *Tables 17 – 20.* Results for M_2 and K_1 at the sill in 1983/84 are shown in *Tables 21 – 24.* The energy fluxes for mode 1, usually the most energetic mode, and the total fluxes up and down-inlet for the best fits, indicated by bold face in *Tables 17 – 24*, are given in *Tables 25 – 26.* All of the cyclesonde data were used, both the velocity and density data, although only the velocity results are presented here. The results are presented as velocity amplitude/Greenwich phase with the velocity given in $cm\,s^{-1}$. A blank entry in the table means that the mode was excluded from the set to be fitted to the observations. The barotropic tidal velocity and density amplitude were fixed for all of the fits. The barotropic velocities of *Tables 17 – 24* are for the up- and down-inlet barotropic modes. The barotropic tidal velocity which would be observed is given by the sum of the two waves which differ in phase by more than 180°. The normalization constant U_0 for each eigenfunction was chosen such that the a_n values are the amplitudes of the dimensional eigenfunctions. It was necessary to scale the

velocity data relative to the density data, a process which is equivalent to weighting the velocity data relative to the density data. The scaling chosen for the fitting was such that $20\,cm\,s^{-1}$ was equivalent to $0.4\,kg\,m^{-3}$. This equivalency was used throughout.

Below each of the fit results, the residual variance of the fit is given. This residual gives the root mean square difference between the fit and the data. It is a measure of the goodness of the fit. Although the results of the density fitting are not included in these tables, the residual variance is for all of the data. The best fit was chosen based upon the minimum value of the residual variance with the smallest number of modes.

Table 17
Fit of M_2 modes to cyclesonde data at the basin station C3. The data are given as (velocity/phase) with the velocity in cm s^{-1}.

Fit#	1	2	3	4	5
8–23 Nov 1983					
Up-inlet mode 0	19.0/172	19.0/172	**19.0/172**	19.0/172	19.0/172
1	6.47/349	4.11/8	**4.41/358**	4.41/351	6.0/343
2	2.88/207	5.18/293	**4.99/293**	–	1.29/52
3	6.16/328	–	–	–	6.09/299
Down-inlet mode 0	19.0/358	19.0/358	**19.0/358**	19.0/358	19.0/358
1	3.09/26	3.34/58	**3.17/53**	2.83/11	–
2	0.45/119	2.00/293	–	–	–
3	1.51/247	–	–	–	–
Residual variance	0.93	2.0	**2.2**	3.9	1.9
25 Nov–10 Dec 1983					
Up-inlet mode 0	19.0/172	19.0/172	**19.0/172**	19.0/172	19.0/172
1	4.86/339	4.06/345	**4.12/344**	5.15/343	
2	2.13/182	3.01/291	**3.17/291**	–	2.31/305
3	2.43/316	–	–	–	2.48/291
Down-inlet mode 0	19.0/358	19.0/358	**19.0/358**	19.0/358	19.0/358
1	2.66/14	2.48/30	**2.49/30**	2.49/11	–
2	0.47/153	0.48/283	–	–	–
3	0.99/292	–	–	–	–
Residual variance	0.99	1.4	**1.4**	2.8	1.8
12–27 Dec 1983					
Up-inlet mode 0	19.0/172	19.0/172	**19.0/172**	19.0/172	19.0/172
1	3.84/7	2.86/0	**2.86/0**	3.15/356	3.91/15
2	2.33/262	1.92/317	**2.01/317**	–	1.54/255
3	2.71/34	–	–	–	2.44/11
Down-inlet mode 0	19.0/358	19.0/358	**19.0/358**	19.0/358	19.0/358
1	1.79/70	1.41/99	**1.40/99**	1.51/87	–
2	1.13/198	0.16/320	–	–	–
3	1.01/352	–	–	–	–
Residual variance	0.17	0.43	**0.42**	0.72	0.38
10–25 Jan 1984					
Up-inlet mode 0	19.0/172	19.0/172	**19.0/172**	19.0/172	19.0/172
1	6.94/44	3.60/61	**3.75/64**	3.26/26	6.94/47
2	3.08/237	1.51/309	**2.17/303**	–	3.26/249
3	2.33/30	–	–	–	2.74/58
Down-inlet mode 0	19.0/358	19.0/358	**19.0/358**	19.0/358	19.0/358
1	4.98/117	4.08/109	**3.27/108**	2.27/101	/
2	1.83/304	1.05/291	–	–	–
3	0.62/114	–	–	–	–
Residual variance	0.023	0.19	**0.20**	0.35	0.40
23 Jan–7 Feb 1984					
Up-inlet mode 0	19.0/172	19.0/172	**19.0/172**	19.0/172	19.0/172
1	2.80/49	1.71/27	**1.72/25**	1.94/18	2.96/55
2	2.86/282	1.26/344	**1.48/337**	–	2.24/265
3	1.70/71	–	–	–	1.93/66
Down-inlet mode 0	19.0/358	19.0/358	**19.0/358**	19.0/358	19.0/358
1	2.92/111	1.74/126	**1.71/126**	1.41/119	–
2	2.80/277	0.45/303	–	–	–
3	1.57/99	–	–	–	–
Residual variance	0.11	0.40	**0.39**	0.45	0.48

Table 18
Fit of M_2 modes to cyclesonde data at the basin station C3 (continued from Table 17).

Fit#	1	2	3	4	5
11–25 Feb 1984					
Up-inlet mode 0	19.0/172	19.0/172	**19.0/172**	19.0/172	19.0/172
1	1.97/49	1.12/22	**1.21/20**	1.51/8	2.24/54
2	2.63/274	1.02/317	**1.48/332**	–	2.15/264
3	1.19/70	–	–	–	1.49/67
Down-inlet mode 0	19.0/358	19.0/358	**19.0/358**	19.0/358	19.0/358
1	2.40/122	1.51/136	**1.45/134**	1.07/227	–
2	2.16/307	0.90/360	–	–	–
3	1.02/109	–	–	–	–
Residual variance	0.053	0.19	**0.19**	0.25	0.25

Table 19
Fit of K_1 modes to cyclesonde data at the basin station C3. The data are given (velocity/phase) with the velocity in $cm\,s^{-1}$.

Fit#	1	2	3	4	5
8–23 Nov 1983					
Up-inlet mode 0	18.2/174	**18.2/174**	18.2/174	18.2/174	18.2/174
1	1.46/306	**1.63/334**	1.64/324	1.51/318	1.66/306
2	0.67/149	**1.74/193**	1.71/191	–	1.72/171
3	1.26/199	–	–	–	1.13/237
Down-inlet mode 0	18.2/356	**18.2/356**	18.2/356	18.2/356	18.2/356
1	1.38/212	**0.82/188**	0.88/194	1.62/193	–
2	0.60/70	**0.65/244**	–	–	–
3	1.14/263	–	–	–	–
Residual variance	0.072	**0.16**	0.19	0.39	0.22

Table 20
Fit of K_1 modes to cyclesonde data at the basin station C3 (continued from Table 19).

Fit#	1	2	3	4	5
25 Nov–10 Dec 1983					
Up inlet mode 0	18.2/174	**18.2/174**	18.2/174	18.2/174	18.2/174
1	1.44/317	**1.47/325**	1.59/318	1.59/314	1.60/301
2	1.48/219	**1.70/221**	1.95/227	–	1.98/223
3	0.69/187	–	–	–	0.59/245
Down-inlet mode 0	18.2/356	**18.2/356**	18.2/356	18.2/356	18.2/356
1	1.07/218	**0.94/207**	0.92/205	1.41/203	–
2	0.73/263	**0.96/261**	–	–	–
3	0.76/298	–	–	–	–
Residual variance	0.087	**0.14**	0.25	0.77	0.34
10–27 Dec 1983					
Up-inlet mode 0	18.2/174	**18.2/174**	18.2/174	18.2/174	18.2/174
1	1.26/310	**1.31/315**	1.40/314	1.40/304	1.64/299
2	1.28/196	**1.53/195**	1.42/220	–	1.60/212
3	0.36/187	–	–	–	0.32/322
Down-inlet mode 0	18.2/356	**18.2/356**	18.2/356	18.2/356	18.2/356
1	0.82/221	**0.74/223**	0.76/231	1.00/228	–
2	1.19/312	**1.20/307**	–	–	–
3	0.10/276	–	–	–	–
Residual Variance	0.041	**0.041**	0.124	0.28	0.165
10–25 Jan 1984					
Up-inlet mode 0	18.2/174	**18.2/174**	18.2/174	18.2/174	18.2/174
1	5.94/286	**4.21/2**	3.80/9	5.69/324	4.37/311
2	2.83/50	**2.33/256**	3.65/283	–	1.67/339
3	3.82/249	–	–	–	2.64/271
Down-inlet mode 0	18.2/356	**18.2/356**	18.2/356	18.2/356	18.2/356
1	4.09/49	**0.90/95**	1.66/337	3.06/309	–
2	3.59/269	**2.90/316**	–	–	–
3	1.71/27	–	–	–	–
Residual variance	0.26	**0.48**	0.63	1.04	0.54
23 Jan–7 Feb 1984					
Up-inlet mode 0	18.2/174	**18.2/174**	18.2/174	18.2/174	18.2/174
1	3.37/307	**2.83/321**	2.96/321	3.10/312	3.68/313
2	1.37/177	**2.45/226**	2.33/244	–	1.70/260
3	1.66/256	–	–	–	0.73/255
Down-inlet mode 0	18.2/356	**18.2/356**	18.2/356	18.2/356	18.2/356
1	1.45/321	**1.31/312**	1.38/313	1.67/294	–
2	1.02/302	**1.22/333**	–	–	–
3	0.81/50	–	–	–	–
Residual variance	0.15	**0.19**	0.22	0.41	0.35
11–25 Feb 1984					
Up-inlet mode 0	18.2/174	**18.2/174**	18.2/174	18.2/174	18.2/174
1	4.23/321	**3.20/340**	3.39/341	3.64/332	4.47/330
2	2.02/138	**2.27/241**	2.18/272	–	0.90/317
3	2.36/274	–	–	–	1.26/282
Down-inlet mode 0	18.2/356	**18.2/356**	18.2/356	18.2/356	18.2/356
1	1.93/352	**1.48/340**	1.67/342	1.96/325	–
2	1.51/304	**1.86/351**	–	–	–
3	1.16/58	–	–	–	–
Residual variance	0.18	**0.28**	0.33	0.44	0.45

Table 21
Fit of M_2 modes to cyclesonde data at the sill station C1.

Fit#	1	2	3	4
8–23 Nov 1983				
Up-inlet mode 0	79.3/171	79.3/171	**79.3/131**	79.3/171
1	139.0/207	16.0/87	**23.2/88**	7.7/30
2	74.5/124	9.7/291	**12.2/287**	–
3	72.1/302	–	–	–
Down-inlet mode 0	79.3/359	79.3/359	**79.3/359**	79.3/359
1	151.9/124	19.4/122	**13.5/139**	23.8/124
2	62.0/302	3.1/271	–	–
3	41.9/127	–	–	–
Residual variance	6.1	6.6	**5.9**	18
25 Nov–10 Dec 1983				
Up-inlet mode 0	79.3/171	**79.3/171**	79.3/171	79.3/171
1	25.9/172	**15.8/239**	23.4/254	17.7/256
2	12.6/120	**7.3/316**	7.8/67	–
3	6.9/297	–	–	–
Down-inlet mode 0	79.3/359	**79.3/359**	79.3/359	79.3/359
1	23.0/209	**23.4/242**	16.9/221	16.9/221
2	9.2/6	**13.2/101**	–	–
3	3.3/157	–	–	–
Residual variance	0.70	**1.7**	3.4	8.2
12–27 Dec 1983				
Up-inlet mode 0	79.3/171	**79.3/171**	79.3/171	79.3/171
1	5.5/65	**13.5/89**	13.2/86	4.6/58
2	1.7/282	**11.4/282**	10.8/280	–
3	3.2/291	–	–	–
Down-inlet mode 0	79.3/359	**79.3/359**	79.3/359	79.3/359
1	15.1/100	**6.5/110**	7.1/115	7.3/114
2	9.4/268	**0.9/154**	–	–
3	3.2/84	–	–	–
Residual variance	0.37	**0.61**	0.54	4.9
25 Dec–10 Jan 1983/84				
Up-inlet mode 0	79.3/171	**79.3/171**	79.3/171	79.3/171
1	189/322	**21.6/140**	15.7/144	7.8/47
2	105/143	**14.9/342**	12.5/348	–
3	27./332	–	–	–
Down-inlet mode 0	79.3/359	**79.3/359**	79.3/359	79.3/359
1	218/131	**8.6/71**	12.9/96	16.0/118
2	120/310	**3.2/131**	–	–
3	28.0/124	–	–	–
Residual variance	1.0	**1.5**	1.3	3.5

Table 22
Fit of M_2 modes to cyclesonde data at the sill station C1 (continued from Table 21).

Fit#	1	2	3	4
10–25 Jan 1984				
Up-inlet mode 0	79.3/171	79.3/171	**79.3/171**	79.3/171
1	114/314	23.6/88	**21.0/90**	10.0/70
2	71/132	9.6/282	**8.5/286**	–
3	23.0/312	–	–	–
Down-inlet mode 0	79.3/359	79.3/359	**79.3/359**	79.3/359
1	152/123	11.5/134	**13.1/123**	16.7/120
2	89.0/302	1.4/75	–	–
3	28.0/119	–	–	–
Residual variance	0.62	0.84	**0.73**	2.3
23 Jan – 10 Feb 1984				
Up-inlet mode 0	79.3/171	79.3/171	**79.3/171**	79.3/171
1	14.1/20	19.2/90	**21.2/96**	7.2/58
2	7.9/185	12.7/290	**14.8/292**	–
3	5.5/330	–	–	–
Down-inlet mode 0	79.3/359	79.3/359	**79.3/359**	79.3/359
1	34.0/115	11.9/113	**9.2/106**	9.8/106
2	21.2/297	2.7/317	–	–
3	7.3/105	–	–	–
Residual variance	0.42	1.9	**1.75**	9.3
10–27 Feb 1984				
Up-inlet mode 0	79.3/171	**79.3/171**	79.3/171	79.3/171
1	4.2/42	**14.8/102**	20.9/113	4.7/77
2	1.6/173	**10.6/294**	16.9/303	–
3	3.4/313	–	–	–
Down-inlet mode 0	79.3/359	**79.3/359**	79.3/359	79.3/359
1	30.9/118	**15.6/130**	7.9/124	8.4/124
2	21.4/296	**7.4/316**	–	–
3	5.6/99	–	–	–
Residual variance	0.25	**1.2**	1.3	10.
23 Feb–7 Mar 1984				
Up-inlet mode 0	79.3/171	79.30/171	**79.3/171**	79.3/171
1	7.14/21	24.4/110	**31.5/112**	5.2/83
2	5.1/172	19.4/296	**26.0/298**	–
3	8.1/311	–	–	–
Down-inlet mode 0	79.3/359	79.3/359	**79.3/359**	79.3/359
1	40.3/120	17.0/123	**9.16/124**	10.1/123
2	27.8/298	7.3/301	–	–
3	6.5/112	–	–	–
Residual variance	0.50	1.9	**1.9**	23.

Table 23
Fit of K_1 modes to cyclesonde data at the sill station C1.

Fit#	1	2	3	4
8–23 Nov 1983				
Up-inlet mode 0	76.1/171	76.1/171	**76.1/171**	76.1/171
1	75.6/263	12.2/48	**13.0/52**	7.7/3
2	41.9/78	5.6/266	**6.0/267**	–
3	40.7/260	–	–	–
Down-inlet mode 0	76.1/355	76.1/355	**76.1/355**	76.1/355
1	74.6/79	2.34/189	**2.6/215**	4.3/114
2	34.5/256	0.48/278	–	–
3	24.0/74.0	–	–	–
Residual variance	1.8	1.9	**1.7**	4.8
25 Nov–10 Dec 1983				
Up-inlet mode 0	76.1/171	**76.1/171**	76.1/171	76.1/171
1	5.9/32	**10.1/81**	10.9/79	2.2/10
2	5.4/230	**12.9/274**	14.0/270	–
3	2.6/314	–	–	–
Down-inlet mode 0	76.1/355	**76.1/355**	76.1/355	76.1/355
1	11.9/99	**3.5/103**	2.9/118	2.8/120
2	11.9/274	**1.5/237**	–	–
3	3.3/86	–	–	–
Residual variance	0.16	**0.84**	0.75	1.1
12–25 Dec 1983				
Up-inlet mode 0	76.1/171	**76.1/171**	76.1/171	76.1/171
1	3.9/242	**5.8/98**	4.4/106	1.3/77
2	5.6/63	**5.4/284**	4.0/296	–
3	3.5/270	–	–	–
Down-inlet mode 0	76.1/355	**76.1/355**	76.1/355	76.1/355
1	10.0/89	**2.8/148**	3.8/119	3.9/120
2	7.7/254	**2.2/74**	–	–
3	3.1/66	–	–	–
Residual variance	0.28	**0.56**	0.55	1.0
25 Dec–10 Jan 1984				
Up-inlet mode 0	76.1/171	76.1/171	**76.1/171**	76.1/171
1	67.4/225	25.8/256	**50.7/272**	28.7/267
2	34.3/34	2.8/55	**15.2/100**	–
3	9.1/215	–	–	–
Down-inlet mode 0	76.1/355	76.1/355	**76.1/355**	76.1/355
1	40.6/312	38.9/268	**15.8/231**	21.7/247
2	21.3/144	14.4/108	–	–
3	1.9/321	–	–	–
Residual variance	0.57	0.73	**1.1**	4.4

Table 24
Fit of K_1 modes to cyclesonde data at the sill station C1 (continued from Table 23).

Fit#	1	2	3	4
10–25 Jan 1984				
Up-inlet mode 0	76.1/171	**76.1/171**	76.1/171	76.1/171
1	177/275	**20.2/101**	5.4/139	4.4/11
2	110/95	**11.7/299**	6.1/342	–
3	35.6/281	–	–	–
Down-inlet mode 0	76.1/355	**76.1/355**	76.1/355	76.1/355
1	193/90	**5.4/139**	6.8/75	7.5/96
2	119/268	**6.1/342**	–	–
3	39/85	–	–	–
Residual variance	0.64	**1.3**	1.5	2.2
23 Jan–10 Feb 1984				
Up-inlet mode 0	76.1/171	76.1/171	**76.1/171**	76.1/171
1	10.7/275	11.1/81	**9.9/71**	2.7/19
2	8.9/82	9.2/274	**7.8/266**	–
3	6.2/272	–	–	–
Down-inlet mode 0	76.1/355	76.1/355	**76.1/355**	76.1/355
1	24.9/77	3.9/39	**4.3/71**	4.6/72
2	17.2/257	2.0/134	–	–
3	6.5/79	–	–	–
Residual variance	0.24	0.87	**0.78**	2.8
10–25 Feb 1984				
Up-inlet mode 0	76.1/171	76.1/171	**76.1/171**	76.1/171
1	10.4/292	10.0/85	**12.0/78**	3.5/24
2	9.1/94	8.7/284	**10.1/274**	–
3	5.8/282	–	–	–
Down-inlet mode 0	76.1/355	76.1/355	**76.1/355**	76.1/355
1	28.2/90	8.4/77	**6.2/88**	6.5/88
2	19.9/270	2.4/230	–	–
3	6.1/93	–	–	–
Residual variance	0.11	0.89	**0.80**	4.0
23 Feb – 7 Mar 1984				
Up-inlet mode 0	76.1/171	76.1/171	**76.1/171**	76.1/171
1	12.0/304	12.1/91	**12.4/80**	4.2/29
2	10..3/108	10.4/290	**9.9/278**	–
3	7.3/298	–	–	–
Down-inlet mode 0	76.1/355	76.1/355	**76.1/355**	76.1/355
1	28.7/87	7.4/59	**6.4/80**	6.8/81
2	19.8/266	2.5/181	–	–
3	6.7/84	–	–	–
Residual variance	0.51	2.2	**1.9**	4.8

Table 25
Total baroclinic energy fluxes and fluxes for mode 1 (in brackets) for the M_2 constituent in 1983/84. Fluxes are in MW.

	Basin		Sill	
Start Date	Up	Down	Up	Down
8 Nov	.0590 (.0317)	.0164(.0164)	.232 (.207)	.0708 (.0708)
25 Nov	.0363 (.0284)	.0104 (.0104)	.221 (.212)	.115 (.112)
12 Dec	.0128 (.0103)	.0025 (.0025)	.0552 (.0367)	.0086 (.0086)
25 Dec	–	–	.0981 (.0732)	.0498 (.0249)
10 Jan	.0245 (.0201)	.0153 (.0153)	.0625 (.1351)	.0515 (.0515)
23 Jan	.0050 (.0035)	.0035 (.0035)	.108 (.0804)	.0153 (.0153)
11/10 Feb	.0030(.0016)	.0023 (.0023)	.115 (.0796)	.0113 (.0113)
23 Feb	–	–	.264 (.1790)	.0153 (.0153)

Table 26
Total baroclinic energy fluxes and fluxes for mode 1 (in brackets) for the K_1 constituent in 1983/84. Fluxes are in MW.

	Basin		Sill	
Start Date	Up	Down	Up	Down
8 Nov	.0071 (.0044)	.00132 (.0013)	.0711 (.0652)	.0026 (.0026)
25 Nov	.0059 (.0036)	.0022 (.0015)	.0454 (.0212)	.003 (.0026)
12 Dec	.0037 (.0021)	.0017 (.0007)	.0110 (.0070)	.0024 (.0016)
25 Dec	–	–	.803 (.766)	.0776 (.0746)
10 Jan	.0333 (.0203)	.0039 (.00039)	.145 (.122)	.0473 (.0330)
23 Jan	.0135 (.0095)	.0030 (.0020)	.0255 (.0177)	.0035 (.0035)
11/10 Feb	.0144 (.0111)	.0046 (.0024)	.0395 (.0263)	.0070 (.0070)
23 Feb	–	–	.0403 (.0266)	.0099 (.0099)

Some measure of the quality of the modal fit can be obtained by looking at the residual variance. *Figure 68* shows the observed and fitted current data in November 1983 for the M_2 constituent at the basin station. As mentioned earlier, the residual variance is not a measure of the dynamical significance of the plot. Some of the fits, which look very good if only the residual variance is considered, also predict more energy to travel down the inlet than up, a physically unrealistic result.

Differentiating between the fits in the basin is difficult. Even fits using only up-inlet propagating waves produce reasonable fits. That the best fits are produced using six internal modes, three up and three down, may be indicative of the presence of down-inlet propagating energy. It may also be a result of having more degrees of freedom to make

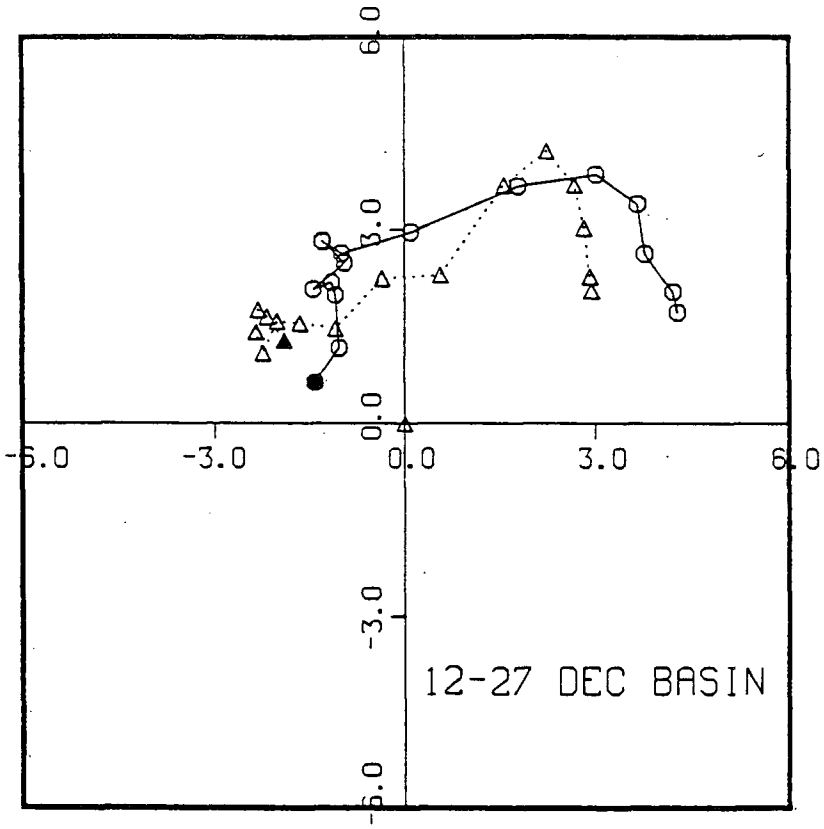

Figure 68 Plot of the raw data and the computed fit for the basin station in December 1983. The raw data is shown by the solid line, the fitted data by the dashed line. The scale is in $cm\,s^{-1}$.

the fit.

In reviewing the data, it was concluded that the best fit using the smallest number of modes was number 3 (using modes 1 and 2 up-inlet and mode 1 down-inlet). Sometimes fit 2, with an extra mode (mode 2 down-inlet), was chosen. For the period beyond 12-December, the residual variances fits # 2 and 3 are the smallest of all fits , except fit # 1 (which almost always has too much energy propagating down-inlet).

Table 21, which presents the fit for the K_1 constituent, shows similar results. There is some variation in the phase of the modes although there is no clear trend. There should be a phase change of 180° for a system that goes completely through resonance. In comparison

with the M_2 fitting the residual variances are small, perhaps indicating less noise at lower frequencies. In general, the best fit for the K_1 was found with waves propagating in both directions.

At the sill no reasonable fit could be found with only up-inlet waves. The residual variance was always 2-3 times greater than the residual variance for the worst other fit. For this reason, fits with only up-inlet modes are not included in *Tables 22 and 23*. As in the basin, the fits at the K_1 frequency appear to be better than those at the M_2 frequency.

In all of these fits, mode 1 is the most energetic with few exceptions. The higher modes generally show decreasing amplitudes and energy. Even if the amplitudes of two modes are the same, the higher mode will transport less energy since the higher modes have lower group velocities. *Tables 25 and 26* show the energy fluxes for the basin and sill stations from the fits indicated in the earlier tables as the best fits. A large amount of energy was found to propagate down-inlet at all times. When the energy flux is small, as it is for the M_2 in January and February, the reliability of the down-inlet fluxes is doubtful. The down-inlet energy flux was about 20-30 % of the up-inlet flux for the basin station. Thus, about 70 % of the internal tide propagating up-inlet is lost, but some reflects off the head of the inlet so that $20 - 30\%$ is left propagating down-inlet at the basin station.

The sill station shows a much larger flux than does the basin station. Because the sill station is on the slope, where the internal tide is being generated, there may be some effect upon the results. If the computed fluxes are true, it indicates that a large percentage of the internal tide generated on the slope does not make it into the basin. In November, for instance, about 0.2 MW propagates up-inlet away from the sill at the M_2 frequency, while only 0.05 MW was observed propagating up-inlet at the basin station. This result was also observed in 1984/85 when more stations were available in the basin and along the slope from the sill. The large energy flux propagating down-inlet at the sill, almost 50% of the total in November, may be indicative of energy loss from the internal tide along the slope.

The loss of the basin data for the second half of December 1983 leaves open the question

as to the significance of the very high energy propagation away from the sill at the K_1 frequency during this period. The energy fluxes do clearly show the increased flux at the K_1 frequency during the 1983/84 winter, and the decreased flux at the M_2 frequency.

The down-inlet fluxes are consistent with a resonance interpretation of the internal tide in 1983/84. Sufficient energy is observed to propagate down-inlet to feed a resonance response in the internal tide.

5.9 Comparison with Stacey's Model

Stacey (1984) developed a linear model, based upon the observed stratification, to predict the energy flux of each mode in an inlet. The model is a slight generalization of a model of Stigebrandt (1976, 1980). Stacey allows for arbitrary stratification and also permits the depths on opposite sides of the sill to differ. The walls of the inlet are assumed to be vertical and the bottom flat. The horizontal velocity field is written as the sum of normal modes which must vanish below sill depth, on either side of the sill. The horizontal velocity is set equal to the barotropic velocity, above the sill. Using this approach, Stacey (1984) estimates the energy flux in the nth mode as:

$$\varepsilon_n = \frac{\bar{\rho}_0 W c_n u_{bt}^2 Z_n(-d)}{2\int_0^H Z'_n{}^2 dz} \quad , \tag{5.77}$$

where ε_n is the energy flux, d is the sill depth, u_{bt} is the barotropic tidal velocity amplitude over the sill , H is the basin depth and Z_n is the nth normal mode.

The normal modes Z_n are computed for the water depth on the side of the sill for which energy fluxes are desired. *Table 27* shows the observed and predicted fluxes at the M_2 and K_1 frequencies for mode 1 in the winter of 1983/84.

Although not the same, the model does predict the fluxes to within a factor of about 4. Except for the December period, the model predicts a fairly constant energy flux for the M_2 constituent, just below 0.01 MW. The observed flux is initially about 3 times greater and then drops to about 1/4 that of the predicted value.

Table 27
Predicted and fitted M_2 and K_1 mode 1 energy fluxes in 1983/84. The predictions are made using the linear model of Stacey (1984).

	M_2		K_1	
Start Date	*Fitted (MW)*	*Model (MW)*	*Fitted (MW)*	*Model (MW)*
8 November	0.0317	0.0101	0.0044	0.0025
25 November	0.0284	0.0093	0.0036	0.0022
12 December	0.0103	0.0059	0.0021	0.0015
10 January	0.0201	0.0093	0.0203	0.0023
23 January	0.0035	0.0077	0.0095	0.0019
11 February	0.0016	0.0077	0.0111	0.0019

The model does not take resonance into account; so if resonance does occur the model can be expected to underestimate the energy flux. Therefore, the M_2 predictions in November and December can be expected to be low, while the January and February predictions should be better. The reverse should hold for the K_1. In fact, the model predicts too large an amplitude for the M_2 in late January and February; a result consistent with the observations of Webb (1985), who found that Stacey's model predicted too much energy flux in Knight Inlet by a factor of 2.5. The K_1 prediction results for November and December in Indian Arm are too low rather than too high. Though too low, they are closer, differing only by a factor of 2 or so. As the M_2 model does in November/December, the K_1 model predicts too low an amplitude in January/February. Different problems with prediction at different frequencies may indicate , as suggested by Webb (1985), that the linear model is too simple and does not adequately represent the generation mechanism of the internal tide.

5.10 Conclusions

In its passage through Indian Arm, the barotropic tide was observed to lose as much as 15% of its energy. Most of this energy goes into heat and tidal mixing, particularly in Burrard Inlet since most of the energy is lost at First and Second Narrows, but as much as 5% of the barotropic flux appears to go into the internal tide.

A shift in the internal response was observed in the winter of 1983/84. The M_2 internal tide was predominant early in the winter, later the K_1 was dominant. No change in the forcing or in the ray path propagation of the tide could be found that explained the cause of the shift. A change in the resonance period was observed, consistent with the change from a M_2 to a K_1 internal response. Fitting of normal modes to the cyclesonde data indicated the down-inlet propagation of energy, necessary for resonance to occur. Estimates of the energy fluxes made using a linear model were also interpreted in the light of a resonance model.

6. The Energy Partition

6.1 Introduction

An assessment of the energy partition in Indian Arm will be made in this chapter. The barotropic tide loses energy as it propagates into and out of the fjord. Three major sinks have been identified: the internal tide, high frequency internal waves and friction. Freeland and Farmer (1980) concluded that friction was the smallest of the three. A simple estimate of the frictional loss in Burrard Inlet will be made at the end of this chapter to allow some assessment of the importance of friction.

In section 6.2 an estimate of the coefficient of diffusion will be made from the CTD data. This estimate will be used to find the work done against the buoyancy force by turbulent diffusion in Indian Arm. Diffusion is primarily driven by turbulence, whose energy is derived from the internal waves. In Indian Arm the most important energy source is the barotropic tide. Neither the wind nor the freshwater flow are as strong as they can be in some other inlets , for example Knight Inlet (Farmer and Freeland, 1983). Most of the energy appears to go into internal waves, which are generated near the sill (see Chapter 5). Most of the energy of these waves is trapped in the fjord and so provides the energy for turbulence. As argued by Osborn (1980), the transfer of energy to do useful work is very inefficient so that less than 15 % of the available energy probably does work against the buoyancy. In section 6.3 an estimate of the energy flux in the high frequency internal wave field will be made using the cyclesonde data. Section 6.4 will present an estimate of the energy flux at the sill using the observed pressure and velocity field. In section 6.5 all these results will be discussed together with the energy flux estimates made in Chapter 5.

6.2 Diffusion Analysis

6.2.1 Theory of Diffusion

Fickian diffusion in seawater is complex for two reasons: first, both temperature and salt diffuse and second, the energy for diffusion comes from turbulence. The first aspect leads to complexity because the density is a function of the diffusion of two properties which may differ in their rates of diffusion. The second factor mitigates the first to some extent, since turbulence driven diffusion will tend to lead to similar rates of diffusion. All diffusion must ultimately take place at the molecular level but the rate of the overall process may be controlled by turbulence. In general, in the ocean the observed rate of diffusion is found to be much larger than the molecular rates of diffusion (Pond and Pickard, 1983). The equation for diffusion is written with both vertical and horizontal terms:

$$\frac{DS}{Dt} = \frac{\partial}{\partial x}(K_h \frac{\partial S}{\partial x}) + \frac{\partial}{\partial y}(K_h \frac{\partial S}{\partial y}) + \frac{\partial}{\partial z}(K_v \frac{\partial S}{\partial z}) \quad , \tag{6.1}$$

where S is the salinity, K_h is the coefficient of horizontal diffusivity and K_v is the coefficient of vertical diffusivity. It is assumed that the process controlling horizontal diffusion is different than that driving the vertical diffusion. In a fjord, which is relatively homogeneous in the horizontal, it is assumed that the first two terms can be neglected. The assumption that $\partial S/\partial y$ (where y is across the channel) is zero is probably quite good. The assumption that $\partial S/\partial x$ is zero, is probably not so robust since there is a long-channel gradient, the result of the freshwater input. It is also assumed that there are periods when there is negligible advective contribution to the diffusion, so the total derivative on the left side of equation (6.1) becomes a partial derivative. If the horizontal terms are dropped then equation (6.1) becomes

$$\frac{\partial S}{\partial t} = \frac{\partial}{\partial z} K_v \frac{\partial S}{\partial z} \quad . \tag{6.2}$$

The diffusion coefficient K_v is almost always greater than the molecular diffusivity because of turbulence. It has usually been assumed that K_v is a constant independent of depth, however, recent work in the ocean suggests that K_v is not a constant but may be a function of the stratification (Osborn, 1980; Gargett, 1984). Gargett and Holloway (1984) suggest that all systems in which the energy source is turbulence from internal waves should exhibit

a relationship between K_v and N. They review observations of the rate of kinetic energy dissipation and find that it tends to vary systematically with the buoyancy frequency N. At steady state, they equate the sum of the mechanical production of energy and the energy which does work against buoyancy to the dissipation rate. From the definition of R_f and K_v they derive

$$K_v = \frac{R_f}{1 - R_f} \varepsilon N^{-2} \quad , \tag{6.3}$$

where R_f is the flux Richardson number and ε is the kinematic energy dissipation. The flux Richardson number is the ratio between the energy flux working against buoyancy and the total mechanical production of energy. Following an analysis of the steady state energy equation, they show that the dissipation should be of the form

$$\varepsilon = \varepsilon_0 N^{+p} \quad , \tag{6.4}$$

where $p = 1$ if all of the waves are of a single frequency and $p = 1.5$ if the waves exhibit the broad-band oceanic spectrum (Munk, 1981). In equation (6.4), ε_0 is a site-specific constant which depends on the actual amount of energy in the local internal wave field. If the flux Richardson number is constant, then equation (6.3) becomes

$$\begin{aligned} K_v &= a_0 N^{-2+p} \\ &= a_0 N^{-q} \end{aligned} \tag{6.5}$$

where $0.5 < q < 1.0$. In equation (6.5), a_0 is a site-specific constant, related to ε_0 by R_f, which is also dependent on the energy in the local internal wave field.

6.2.2 K_v in Indian Arm

In Indian Arm, an investigation of the process of diffusion is important for a number of reasons. First, diffusion is important in the exchange process in that it serves to condition the water between exchanges, reducing the density of the bottom water by the diffusion of salt. Second, diffusion is an important measure of the turbulence in the system. It is also an important sink of the internal wave energy which is generated at the sill (Stigebrandt, 1976, 1980).

The technique for determining the coefficient of diffusion is to solve equation (6.2) using measurements of the salinity or temperature in the fjord. This technique is referred to as the budget method. It assumes that the property being analysed for is conservative; that is, there are no sources or sinks. Because temperature does not fulfill this condition as well as salinity, there is heating and cooling near the surface, the results for temperature are often not as good. Equation (6.2) is solved by integrating from the bottom at z=0 to some height z :

$$K_v(z) = \frac{\frac{\partial}{\partial t}\int_0^z S dz}{\frac{\partial S}{\partial z}} \quad . \tag{6.6}$$

It is necessary to ensure that during the period of integration there is no advection of salt into Indian Arm. The cyclesonde data permit one to see when there is no exchange in the fjord. An attempt was made to use the averaged cyclesonde data to find K_v but the results were not good, indicating the errors in the data ($\sim \pm 0.1$ for salinity) were too great. The CTD data were used for the results presented here. The effects of the internal waves were eliminated by averaging the CTD data over $10\,m$ intervals, a depth range large enough to remove the internal waves but still small enough to allow reasonable vertical resolution.

The period chosen for the diffusion analysis in Indian Arm was January to March 1983, when there was minimal exchange. Results from the analysis over this period are presented in *Figure 69*. Both the temperature and the salinity results are presented. The temperature data produce a much noisier plot, the exact reasons for which are difficult to determine since the sensor resolution of the CTD should produce reliable results. The generally small temperature gradient may be part of the source of the difficulty. Because of the consistently noisier results from the temperature, these data were ignored in the final straight line fit. The best fit for the salinity data of *Figure 69* is:

$$K_v = 2.20 \times 10^{-5}\, N^{-0.86} \quad . \tag{6.7}$$

Data from Saanich Inlet on Vancouver Island were also analysed by this same technique. Although no current meter data were available to determine the exchange conditions, the

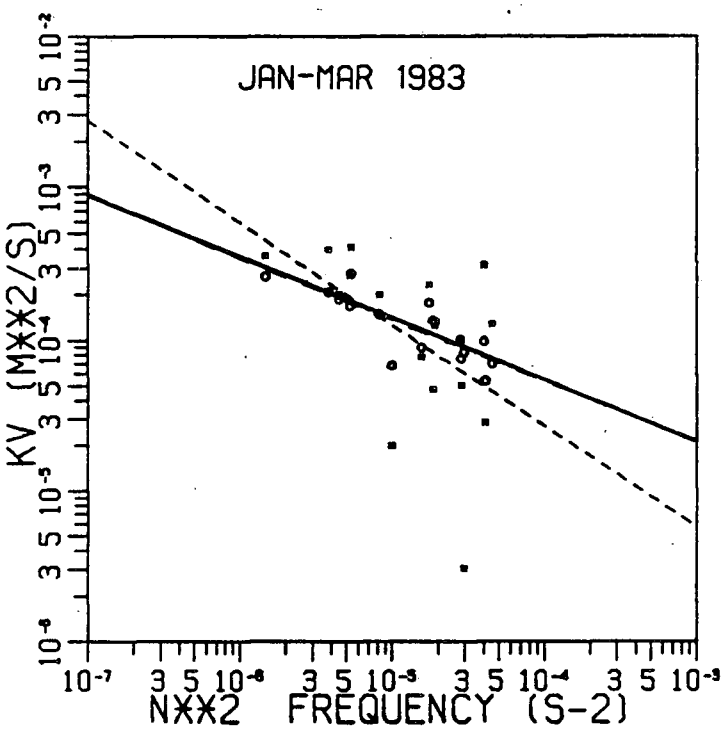

Figure 69 K_v versus N^2 in Indian Arm. The period covered is January to March 1983. The depth range is from $100 - 160\,m$. Open circles are salinity, filled squares temperature. The solid (salinity) and dashed (temperature) lines are least squares fits to the data.

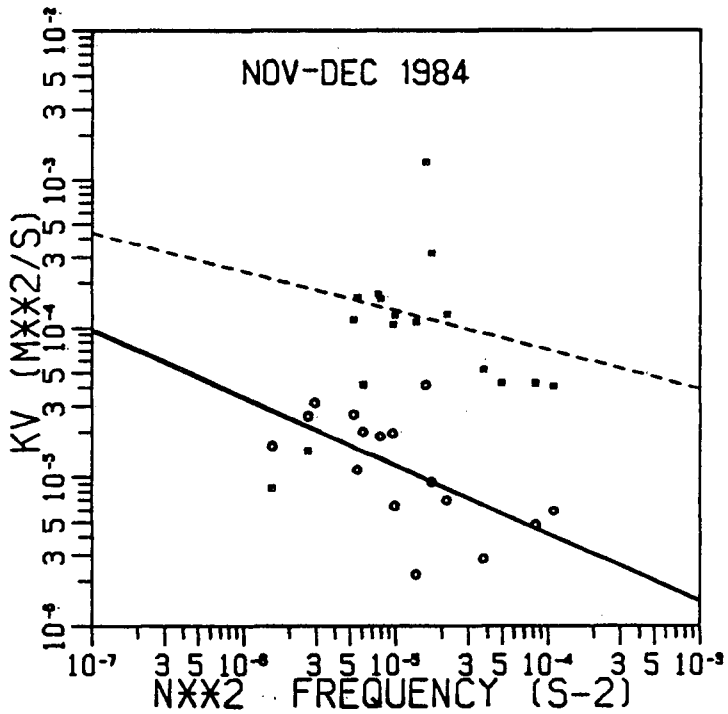

Figure 70 K_v versus N^2 in Saanich Inlet. The period covered is from November to December 1984. The depth range is from $100 - 160\,m$. Open circles are salinity, filled squares temperature. The solid (salinity) and dashed (temperature) lines are least squares fits to the data.

anoxic water at the bottom of the inlet does provide a good test of exchange. The period analysed for was November to December 1984. The results are presented in *Figure 70.* As in the Indian Arm analysis, the temperature data proved to be much noisier than the salinity data. There also seems to be a difference in the degree of diffusion between the salinity and the temperature. It is not known if this effect is real or is some artifact of the data. The same result was not found in Indian Arm. The slope of the salinity data in Saanich Inlet is approximately the same as that for the Indian Arm data. The relationship in Saanich Inlet was $K_v \propto N^{-1.04}$; in Indian Arm the proportionality was found to be $K_v \propto N^{-0.86}$.

These results support the work of Gargett and Holloway (1984) and Gargett (1984) who suggested the form of the relationship between K_v and N. According to their work, the slope of the K_v curve in Indian Arm and in Saanich Inlet indicate that the diffusion is primarily driven by internal wave dissipation and that the internal waves are primarily of one frequency. The latter conclusion is based upon the value of the slope which corresponds to the p of equation (6.4) having a value of approximately 1.

6.2.3 Energy of Diffusion

An estimate of the amount of energy going into mixing will be made in this section. Stigebrandt (1976) estimated this value in Oslofjord and then used this result to estimate the flux Richardson number which he found to be about 0.05. Thus, only about 5 % of the available energy actually did useful work against the buoyancy force. The estimation of the work done against buoyancy forces is made by evaluation of the integral (Stigebrandt, 1976)

$$\int_{Volume} K_v N^2 dV \quad . \tag{6.8}$$

From the results of the previous section, $K_v \propto N^{-0.86}$ in Indian Arm and so the energy going into mixing is proportional to a volume integral of a constant times $N^{1.14}$. As a consequence the buoyancy frequency dependency is less severe than is indicated by the integral (6.8).

The integral (6.8) was evaluated for Indian Arm, which has a volume of $2.45 \times 10^9\, m^3$. The results were determined for a range of N which represent the typical conditions in Indian Arm.

$$10^{-4} > N^2\,(s^{-2}) > 4 \times 10^{-6}$$

$$6 \times 10^{-4} < K_v\,(m^2 s^{-1}) < 3 \times 10^{-4}$$

$$150 > \; Power\,(kW) > 3 \quad .$$

The energy levels are thus quite low, even if the value of N is large. For typical N^2 and K_v values in the basin, a power estimate of about 100 kW is reasonable. Although variable because of the changing N^2 profile in the basin, this power loss serves to represent the approximate level of energy going into mixing. A comparison of the various energy fluxes will be given at the end of this chapter.

6.3 Energy Flux in the High Frequency Internal Waves

The work of Stacey and Zedel (1986) in Observatory Inlet has raised the question of the proportion of energy going into the internal tide versus internal waves. They suggest that even in the presence of strongly non-linear flows most of the energy transfer from the barotropic tide is to the internal tide.

Figure 71 shows an acoustic echogram from the sill of Indian Arm taken on 8 February, 1984. The acoustic energy is backscattered from organisms or density discontinuities which serve as tracers of the fluid motion. In *Figure 71*, taken on an ebb tide, high frequency internal waves with wavelengths of O(100 m) can be seen shedding off the Indian Arm sill. The amplitude of these waves appears great, with values of $10 - 15\, m$. Records indicating large internal motions at short periods have also been collected in other fjords (Farmer and Smith, 1980; Farmer and Freeland, 1983). These observations suggest that the energy in the high frequency internal waves is high.

Cyclesonde data from the top and bottom bumper position at the sill mooring were analysed in an attempt to estimate the energy flux in the high frequency (HF) internal waves. These data were at 1 and 5 minute sampling intervals with gaps when the cyclesonde

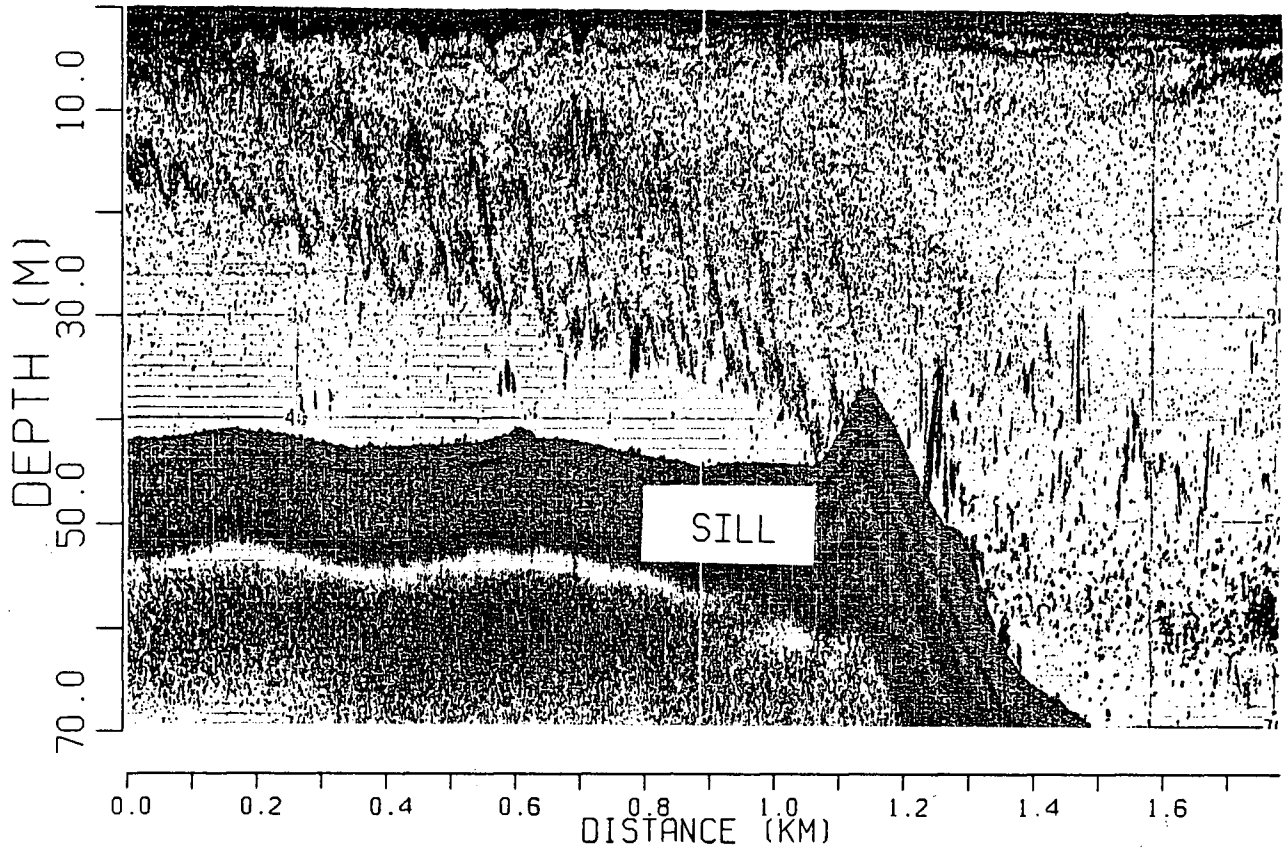

Figure 71 Acoustic echogram from the sill at Indian Arm on 8-February-1984. The frequency of the sounder was 107 kHz. The horizontal scale at the bottom is only approximate.

was profiling or sitting at the other bumper. Harmonic analysis of the records was done and the tidal signal was removed. The variance of the remaining signal was then analysed to get an estimate of the energy density. The energy flux can be determined from

$$E_{Flux} = \rho_o C_g \frac{H}{2} \left[W_{Top} Variance_{Top} + W_{Bot} Variance_{Bot} \right] \quad , \tag{6.9}$$

where ρ_o is the mean density, W is the width at either the top or the bottom, C_g is the group velocity and H is the water depth. All of the terms in equation (6.9) can be evaluated except C_g, which is estimated to be $1\,m\,s^{-1}$. The results of the variance analysis for four separate months are given in *Table 28*.

The average flux for the four months is 0.13 MW. *Table 28* shows that the energy in the internal waves is not always greatest nearest the surface. In January and February

Table 28
Variance and energy flux at the sill in 1984 and 1985.

Period	$Variance_{Top}$ $(cm^2\,s^{-2})$	$Variance_{Bot}$ $(cm^2\,s^{-2})$	*Flux* (MW)
January 1984	28.3	40.9	0.089
February 1984	34.1	45.2	0.11
January 1985	85.3	29.4	0.18
February 1985	54.1	22.4	0.12

1984, the energy levels are higher nearer the bottom.

The results of this analysis must be accepted with some caution because of the limitations of the data used and the assumption of a fixed group velocity. Nevertheless, some estimate of the HF internal wave flux is provided, one which indicates that a significant amount of energy propagates at these frequencies.

6.4 Energy Flux from the Velocity and Pressure

The energy flux in the internal tide was calculated in Chapter 5 as part of the modal fitting. There are, however, some difficulties with this procedure. The modal decomposition itself does not strictly apply to Indian Arm, which has a sloping bottom. As well, the fitting procedure is fraught with difficulties which give rise to some doubt as to the correctness of the fit. Variations in the fit can be very important to the energy flux because of the change in group velocity with mode number. If one mode is left out, or exchanged for another, the energy flux may change greatly.

In this section, a different approach to the energy flux will be taken, one that does not involve the modal decomposition. Gill (1982, pg. 141) writes the energy flux density F' as

$$F' = < p'u > \ , \tag{6.10}$$

where <> represents a time average, u is the velocity and p' is the perturbation pressure. The perturbation pressure is written as

$$p' = \int_0^z -\rho' g dz \ , \tag{6.11}$$

where ρ' is the perturbation density and z is the depth at which the perturbation pressure is to be determined. This equation involves making the hydrostatic assumption that $\omega^2 << N^2$ an assumption which holds here (see Chapter 5). Since a time average is taken, the total flux can be written by integrating from top to bottom and across the inlet

$$E_{Flux} = \int_0^H W(z)\langle p'(z,t)u(z,t)\rangle \, dz \quad , \tag{6.12}$$

where W is the width of the inlet at depth z and H is the water depth. The perturbation density must be integrated from the surface term to the depth of interest and then the perturbation pressure at the various depths is inserted into equation (6.12). This integral was evaluated using the results of the harmonic analysis of the velocity and density data from both the cyclesonde and the Aanderaa current meters. The barotropic tide was removed from the data before making the computations so that only the baroclinic tide is being analysed. Analysis was done at the sill station for January through March 1985. *Table 29* gives the results of the analysis.

Table 29
Net energy flux (in MW) computed using $< p'u >$.

	SILL	
PERIOD	M_2	K_1
1984/85		
16–30Jan	0.0097	0.0059
30Jan-16Feb	0.0091	0.0045
17Feb-5Mar	0.063	0.067
5Mar-25Mar	0.068	0.040

The results of *Table 29* give the net energy flux at the sill station. The energy fluxes correspond to the difference between the up- and down-inlet fluxes from the modal analysis. The 1984/85 modal fits, although not presented here, showed similar fluxes to those observed in 1983/84, as a comparison of the phase plane plots might suggest (*Figures 50-53*). The energy flux differences in *Table 25* for the M_2 tide in 1983/84 are about 0.05–0.1 MW. For K_1 the energy flux differences (*Table 26*) are about the same. The energy flux calculation in *Table 29* is thus in reasonable agreement with the fluxes determined from

modal analysis. Note that the lower fluxes for the first two entries may be caused by the Doppler shifting associated with the strong inflows of January and February 1985. This shift will result in an underestimate of the amplitudes of the tidal constituents from harmonic analysis.

6.5 Comparisons of the Energy Fluxes

A review of the different energy flux calculations will be given in this section. The main purpose is to indicate the relative importance of the different energy sources and sinks in Indian Arm. *Table 30* gives the basic results which have been obtained in earlier sections and which will be discussed here.

Table 30
Energy fluxes (in MW) in Indian Arm.

	M_2	K_1
Lost from barotropic tide (83/84 and 84/85)	0.5	0.2
Up-channel flux from modal fitting (83/84)		
SILL	0.15	0.05
BASIN	0.03	0.02
Net flux from $< p'u >$ calculation		
SILL (1985)	~ 0.05	~ 0.05
Flux in HF internal waves Jan/Feb 1984 and 1985	~ 0.13	
Energy lost to mixing	~ 0.1	

The first line in *Table 30* shows the energy lost between the sill and the basin as estimated by the tidal height analysis. These figures probably underestimate the energy going into the internal tide because the sill station is at the far end of the generating region. Between the Vancouver Harbour station and the sill, almost 3 MW were dissipated in 1983/84 at the M_2 frequency and 1 MW at K_1. Some of this energy is probably lost over Second Narrows although the CTD data show this region to be generally well-mixed indicating that not much energy should go into internal waves. The energy estimates in *Table 30* for the losses from the barotropic tide may be underestimates. The total loss from the M_2 tide may be as high as $1 - 1.5$ MW and from K_1, $0.3 - 0.4$ MW as discussed

in Chapter 5.

The second row of *Table 30* gives the up-channel energy fluxes estimated from the modal analysis of Chapter 5. These fluxes are the averages of the 1983/84 modal analysis with the outliers removed. These averages are the most reasonable estimate of the fluxes in the internal tide at the sill and in the basin. The third row shows the flux estimates from the $< p'u >$ calculations of the previous section. An average of the results for February/March 1985 at the sill is given.

The modal analysis fit shows more flux at the sill than in the basin. The basin flux is 20–40 % that of the sill flux, according to the modal fit. These results indicate that very little of the energy transferred from the barotropic tide to the internal tide at the sill makes its way into the basin as a propagating internal tide. The net energy flux from the $< p'u >$ analysis shows the net flux which propagates away from the sill, presumably up-inlet. The estimates given in *Table 30* are based upon averages of the February and March 1985 data. They show reasonable agreement with the net fluxes from the modal analysis determined during the same period.

The bottom two lines of the table present the flux estimates for high frequency (HF) internal waves at the sill and the energy lost to mixing throughout the basin. The energy lost to the HF internal waves is about $\sim$ 20% of the total power lost from the barotropic tide, if that total is 0.7 MW. The HF internal wave flux is, however, about the same size as the energy flux in the internal tide at the sill, as determined by modal fitting. If the modal fluxes are correct, and the $< p'u >$ analysis supports their validity, then energy from the barotropic tide must be lost somewhere in the vicinity of the sill. Stacey and Zedel (1986) estimated that in Observatory Inlet, which exhibits hydraulic discontinuities and other nonlinear flow processes, only about 5 % of the energy lost from the barotropic tide went into HF internal waves. All of the rest went into the internal tide. The work of Stacey and Zedel (1986) is based, however, upon a three-layer model and not upon observations. In this study, direct observations are used. They are, however, not of the best quality and so

the issue of what percentage of the energy goes into the internal tide remains unresolved.

In Chapter 5 it was argued that 1–1.5 MW was lost from the M_2 tide, and 0.3–0.4 MW from the K_1, over the Indian Arm sill. The fluxes in *Table 30* indicate that much less energy goes into internal processes propagating into Indian Arm. The sum of the modal and the HF internal wave fluxes is 0.31 MW. There is no indication that the 0.7 MW estimate of energy lost from the sill to the basin is too high. The inability to find an energy flux of 0.7 MW propagating away from the Indian Arm sill suggests that energy is lost to other processes such as an internal tide propagating back into Burrard Inlet. Friction is also a likely sink for the energy. The power lost to frictional processes can be estimated using the equation derived by Freeland and Farmer (1980):

$$P = \rho\kappa \int_{Surface} \overline{|u|^3} dA \quad , \tag{6.13}$$

where κ is a drag coefficient set to 3×10^{-3}. Over First and Second Narrows the total frictional loss was estimated at 1.5 MW. This result indicates that friction, particularly through Burrard Inlet, may be an important energy sink for the barotropic tide. Over the Indian Arm sill, the frictional loss was estimated at 0.4 MW indicating that friction may be an important factor in the energy budget there.

The final line of *Table 30*, which gives the energy lost to mixing, will allow the calculation of the flux Richardson number (R_f). If the total power lost from the barotropic tide in Indian Arm is $1 - 2$ MW then R_f is $0.05 - 0.1$, a result in good agreement with Stigebrandt (1980) who found R_f in Oslofjord to be about 0.05. This result is also in agreement with other oceanic observations (Britter, 1974) and the theoretical arguments of Osborn (1980) in which the maximum value of R_f is observed and predicted to be less than 0.15. The transfer of kinetic energy to do useful work in mixing the water is very inefficient in the ocean.

7. Summary and Conclusions

The deepwater exchange cycle in Indian Arm has been described with direct observations of a bottom-water renewal episode in 1984/85. Mid-water renewal has been observed to occur in most years (Burling, 1982); bottom-water renewal takes place every few years. Current and density observations at the sill and in the basin indicate that the timing of the exchange, once the seasonal conditions are appropriate, is tied to the spring/neap tidal cycle. On strong spring tides, the mixing of water through Burrard Inlet reduces the density of the incoming water to the point where deepwater exchange will not occur. As the tidal energy level goes down, with the shift to neap tides, the density of the water reaching the sill goes up and deepwater renewal takes place. Strong freshwater flows were observed to stop the exchange although such flows are fairly infrequent in Indian Arm. The importance of the Fraser River as a freshwater source has not been determined.

The lack of bottom data, the bottom bumper of the cyclesonde at the sill was about $10\,m$ off the bottom, was a problem in determining the effects of bottom friction upon the density current flow just inside the sill. Future work should involve suitably modified moorings. A long time series of temperature and salinity data from outside First Narrows would have been useful in determining the effects of short and long term variability on the exchange. Measurements of the stratification and current data outside Burrard Inlet might have allowed the effects of blocking to be assessed better, though further development of the theory of blocking is also needed (Farmer and Denton, 1985).

During the exchange period, pulsed inflows of water were not detected at the current meter station just inside the sill. The mean current near the bottom was directed into the fjord throughout the exchange. The flow in the basin was observed to be pulsed, as a result of the density current surges associated with the spring/neap mixing cycle.

An analysis of wind at a nearby station (Vancouver Airport) and current data in Indian Arm yielded no conclusive results. There was some significant correlation found between the current and the wind. The forcing does not generate a strong response in the

current because of the weak winds. Wind measurements in Indian Arm were not obtained because of instrumentation and location problems. Summer wind data would be useful in determining the importance of the wind as a source of internal motions in Indian Arm.

The internal tide was observed in all three seasons of data: 1982/83, 1983/84 and 1984/85. A shift in the internal response from a predominantly M_2 internal tide to predominantly K_1 internal tide was observed in 1983/84. After exploring different possible causes for this shift, it was determined to be a partial resonance response. As the stratification changed over the winter of 1983/84, the resonance period gradually lengthened from 14 to 22 hours. A modal analysis, incorporating density and current data, indicated that $20-30$ % of the total internal flux was propagating down the inlet. The reflection of energy from the head of the inlet is a necessary condition for resonance to occur.

The role of the internal tide as an energy source in inlets is gradually becoming clear (Farmer and Freeland, 1983; Webb, 1985). Modal analysis is, however, severely limited if no data from near the surface are obtained. Any future study investigating the internal tide must obtain both density and current data from the upper part of the water column where one has the best chance of differentiating the modes.

From the tidal height, density and current data, an energy budget for the tide in Indian Arm was worked out. Of the $\sim$ 50 MW of tidal energy which enters Burrard Inlet approximately $10-15$ % is dissipated. Most of this energy is lost in the shallows of Burrard Inlet although about 1.0 MW is lost in Indian Arm. About 30 % of the energy lost in Indian Arm goes into the internal tide with about 20 % going into high frequency internal waves. The remaining energy is unaccounted for.

An analysis of the density data determined the vertical diffusion coefficient K_v to depend upon the buoyancy frequency N. The relationship between the two was, $K_v \propto N^{-0.86}$. Using the observed stratification and K_v the amount of energy going into mixing was determined to be about 100 kW. This result, together with the estimate for the total power lost, gives a flux Richardson number (R_f) of $0.05-0.15$, in agreement with the work

of Stigebrandt (1980) who found $R_f \simeq 0.05$ in Oslofjord.

From the energy budget analysis, it appears that a large portion ($\sim$ 20%) of the energy lost from the barotropic tide goes into high frequency internal waves. This result is in conflict with the work of Stacey (1984) and Stacey and Zedel (1986) who predict, based upon a simple linear model, that only about 5 % of the energy of the barotropic tide goes into high frequency internal motions. More work on this problem is warranted. The real effects of friction in the process of dissipation have been ignored here, mainly because of the lack of an effective way in which to deal with them. A properly tuned numerical model, such as the one of Dunbar (1985), together with better data, particularly in Burrard Inlet, might permit one to look into the friction problem. Such a model could also be used to investigate the interaction between the tide and the estuarine circulation. The long-period current averages presented here suggest that the tide has a strong influence on the mean circulation.

Bibliography

ANDERSON, J.J. and DEVOL, A.H. (1973) Deep water renewal in Saanich Inlet, an intermittently anoxic basin. *Est. Coast. Mar. Sci.*, **1**, 1–10.

ASSAF, G. and HECHT, A. (1974) Sea straits: a dynamical model. *Deep-Sea Research*, **21**, 947–958.

BAINES, P.G. (1973) The generation of the internal tides by flat-bump topography. *Deep-Sea Research*, **20**, 179–205.

BAINES, P.G. (1974) The generation of internal tides over steep continental shelfs. *Phil. Trans. Roy. Soc. Lon.*, **A277**, 27–58.

BAINES, P.G. (1982) On internal tide generation models. *Deep-Sea Research*, **29(3A)**, 307–338.

BELL, W.H. (1973) The Exchange of Deep Water in Howe Sound Basin. *Pacific Mar. Sci. Report 73-13*, Institute of Ocean Sciences, Patricia Bay, B.C., 35 pp.

BENJAMIN, T.B. (1968) Gravity currents and related phenomena. *J. Fluid Mech.*, **31**, 20–48.

BERTEAUX, H.O. (1976) *Buoy Engineering*. Wiley Interscience, New York, 313 pp.

BLACKFORD, B.L. (1978) On the generation of internal waves by tidal flow over a sill – a possible nonlinear mechanism. *J. Mar. Res.*, **36(3)**, 529–549.

BLUMBERG, A.F. (1975) A Numerical Investigation into the Dynamics of Estuarine Circulation. *Chesapeake Bay Institute Technical Report 91*, The John's Hopkins University.

BO PEDERSEN, F. (1980) A monograph on turbulent entrainment and friction in two-layer stratified flow. *Inst. of Hydrodynamics and Hydraulic Engineering*, Technical University of Denmark, 397 pp.

BRITTER, R.F. (1974) An experiment on turbulence in a density-stratified fluid. *Ph.D. Thesis , Monash University,* Victoria, Australia.

BURLING, R.W. (1982) Deep circulations in inlets: Indian Arm as a case study. In: *Marine Tailings Disposal*. D.V. Ellis, ed., Ann Arbour Science, Ann Arbour, Michigan, 85–132.

CACCHIONE, D. and WUNSCH, C. (1974) Expermiental study of internal waves over a slope. *J. Fluid Mech.*, **66(2)**, 223–239.

CANNON, G.A. (1975) Observations of bottom-water flushing in a fjord-like estuary. *Est. Coast. Mar. Sci.*, **3**, 95–102.

CANNON, G.A. and LAIRD, N.P. (1978) Variability of currents and water properties from year long observations in a fjord estuary. In: *Hydrodynamics of Estuaries and Fjords*, J. Nihoul, ed., Elsevier, Amsterdam.

CUSHMAN-ROISIN, B. and SVENDSEN, H.(1983) Internal gravity waves in sill fjords: vertical modes, ray theory and comparison with observations. In: *Coastal Oceanography*. H.G. Gade, A. Edwards and H. Svendsen, eds., Plenum Press, New York, 373–396.

DAVIDSON, L.W. (1979) On the physical oceanography of Burrard Inlet and Indian Arm. *M.Sc. Thesis, University of British of Columbia,* Vancouver, British Columbia, 221 pp.

DRINKWATER, K.F and OSBORN, T.R. (1975) The role of tidal mixing in Rupert and Holberg Inlets, Vancouver Island. *Limnology and Oceanography*, **20**, 518–529.

DUNBAR, D.S. (1985) A numerical model of stratified circulation in a shallow-silled inlet. *Ph. D. Thesis, University of British Columbia,* Vancouver, British Columbia, 273 pp.

EBBESMEYER, C.C. and BAINES, C.A. (1980) Control of a fjord basin's dynamics by tidal mixing on embracing sill zones. *Est. Coast. Mar. Sci.*, **11**, 311–330.

EDWARDS, A. and EDELSTEN, A.J. (1977) Deep water renewal of Loch Etive. *Est. Coast. Mar. Sci.*, **5**, 575–595.

ELLIOT, A.J. (1976) A numerical model of internal circulation in a branching tidal estuary. *Chesapeake Bay Institute Technical Report 54*. The John's Hopkins University.

ELLISON, T.H. and TURNER, J.S (1959) Turbulent entrainment in stratified flows. *J. Fluid Mech.*, **6**, 423–448.

EMERY, K.O. (1967) Estuaries and lagoons in relation to continental shelves. In: *Estuaries*, G.H. Lauff, ed., American Association for the Advancement of Science Pub. 83, Washington, D.C., 9-11.

ERIKSEN, C.C. (1982) Observations of internal wave reflection off sloping bottoms. *J. Geophys. Res.*, **87**, 525–538.

FARMER, D.M. and ARMI, L. (1986) Maximal two-layer exchange over a sill and through the combination of a sill and contraction with barotropic flow. *J. Fluid Mech.*, **164**, 53–76.

FARMER, D.M. and DENTON, R.A. (1985) Hydraulic control of the flow over the sill of Observatory Inlet. *J. Geophys. Res.*, **90**, 9051–9068.

FARMER, D.M. and FREELAND, H.J. (1983) The physical oceanography of fjords. *Progress Oceanog.*, **12**, 147–220.

FARMER, D.M. and SMITH, J.D. (1978) Nonlinear internal waves in a fjord. In: *Hydrodynamics of Estuaries and Fjords*, J.Nihoul, ed., Elsevier Oceanography Series, No. 23, 465–494.

———, (1980a) Tidal interaction of stratified flow with a sill in Knight Inlet. *Deep-Sea Research*, **27A**, 239–254.

———, (1980b) Generation of lee waves over the sill in Knight Inlet. In: *Fjord Oceanography*. H.J. Freeland, D.M. Farmer, and C.D. Levings, eds., Plenum Press, New York, 259–270.

FOREMAN, M.G.G. (1977) Manual for Tidal Heights Analysis and Prediction. *Pacific Mar. Sci. Report* 77–10, Institute of Ocean Sciences, Patricia Bay, B.C., 101pp.

———, (1979) Tidal Analysis Based on High and Low Water Observations. *Pacific Mar. Sci. Report* 79–15, Institute of Ocean Sciences, Patricia Bay, B.C., 70pp.

FREELAND, H.J. and FARMER, D.M. (1980) Circulation and Energetics of a Deep, Strongly Stratified Inlet. *Can. J. Fish. and Aquatic Sci.*, **37(9)**, 1398–1410.

GADE, H.G. and EDWARDS, A. (1980) Deep water renewal in fjords. In: *Fjord Oceanography*. H.J. Freeland, D.M. Farmer, and C.D. Levings, eds., Plenum Press, New York, 453–489.

GARETT, C.J.R. (1975) Tides in gulfs. *Deep-Sea Research*, **22(1)**, 23–36.

GARGETT, A.E. (1984) Vertical diffusivity in the ocean interior. *J. Mar. Res.*, **42**, 359–393.

GARGETT, A.E. and HOLLOWAY, G. (1984) Dissipation and diffusion by internal wave breaking. *J. Mar. Res.*, **42**, 15–27.

GEYER, W.R. and CANNON, G.A. (1982) Sill processes related to deepwater exchange in a fjord. *J. Geophys. Res.*, **87**, 7985–7996.

GILL, A.E. (1982) *Atmosphere-Ocean Dynamics*. Academic Press, New York, 662pp.

GILMARTIN, M. (1962) Annual Cyclic Changes in the Physical Oceanography of a British Columbia Fjord. *J. Fish. Res. Bd. Canada*, **19**, 921–974.

GODIN, G. (1972) *The Analysis of Tides*. University of Toronto Press, Toronto, 264 pp.

GRANT, H.L., STEWART, R.W., and MOILLET, A. (1961) Turbulence spectra from a tidal channel. *J. Fluid Mech.*, **12**, 241–263.

HALPERN, D., PILLSBURY, R.D. and SMITH, R.L. (1973) An intercomparison of three current meters operated in shallow water. *Deep-Sea Research*, **21**, 489–497.

HAY, J.E. and OKE, T.R. (1976) *The Climate of Vancouver*. British Columbia Geographical Series, No. 23, Tantalus Research Ltd., 49 pp.

KEELEY, J.R. (1984) Observations of an internal response in a fjord. *J. Mar. Res.*, **42**, 873–891.

LAFOND, C.A. and PICKARD, G.L. (1975) Deepwater exchanges in Bute Inlet, British Columbia. *J. Fish. Res. Bd. Canada*, **32**, 2075–2089.

LEBLOND, P.H. and MYSAK, L.A. (1978) *Waves in the Ocean.* Elsevier Scientific Publishing Co., New York, 602pp.

LEWIS, E.L. and PERKIN, R.G. (1982) Seasonal mixing processes in an Arctic fjord system. *J. Phys. Oceanogr.*, **12(1)**, 74–83.

LIGHTHILL, J. (1978) *Waves in Fluids.* Cambridge University Press, Cambridge, 504pp.

LUMLEY, J.L. (1970) *Stochastic Tools in Turbulence.* Academic Press, New York, 194 pp.

MANTON, M.J. and MYSAK, L.A. (1971) Construction of internal wave solutions via a functional equation. *J. Math. Anal. Appl.*, **35**, 237–248.

MATTHEWS, J.B. (1981) The seasonal circulation of the Glacier Bay, Alaska fjord system. *Est. Coast. Shelf Sci.*, **12**, 697–700.

MCHARDY, R.A. (1961) A Study of the Taxonomy and Some of the Aspects of the Ecology of Marine Ostracods in the Plankton of Indian Arm, British Columbia. *M. Sc. Thesis, University of British Columbia,* Vancouver, British Columbia.

MUNK, W.H. (1981) Internal waves and small scale processes. In: *Evolution of Physical Oceanography.* B.A. Warren and C. Wunsch, eds., MIT Press, 264–271.

OKUDA, T. (1981) Water exchange and the balance of phosphate in the Gulf of Cariaco, Venezuela. In: *Coastal Upwelling.* F.A. Richards, ed., Am. Geophysical Union, 274–281.

OSBORN, T.R. (1980) Estimates of the local rate of vertical diffusion from dissipation measurements. *J. Phys. Oceanogr.*, **10**, 83–89.

PARSONS, T.R., MAITA, Y. and LALLI, C.M. (1984) *A Practical Handbook of Seawater Analysis.* Pergammon Press, Oxford, 173 pp.

PHILLIPS, O.M. (1977) *The Dynamics of the Upper Ocean.* Cambridge University Press, 336 pp.

PICKARD, G.L. (1961) Oceanographic features of inlets in the British Columbia mainland coast. *J. Fish. Res. Bd. Canada*, **18(6)**, 907–999.

———(1975) Annual and longer term variations of deepwater properties of the coastal waters of southern B.C. *J. Fish. Res. Bd. Canada*, **32**, 1561–1587.

PICKARD, G.L. and RODGERS, K. (1959) Current measurements in Knight Inlet, B.C. *J. Fish. Res. Bd. Canada*, **16(5)**, 635–678.

PICKARD, G.L. and STANTON, B.R (1980) Pacific fjords – A review of their characteristics. In: *Fjord Oceanography*. H.J. Freeland, D.M. Farmer, and C.D. Levings, eds., Plenum Press, New York, 1–51.

POND, S. and PICKARD, G.L. (1983) *Introduction to Physical Oceanography*. Pergammon Press, Oxford, 329 pp.

PRITCHARD, D.W. (1967) What is an estuary: Physical viewpoint. In: *Estuaries*. G.H. Lauff, ed., Am. Assoc. Adv. Sci., Publication No. 83, Washington, D.C., 37–44.

RATTRAY, M. (1977) Fjord and salt wedge circulation. In: *Estuaries, Geophysics and the Environment*. C.B. Officier, ed., National Academy of Sciences, Washington, D.C., 36–45.

REGAN, L. (1968) *Euphausia Pacifica* and other Euphausids in the Coastal Waters of British Columbia; Relationships to Temperature, Salinity and Other Properties in the Field and the Laboratory. *Ph.D. Thesis. University of British Columbia,* Vancouver, British Columbia.

ROBINSON, R.M. (1969) The effects of a vertical barrier on internal waves. *Deep-Sea Research*, **16**, 421–429.

SAMUELS, G. (1979) A Mixing Budget for the Strait of Georgia, British Columbia. *M. Sc. Thesis, University of British Columbia,* Vancouver, British Columbia, 261 pp.

SANDSTROM, H. (1976) Effect of topography on propagation of waves in stratified fluids. *Deep-Sea Research*, **16**, 405–410.

SAUNDERS, P.M. (1976) Near-surface current measurements. *Deep-Sea Research*, **23**, 249–257.

SCHUBEL, J.R. and HIRSCHBERG, D.J. (1978) Estuarine and coastal graveyards, climatic change, and the importance of the estuarine environment. In: *Estuarine Interactions*. M. Wiley, ed., Academic Press, 285–302.

SHAN, K. (1962) Systematic and Ecological Studies on Copepoda in Indian Arm, British Columbia. *M. Sc. Thesis, University of British Columbia,* Vancouver, British Columbia.

STACEY, M.W. (1984) The interaction of tides with the sill of a tidally energetic inlet. *J. Phys. Oceanogr.*, **14(6)**, 1105–1117.

STACEY, M.W. and Zedel, L.J. (1986) The time dependent, hydraulic flow over the sill of Observatory Inlet. *J. Phys. Oceanogr.* in press.

STIGEBRANDT, A. (1976) Vertical diffusion driven by internal waves in a sill fjord. *J. Phys. Oceanogr.*, **6**, 486–495.

———, (1979) Observational evidence for vertical diffusion driven by internal waves of tidal origin in Oslofjord. *J. Phys. Oceanogr.*, **7**, 118–122.

———, (1980) Some aspects of tidal interaction with fjord constrictions. *Est. Coast. Mar. Sci.*, **11**, 151–166.

STOMMEL, H. and FARMER, H.G. (1952) Abrupt changes in width in two-layer open channel flow. *J. Mar. Res.***11**, 205–214.

———, (1953) Control of salinity in an estuary by a transition. *J. Mar. Res.*, **12**, 13–20.

STUCCHI, D. and FARMER, D.M. (1976) Deepwater exchange in Rupert-Holberg Inlet. *Pacific Marine Sciences Report , 76-10,* Institute of Ocean Sciences, Patricia Bay, British Columbia.

TABATA, S. (1971) A brief oceanographic description of the waters of Burrard Inlet and Indian Arm. *Appendix D of the Burrard Inlet-Howe Sound Area Preliminary Description of Existing Environmental Conditions.* Mar. Sci. Direct., Pacific Region, Fisheries and Environment Canada.

THOMAS, A.G. (1982) The effect of tidal transport on the zooplankton of a local inlet. *M. Sc. Thesis, University of British Columbia,* Vancouver, British Columbia.

TURNER, J.S. (1973) *Buoyancy Effects in Fluids.* Cambridge University Press, Cambridge, 367 pp.

University of British Columbia (1982) , *Department of Oceanography* Data Report 51.

University of British Columbia (1983) , *Department of Oceanography* Data Report 52.

University of British Columbia (1984) , *Department of Oceanography* Data Report 53.

University of British Columbia (1985) , *Department of Oceanography* Data Report 54.

VAN LEER, J.C., W. DÜING, R. ENRATH, E. KENNELLY and A. SPEIDEL. (1974) The Cyclesonde: An unattended vertical profiler for scalar and vector quantities in the upper ocean. *Deep-Sea Research*, **21**, 385–400.

WALDICHUK, M. (1976) Water exchange in Port Moody, British Columbia and its effect upon waste disposal. *J. Fish. Res. Bd. Canada*, **22(3)**, 801–822.

WEBB, A.J. (1985) The Propagation of the Internal Tide in Knight Inlet, British Columbia. *Ph. D. Thesis, University of British Columbia* Vancouver, British Columbia.

WHITFIELD, P.H. (1974) Seasonal Changes in Hydrographical and Chemical Properties of Indian Arm and their Effect on the Calenoid Copepod *Euchaeta Japonica. M. Sc. Thesis, University of British Columbia,* Vancouver British Columbia.

WOODWARD, M.J., HUGGETT, W.S., and THOMSON, R.E. (1986) Near-surface moored current intercomparisons in coastal waters. *Deep-Sea Research*, (submitted).

WUNSCH, C. (1968) On the propagation of internal waves up a slope. *Deep-Sea Research*, **15**, 251–258.

WUNSCH, C. (1969) Progressive internal waves on slopes. *J. Fluid Mech.*, **35**, 131–144.